Millennial-scale variability in denitrification and phosphorus burial in the Eastern Tropical North Pacific

Thesis submitted for the degree of
Doctor of Philosophy
University of Edinburgh
2009

For Linda, Pino and Luisa

I attest that:

All material presented in this document was compiled and written by myself unless otherwise acknowledged.

Stephen A. Francavilla

Acknowledgements:

First of all, I would like to thank my supervisors Raja Ganeshram and Mary Elliott for getting me started with this challenging project and for supporting me with their advice and many stimulating discussions.

A very warm thank you goes to Laetitia Pichevin, Bryne Ngwenya and Elsa Arellano-Torres who have taken the time and trouble to help me put this thesis into shape through stylistic suggestions and substantive challenges to help me improve my presentation and clarify my arguments.

The technical staff at the University of Edinburgh, especially Ruth Dwyer, Colin Chilcott, Ann Mennim and Nic Odling provided indispensable help throughout my time in the Grant Institute.

Thanks to Steve Moreton at the AMS lab in East Kilbride for assisting with the ^{14}C dating and to Paul Alexandre at SUERC Argon Isotope Facility in East Kilbride for providing the K/Ar dates.

My years in Edinburgh would not have been as enjoyable without all the new friends and flatmates who kept me sane during my years as a postgraduate, especially Natasha Lee, Apo and Phil Crosbie for the endless coffees and discussions in Falcon Avenue. A very warm thank you goes to Louise Kennerley, for opening my eyes to the possibility of a new and exciting career in corporate finance in London. And last but not least, a special thank-you goes to Steven Sawyer for the many enlightening discussions over a pint or three of real ale at the Cloisters pub in Bruntsfield.

Finally I want to thank my family. The encouragement, patience and support from my parents were and will always be a powerful source of inspiration and energy.

ABSTRACT

The remarkable synchrony between changes in temperature recorded in Greenland ice cores and variations in N isotope records from sedimentary cores recovered from the Arabian Sea and the Eastern Tropical North Pacific (ETNP) has provided evidence for teleconnections between changes in marine denitrification in the tropics and climate variations in the northern high latitudes. Changes in tropical denitrification have been attributed to changes in productivity, changes in the source of intermediate waters and the flux of dissolved oxygen to suboxic zones. Variations in marine denitrification and anammox occurring at intermediate depths in proximity to productive continental margins have had profound effects on the N:P ratio of upwelled waters between stadials and interstadials, and may have indirectly affected carbon sequestration in the ocean by changing the balance of nutrients available to primary productivity. Competitive equilibrium, the changing stoichiometric balance of elements available as nutrients and the shorter residence time of N compared to P are factors that are believed to favour diazotrophs (N_2-fixing organisms) during interstadials and shift the competitive advantage to non-N_2-fixing ecosystems during stadials.

This study presents a very high-resolution analysis of sedimentary nitrogen isotope records, phosphorus concentrations and bulk detrital element concentrations from two cores collected along the Pacific Mexican Margin. The results show that the oxygen minimum zone (OMZ) bathing intermediate waters in ETNP is modulated by the interaction of a Northern Hemisphere climate component with the “leakage” of heavy nitrate believed to derive from the Eastern South Pacific (ESP). This southerly component has a more “Antarctic” timing and is similar to records from the Peru-Chile margin. The sedimentary core recovered from the Mazatlan margin shows a “Greenland” timing of millennial-scale events, with reduced upwelling and reduced primary productivity, a less intense OMZ leading to reduced denitrification and a more southerly position of the mid-tropospheric subtropical ridge during stadials. This would have increased the onshore flow of moist air, ultimately leading to increased precipitation along the western Mexican Margin. Interstadials show a reversal of these conditions.

In contrast to the Mazatlan core, the N isotope record from the core recovered from the Gulf of Tehuantepec records an element of “Antarctic” timing superimposed on local, millennial-scale variations in denitrification that are more similar in timing to Greenland temperature changes. In addition, the interpretation of observed variations in detrital elements from the Gulf of Tehuantepec highlights latitudinal displacements of the ITCZ that are consistent with those observed in the Cariaco Basin in Venezuela. Bulk P concentrations from both cores suggest that although phosphorite formation in the ETNP during interstadials is not as widespread as previously thought, the very high accumulation rates in the Gulf of Tehuantepec and Mazatlan Margin lead to total Holocene phosphorus burial rates that are up to 4-5 times higher than had been estimated in previous studies. These observations lead to the argument that the ETNP may play a more important role in regulating global P budgets than was previously thought and call for an improved appreciation of the benthic microbial communities that modulate biomes at tropical latitudes.

Contents

Declaration…….*ii*
Acknowledgements…….*iii*
Abstract.....*iv*
Contents…….*v*

1. Introduction
- 1.1 Late Quaternary millennial-scale climate variability…….*2*
- 1.2 The Eastern Tropical North Pacific: the Oxygen Minimum Zone, water-column denitrification and phosphorite deposition 6
- 1.3 Objectives …….*12*

2. Oceanographic, atmospheric and physiographic settings: Upwelling, the Oxygen Minimum Zone and ocean currents in the Eastern Tropical North Pacific
- 2.1 Oceanography…….*18*
- 2.2 El Niño in the Eastern Pacific over Interannual and Millennial Time-Scales …….*20*
- 2.3 The ITCZ in the Eastern Pacific…….*22*
- 2.4 Upwelling in Mazatlan and the Mexican monsoon …….*23*
- 2.5 Upwelling in the Gulf of Tehuantepec as a consequence of Central American Cold Surges …….*24*
- 2.6 Geology of western Mexican plains and the Sothern Highlands…….*26*
- 2.7 Climate and Vegetation…….*27*

3. Methodology
- 3.1 Core description…….*32*
- 3.2 Sampling…….*33*
- 3.3 Carbon and Nitrogen…….*33*
- 3.4 X-Ray Fluorescence…….*33*
- 3.5 Colour reflectivity…….*34*
- 3.6 ^{14}C dating of samples…….*36*
- 3.7 K-Ar dating…….*36*

4. Stratigraphy
- 4.1 Age model…….*40*

5. Nitrogen isotope, organic carbon and sediment chromaticity records from the Eastern Tropical North Pacific: remote vs. local forcing of millennial- and orbital-scale variability over the past 200,000 years
- 5.1 Introduction…….*55*
- 5.2 Environmental Setting…….*57*
- 5.3 Methods…….*59*
- 5.4 Results: $\delta^{15}N$ and Organic Carbon…….*59*
- 5.5 Results: Detrital Elements…….*65*
- 5.6 Discussion: Past Changes in Water-Column Denitrification Throughout the Past 200,000 years …….*68*
- 5.7 The nitrogen cycle in the ETNP: a dynamic equilibrium or a catalyst for glacial-interglacial CO2 variations?…….*71*
- 5.8 Cyclical changes in detrital elements and latitudinal shifts in the Pacific mid-tropospheric subtropical ridge…….*76*
- 5.9 Conclusion…….*80*

6. Glacial-Holocene $\delta^{15}N$ record from the Gulf of Tehuantepec, Mexico: Implications for denitrification in the eastern equatorial Pacific

- 6.1 Introduction…….*87*
- 6.2 Environmental Setting: Upwelling in the Gulf of Tehuantepec as a consequence of Central American Cold Surges…….*89*
- 6.3 Methods…….*90*
- 6.4 Results: $\delta^{15}N$ and Organic Carbon…….*91*
- 6.5 Results: Detrital Elements…….*94*
- 6.6 Discussion: Origin of the $\delta^{15}N$ signal in the Gulf of Tehuantepec…….*96*
- 6.7 Advection of heavy nitrate from the southern OMZ…….*100*
- 6.8 Gap winds and moisture transport across Central America as a positive feedback on denitrification and abrupt climate change…….*103*
- 6.7 Conclusion…….*108*

7. Millennial-scale variations in phosphorite deposition in the Eastern Tropical North Pacific

- 7.1 Introduction…….*115*
- 7.2 Methods…….*117*
- 7.3 Results: Phosphorus burial in total P concentrations in cores MD02-2518 and MD02-2520…….11*7*
- 7.4 Discussion…….*126*
- 7.5 Conclusion…….*135*

Appendix A

- Core MD02-2518 (Mazatlan) – Carbon & Nitrogen…….*140*

Appendix B

- Core MD02-2520 (Tehuantepec) – Carbon & Nitrogen…….*147*

Appendix C

- Core MD02-2518 (Mazatlan) – Major Elements…….*159*

Appendix D

- Core MD02-2520 (Tehuantepec) – Major Elements…….*168*

Appendix E

- Core MD02-2518 (Mazatlan) – Colour Reflectivity…….*173*

Appendix F

- Core MD02-2520 (Tehuantepec) – Colour Reflectivity…….*174*

CHAPTER 1

Introduction

1.1 Late Quaternary millennial-scale climate variability

Climate instability and Dansgaard-Oeschger events

Climatic instability on orbital and sub-orbital cycles is one of the most prominent features of ice-core and marine records retrieved from all over the globe. Climatic instability on orbital timescales has been shown to occur with periodicities of 100, 40 and 23kyrs, respectively coinciding with variations in eccentricity, obliquity and precession of the Earth (Hays et al., 1976). Details of dramatic sub-orbital (10^3 to 10^4 years) climate variability over the past 120,000 years were first discovered and documented most prominently in GRIP and GISP2 Greenland ice cores (Johnsen et al, 1992 and Grootes et al., 1993). The temperature ($\delta^{18}O$) records from these ice cores have shown that episodes of abrupt warming took place on average every 1000 to 3000 years during the glacial period spanning from 25 to 60kyrs BP (Bond et al., 1999; Schultz, 2002). The timing of these short and abrupt warming events seems to have varied more considerably between 60 to 90kyrs BP, with recurrence times varying between 1 to 12 kyrs. These interstadial periods are known as Dansgaard-Oeschger (D-O) events (Dansgaard et al, 1993), and are characterised in the Greenland ice-core oxygen isotope records of temperature variability as episodes of very rapid warming, which are followed by a gradual cooling of the Northern Hemisphere (Fig. 1.1). There is no uniform consensus on the origin and pacing of D-O events: periodic calving of icebergs from the Laurentide and Greenland ice sheets, internal oscillations within the ocean – atmosphere system in the Northern Hemisphere, external astronomical forcing and the intrinsic instability of interstadials are among the most relevant controlling factors for the rapid and large temperature fluctuations recorded in ice cores (see Schultz et al., 2002 for a comprehensive review of pacing mechanisms for D-O events). However, this millennial time-scale variability in the climate system recorded in ice cores was not only restricted to the last glacial period but appears to be a recurrent feature of the Pleistocene; sediment records recovered from the North Atlantic have documented millennial-scale climate instability recurring throughout the past 0.5 million years (Oppo et al., 1998; McManus et al., 1999) and during the early Pleistocene epoch (Raymo et al., 1998). This evidence suggests that millennial-scale instability is most likely a dominant characteristic of the Earth's climate.

Heinrich Events

An important feature of marine records recovered from the North Atlantic was the discovery of periodic horizons rich in limestone and dolomite fragments (>150 μm), which are believed to have derived from the discharge of icebergs from eastern Canada during glacial periods (Broecker, 1994). These layers of 'ice-rafted debris' (IRD) are known as Heinrich deposits (Heinrich, 1988) and are thought to have occurred after increases in ice volume in the Northern Hemisphere reached a peak, leading to a catastrophic discharge of icebergs into the North Atlantic (Bond et al., 1993 and references within; McManus et al., 1999, Hiscott et al., 2001). Evidence from sedimentary records from the North Atlantic shows that on an average 19kyr cycle, which is shorter than the 23kyr orbital precession cycle, surface temperatures in the Northern Hemisphere began to drop, eventually leading to an advance in ice streams into the North Atlantic from eastern Canada and Greenland. As the ice fronts reached their maximum seaward position and began to calve, the lithic grains incorporated in the ice were transported to the deep sea by the melting icebergs. Episodes of maximum IRD have been found to correlate with minima in $\delta^{18}O$ atmospheric temperature records from Greenland, and with short, pronounced negative excursions of up to 0.5‰ in $\delta^{18}O$ records from both planktonic (Bond and Lotti, 1995) and benthic foraminifera (Raymo et al, 1998). The oxygen isotope data from the planktonic foraminifera indicates that the periodic discharge of icebergs lead to a decrease in sea surface salinity by melt water, whereas the negative excursion recorded in benthic foraminifera indicates a likely change in deep-water circulation resulting in a perturbation of the north Atlantic thermohaline circulation which would have had repercussions on the global climate.

When observing the pattern of D-O and IRD events during the last glacial, it becomes obvious that variability on millennial time scales has been the rule throughout the Late Pleistocene and that these events assume a progressively colder and shorter nature within longer cooling cycles. These cycles were first observed by Bond et al. (1993) who speculated that the maximum expansion of ice sheets and consequent iceberg discharge into the North Atlantic (Heinrich event) occurs at the most intense cold phase of a package of a D-O cycles, and that each Heinrich event is

followed by an abrupt warming which ultimately leads to a new package of D-O cycles.

A comparison of ice-core records from Greenland vs. Antarctica

Climate instability is a typical feature of records retrieved not only from Greenland and the North Atlantic, but also from a variety of complementary proxy records recovered in Northern Hemisphere from deep sea sediments, continental loess deposits, speleothems and floral records (Tzedakis et al., 1997). The similar characteristics of many geographically disparate proxy records for climate change eventually lead to the interpretation of a hemispheric synchronicity in millennial-scale climate variability. But do Northern Hemisphere ice-core climate records have analogues in Antarctica?

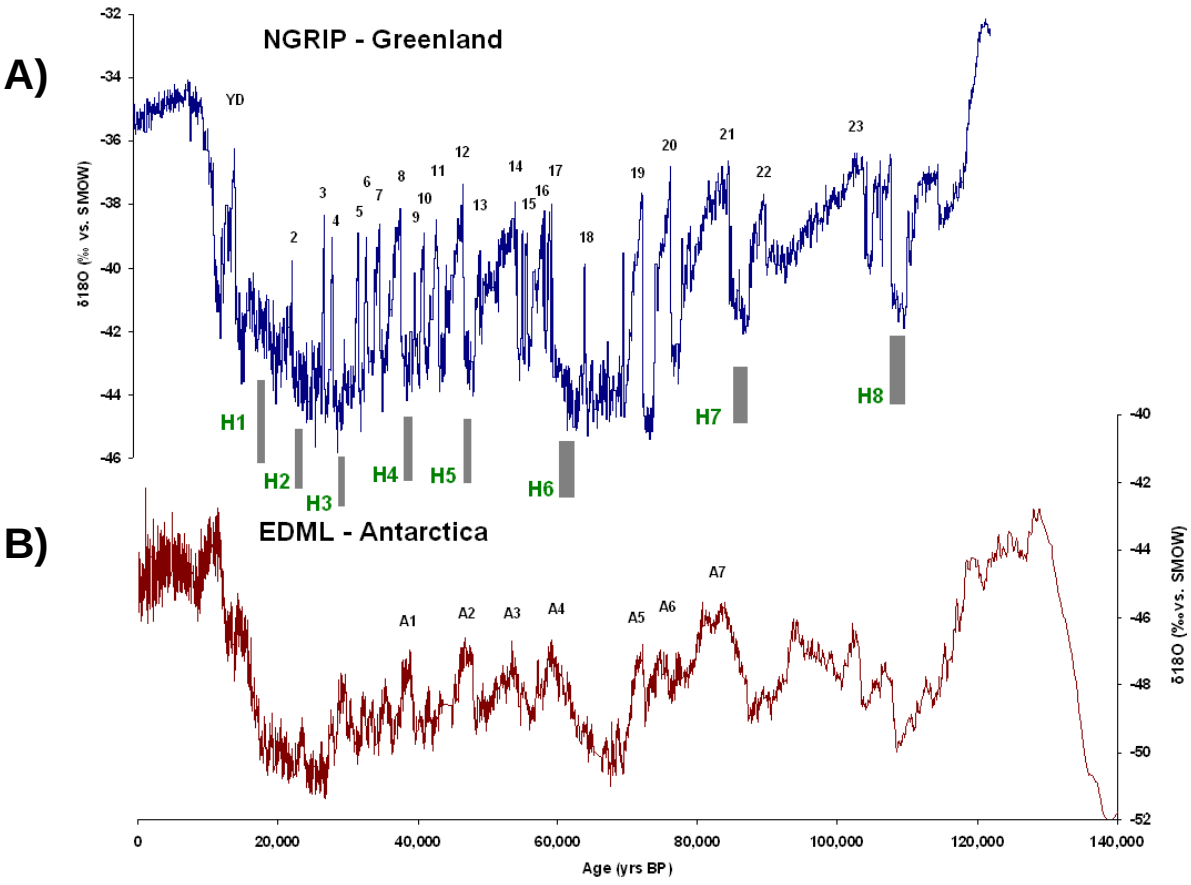

Figure 1.1: A) Oxygen isotope ($\delta^{18}O$) record from Greenland NGRIP ice core, where numerals above the maxima indicate Dansgaard / Oeschger events. B) $\delta^{18}O$ record from EPICA Dronning Maud Land (EDML) in the Atlantic sector of the East Antarctic Plateau. Numerals (A1, A2…) indicate Antarctic warm events. The grey bars beneath the NGRIP record represent the onset of compositionally distinctive ice-rafted deposits (Heinrich layers) observed in a number of cores recovered from the North Atlantic (Hiscott et al., 2001).

Drilling at the Vostok station in East Antarctica has covered the past 420,000 years and revealed the existence of repeating climate cycles in the Southern Hemisphere varying in accordance to precession, obliquity and eccentricity cycles of the Earth's orbit throughout the past four glacial-interglacial cycles (Petit et al., 1999). By complementing data from Vostok with ice-core drillings from the Byrd station in West Antarctica, and using methane records to correlate Greenland and Antarctic records, Blunier et al. (1998) was able to compare the inter-hemispheric relationships between millennial-scale warming events over the last 90kyrs. Additional data from high resolutions ice cores drilled at EPICA Dronning Maud Land (EDML) in the Atlantic sector of the East Antarctic Plateau found that warming events from Antarctica (denominated as A1, A2…) chronologically led Greenland D-O events by 1.5 to 3kyrs. In addition, the temperature rises in Antarctica had amplitudes of only 1-3°C (compared to D-O interstadial isotopic excursions revealing atmospheric temperature increases of >5°C, Blunier and Brook, 2001), were more gradual than the Greenland interstadials and appear to terminate as Greenland temperatures rose abruptly to interstadial levels. This created a see-saw pattern of warm events in the Northern high latitudes concurrent with cold events in Southern Hemisphere and vice versa. The coupling of millennial scale warmings in Antarctica has been extended to all D-O events in Greenland that occurred throughout the last glacial (EPICA Community Members, 2006).

The amplitude of warming events in Antarctica has been found to show a linear relationship with the duration of stadials in Greenland (the longer the Greenland stadial, the greater the Antarctic warming), which suggests the existence of either atmospheric or oceanic teleconnections linking the formation of North Atlantic Deep Water with heat accumulation in the Southern Ocean (Stocker & Johnsen, 2003). The EPICA Community Members (2006) speculated that changes in Southern Ocean sea-ice cover, especially a reduced cover during Antarctic warmings, may control the timing of reinstatement of deep-water formation in the North Atlantic. The trigger mechanism, however, remains yet unclear and may involve not only sea-ice cover, but also freshwater inputs, with the potential to affect Antarctic Intermediate Water Production (Pahnke and Zahn, 2005).

Sachs and Anderson (2005) found widespread evidence for increased productivity in the Southern Ocean during each of the eight Heinrich events which occurred in the last 70kyrs. The synchronous changes in chemistry and biology of sediments in both North Atlantic and Southern Ocean suggest that Heinrich events, as well as D-O events, may have affected climate on a global scale through perturbations in the global thermohaline circulation, with perturbations affecting climate regimes at lower latitudes (Rahmstorf, 2002, provides a global overview of palaeoclimatic proxy data characterizing warm phases and cold phases). As the Southern Ocean plays an important role in the formation of global intermediate waters, it is likely that changes in stratification and upwelling at high latitudes will have an effect on global circulation. There appears to be an antiphase between NADW-AAIW, suggesting that the northward surface heat transport "push" change as a result of freshwater inputs. It is believed that during periods of enhanced freshwater stratification, which lead to the cessation of NADW production at high latitudes in the northern hemisphere (i.e. Heinrich events), there was an intensified production and northward flow of AAIW (Pahnke and Zahn, 2005). This would in turn have had an effect on the global distribution of nutrients and dissolved oxygen and would ultimately have affected marine ecosystems that thrive in the large oxygen minimum zones of the globe, including the Eastern Tropical North Pacific (ETNP; Fig. 1.2).

1.2 The Eastern Tropical North Pacific: the Oxygen Minimum Zone, water-column denitrification and phosphorite deposition

The Oxygen Minimum Zone

Oxygen minimum zones (OMZs), as the name implies, are areas of the ocean where water-column oxygen saturation levels are at their lowest. OMZs are known for playing a key role in the global nitrogen cycle, as the absence of oxygen is conducive to the bacterial conversion of nitrate into gaseous nitrogen (N_20 and N_2) through denitrification and anammox, processes that can only occur in O_2 deficient regions (Hattori, 1983; Codispoti et al., 2001; Kuypers et al., 2005). In addition, the oxic conditions at the upper boundary of an OMZ lead to the two step transformation of NH_4^+ to NO_3^- via nitrite by means of nitrification, thus playing a pivotal role in

linking organic matter mineralization to anaerobic nitrogen removal. At present, global OMZs, defined as areas with O_2 concentrations <20μM cover an area of 30.4 10^6 km^2 (Paulmier and Ruiz-Pino, 2008), with the OMZ in the ETNP covering 12.4 x 10^6 km^2 (or 41% of the entire OMZ surface) and having a vertical extent of about 400m (from ~700-300m water depth) with minimal seasonal variability.

The structure of an OMZ is different from the classical O_2 minimum that is observed at 1000-2500m depth in all oceans, as the oxygen depletion may be up to 50 times more intense and occurs at shallower depths (50-700m). The intensity of the OMZ in the ETNP results primarily from the lateral advection of oxygen-deficient intermediate waters that have a predominantly northern source, coupled with high surface productivity and high rates of O_2 utilisation in subsurface waters due to the decomposition of sinking organic matter. Directly measured productivity data in this region show annual primary productivity ranging from 200-350g C m^{-2} yr^{-1} estimated using satellite radiometer data (Longhurst et al., 2005). This high flux of organic matter through the water column sustains the OMZ offshore western Mexico from 5ºN to 25ºN and out to 140ºW, where dissolved oxygen concentrations may be as low as <5μM (Nameroff et al., 2002).

Water-column denitrification

As dissolved oxygen is consumed within subsurface waters during the respiration of sinking organic matter, the OMZ also becomes gradually depleted in NO_3^- as this is the next thermodynamically most favourable electron acceptor in the bacterially-mediated oxidation of sinking organic matter. The reduction of NO_3^- in suboxic waters is a process known as denitrification, which at present occurs in the ETNP, off Peru-Chile and in the Arabian Sea. Denitrification represents an important loss of biologically available nitrogen from the oceans' OMZs and occurs primarily in sediments and in the water column beneath areas of high plankton productivity, where oxygen demand for the reduction of sinking organic matter exceeds its supply. As denitrification intensity increases in the water column with increasing oxygen demand, the reduction of nitrate leads to the formation of nitrite (NO_2^-) > nitric oxide (NO) > gaseous nitrous oxide (N_2O) and finally gaseous nitrogen (N_2). These processes together represent a significant loss of biologically available nitrogen from

the ocean as the gaseous products of denitrification (N_2O and the inert, least biologically available gaseous N_2) are eventually lost to the atmosphere. The inorganic nitrogen needs of primary production in the surface ocean are eventually supplied by the large reserves of nitrogen (in the form of nitrate) in the deep ocean and by N_2 fixation occurring in subtropical oceanic gyres, although estimating nitrogen fixation and precisely quantifying sources of nitrogen fixation in the open ocean remain a major challenge (Karl et al., 2002). Water-column denitrification in the ETNP is confined to oxygen-deficient regions in the density range σ = 26.7-27.4 (200-700m depth), where the supply of O_2 from lateral transport and vertical advection is less than its demand for the remineralisation of sinking organic matter.

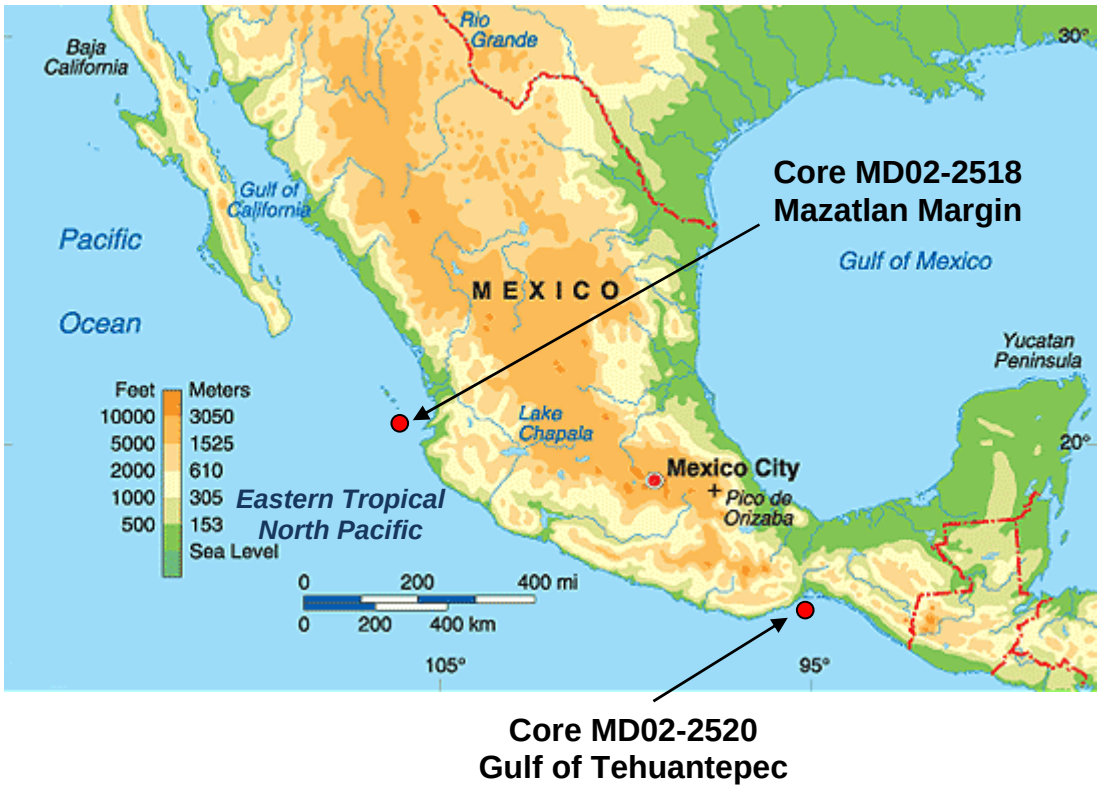

Figure 1.2 Location of core MD02-2518 collected at 454m water depth on the upper slope of the northwestern Mexican Margin, offshore Mazatlan (22º40.39N, 106º29.19W), and core MD02-2520 collected at a water depth of 719m in the Gulf of Tehuantepec (015º40.1N, 095º18.00W)

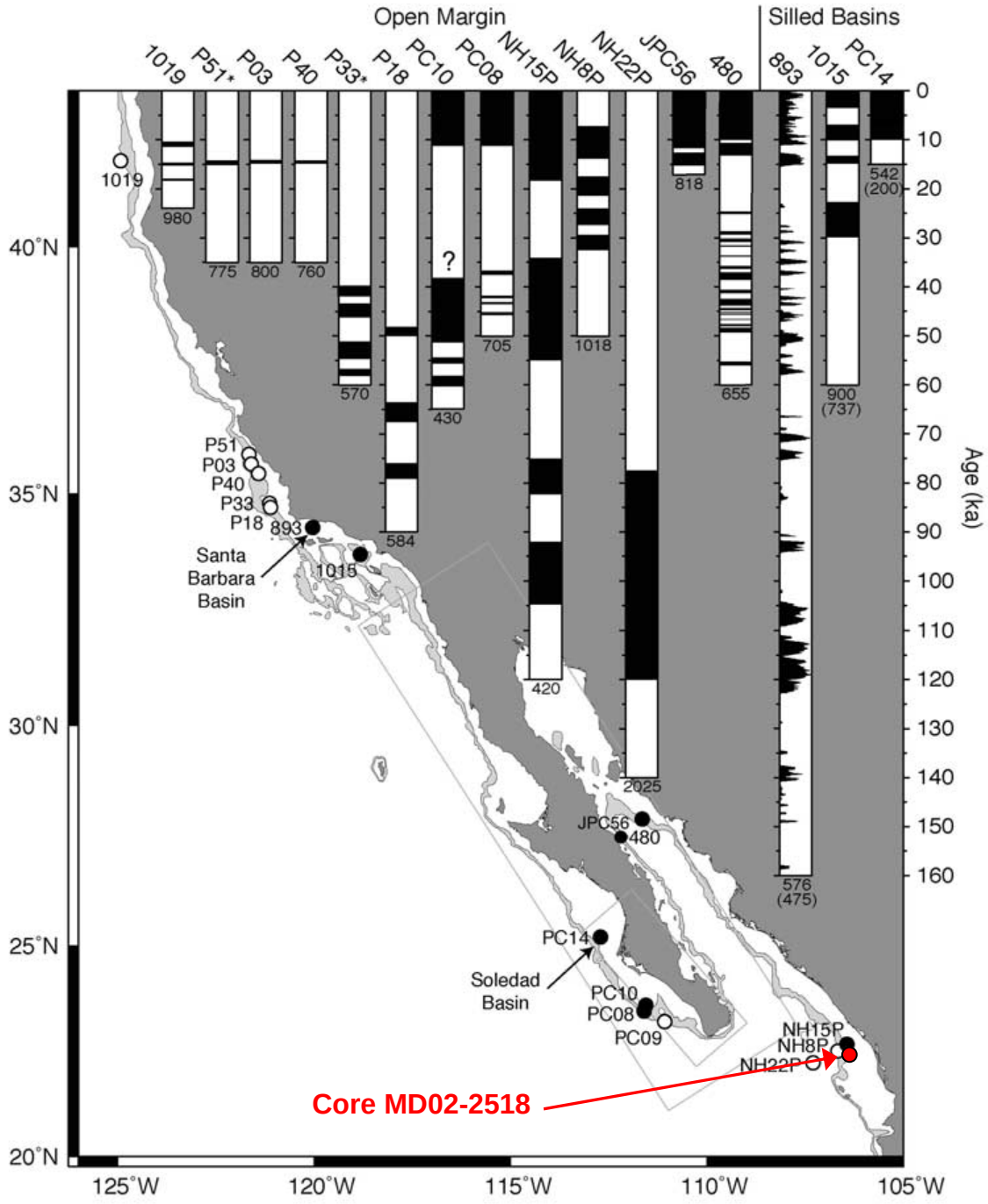

Figure 1.3: Distribution and timing of preservation of laminated sediments (black) vs. bioturbated sections (white) in piston cores collected along the western margin of North America. The depth of each record (m) is listed below each bar (with sill depth in parentheses where relevant). The most recent transition from bioturbated late glacial sediments to laminated Holocene sediments was not synchronous at southern Baja California sites, despite their proximity. This implies that records from different locations are subject to an OMZ which has varied in lateral and vertical extent throughout the past, and is subject to variable organic C rain rates and lateral ventilation from different sources.
The figure is taken from Figure 1 in van Geen et al., 2003.

Denitrification (and nitrification) in the oceans are major contributors of nitrous oxide (N_2O) to the atmosphere (Codispoti and Christensen, 1985; Yoshinari et al., 1997). The importance of N_2O as a greenhouse gas in the atmosphere stems from the fact that on a molecular basis it is 180 times more powerful than CO_2 (Lashof and Ahuja, 1990). N_2O measurements made on gas bubbles extracted from polar ice indicate that the atmospheric concentration of this gas varied in tandem with temperature, increasing dramatically during D-O warm stadials and reducing throughout cold interstadials (Blunier et al., 1998; Flückiger et al., 1999; Flückiger et al., 2004).

All OMZs are associated with nitrogen loss from the oceans, although the lateral and vertical extent of denitrification regions is generally smaller than the core area of the associated OMZ. By using criteria defined by Broecker and Peng (1982) and Hattori (1983) to define denitrification zones ("nitrate deficit maximum" zone = $15PO_4^{3-} - NO_3^- > 10$ μM), Paulmier and Ruiz-Pino (2008) found the "nitrate deficit maximum" zone in the ETNP to extend 7.8 x 10^6 km^2 (56% of the ETNP OMZ core) with a vertical average from 220-480m depth (62% of ETNP OMZ vertical extent). This difference may be reconciled by the variable oxygen threshold value below which denitrification occurs, which may vary between <0.8 - < 20 μM O_2 according to the local denitrifying bacterial community (Smethie, 1987) and will occur in a restricted volume compared to the OMZ core.

Fig. 1.3 provides an overview of how the OMZ in the ETNP has varied in both lateral and vertical extent throughout the past. The numerous transitions from laminated to bioturbated sediments observed in sedimentary cores retrieved from the Californian and Mexican Margin, where the OMZ impinges on the continental shelf, are testament to the variability in past productivity and changes in O_2 concentrations. The similar timing and order of succession between laminated and bioturbated intervals along the western margin of North America indicates that many records are related to broad-scale changes in the intensity of the OMZ along the ETNP (van Geen et al., 2003). At present, laminations are preserved on the open margin only in regions south of 25ºN (Fig. 1.3), which reflects a northern and Central Californian OMZ which is deeper, more proximal to areas of ventilation and considerably less intense than the OMZ bathing the Mazatlan Margin (23ºN – Fig. 1.3). However, the

striking correlation between the pattern of laminations in cores from the western margin of North America and the Greenland isotope record is testament to the sensitivity of low-oxygen environments at low latitudes to climate change. In particular, oxygen levels within the OMZ bathing the western margin of North America were sufficiently low for bioturbation to be a dominant feature during the Last Glacial Maximum (LGM), as evidenced by a number of piston cores collected between 20°-30°N and 105°-115°W (Fig. 1.3). What emerges from these observations is that high frequency climate variability first recognized in the Greenland (and Antarctic) ice-cores is also present in the tropics and there is increasing evidence for a pronounced role of the tropics being responsible for acting as a trigger and/or amplifier of millennial-scale climatic cycles.

Phosphorites

Phosphogenesis (the authigenic formation of carbonate fluorapatite - CFA) and phosphorite deposition (the accumulations of P-rich sediments) are common features in marine sediments where the porewater HPO_4^{2-} concentrations exceed CFA saturation thresholds (Filippelli and Delaney, 1992). Phosphorite deposition represents a particularly important sink in the marine P cycle and has been found to occur predominantly in continental margins that coincide with higher rates of plankton productivity and an increase in intensity of the oxygen minimum zone – which together combine to preserve plankton deposition and contribute to an increased supply of HPO_4^{2-} to the sediments (Ingall and Jahnke, 1994, 1997).

Denitrification and phosphogenesis are the largest sinks of fixed nitrogen and dissolved phosphorus in the oceans. Next to light, these two elements (N and P), together with a number of micronutrients (i.e. Fe) are the main limitation to biological productivity over most of the ocean (Tyrell, 1999). For the above reasons, reconstructing the history of variations in marine denitrification and phosphorus deposition throughout the Late Quaternary from sedimentary cores is necessary to provide a clearer picture of past nutrient cycling in the oceans and how local changes in nutrient inventories may have affected plankton ecosystems, N_2O emissions and the biological pump for CO_2 (Codispoti, 1985; Arrigo, 2005).

1.3 Objectives

The purpose of this study is to interpret two new, high-resolution archives of past climate change recovered from the Mexican Margin (Fig. 1.2). The conclusions presented in this work are based on the comparison of paleoenvironmental records of denitrification, phosphogenesis, organic carbon preservation and major element distribution from two previously undocumented sediment cores collected from Mazatlan Basin and the Gulf of Tehuantepec, Mexico, with existing records of climate change. The two core sites are roughly 800 miles apart from each other on the continental slope of western Mexico and were chosen for their proximity to atmospheric and topographic environmental boundaries, the pronounced variability in sedimentation rates and their individual oceanographic settings. The key principles that form the basis of the discussion are:

- the reconstruction of very high resolution records of denitrification and organic matter preservation from two cores collected along the ETNP and the comparison of the timing and amplitude of these with other published paleogeographic records from both the northern and southern hemispheres.
- the reconstruction of past shifts in rainfall patterns in the Gulf of Tehuantepec throughout the last 40,000 years by analysing changes in detrital inputs from land (Si/Al, K/Al, Ti/Al) as a reliable index of the relative position of the Intertropical Convergence Zone with respect to the equator.
- analysis of the role of millennial-scale denitrification and phosphogenesis in the ETNP for regulating ecosystems and attempt to estimate the rates of removal of P in phosphogenic areas off the coast of Mazatlan and the Gulf of Tehuantepec and assess variations in total P burial between stadials and interstadials.

Chapter 2 provides an introduction to the oceanographic settings, El Niño in the Eastern Pacific over interannual and millennial time-scales, the Intertropical Convergence Zone and an overview of the wind patterns, the regional geology and vegetation of western Mexico.

Chapter 3 provides a description of the two cores, the description of the analytical methods employed for this study and the rationale behind each

geochemical proxy used for the assessment of past changes in the regional environment.

Chapter 4 presents the construction of the stratigraphy and the age models for both cores through the use of both AMS ^{14}C dating and correlations of the $\delta^{18}O$ and $\delta^{15}N$ records.

Chapter 5 is an investigation of the millennial-scale variability in ventilation changes in intermediate waters, organic matter deposition and the distribution of phosphorites and major elements in the Mazatlan Margin. The proxy records are used to generate a picture of changes in wind-driven upwelling, productivity and the reorganization of wind systems over the past 130 kyrs.

Chapter 6 investigates proxies for millennial-scale variability in sediments deposited in the Gulf of Tehuantepec, where water mass properties of the Pacific Ocean are highly asymmetric. The Antarctic character imprinted on nitrogen isotope records and the decoupling of these records from records of organic matter preservation highlight the importance of remote vs. local variations in productivity and denitrification over millennial time-scales. In addition, the distribution of major elements in this core suggests that the relative position of the Intertropical Convergence Zone may have varied in synchrony with changes previously observed in the Cariaco Basin.

Chapter 7 analyses distribution of P in sediments from the Mexican Margin and leads to the interpretation that laminated sediments in the ETNP may constitute a larger sink for phosphorus than has been previously observed.

Chapter 8 provides an overview of the main concepts discussed in chapters 3-7 and a brief summary of this thesis.

All measurements produced during this study are presented in Appendices A-F.

References

Arrigo, K.R. (2005) Marine microorganisms and global nutrient cycles. *Nature*, vol. **437**, pp. 349-355

Blunier, T., Chappellaz, J., Schwander, J., DaÈllenbach, A., Stauffer, B., Stocker, T.F., Raynaud, D., Jouzel, J., Clausen, H.B., Hammer, C.U., Johnsen, S.J. (1998) Asynchrony of Antarctic and Greenland climate change during the last glacial period. *Nature*, vol. **394**, pp. 739-743

Blunier, T. and Brook, E.J. (2001) Timing of Millennial-Scale Climate Change in Antarctica and Greenland During the Last Glacial Period. *Science*, vol. **291**, pp. 101-111

Bond, G.C., Broecker, Johnsen, S.J., McManus, J.F., Labeyrie, L., Jouzel, J., Bonani, G. (1993) Correlations between climate records from North Atlantic sediments and Greenland Ice, *Nature*, vol. **365**, pp 143-147

Bond, G.C. and Lotti, R. (1995) Iceberg discharge into the North Atlantic on millennial time scales during the last glaciation. *Science*, vol. **267**, pp. 1005-1010

Bond, G.C., Showers, W., Elliot, M., Evans, M., Lotti, R., Hajdas, I., Bonani, G., Johnson, S., (1999) The North Atlantic's 1-2 kyr climate rhythm: Relation to Heinrich events, Dansgaard/Oeschger cycles, and the Little Ice Age, in *Mechanisms of Global Climate Change at Millennial Time Scales*, Geophys. Monogr. Series, vol. **112**, pp. 35-58

Broecker W.S. (1994) Massive iceberg discharges as triggers for global climate change. *Nature*, vol. **372**, pp. 421-424

Broecker, W. S. and Peng, T.-H (1982) *Tracers in the Sea*. Lamont-Doherty Geological Observatory, Eldigio Press, Palisades, N.Y.

Codispoti, L.A. and Christensen, J.P., (1985) Nitrification, denitrification and nitrous oxide cycling in the eastern tropical South Pacific Ocean. *Mar. Chem.*, vol. **16**, pp. 277-300.

Codispoti, L.A., Brandes, J.A., Christensen, J.P., Devol, A.H., Naqvi, S.W.A., Paerl, H.W., and Yoshinari, T. (2001) The oceanic fixed nitrogen and nitrous oxide budgets: Moving targets as we enter the anthropocene?, *Sci. Mar.*, vol. **65**, pp. 85–105

Dansgaard, W (1993) Evidence for general instability of past climate from a 250-kyr ice-core record. *Nature*, vol. **364**, 218-220

EPICA Community Members (2006) One-to-one coupling of glacial climate variability in Greenland and Antarctica. *Nature*, vol. **444**, pp. 195-198

Filippelli, G.M. and Delaney, M.L. (1992) Similar Phosphorus fluxes in ancient phosphorite deposits and a modern phosphogenic environment. *Geology*, vol. **20**, pp. 709-712

Fluckiger, J., Dallenbach, A., Blunier, T., Stauffer, B., Stocker, T.F., Raynaud, D. Barnola, J.M. (1999) Variations in atmospheric N_2O concentration during abrupt climatic changes. *Science*, vol. **285**, pp. 227–230

Fluckiger, J., Blunier, T., Stauffer, B., Chappellaz, J., Spahni, R., Kawamura, K., Schwander, J., Stocker, T., Dahl-Jensen, D. (2004) N_2O and CH_4 Variations during the last glacial epoch: insight into global processes, *Glob. Biogeochem. Cycles*, vol. **18**, DOI: 10.1029/2003GB002122

Grootes, P.M., Stuiver, M., White, J. W. C., Johnsen, S., Jouzel, J. (1993) Comparison of oxygen isotope records from the GISP2 and GRIP Greenland ice cores, *Nature*, vol. **366** pp. 552-554

Hays, J., Imbrie, J., and Shackleton, N. (1976) Variations in the Earth's Orbit: Pacemaker of the Ice Ages. *Science*, vol. **194**, p.1121

Hattori, A. (1983). Denitrification and dissimilatory nitrate reduction. 1n Carpenter, E.J. and Capone, D.G., *Nitrogen in the marine environment*. Academic. pp.19l-232

Heinrich, H. (1988) Origin and consequences of cyclic rafting in the Northeast Atlantic Ocean during the past 130,000 years. *Quat. Res.*, vol. **29**, pp. 143-152

Hiscott, R.N., Aksua,A.E., Mudieb, P.J. and Parsonsa, D.F. (2001) A 340,000 year record of ice rafting, palaeoclimatic fluctuations, and shelf-crossing glacial advances in the southwestern Labrador Sea. *Global and Planetary Change*, vol. **28**, Issues 1-4, pp. 227-240

Ingall, E. and Jahnke, R. (1994) Evidence for enhanced phosphorus regeneration from sediments overlain by oxygen depleted waters. *Geochimica et Cosmochimica Acta*, vol. **58**, pp. 2571-2575

Ingall, E. and Jahnke, R. (1997) Influence of water column anoxia on the elemental fractionation of carbon and phosphorus during sediment diagenesis. *Marine Geology*, vol. **139**, pp. 219-229

Johnsen, S. J., Clausen H. B., Dansgaard W., Fuhrer K., Gundestrup N., Hammer C. U., Iversen P., Jouzel J., Stauffer B. & Steffensen J. P. (1992) Irregular glacial interstadials recorded in a new Greenland ice core. *Nature* vol. **359**, pp. 311–313

Karl, D., Michaels, A., Bergman, B., Capone, D., Carpenter, E., Letelier, R., Lipschultz, F., Paerl, H., Sigman, D. and Stal L. (2002) Dinitrogen fixation in the world's oceans. *Biogeochemistry*, vol. **57/58**, pp. 47– 98

Kuypers, M.M.M., Lavik, G., Woebken, D., Schmid, M., Fuchs, B.M., Amann, R., Jørgensen and Jetten, M.S.M. (2005) Massive nitrogen loss from the Benguela upwelling system through anaerobic ammonium oxidation, *Proc. Nat. Acad. Sci*., vol. **102**, pp. 6478–6483

Lashof, D.A. and Ahuja, D.R., (1990) Relative contributions of greenhouse gas emissions to global warming. *Nature*, vol. **344**, pp. 529-531

Longhurst, A.R., Sathyendranath, S., Platt, T. and Caverhill, C. (1995) An estimate of global primary production in the ocean from satellite radiometer data. *Journal of Plankton Research*, vol. **17**, pp. 1245-1271

McManus, J., Oppo, D.W., Cullen, J.L. (1999) A 0.5-Million-Year Record of Millennial-Scale Climate Variability in the North Atlantic. *Science*, vol. **283**, pp 971- 975

Nameroff, T. J., L. S. Balistrieri, and J. W. Murray (2002), Suboxic trace metal geochemistry in the eastern tropical north Pacific. *Geochim. Cosmochim. Acta*, vol. **66**, 1139– 1158.

Oppo, D.W., McManus, J.F., Cullen, J.C., (1998) Abrupt climate change events 500,000 to 340,000 years ago: evidence from sub polar North Atlantic sediments. *Science*, vol. 279, pp. 1335-1338

Pahnke, K. and Zahn, R. (2005) Southern Hemisphere water mass conversion linked with North Atlantic climate variability. *Science*, vol. **307**, pp. 1741-1746

Paulmier, A., and Ruiz-Pino, D. (2008) Oxygen Minimum Zones (OMZs) in the Modern Ocean. *Progress In Oceanography* (in revision). doi:10.1016/j.pocean.2008.08.001

Petit, J.R., J. Jouzel, D. Raynaud, N.I. Barkov, J.-M. Barnola, I. Basile, M. Bender, J. Chappellaz, M. Davis, G. Delayque, M. Delmotte, V.M. Kotlyakov, M. Legrand, V.Y. Lipenkov, C. Lorius, L. Pépin, C. Ritz, E. Saltzman, and M. Stievenard (1999) Climate and atmospheric history of the past 420,000 years from the Vostok ice core, Antarctica, *Nature*, vol. **399**, pp. 429-436.

Raymo, M.E, Ganley, K., Carter, S., Oppo, D.W., McManus, J. (1998) Millennial-scale climate instability during the early Pleistocene epoch. *Nature*, vol. **392**, pp. 699-702

Sachs, J.P. and Anderson, R.F. (2005) Increased productivity in the subantarctic ocean during Heinrich events. *Nature*, vol. **434**, pp. 1118-1121

Schultz, M (2002) On the 1470-year pacing of the Dansgaard-Oeschger warm events. *Paleoceanography*, vol. **17**, pp. 4-1 – 4-10

Smethie, W.M. (1987) Nutrient regeneration and denitrification in low oxygen fjords. *Deep Sea Research*, vol. **34**, pp. 983-1006.

Stocker, T.F. and Johnsen, S.J.A. (2003) A minimum thermodynamic model of the bipolar seesaw. *Paleoceanography*, vol. **18**, doi:10.1029/2003PA000920.

Tyrell, T. (1999) The relative influences of nitrogen and phosphorus on oceanic primary production. *Nature*, vol. **400**, pp. 525-531

Tzedakis, P.C., Andrieu, V., de Beaulieu, J.-L., Crowhurst, S., Follieri, M., Hooghiemstra, H., Magri, D., Reille, M., Sadori, L., Shackleton, N.J. & Wijmstra, T.A. (1997) Comparison of terrestrial and marine records of changing climate of the last 500,000 years. *Earth and Planetary Science Letters*, vol. **150**, pp. 171-176

van Geen, A., Zheng, Y., Bernhard, J. M., Cannariato, K. G., Carriquiry, J., Dean, W.E., Eakins, B. W., Ortiz, J. D., Pike, J. (2003) On the preservation of laminated sediments along the western margin of North America. *Paleoceanogr.*, vol. **18**, Issue 4, DOI 10.1029/2003PA000911

Yoshinari T., Altabet, M.A., Naqvi, S.W.A., Codispoti, L., Jayakumar, A., Kuhland, M., Devol A. (1997) Nitrogen and oxygen isotopic composition of N_2O from suboxic waters of the eastern tropical North Pacific and the Arabian Sea - measurement by continuous-flow isotope-ratio monitoring. *Marine Chemistry*, vol. **56**, pp. 253-264

CHAPTER 2

Oceanographic, atmospheric and physiographic settings: Upwelling, the Oxygen Minimum Zone and ocean currents in the Eastern Tropical North Pacific

2.1 Oceanography

The high rates of primary production in the ETNP are among the highest in the world and are mostly due to regional wind forcing dominated by the Mexican monsoon, trade winds converging into the Intertropical Convergence Zone (ITCZ) and jets blowing through gaps in the Central American cordillera. The intermediate waters along the Mexican Pacific plains and the Gulf of Tehuantepec have a complex origin coinciding with the mixing zone between the West Mexican Current (WMC; Kessler, 2006) from the south and Pacific Intermediate Water (PIW) from the north. The temperature, salinity and density properties of the WMC in the ETNP south of ~20ºN coincide with those of the "equatorial 13ºC water", a water mass that lies at depths of 75-300m east of 150°W. CTD (Conductivity-Temperature-Depth) transects conducted along the Equator in the mid-1960s highlighted the uniformity of physical properties of the 13°C Water, with salinity ranging between 34.8-35‰ and temperatures between 11-14°C. The properties are maintained throughout the equatorial Pacific and the water mass has been found to originate between the northeast of New Zealand and the Tasman Sea during the southern winter mixing (Tsuchiya, 1981). Tsuchiya proposed that this surface water is convected into the intermediate depths of the Equatorial Pacific and flows eastward next to the Equatorial Undercurrent and the subsurface North and South Equatorial Countercurrents, providing the evidence for a Southern Hemisphere origin of a portion of the nitrate-deficient intermediate waters upwelled in the ETNP. Kessler (2006) provided the most comprehensive review to date of the circulation in the eastern tropical Pacific and has identified the 13°C Water as an eastward flow found at 5-6º N associated with the Tsuchiya Jet and with the North Equatorial Countercurrent (NECC) at shallower depths (see Figure 2.1). These eastward-flowing Tsuchiya Jets coincide with tongues of higher salinity and higher dissolved oxygen and lower nitrate and phosphate extending from 170°W to 90°W at depths of about 300m (Tsuchiya, 1981). The speed of these tongues is high enough to allow the water mass to maintain their properties against the action of lateral mixing from westward-flowing low-oxygen equatorial currents. In addition, the water masses become shallower as they flow eastward, a property that reflects the eastward rising trend of the thermocline in the Pacific. It is assumed that once the eastward-flowing

North Equatorial Counter Current (NECC) and Tsuchiya Jets reach the longitude of the Galapagos Islands, they will either return to the west along the equatorial currents or flow poleward along the American coast to 15-20°N and 8-12°S (see Fig 2.1 for a schematic representation of circulation in the ETNP). It is thought that the eastward equatorial countercurrents may entrain 15 Sv of Subantarctic Mode Water (SAMW) and Antarctic Intermediate Water (AAIW) leaked through western boundary undercurrents near Papua New Guinea (Tsuchiya and Talley, 1996). Even though the geostrophic flow of NECC is reduced from 9 Sv (9 Sv = 9 × 10^6 m^3/s) at 125°W to only 1Sv east of 110°W, it is highly likely that a fraction of AAIW flows all the way to the Central American coast flowing north along the Costa Rica Dome, thus providing a source of intermediate waters bathing the Gulf of Tehuantepec and the site of core MD02-2520 presented in this study.

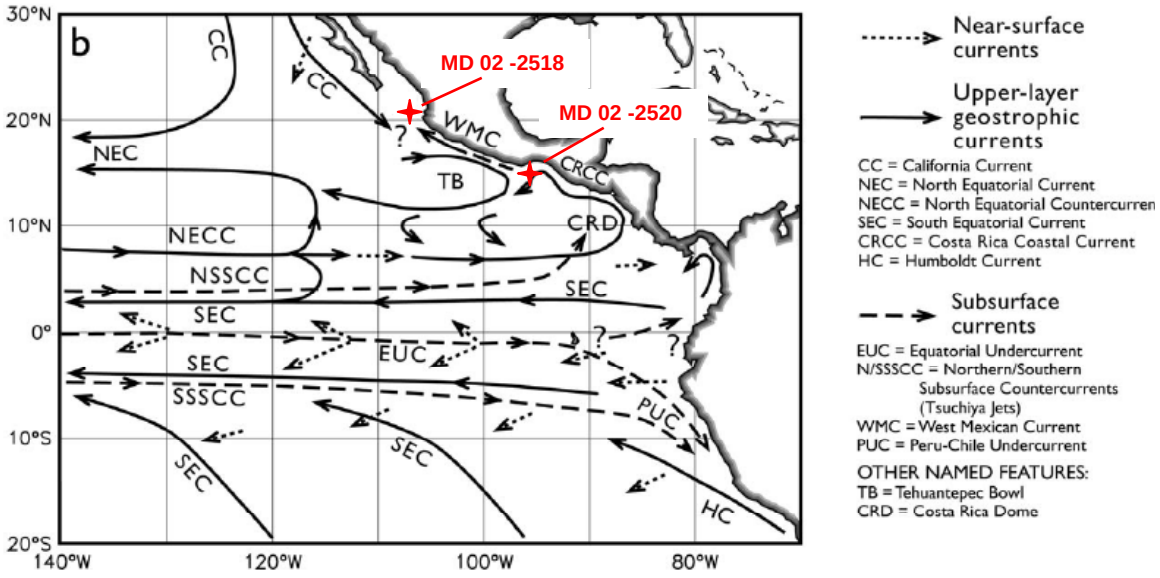

Figure 2.1. Schematic circulation in the eastern tropical Pacific showing the location of the two cores analysed in this thesis; from Fig 5b in Kessler, 2006.

The equatorial countercurrents start to progressively weaken between 110°W and the Central American land mass, where surface and subsurface circulation is affected by gap winds influenced by the topographic depressions. The main feature in the eastern pacific is the Costa Rica Dome (CRD) centred at 9°N, 90°W, where the thermocline rises to 25m depth. The counter-clockwise current speeds along the dome reach 20-50 cm s^{-1} leading to centrifugal- and wind-forced upwelling of 3 Sv of oxygen-poor and phosphate-rich waters from beneath the thermocline (Kessler,

2006; Wyrtki, 1964). These waters flow along the Mexican coast into the Gulf of Tehuantepec along the Costa Rica Coastal Current (CRCC in Fig. 2.1), a current that extends up to 400m depth in the water column which may extend north along the Pacific coastal plain to Cabo Corrientes at 20°N (mean speed of 3-5 cm s^{-1} and transport of 3 Sv – Kessler, 2006). The lower salinity and higher oxygen levels of intermediate waters to the north of 20°N allow for a distinction of the southern intermediate water component from the northern Pacific Intermediate Water. The latter has salinity and temperature range which is closer to waters formed in the north-western subarctic Pacific (salinity values of ~34‰ and temperatures ranging from 0-10°C) and is thought to be transported south by the California Current to the northwestern Mexican Margin (Nameroff et al., 2004), where core MD02-2518 was collected. It emerges that the oceanographic settings of the core locations and the structure of currents in the eastern equatorial Pacific are rather complex and any exchange of water masses across the equator are not yet completely understood.

2.2 El Niño in the Eastern Pacific over Interannual and Millennial Time-Scales

During modern La Niña / El Niño patterns, the tropical Pacific experiences dramatic changes in atmospheric circulation and precipitation patterns, typically lasting less than a year (Fig. 2.2). The onset of an El Niño event is characterised by a weakening and reversal of the trade winds in the western and central equatorial Pacific, which leads to the rapid development of unusually high sea-surface temperatures east of the International Date Line (McPhaden, 1999). The western Pacific warm pool, where surface waters are greater than about 29°C, gradually migrates eastward with the collapse of the trade winds. In the eastern Pacific, the colder sea surface temperatures that characterise equatorial cold tongue (the strip of cool water indicative of equatorial upwelling that normally occupies the eastern and central Pacific) fail to develop in boreal summer and autumn, ultimately causing the advection of warm water eastward near the equator, the depression of the seasonal thermocline in the eastern Pacific by more than 90 m and temporary reduction or even suppression of upwelling along central and south American margins (Stott et al., 2002). By contrast, La Niña patterns are characterised by a westward Pacific

warm pool and the overlying atmospheric convection lying above Indonesia, a steeper thermocline gradient that leads to enhanced upwelling and colder sea surface temperatures in the eastern Tropical North Pacific (ETNP) and off Peru.

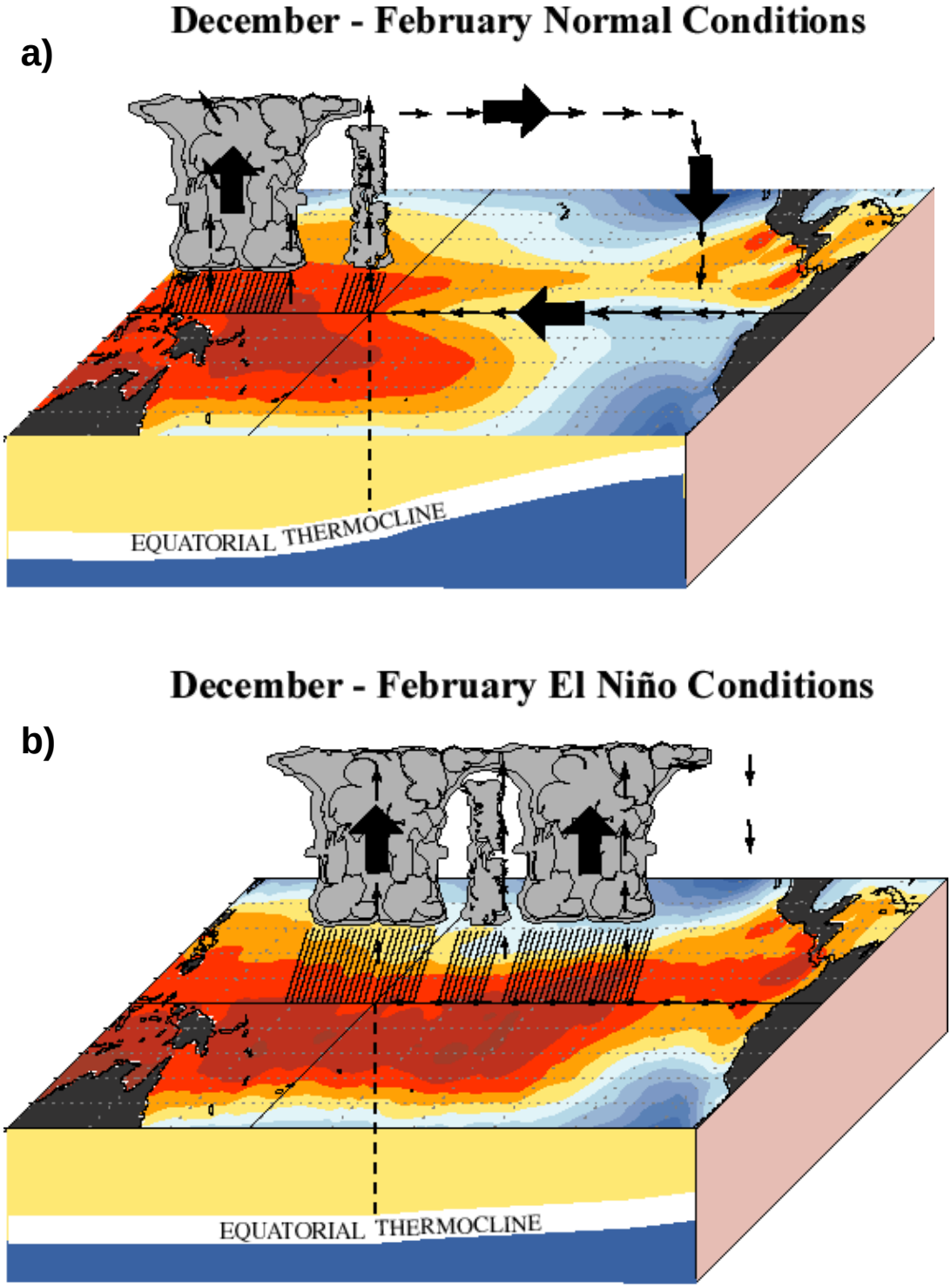

Figure 2.2. Schematic representation of: *a*) La Nina conditions across the tropical Pacific (Equatorial winds gather warm water pool toward west and cold water wells up along the ETNP) and *b*) El Nino conditions (the warm water pool approaches the Central American coast and reduced upwelling increases surface warming in the Eastern Pacific).

A number of records from the tropics have pointed to a dominant link between stadials and persistent El Niño conditions, referred to as a "Super-ENSO" state (Stott et al. 2002). Temperature variations in the Pacific warm pool during stadials point to shifts in the locus of convection towards the east or south, as happens during modern El Niño events. By contrast, La Niña conditions (higher salinities in the western Pacific, a western displacement of the Pacific warm pool, increased upwelling along central American margins) are found to be more common during interstadials, when warmer sea-surface temperatures shift from high-to-low latitudes following the reduction in land- and sea-ice cover (Tudhope et al., 2001). The warmer tropical SSTs (during interstadials) influence the hydrologic cycle across the Pacific (Xie, 1999; Xie and Saito, 2001), ultimately displacing the trade winds meridionally towards the hemisphere with a reduced ice extent and affecting the position of where the trade winds converge: the Intertropical Convergence Zone (ITCZ).

2.3 The ITCZ in the Eastern Pacific

The ITCZ is a circum-global atmospheric belt of intense convection and rainfall that results from the convergence of the trade winds (Koutavas and Lynch-Stieglitz, 2004). The modern-day ITCZ has a northern hemisphere bias, lying just north of the Equator over the Atlantic and eastern Pacific Oceans despite the annual-mean solar radiation at the top of the atmosphere being symmetric with respect to the equator (Waliser and Gautier, 1993). The global latitudinal asymmetry of the ITCZ is due to a variety of factors, including:

1) the distribution of land and sea between hemispheres;
2) the asymmetric sea-surface temperatures (SST) in areas of eastern boundary equatorial upwelling, as SSTs at the ITCZ are a few degrees higher than those at the same latitudes south of the equator due to the southeast-to-northwest tilted coastal geometry (Philander al., 1996);
3) the bulge of West Africa that provides a monsoonal influence over the equatorial Atlantic and favours the establishment of the ITCZ in the northern hemisphere (Xie and Saito, 2001).

The ITCZ is in constant seasonal migration, reaching its northernmost latitude in late

boreal summer and moving towards the equator in March-April. A southward displacement of the ITCZ in the eastern Pacific tends to occur during an El Niño event (Walisser and Gautier 1993), which initiates positive feedback processes that keep the ITCZ southwards by maintaining the reduced meridional SST gradient through a reduction in equatorial upwelling (Xie and Saito, 2001).

By analysing planktonic foraminiferal $\delta^{18}O$ records of the last 30,000 years in a suite of cores located between 5ºS and 3ºN at around 90ºW, Koutavas and Lynch-Stieglitz (2003 , 2004) observed a reduced cross-equatorial SST gradient during the LGM and interpreted this as a southward shift of the mean ITCZ latitude. The early Holocene was characterized by a stronger SST gradient in the equatorial Pacific and a wetter climate in the Cariaco Basin in Northern Venezuela, up to about 5,000–6,000 BP, and a shift to more arid conditions thereafter (Haug et al. 2001). These trends have been interpreted in terms of a more northerly ITCZ position in the early and middle Holocene followed by a gradual southward retreat. However, the available records from the eastern tropical Pacific are as yet unable to resolve millennial climate changes with enough dating precision to ascertain any variability of the ITCZ in the eastern Pacific at latitudes ranging from 5º - 20º N.

2.4 Upwelling in Mazatlan and the Mexican monsoon

The area surrounding the location of core MD02-2518 in Mazatlan is affected by the differential warming of the Tropical Pacific and the arid continental land to the east (Douglas et al., 2007). This leads to a monsoon regime of semi-annual reversing winds, with strong, cool and dry NW winds leading to upwelling in winter and spring, and southerly, wet and warm winds suppressing upwelling during the summer months. Upwelling offshore Baja California and Northwestern Mexico takes place when the North Pacific high-pressure fields move south to ~28ºN and low pressure builds up over south-western United States and northern Mexico. As a consequence, the pressure gradients channel strong northwesterlies down the axis of the Gulf of California. The resulting shore-parallel northwesterly winds move surface water masses away from the coastline and cause deeper, nutrient-rich water to rise into the euphotic layer and support high rates of primary productivity (Pride et al., 1999). The width of the upwelling zone is generally in the order of 100-150km with

an upwelling speed of 5-10 m/day (Thunnel and Kepple, 2004). In summer, the pressure field is dominated by a thermal low over the head of the Gulf of California and the ensuing southeasterlies bring an end to upwelling from late spring to early autumn. Upwelling along the margin of the ETNP is strongest during La Niña and decreases significantly during El Niño (see chapter 1.2), when the northwesterly winds typical of winter and early spring may diminish or even reverse direction (Pride et al., 1999).

2.5 Upwelling in the Gulf of Tehuantepec as a consequence of Central American Cold Surges

Surges of cold air along the eastern slopes of the Sierra Madre mountain range during the winter months produce northerly winds over the Gulf of Tehuantepec, which are commonly known as *tehuanos*. These northerly winds tend to occur on an average 11-16 times per cold season (November-April), commonly reaching 10-20m s^{-1} and tend to last for 2-6 days, though some of these occurrences have been documented to last for up to 13 days. As the *tehuanos* emerge into the Gulf of Tehuantepec, they entrain subsurface waters into the surface layer, thus enhancing upwelling, primary productivity and reducing sea surface temperatures by as much as 8°C (Chelton et al., 2000). The arrival of high-pressure systems associated with the *tehuanos* may also indirectly affect the tropical atmospheric dynamics by strengthening trade winds over the eastern North Pacific Ocean by up to 10 m s^{-1}, enhancing convection along the ITCZ and dramatically reducing lower tropospheric temperatures (Schultz et al., 1997).

The conditions for the development of the *tehuanos* are set by the interaction of Central American cold surges with the Sierra Madre. A Central American cold surge is defined as the leading edge of a cold anticyclone that originated at mid-latitudes and propagated equatorward to at least 20°N (Schultz et al., 1998). These anticyclones propagate southwards from Canada or the Northeastern Pacific into the southeast United States, thus bringing cooler air to low latitudes. As the cold fronts progress equatorward to the Gulf of Mexico, they find that the topography of Sierra Madre mountains acts as a natural barrier. These mountains do not allow cold fronts to travel freely over the Mexican mainland. However, this barrier to low-level air

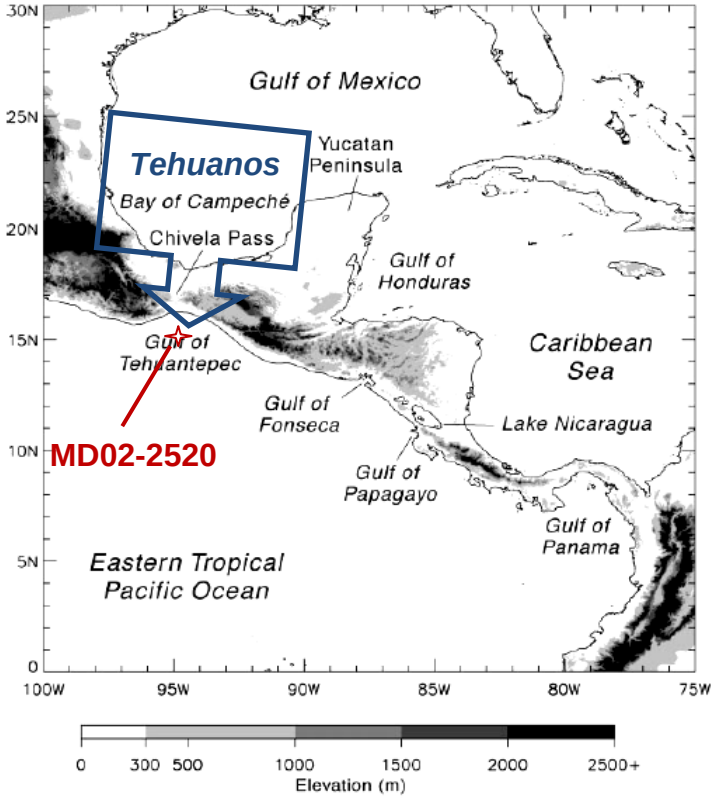

Figure 2.3: Map of the location of core MD02-2520 on the lee side of the Chivela Pass and elevation ranges of the Sierra Madre del Sur. The three most prominent gaps in the Central American mountain range are the Chivela Pass, the region surrounding Lake Nicaragua and the Panama Isthmus. The blue arrow shows the trajectory of the *Tehuanos* wind surges across the Sierra Madre.

masses is broken by a mountain gap, the Chivela Pass, which is 40km wide, has a maximum elevation of only 250m and runs north-south from the Gulf of Mexico's Bay of Campeche to the Pacific Ocean's Gulf of Tehuantepec (Fig. 2.3). The arrival of a cold surge in the Gulf of Mexico during winter and spring, when high pressure is resident east and north of the Sierra Madre, creates a cross-isthmus pressure gradient of 5 hPa or more (Chelton et al., 2000). This pressure gradient produces a strong offshore wind in the lee of the Chivela Pass, a phenomenon known as a "gap wind" or *tehuano* when referring to a gap wind extending into the Gulf of Tehuantepec. The equatorward extent of cold fronts varies from event to event, though it is likely that an anticyclone of North American origin may penetrate as far south as 7°N and eventually lead to a "surge of the trades" by up to 10m s^{-1} from Costa Rica to 140ºW (Schultz et al., 1998).

Empirical observations have demonstrated that the Tehuantepec wind jet has noticeably different characteristics compared to the winds over Papagayo and

Panama. The winds in the Gulf of Tehuantepec tend to have an irregular temporal distribution, attain higher speeds and are offshore (northerly) in more than 90% of documented cases from October through May (Chelton et al., 2000). By contrast, the winds in the Gulf of Papagayo and Gulf of Panama are not attributed to Central American cold surges, are generally less energetic (over 50% of wind speeds are in the range 5-8m s^{-1}), have lower variability and tend to alternate seasonally between onshore and offshore flow.

2.6 Geology of the Western Mexican plains and the Southern Highlands

Over half of the Mexican territory is higher than 900 m above sea-level (Davis et al., 1997). The Central Plateau or Altiplano extends southward from the U.S border to the latitude of Mexico City as a continuation of the Basin and Range region of the U.S. The Sierra Madre Occidental and Sierra Madre Oriental form borders respectively on the western and eastern edges of this plateau. The Sierra Madre Occidental rises to well over 3000 m and is the main source area for sediments reaching the site area of core MD02-2518 in Mazatlan Basin. The source rocks of these sediments are most likely to be Tertiary volcanics from the Trans-Mexican Volcanic Belt, metamorphic quartz-rich gneiss and Early Cretaceous gabbroic and dioritic intrusives from the Sierra Madre, where the western slope forms rugged canyons and narrow ridges descending to the Quaternary Pacific Coastal Plain.

The Trans-Mexican Volcanic Belt constitutes a major geological break with the Central Plateau and comprises hundreds of volcanic peaks, cinder cones, lava flows and ash deposits as evidence of past and present volcanic activity. Mexico's highest and best known volcanic peaks are included in this belt: Pico de Orizaba or Citlaltépetl (c. 5700m), Popocatépetl (5452m), Ixtaccíhuatl (5286m) and Nevado de Toluca or Zinantécatl (4392m), some of which may have been the source of ash layers in the cores presented in this study.

The Highlands of Southern Mexico are a geologically complex region separated into two sections by the Isthmus of Tehuantepec (see Fig. 2.3 for elevation ranges of the Sierra Madre del Sur), namely the Sierra Madre del Sur in the Oaxaca region to the northwest and the Chiapas Highlands in the southeast. Tectonic activity in the Gulf of Tehuantepec is due to active subduction of the Cocos plate beneath the

Caribbean plate. This tectonic activity has created numerous faults cutting the Sierra Madre del Sur mountain system with narrow valleys perpendicular to the coastline, which extend below sea level as narrow canyons channeling both weak turbidity and strong wind-induced upwelling currents (Boumaggard et al., 1998). The southeastern highlands are dominated by the Chiapas Highlands, a plateau rising to 2500m, which is composed predominantly of intrusive formations, and are the most likely source of detrital sediments within core MD02-2520.

2.7 Climate and Vegetation

Mexico's climatic diversity is primarily due to the wide range of elevations ranging from sea-level to 5000m and the oceanic influences from the Gulf of Mexico and the Pacific over the narrow continental mass. The Tropic of Cancer approximately marks the transition from arid and semi-arid climates due to anticyclonic high pressures systems to the north, and humid to semi-humid climates under the influence of trade winds and the ITCZ to the south (Magana et al., 1999).

The precipitation also presents notable contrasts, from annual average values less than 50 mm with no wet season (e.g. in parts of Baja California), to more than 5500mm with no dry season (e.g. in parts of Tabasco and Chiapas) on the Gulf of Mexico. Average annual precipitation below 500 mm is found north of 20°N, where the Sierra Madre Occidental separates the two principal dry zones of Mexico: the Chihuahuan Desert to the east and the Sonora Desert to the west. In the Sonora Desert, comprising the Sonora Coastal Plain and the major part of Baja California, the precipitation is less than 400m.

The distribution of rainfall during the year constitutes a factor of the greatest importance for the distribution of vegetation. Thorn scrub and tropical deciduous forests are the main vegetations types in the on the Pacific coast of Sinaloa (adjacent to the Mazatlan Basin core MD02-2518), where the months of November to April usually are predominantly dry. The areas with the most abundant precipitation, with annual values exceeding 4000mm, are on the windward (eastern) slopes of the Sierra Madre Oriental and on the hills north of Oaxaca and the Central Massif of Chiapas. However, the Pacific slope surrounding the Gulf of Tehuantepec and core MD02-2520 is characterized by drier climate and an annual dry period of five to nine

months. Vegetation consists mostly of tropical deciduous forests with rainfall and ranging from 750-1500mm yr-1 (Magana et al., 1999). The majority of this rainfall occurs with bimodal maxima during June and September-October, and a minimum throughout July and August (Magana et al., 1999; Therrell et al, 2002).

References

Boumaggard, El H., Gayet, J., Bobier, C., Machain-Castillo, M.L., Aguayo_Camargo, E. (1998) Distribution des sediments sur la marge du golfe de Tehuantepec (Pacifique Oriental). Exemple d'interaction tectonique-eustatisme. *Oceanologica Acta*, vol. **21**, pp. 21-31

Chelton, D.B., Freilich, M.H. and Esbensen, S.K. (2000) *Satellite Observations of the Wind Jets off the Pacific Coast of Central America. Part I: Case Studies and Statistical Characteristics.* Monthly Weather Review, **128**, pp.1993-2018

Davis, S.D., Heywood, V.H., Herrera-MacBryde, O., Villa-Lobos, J. and Hamilton, A. (eds.). 1997. *Centres of Plant Diversity: A Guide and Strategy for Their Conservation. Volume 3: The Americas*. IUCN Publications Unit, Cambridge, England

Douglas, R., Gonzalez-Yajimovich, O., Ledesma-Vasquez, J., Staines-Urias, F. (2007) Climate forcing, primary production and the distribution of Holocene biogenic sediments in the Gulf of California. *Quat. Sci. Reviews*, vol. **26**, pp. 115-129

Haug, G.H., Hughen, K.A., Sigman, D.M., Peterson, L.C. and Rohl, U. (2001) Southward migration of the intertropical convergence zone through the Holocene. *Science*, vol. **293**, pp. 1304–1308

Kessler, W.S. (2006) The circulation of the eastern tropical Pacific: A review. *Progress in Oceanography*, vol. **69**, pp. 181-217

Koutavas, A. and Lynch-Stieglitz, J. (2003) Glacial-interglacial dynamics of the eastern equatorial–Pacific cold tongue–Intertropical Convergence Zone system reconstructed from oxygen isotope records. *Paleoceanography*, vol. **18**, doi: 10.1029/2003PA000894.

Koutavas, A. and Lynch-Stieglitz, J. (2004) Variability of the marine ITCZ over the eastern Pacific over the past 30,000 years. In Chapter 12 "*The Hadley circulation: Present, Past and Future*", Diaz, H.F. and Bradley, R.S. (Eds), Springer-Kluwer Academic Press.

Magana, V., Amador, J.A., Medina, S. (1999) The Midsummer Drought over Mexico and Central America. *Journal of Climate*, vol. **12**, pp 1577-1588

McPhaden, M.J. (1999) Genesis and Evolution of the 1997-98 El Niño. Science, vol. **283**, pp. 950-954

Nameroff, T.J., Calvert S.E. and Murray, J.W. (2004) Glacial-interglacial variability in the eastern Tropical North Pacific oxygen minimum zone recorded by redox-sensitive trace metals. *Paleoceanography*, vol. **19**, pp. 1-19

Philander, S.G.H., et al., (1996) The role of low-level stratus clouds in keeping the ITCZ mostly north of the equator. *Journal of Climate*, vol. **9**, pp. 2958-2972

Pride, C., Thunell, R., Sigman, D., Keigwin, L., and Altabet, M.A., (1999) Nitrogen isotopic variations in the Gulf of California since the last deglaciation: response to global climatic change. *Paleoceanography*, vol. **14** (3). doi:10.1029/1999PA900004

Schultz, D.M., Bracken, W.E. and Bosart, L.F, Hakim, G.J., Bedrick, M.A., Dickinson M.J. and Tyle, K.R. (1997) The 1993 Superstorm Cold Surge: Frontal Structure, Gap Flow, and Tropical Impact. *Monthly Weather Review*, vol. **125**, pp.5-39

Schultz, D.M., Bracken, W.E. and Bosart, L.F. (1998) Planetary- and Synoptic-Scale Signatures Associated with Central American Cold Surges. *Monthly Weather Review*, **126**, pp.5-27

Stott, L., Poulsen, C., Lund, S., Thunell, R. (2002) Super ENSO and Global Climate Oscillations at Millennial Time Scales. *Science*, vol. **297**, pp. 222-226

Therrell, M.D., Stahle, D. W., Cleaveland, M.K. and Villanueva-Diaz, J. (2002) Warm season tree growth and precipitation over Mexico. *J. Geophys. Res.,* vol. **107,** doi:10.1029/2001JD000851.

Thunell, R.C., and Kepple A.B. (2004), Glacial-Holocene $\delta^{15}N$ record from the Gulf of Tehuantepec, Mexico: Implications for denitrification in the eastern equatorial Pacific and changes in atmospheric N2O. *Global Biogeochem. Cycles*, vol. **18,** GB1001, doi:10.1029/2002GB002028

Tsuchiya, M. (1981) The Origin of the Pacific 13°C Water. *Journal of Physical Oceanography*, pp 794-812.

Tsuchiya, M., and Talley, L.D., (1998) A Pacific hydrographic section at 88°W: water-property distribution. *J. Geophys. Res.,* vol. **103**, pp. 12899–12918

Tudhope, A.W., Chilcott, C.P., McCulloch, M.T., Cook, E.R., Chappell, J., Ellam, R.M., Lea, D.W., Lough, J.M., Shimmield, G.B. (2001) Variability in the El Nin˜o-Southern Oscillation through a glacial-interglacial cycle. *Science*, vol. **291**, pp. 1511–1517

Waliser, D. E., and Gautier, C. (1993) A satellite-derived climatology of the ITCZ. *J. Climate,* vol. **6,** pp. 2162–2174

Wyrtki, K. (1964) Upwelling in the Costa Rica Dome. *Fishery Bulletin*, vol. **63**, pp. 355–372.

Xie, S.P. (1999) A dynamic ocean-atmosphere model of the tropical Atalantic decadal variability. *Journal of Climate*, vol. **12**, pp. 64–70

Xie, SP, and Saito, K. (2001) Formation and variability of a northerly ITCZ in a hybrid coupled AGCM: Continental forcing and oceanic-atmospheric feedback. *Journal of Climate*, vol. **14**, pp. 1262–1276

CHAPTER 3

Methodology

3.1 Core description

The piston cores presented in this study were collected during the 2002 MONA (Margins Ouest North America) Cruise on board the French research vessel "Marion Dufresne" and the location and length of the cores is summarised in Table 3.1.

Core **MD02-2518** was raised from the heart of the modern oxygen minimum at 450m water depth on the upper slope off Mazatlan margin. The core recovered a total of 40.76m of sediments, consisting predominantly of silty clay, with minor amounts of diatoms and/or nanofossils. The colors range from olive grey and dark olive grey to very dark grey, with the lighter colours distinguishing massive and sometimes bioturbated intervals from the darker, laminated intervals.

A few shell fragments occur in the massive and bioturbated section; fish scales and wood fragments can be found in the laminated sections. A large angular cobble of grey apatite occurs at 35.80m, whereas beige and white tephra layers occur at 12.20m, 27.80m and 33.40m.

Core **MD02-2520** was collected at a water depth of 719m in the Gulf of Tehuantepec. The dominant sediment consists of olive grey and olive green to dark olive grey silty clay, which grades to very dark grey and black silty clay from 12.00m to 30.00m, and to dark olive and dark olive grey in the lower part of the core. The sediment is mostly very finely laminated throughout the core, which are occasionally interrupted by rare slightly bioturbated intervals and a few fine, light sandy layers are present from 3.00m to 12.00m. Grey to brown thin (1 - 6mm-thick) layers of coarse tephra are present throughout the core.

Core number	Location	Depth (m)	Latitude ºN	Longitude ºW	Core Length (m)
MD02-2518	Mazatlan Basin	454	022º40.39	106º29.19	40.76
MD02-2520	Gulf of Tehuantepec	719	015º40.14	095º18.00	37

Table 3.1: location and length of cores presented in this study.

3.2 Sampling

Samples for carbon & nitrogen analysis for core MD02-2518 (Mazatlan) were taken at 2cm intervals from the surface to 1772cm depth. X-ray Fluorescence analysis was conducted on samples at 2-cm intervals down to 1226cm depth. An additional nine samples among laminated sediments deposited between 1810-1920cm depth were analysed by X-Ray Fluorescence to verify the existence of phosphorites within lower sections of the core (see Appendix C for a list of these intervals).

The entire core MD02-2520 (Tehuantepec) was sampled at 5cm resolution for both C & N and X-ray Fluorescence analysis.

3.3 Carbon and Nitrogen

In order to determine organic carbon and nitrogen, aliquots of approximately 6mg (laminated intervals) - 12mg (bioturbated intervals) of sample were placed in silver capsules and digested overnight in 6N HCl solution. The samples were then combusted in a Carlo Erba NH2500 elemental analyser at 1000° C. The instrumental settings are described in Verardo et al. (1990) and Acetanelide and certified sediments (PACS) were used as standards and run together with blanks every 10 samples. Nitrogen ($\delta^{15}N$) and carbon ($\delta^{13}C$) isotope analyses of acidified sediments were determined on a VG PRISM stable isotope ratio mass spectrometer linked to the Carlo Erba NH2500 elemental analyser. Isotopic ratios are reported in ‰ relative to atmospheric N_2 and Pee Dee Belemnite (PDB) standards and the precision of this instrument is better than ± 0.2‰. All the nitrogen isotopic data in this study are presented as follows:

$$\delta^{15}N = [(^{15}N/^{14}N)_{sample}/[(^{15}N/^{14}N)_{standard}]-1$$

3.4 X-ray Fluorescence

Major element (Si, Al, Fe, Mg, Ca, Na, K, Mn, Ti and P) concentrations were determined using a Philips PW-2404 wavelength-dispersive X-ray fluorescence spectrometer fitted with a Rh-anode tube. Instrumental settings were similar to those described in Calvert et al. (1985). Sediment samples were dried for 2 hours at 110°C

to remove excess moisture. A small fraction of each sample (~1g) was ignited overnight in ceramic crucibles at 500°C in order to remove organic carbon and preserve the carbonate phases within the sample. About 0.9g of ignited sediments were then mixed with a borate flux (47% lithium tetraborate, 37% lithium oxide and 16% lanthanum oxide) in the proportions 1:5 (sample:flux), fused in a furnace at 1100°C and cast into glass disks. Standardisation was achieved using USGS and CRPG rock standards; analytical precision and accuracy were better than ±2% for all major elements reported here.

3.5 Colour Reflectivity

The colour of sediments in the cores presented this study has been described in section 3.1 by shipboard visual observation according to the Munsell rock colour chart, which is based on hue, value and chroma evaluations through a naked eye. For this reason, colour interpretation tends to be highly subjective, as varying conditions of illumination aboard a ship may lead to different interpretations of the colour of sediments, and needs to be complemented by quantitative data on the reflectance spectra of sediments. This requirement has lead to the shipboard implementation of a colorimeter. The spectral reflectance data for the cores reported in this thesis was collected aboard the *RV Marion Dufresne* by means of a handheld Minolta spectrophotometer 2022 at 2-cm intervals on split core surfaces. Colour reflectance in marine sediments can provide initial detailed information on time series changes in the mineralogical composition of a core and help correlate sections from cores collected from separate locations (Blum, 1997). Spectral analysis of sediment reflectance has helped to detect the presence of carbonate, opal, hematite and goethite and organic matter in marine cores (i.e. Ortiz et al., 2004).

Colour reflectance in core MD02-2520 has been defined based on the L*a*b* system, commonly referred to as the CIELAB system (Blum, 1997). This system can be interpreted as an imaginary cylinder in which the axis represents lightness (L*) ranging from 0% to 100%, whereas the two perpendicular radii of the cylinder represent chromaticity. These radii are variable (a*) ranging from green (negative) to red (positive), and variable b* with values ranging from blue (negative) to yellow

(positive). The colour reflectance measured on the surface of a split core may diverge from original values when affected by a series of factors such as:

- Moisture content of the sediments: as soon as the core is exposed to air, the sediments will start to dry and thus give the sediments a lighter colour. Nagao and Nakashima (1992) found that in wet marine sediments the L* factor is up to 20% higher than in dried sediments.
- Irregularity of the surface between softer sediments near the core-top and harder, more compacted sediments at depth.
- Grain Size, where coarser grain sizes tend to lead to increase (L*) and give more positive (a*) measurements.
- Oxidation: the oxidation of Fe-based greenish compounds will tend to increase reflectance at the red end of the spectrum, thus affecting a* values.

Measured reflectance in L*a*b* colour space from core MD02-2518 and core MD02-2520 can be respectively be seen in Appendices E and F. By observing the plots in both cores it is possible to infer that lightness (L*) shows increased values in bioturbated intervals, which in the north-western Mexican margin tend to contain lower amounts of organic carbon and have a larger grain size. By contrast, the organic-rich and finer-grained clays found in laminated intervals display lower (L*) values. This parameter shows a greater degree of variability in core MD02-2518 than MD02-2520, as the former core contains intermittent darker, laminated and lighter, bioturbated horizons, whereas core MD02-2520 is predominantly finely laminated throughout its entire length. The two (L*) peaks at ~27m and 33m in core MD02-2518 correspond to the two white tephra layers described in section 3.1.

Chromaticity value (a*) has been referred to in previous literature as Diffuse Spectral Reflectance (DSR) Factor 3 (Ortiz et al., 1999 and 2004). This chromaticity value ranges from green to red and has been shown to bear resemblance to the C_{org} content of the cores (see Chapter 5.1). The contrast between positive and negative (a*) values can be seen to gradually dampen below 20m depth in core MD02-2518. This is probably due to sediments becoming more compressed with depth, leading to lower water contents and reduced oxidation of the laminated sediments when exposed to air. Plots of yellow-blue chromaticity variable (b*) in both cores are more

complex and do not show a direct relationship between C_{org} content of the cores or laminated / bioturbated intervals.

3.6 ^{14}C dating of samples

The age of samples in the uppermost 4.3m (corresponding to 0-40kyrs - the ^{14}C dating window) of core MD02-2520 was constrained by means of 8 accelerator mass spectrometry (AMS) ^{14}C dates obtained from acidified organic matter. The poor preservation of calcium carbonate in organic-rich sections of the cores prevented the use of foraminifera as a dating tool. Due to similar constraints, the entire age model of core MD02-2520 was reconstructed by means of 23 AMS ^{14}C dates of acidified, C_{org}-rich sediments. A description of how all AMS ^{14}C dates were determined and what reservoir ages have been applied can be found at the end of chapter 4.1 (Age model - *Core MD02-2520 – Gulf of Tehuantepec*)

3.7 K-Ar dating of samples

A provisional assessment of the age of the entire core was made by comparing the reflectance data for core MD02-2518 by meticulously matching prominent peaks and troughs of the red-green chromaticity (a*) record to high-resolution foraminiferal δ^{18}O records from with records of δ^{18}O from the North Atlantic that spans the last 13 Marine Isotope Stages (MIS) – approximately 500kyrs (Fig. 4.1). Any ^{14}C dating of organic matter in sediments will be restricted to the top two metres of the core, as the sediments deposited below this depth will fall outside the 40kyr-dating window for ^{14}C. Visual analysis of the sediments indicated that the piston core contains two 2.5cm-thick tephra layers at approximately 27 and 33 metres depth, which derived from volcanic eruptions in the Sierra Madre. The good preservation and sufficient K content of the tephra shards observed by microscopic and X-Ray Fluorescence analysis indicated that the two tephra layers could provide independent dates for core MD02-2518 by means of K/Ar dating.

K/Ar dates were provided by the SUERC Argon Isotope Facility in East Kilbride, Scotland, where Ar^{40} was extracted by furnace step-heating of the tephra

samples, purified on an extraction line and then measured with a mass spectrometer equipped with 5 high-sensitivity Faraday collectors for simultaneous measurement of all five argon peaks (36 through 40). The results of the K/Ar dating of the two tephra layers in core MD02-2518 can be seen in Table 3.2.

Sample depth	Sample weight	K, wt%	K/Ar age (years BP)	K/Ar Average age (years BP)
2791-2793	281 mg	3.9591	433000	**385000**
2791-2793	685 mg	3.9591	336000	±69000
3319-3321	771 mg	3.7184	888000	**900000**
3319-3321	648 mg	3.7184	912000	±17000

Table 3.2: Sample weight, potassium content and calculated K/Ar age of samples from MD02-2518.

The sample at 27.92m depth provided an average age of 385kyrs and a standard deviation of ±69kyrs. The sample at 33.20m depth provided and average age of 900kyrs and a standard deviation of ±17kyrs. While the first tephra sample provides an age that, within the standard deviation, is consistent with our proposed age model (see section 4 - stratigraphy), the error range is too large to help resolve the marine isotope stage (MIS) in which the tephra horizon was deposited. By contrast, the second tephra layer has a relatively narrow error range, but the K/Ar apparent age is too old to be consistent with the proposed age model based sedimentation rates of around 8-20cm kyr^{-1}. Possible explanations for the inconsistent age of the latter sample include:

a) extraneous ^{40}Ar being inherited from incompletely degassed xenocrysts entrained from the magma conduit during eruption or;
b) excess ^{40}Ar entrapped in submicroscopic inclusions or defects within the tephra during residence in the magma chamber.

References

Blum, P (1997) Chapter 7 in: Physical Properties Handbook: A guide to the shipboard measurement of physical properties of deep-sea cores. Ocean Drilling Program Technical Note **26.**
An online version can be found at: http://www-odp.tamu.edu/publications/tnotes/tn26/TOC.HTM

Nagao, S., and Nakashima, S. (1992) The factors controlling vertical color variations of North Atlantic Madeira Abyssal Plain sediments. *Marine Geology*, vol. **109**, pp. 83–94

Ortiz, J.D., Mix, A., Harris, S. and O'Connell, S. (1999) Diffuse spectral reflectance as a proxy for percent carbonate content in North Atlantic sediments. *Paleoceanography*, vol. **14**, pp. 171-186

Ortiz, J.D., O'Connell, S., DelViscio, J., Dean, W., Carriquiry, J., Marchitto, T., Zheng, Y., and van Geen, A. (2004) Enhanced marine productivity off western North America during warm climate intervals of the past 52 kyr. *Geology*, vol. **32**, n.6, pp. 521-524

Verardo, D.J., Froelich, P.N., McIntyre, A., 1990. Determination of organic carbon and nitrogen in marine sediments using the Carlo Erba NA-1500 Analyzer. Deep Sea Res. 37, 157-165.

CHAPTER 4

Stratigraphy

4.1 Age model

Core MD02-2518 – Mazatlan Margin

The age determination for the entire 40.76 metre-long core at site MD02-2518 (Mazatlan Margin) is based on accelerator mass spectrometry (AMS) ^{14}C dates between 0 - 4.3 m depth of acidified, C_{org}-rich sediments.

From 4.3m up to 18m depth these AMS ^{14}C dates are corroborated by the correlation between $\delta^{15}N$ variations and the chromaticity (a*) record at sub-millennial resolution of core MD02-2518 with oxygen isotope records from Greenland NGRIP ice core and benthic and planktonic foraminifera of a reference core from the North Atlantic - core ODP 980. The remaining portion of the core (18m - 40.7m) was dated by correlation between the chromaticity (a*) record of MD02-2518 with $\delta^{18}O$ records from core ODP 980.

The age of samples in the uppermost 4.3m (corresponding to 0-40kyrs - the ^{14}C dating window) was constrained by means of 8 accelerator mass spectrometry (AMS) ^{14}C dates (table 4.1) obtained from acidified organic matter. The age model constructed for sediments deposited between 0-40kyrs highlights a correlation (within dating errors) between events documented in climate proxy records from three separate locations (Fig. 4.1), namely:

- temperature transitions in the NGRIP Greenland ice core;
- foraminiferal $\delta^{18}O$ records of millennial scale variability from core ODP 980 from the North Atlantic (McManus et al., 1999; Siddall et al., 2006); and
- chromaticity (a*) and $\delta^{15}N$ variations in core MD02-2518.

Colour reflectance data was measured on the archive halves of all split cores at 2-cm intervals onboard the RV Marion Dufresne and provides a rapid method of constructing an age model of the lower sections of the core by revealing patterns of millennial-scale climate variability recorded in rapid excursion in chromaticity values, which are comparable to variability observed in climate records from the North Atlantic (Helmke et al., 2002). The chromaticity excursions indicate compositional changes in the sediments, most likely due to climate cycles in the northern hemisphere ultimately affecting the composition of sediments along the

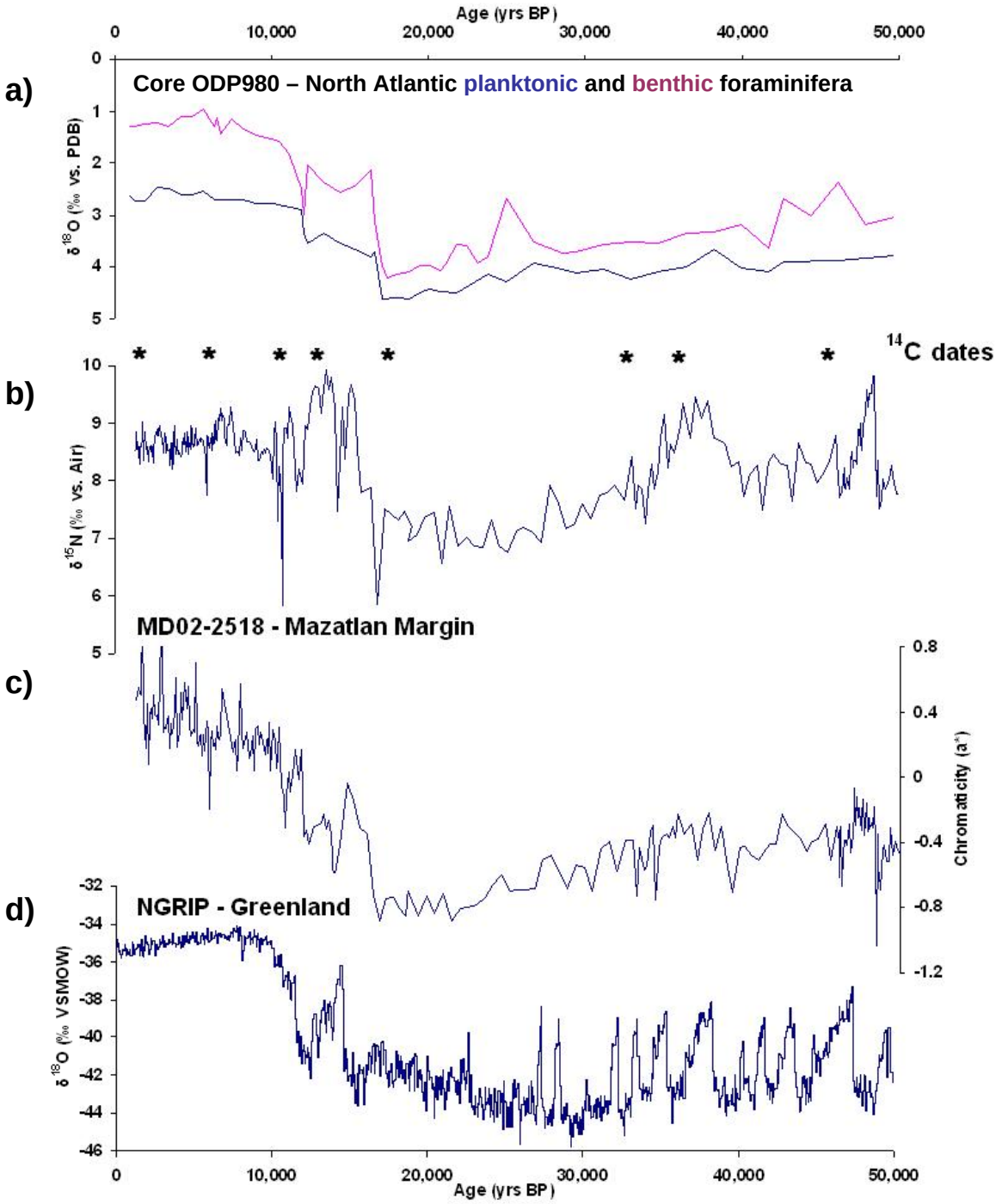

Figure 4.1: comparison between *a)* planktonic and benthic foraminiferal $\delta^{18}O$ records from core ODP 980 from the North Atlantic (McManus et al., 1999); *b)* chromaticity (a*) and *c)* $\delta^{15}N$ variations in core MD02-2518; and *d*) temperature transitions in the NGRIP Greenland ice core. Black star between records *a)* and *b)* indicate the position of AMS ^{14}C dates obtained for core MD02-2518. The correlation between records from the Mazatlan Margin indicates that the rapid millennial- to centennial-scale events seen in Greenland and the northern North Atlantic are also an important element of low-latitude climate variability during the past 50,000 years. For this reason, the correlation between these records may be extended to the remaining portion of core MD02-2518 and provide an age model for sediments deposited prior to 50,000 yrs BP.

Mexican margin. As chromaticity parameter (a*) is thought to be related, among other factors, to the grain size of sediments (Nagao and Nakashima, 1992), a preliminary assessment of the age of the entire core was done by correlating negative (a*) excursions (thought to represent sandy, carbonate-rich sediments typically observed in the stadial portions of sediment records from the ETNP - Ganeshram et al., 1995) with glacial Terminations (I, II, III...) recorded in a marine oxygen isotope record from the North Atlantic (Fig. 4.2). This initial correlation provides us with an approximate age of 450,000 years (i.e. five glacial periods and terminations) for the entire core, which corresponds to average sedimentation rates of ~9cm kyr^{-1}. These values are in close agreement with published sedimentation rates for core NH15P (Ganeshram et al., 1995) recovered from 420m depth in the Mexican margin.

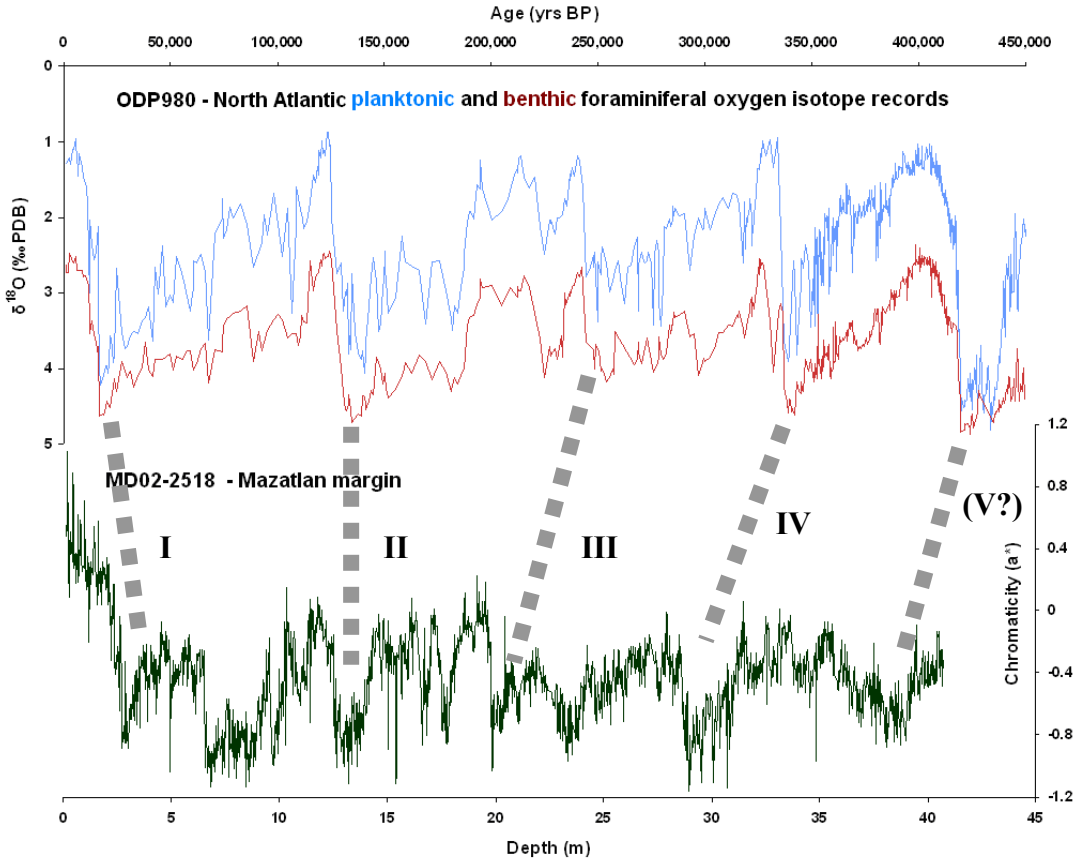

Figure 4.2: Construction of a time series for the entire 40.76m of core MD02-2518. The time series was achieved through visual correlation of glacial terminations between $\delta^{18}O$ of benthic and planktonic foraminifera from core ODP980, representing a 0.5 million year record of millennial-scale variability in the North Atlantic (McManus et al., 1999), with the chromaticity (a*) record from core MD02-2518. The age of glacial terminations is as follows: Termination I (16-18 kyr BP); II (128-135 kyr BP); III (240-245 kyr BP); IV (325-330 kyr BP); V (425-430 kyr BP) – Mc Manus et al., 1999.

The stretching of the sedimentary record within the top sections and compression of sediments at the bottom of the core end are features that have been previously observed in cores recovered by means of giant Calypso piston corers (i.e. Hiscott et al., 2008), and it is fair to say that neither core MD02-2518 is immune from these moderate coring disturbances. The higher compression rate of the lower sections of MD02-2518 (highlighted by reduced variations in chromaticity and the visual observations of inverted-U-shaped laminations in sediments deposited lower than 37m depth) are a coring artefact and result in lower apparent sedimentation rates at the bottom of the core.

In order to constrain the chronology of sediments deposited beyond ^{14}C dating window, the $\delta^{15}N$ record was compared to the NGRIP $\delta^{18}O$ record of temperature changes in Greenland. As the calculated Calendar Ages for sediments deposited within the top 4.3m of core MD02-2518 indicate a strong correlation between peaks in the $\delta^{15}N$ record and D-O cycles evident in the NGRIP temperature record (Figs. 4.1 *a* and *b*), the chronology of the remaining portion of the $\delta^{15}N$ record was developed by tying five major peaks within the $\delta^{15}N$ record with prominent interstadials and in the NGRIP temperature records (Fig. 4.3a). The age of sediments is then allowed to "float" between these five tie-points, thus giving an age of 190,000 for the 17.72m $\delta^{15}N$ and Corg record of core MD02-2518 and a near-linear sedimentation rate of approximately 9.3cm kyr^{-1} (Fig 4.3b).

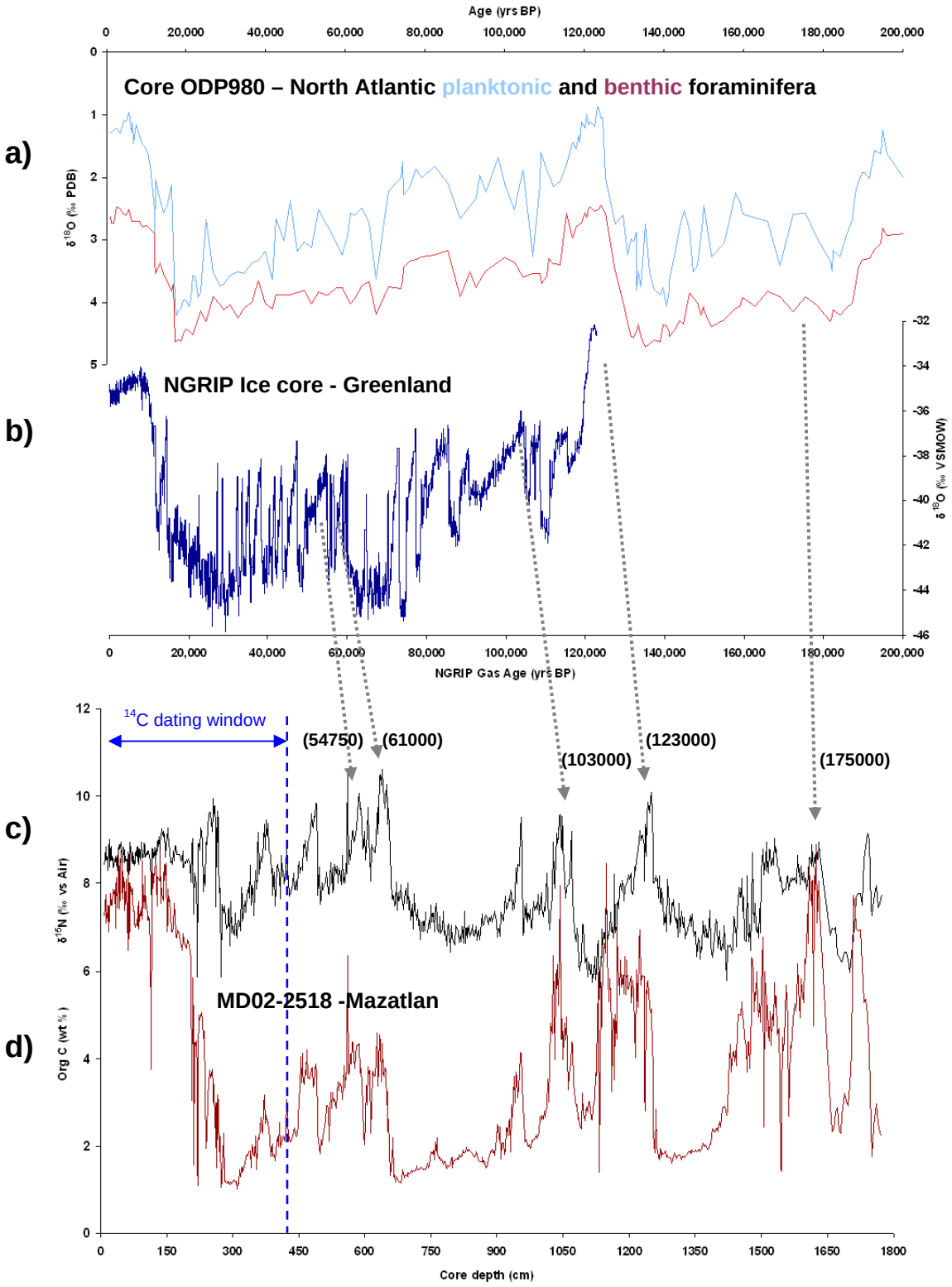

Figure 4.3a: The development of a chronology for core MD02-2518. The dates up to 430cm depth were obtained by means of eight AMS ^{14}C dates, the positions of which can be seen in Fig. 4.1. The five arrows and dates visible from 430 to 1772cm correspond to tie points between major peaks in the $\delta^{15}N$ record with prominent interstadials in the NGRIP temperature record and $\delta^{18}O$ minima in core ODP 980 from the North Atlantic. A description of *a); b); c);* and *d)* is outlined in Fig. 4.3b.

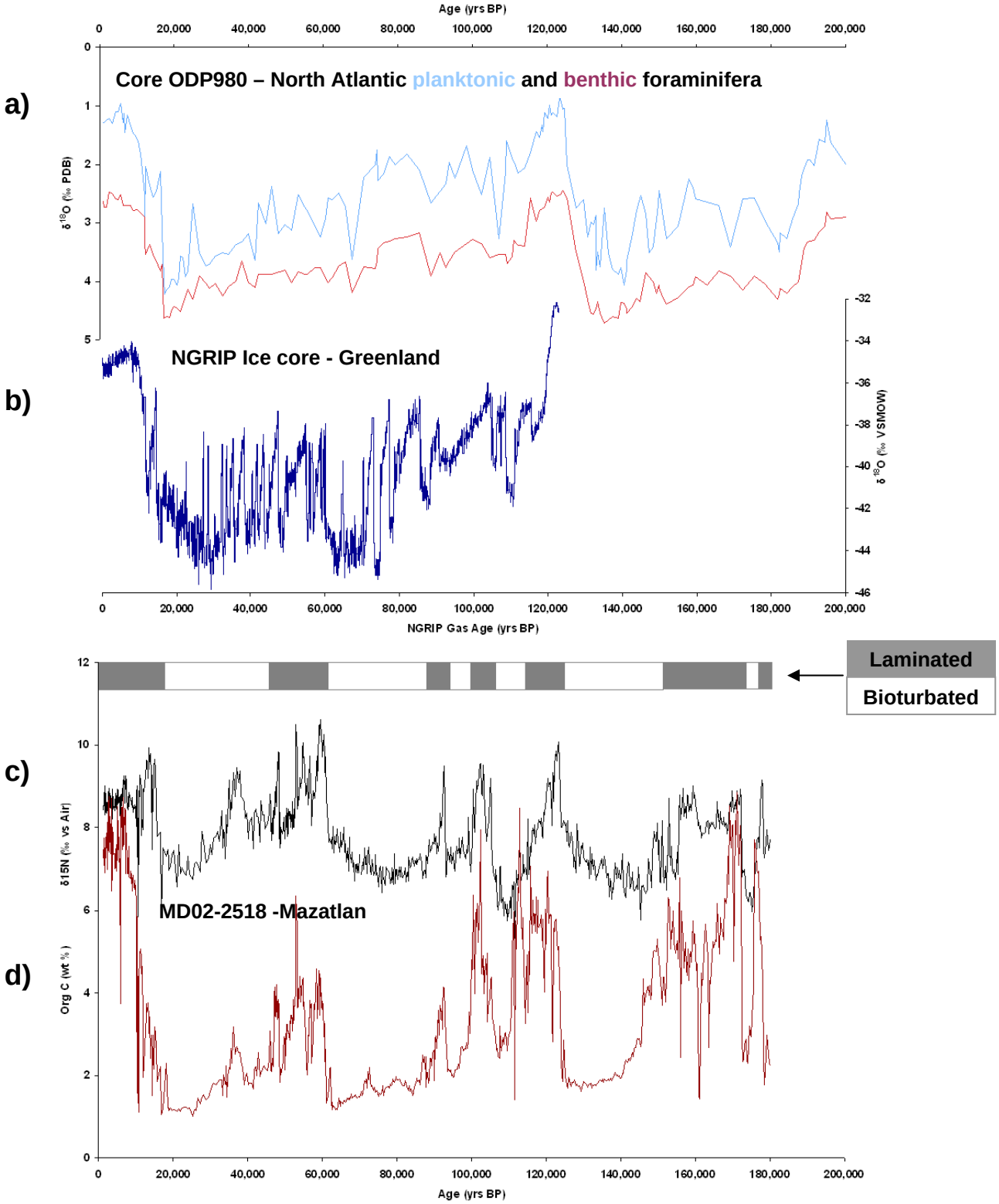

Fig 4.3b: Time series for the top 1772cm of core MD02-2518 following the initial correlation outlined in Fig 4.3a. *a)* planktonic and benthic foraminiferal $\delta^{18}O$ records from core ODP 980 from the North Atlantic (McManus et al., 1999); *b)* $\delta^{18}O$ transitions in the NGRIP Greenland ice core; *c)* $\delta^{15}N$ variations and *d)* Corg weight % in core MD02-2518. The grey and white bars represent laminated/bioturbated intervals in core MD02-2518. The low $\delta^{15}N$ and Corg values in bioturbated sediments do not allow any correlation of these sections with D-O events observed in Greenland.

Core MD02-2520 – Gulf of Tehuantepec

The age model of the 37.06 m core MD02-2520 was reconstructed by means of 23 AMS ^{14}C dates (table 4.2) obtained from acidified organic matter. The samples were chosen to specifically match events previously identified in the nitrogen isotope record. Hence, D-O interstadials, Antarctic warming events and Heinrich Events were dated, as well as transitions through the Bølling-Ållerød (ACR) and the Younger Dryas. Ten samples were dated throughout the Holocene to provide general coverage. These radiocarbon dates are supported by oxygen isotope records for planktonic (*G. rubber*), thermocline dwelling (*N. dutertrei*) and benthic (*U. peregrina*) foraminifera provided by Cecile Blanchet at the CEREGE laboratories in Aix-en-Provence, France.

All AMS ^{14}C dates reported in this study were determined at the NERC radiocarbon laboratory in East Kilbride, Scotland. The raw samples were digested in 2M HCl (80°C, 8 hours), washed free from mineral acid with deionised water then dried and homogenised. The total carbon in a known weight of the pre-treated sample was recovered as CO_2 by heating with CuO in a sealed quartz tube. The gas was converted to graphite by Fe/Zn reduction. All AMS ^{14}C dates from both cores younger than 21,381 years were calibrated with CALIB Radiocarbon Calibration software version 5.0.2 (http://calib.qub.ac.uk/calib/), which is based on a calibration curve developed by Hughen et al. (2004) for the conversion of radiocarbon ages to calibrated ages. As the upwelling of nutrient-rich waters from intermediate depths within the ETNP supplies the surface waters with "older" water which has been isolated from the atmosphere for a number of years, the calibration incorporates a standard global ocean reservoir correction of about 400 years (Butzin et al., 2005). This is because marine organic matter preserved in sedimentary cores would have been exposed to different levels of ^{14}C compared to organic matter in contact with the atmosphere, and radiocarbon ages of samples formed in the ocean have been found to be several hundred years older than terrestrial samples.

It has been noted (Ivanochko, 2005) that the reservoir age of samples collected within upwelling regions (such as the western Arabian Sea) are larger than the global average of 400 years and that the local reservoir age may change over time. The average reservoir age for the Arabian Sea has been calculated to average

around 600, though reservoir ages of over 1000 years have been documented in the Northern Arabian Sea (Staubwasser et al., 2002).

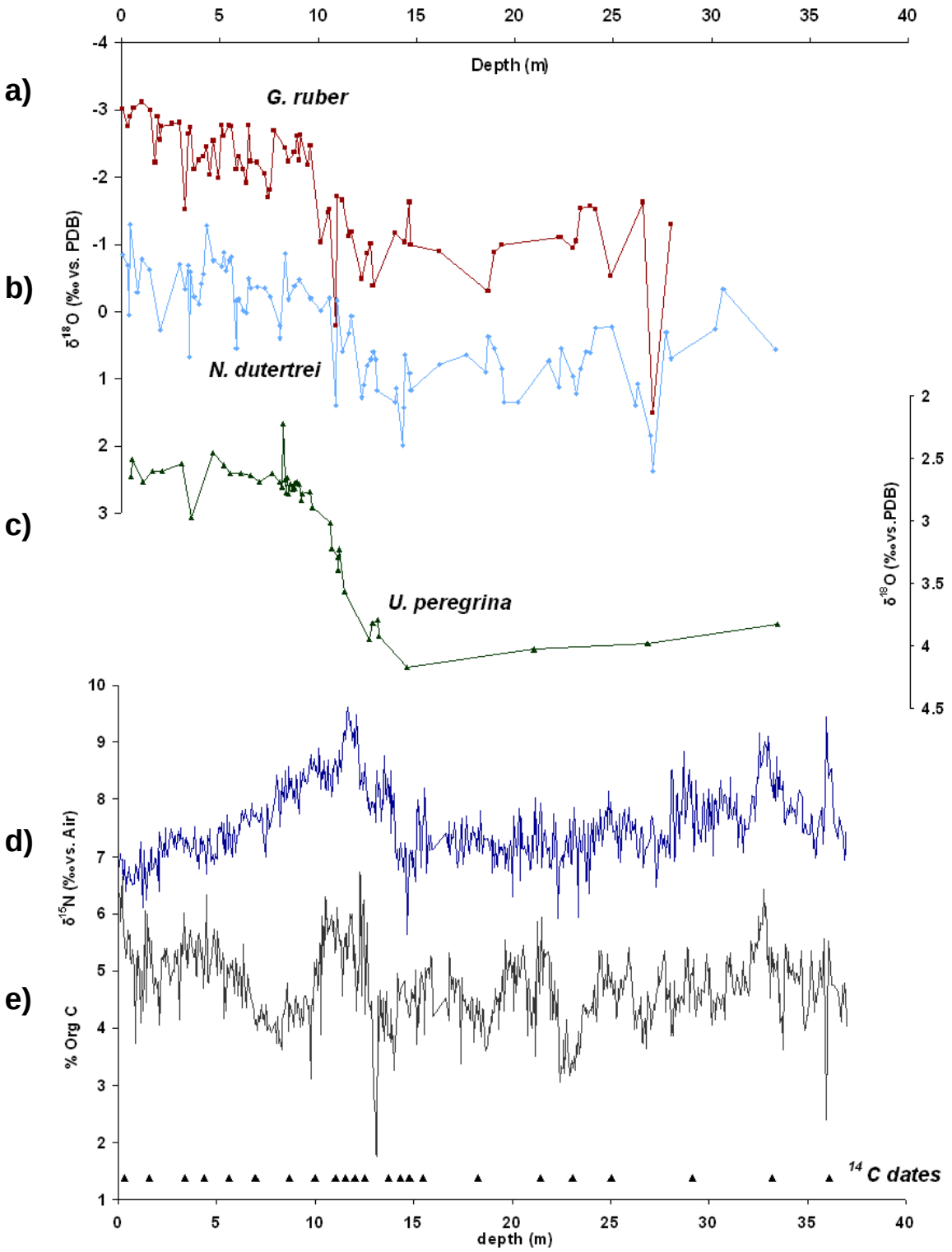

Figure 4.4a: Construction of an age model for core MD02-2520 by means of 23 AMS ^{14}C dates. These radiocarbon dates are supported by oxygen isotope records for planktonic (G. ruber), thermocline dwelling (N. dutertrei) and benthic (U. peregrina) foraminifera.

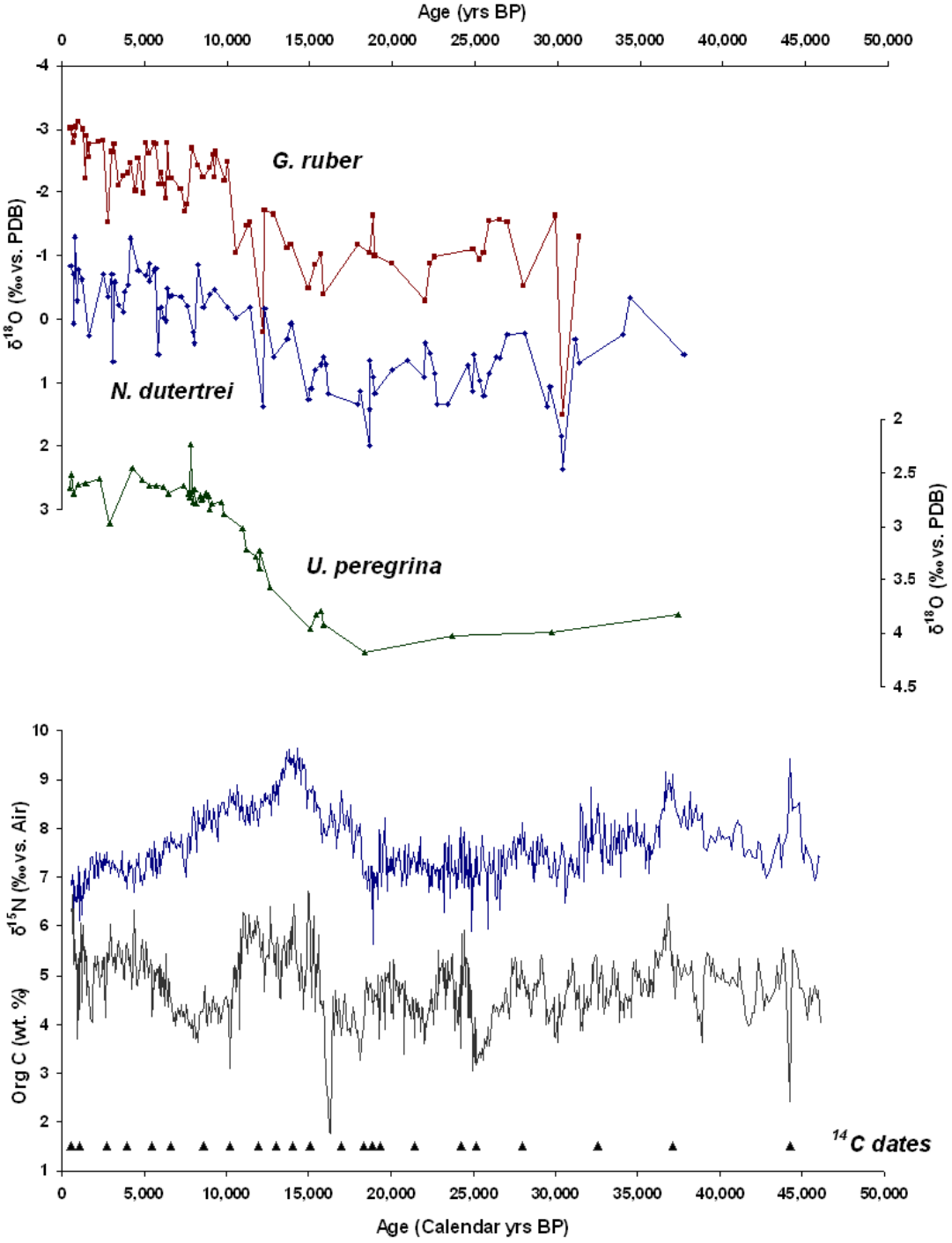

Figure 4.4b: Complete time series for the entire core MD02-2520 by means of 23 AMS ^{14}C dates. These radiocarbon dates are supported by oxygen isotope records for planktonic (G. ruber), thermocline dwelling (N. dutertrei) and benthic (U. peregrina) foraminifera.

For this reason, in addition to the standard global ocean reservoir correction of 400 years, the difference in reservoir age of the local region of interest and the model ocean (ΔR) was determined according to the global database of values kept at http://www.calib.qub.ac.uk/marine, which takes into account local effects such as upwelling, marine currents and riverine inputs. This correction is necessary in order to compare marine and terrestrial samples, but because of complexities in ocean circulation the actual correction will depend on the individual location of the sedimentary cores.

The ΔR for core MD02-2518 from Mazatlan Basin is 203 ±48 years, giving a total reservoir correction of 603 years (400 years + 203 years). By contrast, the ΔR for core MD02-2520 from the Gulf of Tehuantepec is assumed to be 162 ±50 years, giving a total reservoir correction of 562 years (400 + 162 years). Radiocarbon ages older than 21,381 years BP were calibrated by means of the equation outlined by Bard et al. (1997):

Calendar Age = -1,807 + 1.39 x (^{14}C age yrs BP) – 5.85 x 10^{-6} x (^{14}C age yrs BP) ^{2}

One sample from the Mazatlan core (depth interval: 486-487cm, highlighted in red in table 4.1) represents an age reversal in the sequence and may have been contaminated by carbon derived from plastic from the core liner (Dr. Steve Moreton, *pers. comm.*). Another sample (depth interval: 586-587cm; highlighted in red in table 4.1) most likely constitutes a dating anomaly, due to the large reported ^{14}C age error and the large variation in resulting sedimentation rates in samples between 422-586cm depth.

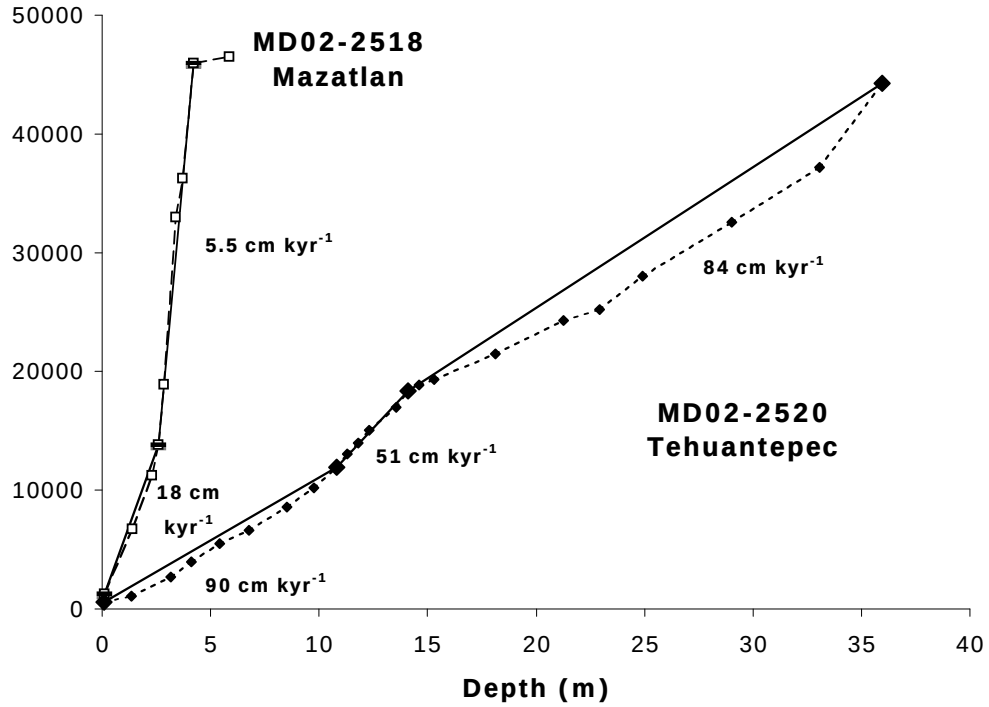

Figure 4.5: Age-depth plots for calibrated AMS ^{14}C dates for the two piston cores presented in this study: core MD02-2520 (solid diamonds) and core MD02-2518 (open squares). The numbers indicate maximum and minimum linear sedimentation rates in cm kyr^{-1}. The solid lines tie sections of the cores along which the average sedimentation were calculated (i.e. the average sedimentation rate between 14m and 37m depth in MD02-2520 is 84cm kyr^{-1}).

It is worth noting that there has been some debate regarding the preservation of sediments extracted with a Calypso piston corer (as used on the RV Marion Dufresne) compared to other long coring systems, as it was found that Calypso cores tend to suffer from some stretching in the upper sections and also compression in the lower sections. If this were there the case, it would give rise to increased sedimentation rates at the top of the core and reduced sedimentation rates within the lower sections.
The lower sedimentation rates observed in MD02-2518 (Mazatlan) are unlikely to be due to core compression, as the reduction in sedimentation rates occurs at 3-4m depth, which is within the top 10% of the length of the core. A change in the source and nature of sediments is far more likely to provide an explanation for the observed changes.

MD02-2518 - Mazatlan

Sample depth (cm)	^{14}C age	^{14}C age error (1σ)	% Carbon	Calibrated Age (years BP)
10-11	1891	35	9.7	**1286**
140-141	6442	44	11.2	**6744**
230-231	10413	72	6.4	**11253**
260-261	12515	97	3.4	**13824**
284-285	16204	162	1.5	**18916**
340-341	28838	850	2.2	**33005**
372-373	31772	1234	3.5	**36264**
422-423	40188	3555	2.9	**45956**
486-487	37751		4.2	**42500 - Age reversal**
586-587	40682	3783	4.9	**46500 – Dating Anomaly (?)**
586-587	/			54750
654-655	/			61000
1050-1051	/			103000
1248-1249	/			123000
1632-1633	/			175000

Table 4.1: AMS ^{14}C ages reported as conventional radiocarbon years BP (relative to AD 1950), ^{14}C age errors (1σ), percentage carbon and calibrated ages (using Calib 5.0.2 software and equation outlined by Bard et al. (1997), see text for details) for core MD02-2518. The ^{14}C age in red corresponds to a dating anomaly, which is most likely due to the sample being at the bottom end of the ^{14}C dating window. The last five data points (in blue) correspond to tie points between maxima in the δ^{15}N record from core MD02-2518, corresponding δ^{18}O minima in the NGRIP ice core record and, for values that lie beyond 125,000 years BP, corresponding δ^{18}O minima in core ODP 980 from the North Atlantic.

MD02-2520 - Tehuantepec

Sample depth (cm)	^{14}C age	^{14}C age error (1σ)	% Carbon	Calibrated Age (years BP)
8-9	1063	24	8.8	**560**
136-137	1658	37	6	**1093**
316-317	3048	36	6.6	**2704**
411-412	4084	38	6.8	**3955**
541-542	5246	41	5.4	**5510**
676-677	6295	43	5.4	**6613**
851-852	8233	55	5.0	**8567**
976-977	9480	63	5.4	**10208**
1081-1082	10764	82	7.0	**11943**
1131-1132	11648	86	6.5	**13051**
1181-1182	12662	99	6.6	**13992**
1231-1232	13279	108	7.6	**15034**
1356-1357	14750	133	5.3	**16982**
1411-1412	15588	149	4.8	**18379**
1461-1462	16046	158	5.4	**18849**
1531-1532	16652	172	4.5	**19314**
1811-1812	18589	224	5.1	**21478**
2126-2127	21177	316	5.3	**24302**
2291-2292	21957	349	4.7	**25209**
2491-2492	24387	480	6.1	**28012**
2901-2902	28392	803	5.2	**32554**
3306-3307	32557	1363	8	**37174**
3596-3597	39133	3116	2.1	**44256**

Table 4.2: AMS ^{14}C ages reported as conventional radiocarbon years BP (relative to AD 1950), ^{14}C age errors (1σ), percentage carbon and calibrated ages (using Calib 5.0.2 software and equation outlined by Bard et al. (1997), see text for details) for core MD02-2520 from the Gulf of Tehuantepec.

References

Bard, E., Rostek, F., Sonzogni, C., (1997) Interhemispheric synchrony of the last deglation inferred from alkenone paleothermometry. *Nature*, vol. **385**, pp. 707-710

Butzin, M., Prange, M., and Lohmann, G., (2005). Radiocarbon simulations for the glacial ocean: the effects of wind stress, Southern Ocean sea ice and Heinrich events. *Earth & Planet. Sci. Lett.*, vol. **235**, pp.45-61

Ganeshram, R.S., Pedersen, T.F., Calvert, S.E. and Murray, J.W. (1995) Large changes in oceanic nutrient inventories from glacial to interglacial periods. *Nature*, vol. **376**, pp. 755-757

Helmke, J.P., Schulz, M and Bauch, H.A. (2002) Sediment-Color Record from the Northeast Atlantic Reveals Patterns of Millennial-Scale Climate Variability during the Past 500,000 Year, *Quaternary Research*, Vol. **57**, Issue 1, pp. 49-57

Hiscott, R.N., Aksua, A.E., Mudie, P.J. (2008) Comment on "The timing and evolution of the post-glacial transgression across the Sea of Marmara shelf south of İstanbul" by Eriş et al., Marine Geology 243, 57–76. *Marine Geology*, Vvl. 248, Issues 3-4, pp. 228-236

Hughen, K.A., Baillie, M.G.L., Bard, E., Bayliss, A., Beck, J.W., Bertrand, C.J.H., Blackwell, P.G., Buck, C.E., Burr, G.S., Cutler, K.B., Damon, P.E., Edwards, R.L., Fairbanks, R.G., Friedrich, M., Guilderson, T.P., Kromer, B., McCormac, F.G., Manning, S.W., Bronk Ramsey, C., Reimer, P.J., Reimer, R.W., Remmele, S., Southon, J.R., Stuiver, M., Talamo, S., Taylor, F.W., van der Plicht. J., Weyhenmeyer, C.E. (2004) Marine04 marine radiocarbon age calibration, 26–0 kyr BP. Radiocarbon, vol. **46**, pp. 1029-1058

Ivanochko, T.S. (2005) Sub-Orbital Scale variations in the Intensity of the Arabian Sea Monsoon. PhD Thesis, The University of Edinburgh.

McManus, J., Oppo, D.W., Cullen, J.L. (1999) A 0.5-Million-Year Record of Millennial-Scale Climate Variability in the North Atlantic. *Science*, vol. **283**, pp 971- 975

Nagao, S., and Nakashima, S. (1992) The factors controlling vertical color variations of North Atlantic Madeira Abyssal Plain sediments. *Marine Geology*, vol. **109**, pp. 83–94

Staubwasser, M., Sirocko, F., Grootes, P.M. and Erlenkeuser, H. (2002) South Asian monsoon climate and radiocarbon in the Arabian Sea during early and mid Holocene. *Paleoceanography*, vol. **17** (4), DOI 10.1029/2000PA000608

CHAPTER 5

Nitrogen isotope, organic carbon and sediment chromaticity records from the Eastern Tropical North Pacific: remote vs. local forcing of millennial- and orbital-scale variability over the past 200,000 years

ABSTRACT

Millennial-scale variations in denitrification and productivity are assessed by means of a sediment core collected from the Mazatlan Margin at 420m depth. The nitrogen isotope record ($\delta^{15}N$) spans nearly 200kyr and ranges from 5.7‰ in bioturbated sediments to 10.6‰ in finely laminated horizons. The organic carbon content of the sediments, which records the history of productivity in the Mazatlan Margin, ranges between 1.5 – 8 weight % and is tightly coupled to variations in the nitrogen isotope record with a frequency that is rather similar in timing to that of the major millennial-scale warming events observed in Greenland ice cores. Millennial-scale reorganizations of the wind systems off Baja California and Mazatlan Margin are also identified through variations in detrital element concentrations in the core, expressed through Ti/Al, K/Al and Si/Al ratios. High-frequency variations in the concentration of detrital elements occur in tandem with Greenland D-O events, with the lowest concentrations occurring during D-O events, suggesting drier conditions, reduced precipitation and fluvial transport of terrigenous material from the North American continent during Greenland warming events.

5.1 Introduction

The relationship between biological productivity, the oceanic fixed-N budget and past variations in the atmospheric concentrations of carbon dioxide and nitrous oxide have stimulated an avalanche of research into the sources and sinks for oceanic nitrogen. This is primarily because biologically available (or ‘‘fixed’’) N is an essential nutrient that will directly affect plankton productivity and the associated drawdown of CO_2 over large regions of the ocean. In addition, the process of water-column denitrification, where nitrate is used as an electron acceptor in the remineralisation of organic matter in the absence or near absence of oxygen, may have contributed up to 50% of any past variations in atmospheric N_2O (Altabet et al., 1995, Deutsch et al., 2004, Fluckiger et al., 2004; Ganeshram et al., 1995; Karl et al., 1997). For the above reasons, monitoring past changes in the oceanic inventory of fixed N has become a major topic of research at the interface between climate change and biogeochemistry, especially at low latitudes, where the availability of nitrate and phosphate may pose a constraint on the biological carbon pump (Volk and Hoffert, 1985). Analyses of sedimentary records recovered from the western Mexican (Ganeshram, 2000, 2002; Thunell and Kepple, 2004), Californian margins (Behl and Kennett, 1996; Hendy and Kennett, 2000; Hendy et al., 2004) suggest that the Pacific Ocean’s intermediate-depth waters have undergone intermittent episodes of enhanced and reduced ventilation and surface productivity which, as a consequence, have led to variations in subsurface denitrification. Variations in the intensity of oxygen minimum zones (OMZs) and denitrification are primarily due to two mutually inclusive mechanisms: a) variations in regional productivity leading to a change in remineralisation rates and the consumption of dissolved oxygen (Ortiz et al, 2004) and/or b) changes in temperature, in ocean circulation and in the lateral mixing of water masses, ultimately resulting in variations of the physical supply of dissolved oxygen to intermediate depths (Galbraith et al., 2004; Meissner et al., 2005). While nitrogen fixation in the Pacific and Atlantic oceanic gyres accounts for the largest source of biologically available fixed nitrogen, the major sinks are found in ‘canonical’ denitrification (Codispoti et al, 2006) occurring in OMZs and shelf sediments (Brandes and Devol, 2002) and through the anammox pathway (Kuypers et al., 2005) which leads to the anaerobic oxidation of ammonium with nitrite to N_2.

Water-column denitrification is the most important process affecting deviations in the stable isotopic ratio between the heavier and rarer isotope ^{15}N and the lighter, more abundant ^{14}N. This occurs as the lighter isotope reacts faster than the heavier ^{15}N, thus generating a product pool that is depleted in ^{15}N and a remaining pool that is enriched in ^{15}N, in a similar fashion to a "geochemical dye" tracing the history of processes affecting the nitrogen pool. The ratio between $^{15}N/^{14}N$ is expressed as $\delta^{15}N$ (where $\delta^{15}N = [(^{15}N/^{14}N)_{sample} / [(^{15}N/^{14}N)_{standard}] - 1$), with the $\delta^{15}N$ of exported organic matter preserved in sediments reflecting the state of the surface ocean nitrogen cycle. For this reason, if the surface NO_3^- pool is completely used up by primary production, variations in $\delta^{15}N$ from exported organic matter will provide a direct record of variations in the $^{15}N/^{14}N$ of the upwelled NO_3^-. In areas where the nutrient pool is not completely utilised, the $\delta^{15}N$ of sedimentary organic matter will provide a record of variations in nitrate utilisation. Areas of N_2 fixation, by contrast, lead to the production of organic matter by diazotrophic organisms that is very close to that of atmospheric N_2 (around 0‰; Capone et al., 1997; Karl et al., 1997 and 2002) and noticeably lower than the mean ocean $\delta^{15}N$ of NO_3^-, which lies in the region of 5‰ to 6‰ (Brandes and Devol, 2002).

The growing database obtained through deep-sea sediment core records collected in the world's three quasi-permanent oxygen minimum zones - the Eastern Tropical North Pacific (ETNP), the Arabian Sea and the Eastern Tropical South Pacific (ETSP) - is providing an increasingly precise understanding of the factors that control the timing and extent of marine denitrification (Ganeshram et al., 1998; 2002; Galbraith et al., 2004; Altabet et al., 1999). The records highlight a cycle of water-colum nitrate depletion during interstadials and nitrate build-up throughout colder stadials. The correspondence between changes in the nitrogen cycle and climate change has led to speculation that an increase in the nitrogen inventory during the stadials through reduced denitrification was one of the major contributing factors for lower glacial atmospheric pCO_2 (McElroy, 1983). Regardless of the intensity of past perturbations of the marine nitrogen cycle, Sigman and Haug (2003) speculated that the fertility of the ocean has been remarkably stable throughout the Late Quaternary. This stability is likely to be a result of negative feedbacks involving increases in N_2 fixation in subtropical gyres (Ganeshram et al., 2002; Tyrrell, 1999)

occurring in tandem with increased water-column denitrification following an increase in primary productivity (Codispoti, 1989; Deutsch et al., 2004).

The N_2 fixation feedback mechanism suggests that, as available N becomes depleted relative to P and the Redfield Ratio shifts to ratios <16, N_2 fixers and organisms capable of assimilating low N:P ratios will have an ecological advantage. This advantage will last until nitrate availability and N:P ratios are restored to the original P-limiting conditions, thus eventually discouraging nitrogen fixing. The nitrogen cycle is also regulated by the latter feedback mechanism, which involves increased N sinks as OMZs expand following increased nutrient availability and the associated primary productivity. Denitrification associated with the enlarged OMZs is will eventually deplete nitrate reservoirs, thus reducing productivity, remineralisation rates and causing OMZs to weaken. A conservative estimate of nitrogen loss from the oceans as a result of present day water-column denitrification is in the order of ~150-200 Tg N yr^{-1} (Codispoti et al., 2001), of which about half (~100Tg N yr^{-1}) occurs in the OMZs of the ETNP, the ETSP and the Arabian Sea (Ganeshram et al., 2000).

In this study, we examine a 40.7m piston core collected from 420m depth in the Mazatlan Margin in order to reconstruct past variability of denitrification through $\delta^{15}N$ records and past reorganizations of wind systems off Baja California and Mazatlan Margin through the bulk composition of detrital elements in the core. The new high-resolution record sheds new light on high-frequency climate variability in the Pacific during the past 200,000 years. In addition, the comparative similarity between the high-frequency oscillations observed in Mazatlan and Greenland ice core allows us to infer that rapid reorganization of the climate through in Western Mexico has been a prominent feature throughout the past two glacial cycles.

5.2 Environmental Setting

The Mazatlan Margin in the ETNP is a rather dynamic environment because of tidal currents, wind stress, upwelling and a high degree of solar heating that leads to the differential warming of ocean and land (Douglas et al., 2007). The area is characterized by marked seasonal changes in circulation and primary productivity driven by changes in atmospheric circulation over the Eastern Tropical North Pacific

(ETNP) and the adjacent North American continent. Upwelling of subsurface waters occurs primarily in winter and early spring, when the subtropical North Pacific high-pressure cell is at its most southerly position and the eastern North Pacific is characterized by strong northwesterly winds that transport water away from the shores and lead to high organic productivity (Thunell et al., 1994; Thunell, 1998). The summer months (April to October) see the introduction of tropical temperatures, high humidity and rainfall when northwesterly winds diminish as the East Pacific High and the ITCZ shift northward (Douglas et al., 2007).

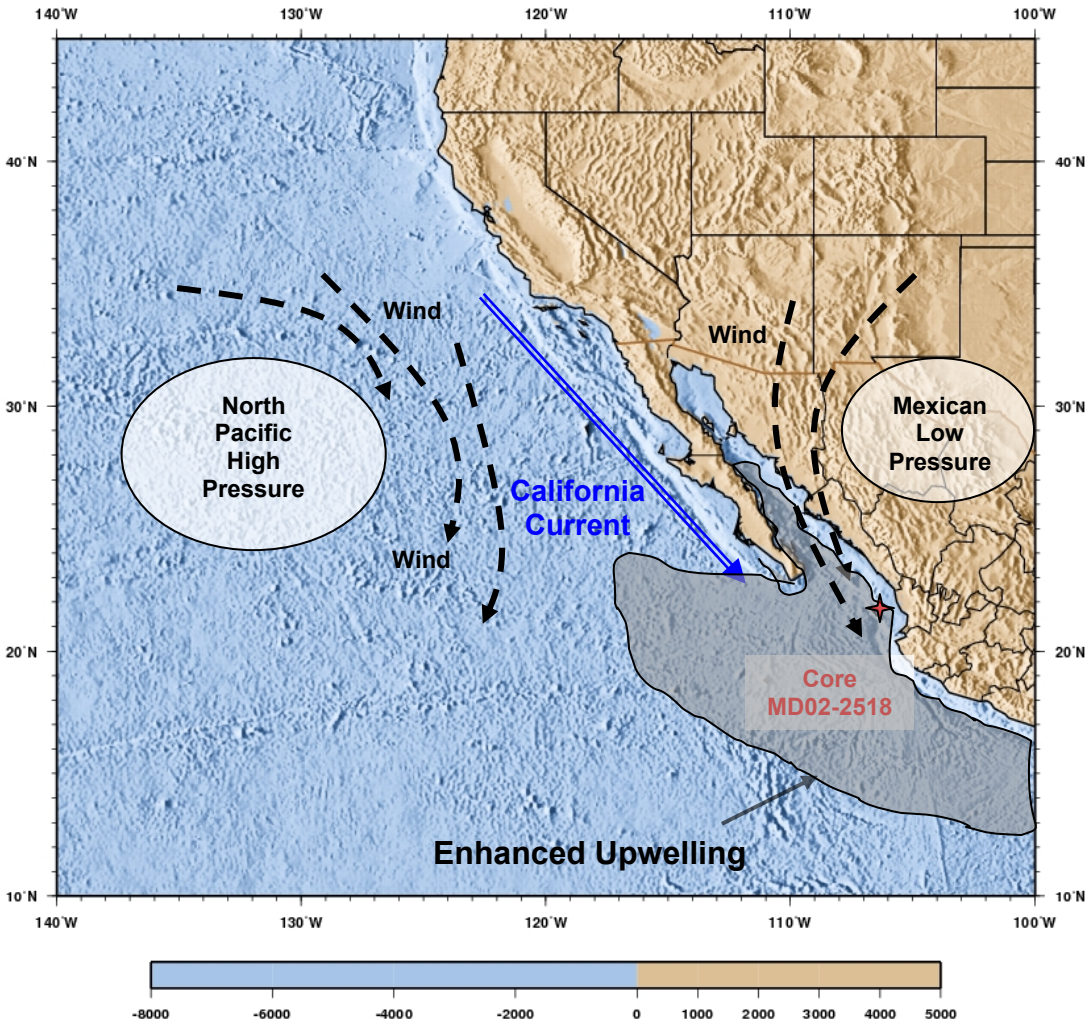

Figure 5.1 Location of core MD02-2518 collected at 454m water depth on the upper slope of the northwestern Mexican Margin, offshore Mazatlan (22º40.39N, 106º29.19W).

The productive Mazatlan Margin is characterized by high sedimentation rates that may range between 8–25cm/kyr due to higher input of organic matter produced in overlying water column coupled to a greater supply of detrital matter resulting

from continental erosion (Van Geen et al., 2003). Intermediate waters that bathe the site in which core MD02-2518 was collected have a predominantly northern source, as North Pacific Intermediate Water (NPIW) that circulates clockwise in the North Pacific gyre reaches the Eastern Pacific continental slope and the California Current moves south along the western coast of North America.

5.3 Methods

See chapter 3 of this thesis

5.4 Results: $\delta^{15}N$ and Organic Carbon

The $^{15}N/^{14}N$ ratio of sinking organic matter is expressed as $\delta^{15}N$ (in ‰ - where $\delta^{15}N = [(^{15}N/^{14}N)_{sample}/(^{15}N/^{14}N)_{standard}]-1$ and the reference is atmospheric N_2). High $\delta^{15}N$ values are a result of both source waters that are enriched in heavier nitrate ($^{15}NO_3$) and the complete utilisation of the source nitrate pool by phytoplankton. By contrast, lower $\delta^{15}N$ values occur in sediments underlying waters where either nutrients are abundant and phytoplankton preferentially take up ^{14}N through isotopic fractionation (Altabet et al. 1995; Ganeshram et al., 1995) and/or pelagic N_2-fixation, which hardly discriminates against ^{15}N and leads to the addition of isotopically light NO_3 (between 1 and -1‰) resulting from the remineralisation of diazotrophic organic matter (Capone et al., 1997; Brandes and Devol; 2002). The average $\delta^{15}N$ composition of global seawater is 4.5-5‰ (Sigman et al., 1997), which reflects a dynamic equilibrium between various degrees of marine nitrogen fixation, water-column and sedimentary denitrification and anammox reactions. Water-column samples collected in the ETNP (Fig 5.2) show that present-day fractionation of the stable nitrogen isotopes measured as $\delta^{15}NO_3$ varies between 7‰ at 1,500m depth to 14-16‰ at 450m depth (Brandes et al., 1998; Ganeshram et al, 2002). This heavy isotopic signature of the upper water-column NO_3 pool is reflected in the $\delta^{15}N$ record of core MD02-2518, which spans nearly 200kyr BP and ranges from 5.7‰ – 10.6‰ (Fig 5.3). The lowest values are from bioturbated sections in the sedimentary record, indicating a reduction in intensity of the OMZ in the ETNP coinciding with episodes of cooling (stadials) recorded at high latitudes. By contrast, the highest $\delta^{15}N$ values are found in laminated intervals of the core as a series of 13 abrupt and mostly asymmetric peaks (table 5.1), which the author has designated as events “N1 – N13”.

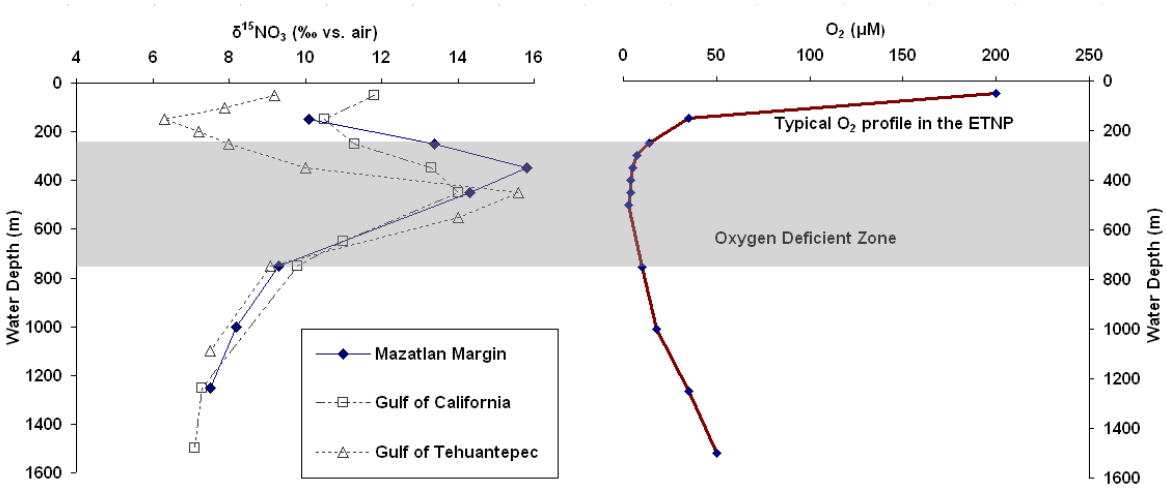

Figure 5.2: Water column profiles of $\delta^{15}NO_3$ from Mazatlan Margin (as reported in Ganeshram et al., 2002); the Gulf of Tehuantepec (Thunell and Kepple, 2004); the Gulf of California (Pride et al., 1999); and a typical oxygen profile from the Eastern Tropical North Pacific. The shaded area represents the approximate depth of the OMZ in the ETNP.

Mazatlan Margin $\delta^{15}N$ events (author's own designation)	Calendar Age of $\delta^{15}N$ maxima (kyr BP)	Corresponding Greenland Interstadial (or MIS)
N1	12.5 - 15	B/A
N2	36 – 38	D-O **8**
N3	47 – 48	D-O **12**
N4	53 – 55	D-O **14**
N5	58 – 60	D-O **16**
N6	91 – 92	D-O **22** (MIS 5.1)
N7	101 – 103	D-O **23**
N8	105 – 106	D-O **24** (MIS 5.3)
N9	121 – 125	Eemian (MIS 5.5)
N10	149 – 150	MIS 6
N11	155 - 159	MIS 6
N12	169 – 172	MIS 6
N13	176 - 179	MIS 7.1 (?)

Table 5.1: Age of $\delta^{15}N$ maxima in core MD02-2518 from the Mazatlan Margin and corresponding major interstadials in Greenland ice cores (from present day to MIS 5.5) and in core ODP 980 from the North Atlantic (McManus et al., 1999) as can be seen in Fig 5.3. B/A = Bølling-Allerød interstadial event; D-O = Dansgaard-Oeschger interstadial event; MIS = Marine oxygen Isotope Stage.

These millennial-scale increases in denitrification appear to be synchronous, within dating errors, with major D-O events recorded in the Greenland NGRIP and GISP2 ice-core record (Bender et al., 1994; NGRIP Members, 2004) throughout the last two glacials (i.e. over the past 190,000 years). Sedimentation rates documented in the Mazatlan core average 9.2 cm kyr^{-1} and are between five times to an order of magnitude lower than those recorded in the Gulf of Tehuantepec. Nevertheless, as has been previously documented by Ganeshram et al. (1995, 2000 and 2002), the C_{org} record from core MD02-2518 is likely to indicate changes in paleoproductivity rather than variations in organic matter preservation (Calvert et al., 1992; Calvert et al., 1995). The C_{org} content ranges between 1.5 - 2% in coarser, bioturbated sections and between 4 – 8% in the finely laminated sections. The carbon record is tightly coupled to variations in the nitrogen isotope record with a frequency that is rather similar in timing to that of the major millennial-scale warming events observed in Greenland. The highest C_{org} values (>6%) were deposited during conditions of anoxia (laminated sediments) in MIS 1, 5.3, 5.5 and 6 - 7.1.

The relative proportions of marine vs. terrestrial sources of the preserved organic matter in marine sediments can be interpreted in terms of their $\delta^{13}C_{org}$ and $\delta^{15}N$ content (Sackett, 1964; Hedges & Parker, 1976). The isotopic composition of organic matter in the core reflects the bulk signal derived from the mixture of all sources of OM that accumulated on the Mazatlan Margin. Hence, any terrestrially-derived organic matter is likely to reflect the $\delta^{15}N$ and $\delta^{13}C$ signal of C_3 plants from surrounding areas ($\delta^{15}N_{C3\ plants} \approx 2‰$; Sweeney and Kaplan, 1980; $\delta^{13}C_{\ C3\ plants} = -26‰$ to -28‰ PDB; Jasper and Gagosian, 1990). By contrast, the isotopic signal of marine organic matter is noticeably heavier than the terrestrial signal, with average $\delta^{13}C$ values for low-latitude plankton ranging from -18‰ to -22‰ PDB (Rau et al., 1989; Wakeman and Ertel, 1988). The $\delta^{13}C$ range of -20.5‰ to -22‰ provides evidence for the dominantly marine origin of the organic matter preserved in core MD02-2518 (Fig. 5.3).

It is assumed that the C_{org} content of core MD02-2518 records the history of productivity offshore Mazatlan, as the character of the organic matter preserved in

the core is predominantly marine, and Ganeshram et al. (1998) observed biogenic opal concentrations to follow percentage C_{org} quite closely in core NH15P collected at a very similar depth offshore Mazatlan. The direct relationship between C_{org} and chromaticity value (a*) in the top 15m of core MD02-2518 (Fig. 5.3) allows for a rapid method for estimating the organic C content of remaining sections of the core (i.e. up to 40.5m depth), which the author believes to range between 1.5 – 7% (Fig 5.4).

(*Next page*) Figure 5.3: A comparison between planktonic and benthic foraminiferal $\delta^{18}O$ records from core ODP 980 from the North Atlantic (McManus et al., 1999); $\delta^{18}O$ transitions in the NGRIP Greenland ice core; $\delta^{15}N$ variations and organic C weight % in core MD02-2518 from Mazatlan; and $\delta^{13}C$ records from acidified organic matter in core MD02-2518. The grey and white bars above the Mazatlan core records represent laminated/bioturbated intervals in core MD02-2518. The numbers above the Greenland record represent major D/O events that have been used to correlate peaks in the $\delta^{15}N$ record of core MD02-2518. Numbers (N1-N13) above the $\delta^{15}N$ maxima correspond to the events outlined in Table 5.1. The blue lines indicate the author's proposed correlation between events outlined in the three records.

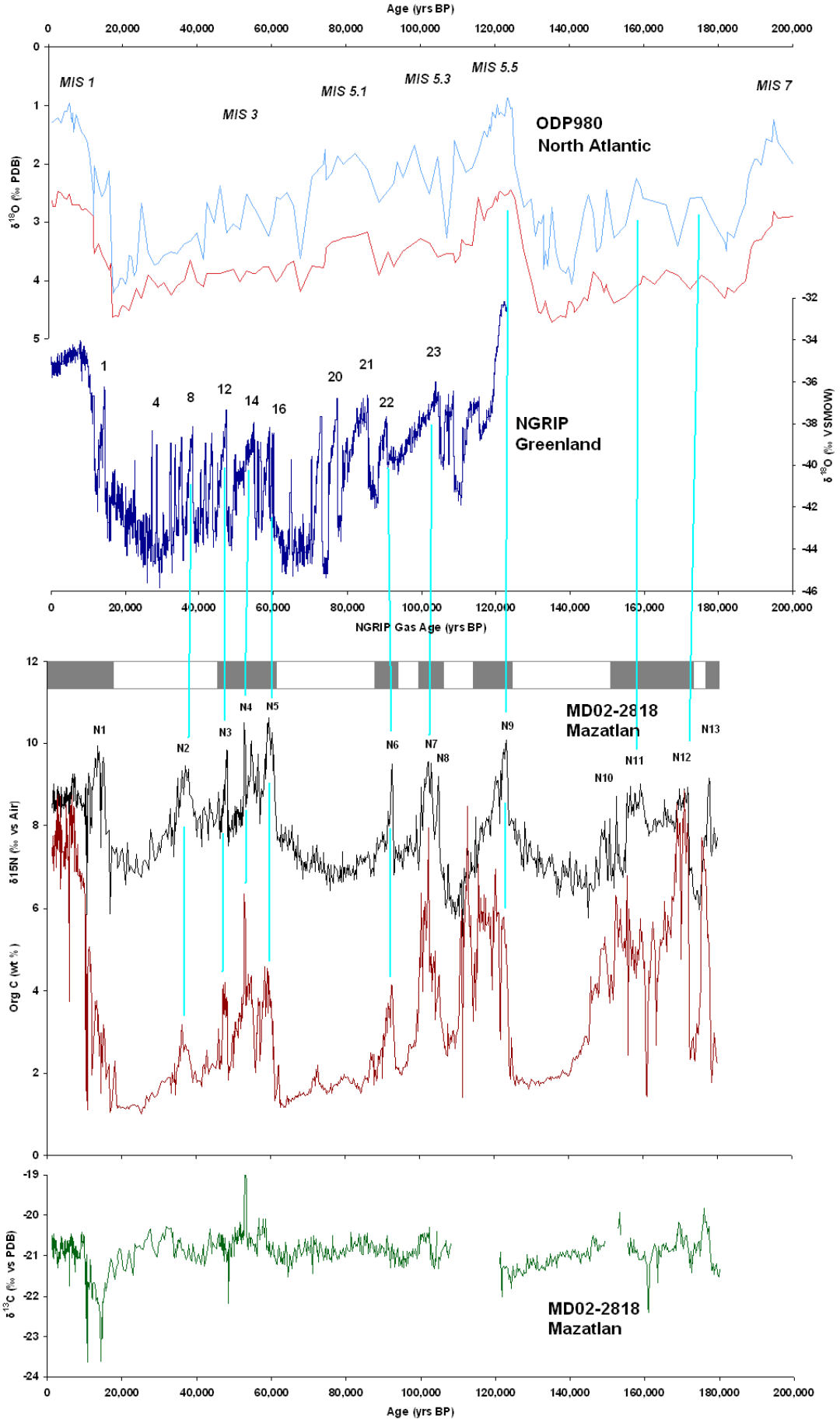
Age (yrs BP)
MIS 1
MIS 3
MIS 5.1
MIS 5.3
MIS 5.5
MIS 7
ODP980
North Atlantic
δ18O (‰ PDB)
NGRIP
Greenland
δ18O (‰ VSMOW)
NGRIP Gas Age (yrs BP)
MD02-2818
Mazatlan
δ15N (‰ vs Air)
Org C (wt %)
δ13C (‰ vs PDB)
MD02-2818
Mazatlan
Age (yrs BP)

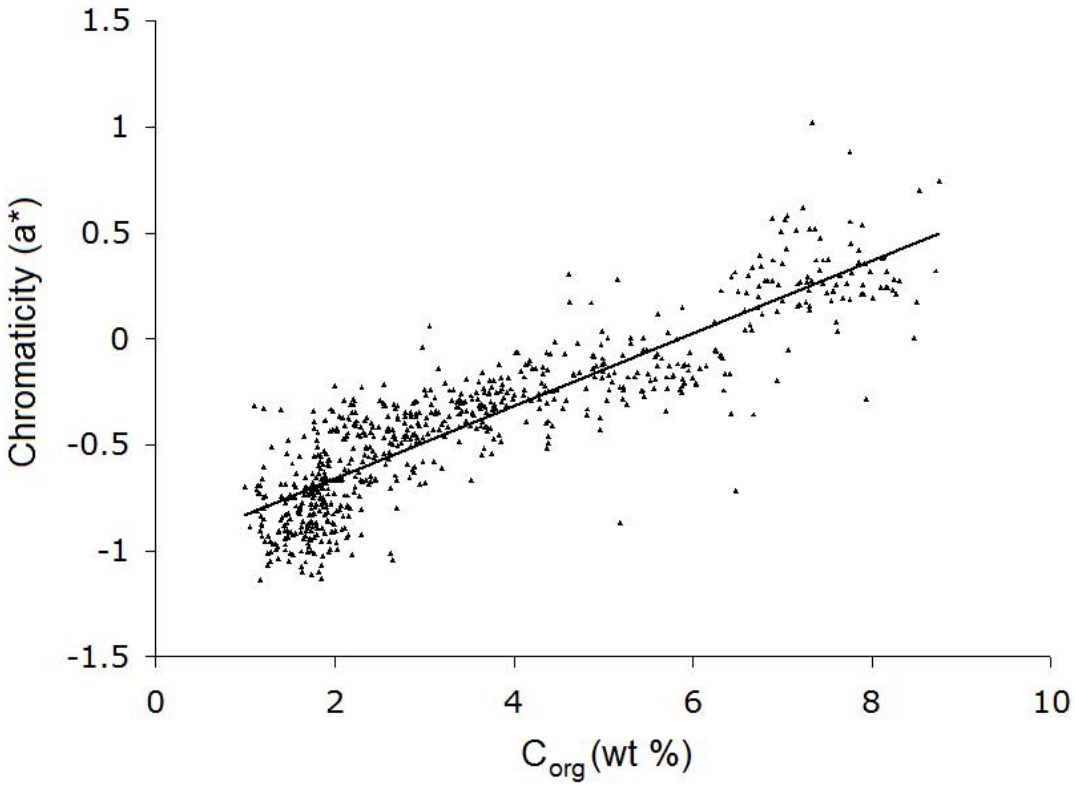

Figure 5.4: Scatter-plot highlighting the direct relationship between C_{org} (wt%) and chromaticity value (a*) in the top 15m of core MD02-2518. The plot was constructing by comparing 722 shipboard (a*) measurements with organic C measurements conducted at the University of Edinburgh from samples at equivalent depths, which span at least five bioturbated and six laminated horizons. The trendline highlights the following relationship in the Mazatlan core:

$$C_{org} = 4.55\ (a^*) + 5.35$$

However, while such a relationship may provide a relatively rapid and inexpensive method for estimating the organic C content of the core, we must note that the contrast between positive and negative (a*) can be seen to gradually dampen below 20m depth (equivalent to ~ 220,000 yrs BP), as sediments become more compressed, leading to lower water contents and reduced oxidation of the laminated sediments when exposed to air (See chapter 3.5).

5.5 Results: Detrital Elements

Fluctuations in the bulk concentrations of detrital source elements (Si, K, Ti as aluminium-normalised ratios) are presented in Fig. 5.5 in order to understand the variations of terrigenous sediments discharges in the northwestern Mexican margin during the last 140 ka. When used together, these geochemical tracers can provide an indication of past variability in humidity and weathering conditions affecting the sediment source regions (i.e. Beckmann et al., 2005), where more humid climates would have led to increased chemical weathering and clay mineral formation and drier periods would have resulted in more intense sorting by winds and marine currents.

Increases in K/Al ratios are associated with continental siliciclastics (clay minerals and K-feldspars) that have undergone only moderate amounts of chemical alteration (Yarincik et al., 2000). K/Al ratios in core MD02-2518 range from 0.24 – 0.39, with the highest ratios reflecting an illite-kaolinite-dominated sediment mineralogy during the LGM and throughout each cold period that separates interstadials as recorded in the Greenland ice cores.

Titanium minerals (ilmenite, augite, rutile and anatase) are classically considered to be very resistant to weathering in soils and Ti is generally insensitive to environmental redox variations (Haug et al., 2001). Titanium is typically enriched in coarser sediments and heavy minerals, hence increased Ti/Al ratios in marine sediments can be interpreted to reflect either an increase in aeolian supply or increased current energy during lower sea-level episodes (Peterson et al., 2000; Beckmann et al., 2005). Ti/Al ratios range from 0.034 – 0.048 and are similar to values published by Nameroff et al. (2004) for core NH15P (22°41.0'N, 106°28.8'W) collected 1.3km from core MD02-2518 presented in this study, with the highest values occurring during Greenland stadials and the lowest during interstadials.

The Si/Al record in core MD02-2518 records both variations in the biogenic Si (opal) from diatoms and other siliceous phytoplankton and lithogenic (detrital) Si. However, as Si/Al, Ti/Al and K/Al tend to covary in the core, we can assume a detrital origin of the silica to be more likely. The Si/Al ratios range from 2.5 during interstadials to 4.1 during stadials and are generally above the crustal average of 3.1 (Wedepohl, 1995). Ganeshram and Pedersen (1998) found that biogenic opal

contents in the Mazatlan Margin follow the organic carbon record quite closely. As C_{org} percentage in core MD02-2518 is lower during colder periods, it suggests that the high Si/Al ratios recorded during stadials are due to the fluvial and/or aeolian input of quartz grains, Si-rich silt and volcanic tephra shards from the Sonoran desert or the Central Mexican Volcanic Belt.

(*Next page*) Figure 5.5: A reconstruction of millennial-scale deposition of detrital elements in the Mazatlan Margin. Changes in the detrital source element content of core MD02-2518 are represented by the K/Al; Ti/Al; and Si/Al records (note the inverted y-axis). Minima in the three records from core MD02-2518 are correlated with the main D-O events (numbered 7-23) in the Greenland (NGRIP) $\delta^{18}O$ record, which indicates temperature variations in the northern polar region. The dark and light shading indicate respectively laminated and bioturbated intervals in core MD02-2518. B/A = Bolling-Allerod Period (14,500-12,900 yrs BP); H1-H8 indicate the chronology of Heinrich events.

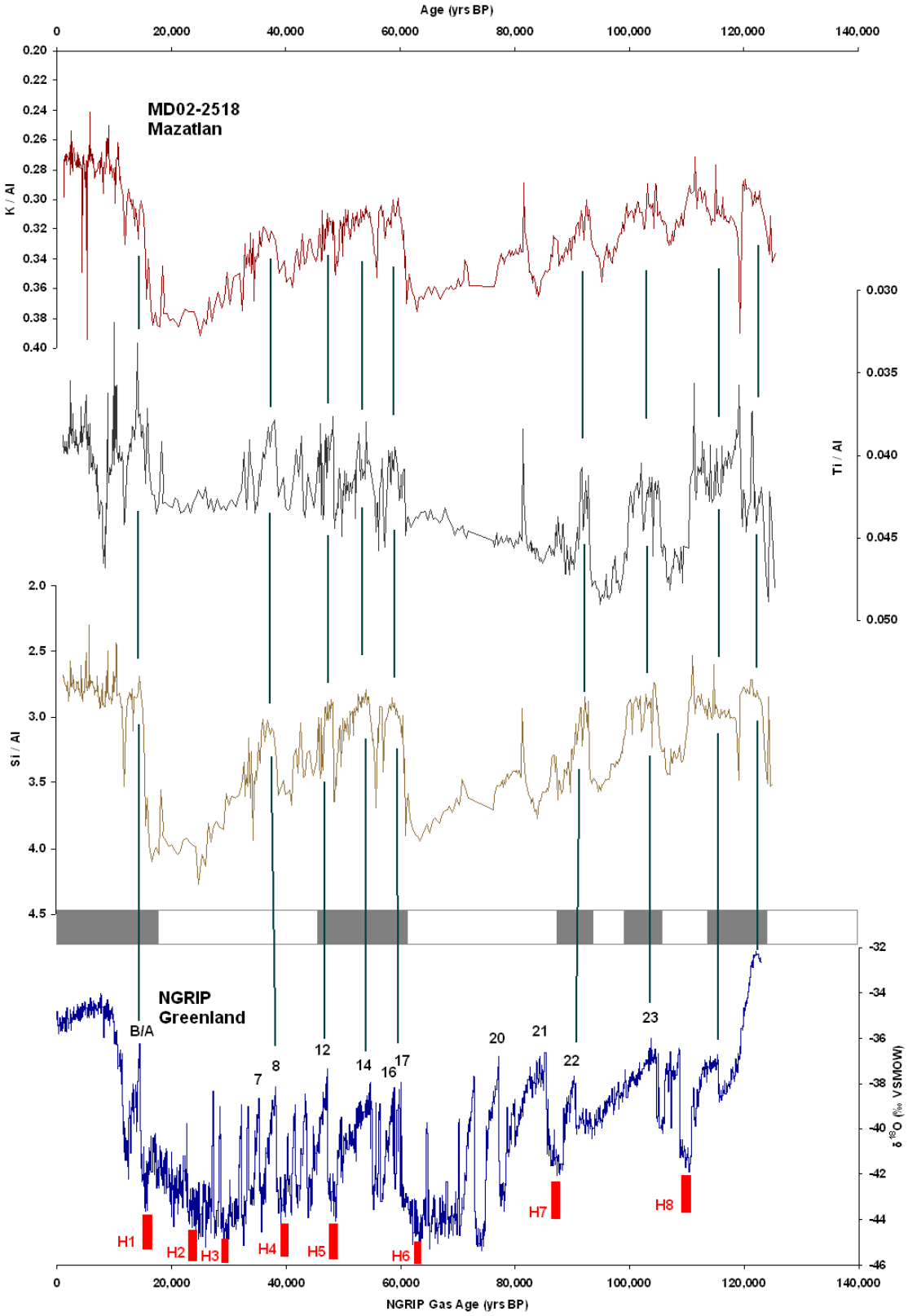
Age (yrs BP)
0
20,000
40,000
60,000
80,000
100,000
120,000
140,000
MD02-2518
Mazatlan
K / Al
0.20
0.22
0.24
0.26
0.28
0.30
0.32
0.34
0.36
0.38
0.40
Ti / Al
0.030
0.035
0.040
0.045
0.050
Si / Al
2.0
2.5
3.0
3.5
4.0
4.5
NGRIP
Greenland
B/A
7
8
12
14
16
17
20
21
22
23
H1
H2
H3
H4
H5
H6
H7
H8
δ18O (‰ VSMOW)
-32
-34
-36
-38
-40
-42
-44
-46
NGRIP Gas Age (yrs BP)

5.6 Discussion: Past Changes in Water-Column Denitrification throughout the Past 200,000 years

Any variation in the global ocean nitrogen budget has the capacity to affect the biogeochemistry and productivity of the oceans through a change in nutrient inventories. Oceanic biochemistry and productivity assert a direct control on the budget of atmospheric greenhouse gases, primarily through the uptake of CO_2 by marine plankton and the release of N_2O as a by-product of nitrification and denitrification (Elkins et al, 1978; Cline et al., 1987; Yoshinari et al., 1997). At present, there are three main areas of the global ocean where biologically available NO_{3-} is lost to the atmosphere through denitrification and anaerobic ammonium oxidation (anammox - Dalsgaard et al., 2003): The Eastern Tropical North Pacific (ETNP), the Eastern South Pacific (ESP) and the Arabian Sea. The increasing number of marine piston and gravity cores obtained from these areas, coupled with longer core lengths and sampling resolutions of the sedimentary record has led to an improved understanding of the geographical and temporal extent of denitrification in the global ocean. Marine records from the Arabian Sea and Californian and Mexican margin up to a latitude of 20°N have highlighted that variations in $\delta^{15}N$ in organic matter have occurred in synchrony with changes in temperatures recorded in Greenland ice cores (Altabet at al., 1995; 2002; Ganeshram and Pedersen, 1998; Ganeshram et al., 2000; Kienast et al., 2002; Schult et al., 1998). In addition, high resolution records from the Santa Barbara basin (Behl and Kennett, 1996; Hendy et al., 2004) have highlighted that variations in $\delta^{15}N$ also occurred on frequencies which are in synchrony with stadial-interstadial temperature variations recorded in Greenland, with the timing and relative magnitude of $\delta^{15}N$ variations matching Dansgaard/Oeschger (D-O) events recorded in Greenland ice cores. Core MD02-2518 shows dark, finely laminated, C_{org}-rich sediments with higher $\delta^{15}N$ values that correlate, within AMS ^{14}C dating errors, with Greenland interglacials, whereas light-coloured, C_{org}-poor, bioturbated sediments occurred in synchrony with stadials (Fig 5.3). Sediments below the depleted waters of the Eastern Tropical North Pacific (ENTP) have $\delta^{15}N$ values ranging between 6-10 ‰, which reflect the intense denitrification occurring within intermediate waters of the ETNP (Ganeshram et al., 1995, Kiefer and Kienast, 2005). These records suggested a decrease in intensity of

the OMZ led by reduced upwelling-driven productivity during cold intervals and a reversal of these conditions during warmer interglacials. Fig. 5.3 shows that the Bolling Allerod warming (13-15 kyr BP) and all major D-O events recorded in Greenland are expressed in the climate variability of the NW Mexican Margin through high-frequency perturbations in the organic carbon record and through reorganizations in the intensity of the OMZ. Organic matter in the sediments in Mazatlan Margin contain predominantly marine organic matter (Fig. 5.6), as the $\delta^{13}C$ values range between -19‰ and -23‰ and C_{org}/N_{total} ratios range predominantly between 8-13 (with the exception of a small number of samples in sediments younger than 20kyrs BP, where C/N ratios may be as high as 37 due to the small levels of N_{total} in organic matter with a potential terrestrial source). Core MD02-2518 spans the last ~200kyr BP, and as the high-frequency variability in $\delta^{15}N$ values extends to sediments older than MIS 5.5 we can infer that D-O events and millennial-scale cycles extend to MIS 6 and 7, in a similar fashion to rapid climate variations observed in sediments from the North Atlantic by McManus et al. (1999). Major interstadials occurred between 160 - 163 kyr BP, 167 - 171 kyr BP, 177 – 181 kyr BP and 189 – 192 kyr BP and each one of these events is likely to be linked to significant Greenland D-O (warming) events that have not yet been traced in boreal high-latitude ice-records of temperature change. Each variation in the intensity of OMZs and water-column denitrification between stadials and interstadials had profound effects not only on the global nitrogen cycle, but also affected the carbon cycle. This resulted from water-column denitrification and anammox activity (the anaerobic oxidation of NH_4 to N_2 by microbes using NO_2^- as an oxidant) accounting for 25-60% of the loss of fixed N from the oceans (Gruber and Sarmiento, 1997; Codispoti et al., 2001), with the remaining portion of the loss of fixed N being due to sedimentary denitrification. In addition, variations in denitrification also indirectly contributed to atmospheric CO_2 variations by modulating the level of fixed nitrogen available to primary productivity (Yoshinari et al., 1997; Altabet et al., 2002; Ganeshram et al., 2000; 2002; Galbraith et al., 2004).

The gradual increases in $\delta^{15}N$ that occur before the onset of a higher C_{org} values sediments at 65kyr BP and 135 kyr BP (Fig. 5.3) show that changes in water-column denitrification may also be due to remote ventilation changes originating at

high latitudes. The most likely cause of changes in ventilation changes in intermediate waters bathing the Mazatlan Margin are alterations in the intensity of the California Current that followed changes in the gradient between high-pressure cells of the North Pacific and the Aleutian and Mexican lows (Fig. 5.1; Herbert et al., 2001).

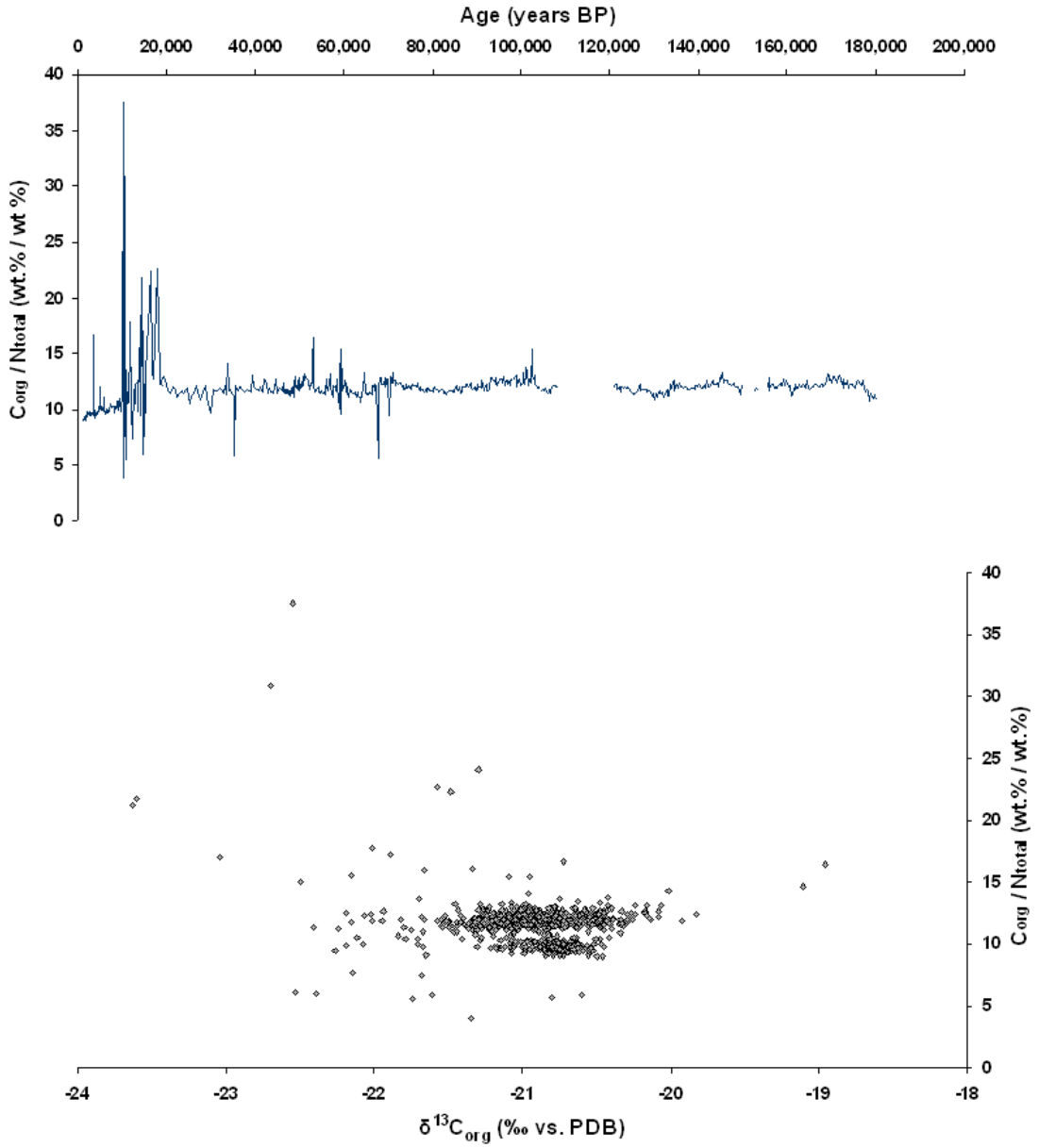

Figure 5.6: a) Time-series of C_{org} / N_{total} ratio; and b) relationship between C_{org} / N_{total} ratio and δ^{13}Corg values in sediments in core MD02-2518 from the Mazatlan Margin. Some samples from sediments younger than 20kyrs BP display C/N ratios may be as high as 37 due to the small levels of Ntotal in organic matter. This could be due to the presence of terrestrial organic matter impoverished in N.

It is believed that the California Current weakened at the end of major stadials, when large ice sheets reorganized wind systems over the North Pacific. This would have reduced lateral oxygen transport to the Mazatlan margin at the end of stadials, thus intensifying the OMZ in the portion of the ETNP that lies to the north of 20°N in advance of the onset of increased primary productivity. This may explain why the increases in $\delta^{15}N$ at the end of major stadials are gradual and not as abrupt as those observed in the C_{org} record and provide evidence for the importance of later ventilation changes as a driver of variations in the $\delta^{15}N$ record.

Denitrification and anammox activity in the oceans are major contributors of nitrous oxide (N_2O) to the atmosphere (Codispoti and Christensen, 1985; Yoshinari et al., 1997). Anammox is known to occur within the OMZ of the ETNP (Dalsgaard et al., 2003), and together with denitrification is thought to be responsible for a global loss of 80-150 Tg of fixed N yr^{-1} (Gruber and Sarmiento, 1997). Over timescales of hundreds to thousands of years the losses of fixed N are thought to be balanced in subtropical gyres by biological N_2 fixers such as the cyanobacterium *Trichodesmium* (Karl et al., 1997), and the diatom genera *Rhizosolenia* and *Hemiaulus*, which contain the endosymbiotic N_2-fixing cyanobacterium *Richelia intracellularis* (Venrich, 1997). Neither the taxonomic distribution in the oceans, nor the exact N_2-fixation rates of these microorganisms is well known (Arrigo, 2005), though it believed that annual N_2-fixation rates are in the range of 100-200 Tg N yr^{-1} (Karl et al., 2002). The millennial-scale frequency of variations in denitrification recorded in the ETNP is likely to have affected the stoichiometric balance between N, P and C available as nutrients, shifting ecological advantage toward N_2-fixers during interstadials and non-N_2-fixing organisms during stadials.

5.7 The nitrogen cycle in the ETNP: a dynamic equilibrium or a catalyst for glacial-interglacial CO_2 variations?

At present, the largest mass of denitrifying waters in the ocean resides beneath the highly productive waters of the eastern tropical North Pacific (ETNP), and the observed past variations in $\delta^{15}N$ during transitions between stadials and

interstadials show the existence of a close connection between the marine nitrogen cycle, the carbon cycle (via feedbacks between primary production and atmospheric CO_2) and global climate (Falkowski, 1997; Fluckinger et al, 2006). Fig. 5.7 highlights the main feedbacks between the nitrogen cycle (light grey ellipse) and the carbon cycle and atmospheric CO_2 (dark grey circles).

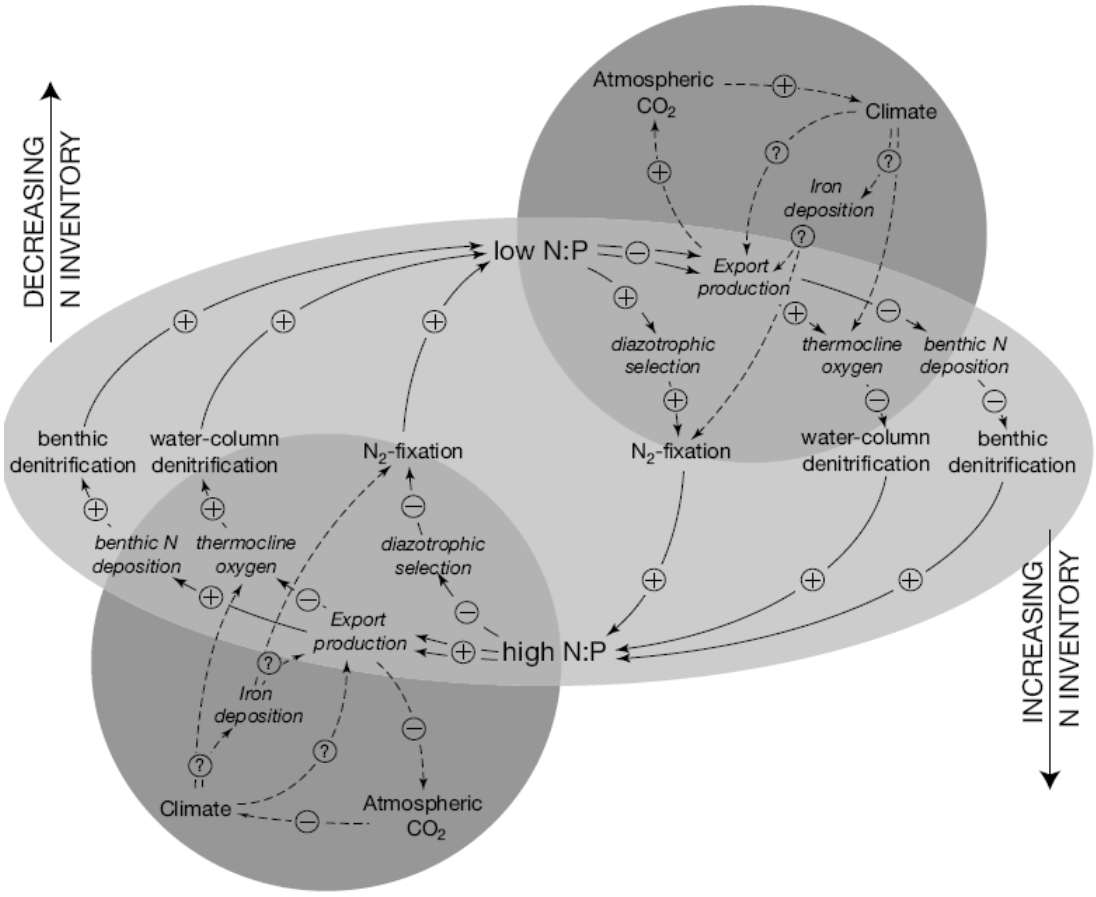

Figure 5.7: Schematic representation of negative feedback processes responsible for stabilising the oceanic nitrogen cycle (light grey ellipse). The interactions between the nitrogen and carbon cycles are highlighted by the dark-grey circles. The relationship between elements in the loops may lead to either a direct proportionality (+) or an inverse proportionality (-), although the processes in each case (increasing or decreasing N inventory) give rise to a negative feedback. The feedback loops are predominantly controlled by the ratio of surface-water N:P; which is in turn modulated by the intensity of water-column and benthic denitrification along western continental margins, and nitrogen fixation in subtropical gyres. The representation is taken from Fig. 1.7 in Gruber, 2004.

If we are to apply this schematic feedback-loop diagram to the ETNP, the picture that emerges suggests that denitrification governs the ratio of surface-water $[NO_3^-]$:$[PO_4^{3-}]$ and nitrogen fixation in the more distant subtropical gyres. Throughout stadials, the lower export production along the Mexican Margin occurring as a result of reduced wind-induced upwelling would have reduced the

intensity of denitrification in the ETNP. The close coupling between records of organic carbon and $\delta^{15}N$ in core MD02-2518 (Fig. 5.3) suggest that past changes in water-column denitrification are likely to be related to changes in local productivity as much as changes in the remote ventilation of intermediate waters (Meissner et al., 2005). The reduced denitrification would ultimately lead to an increased supply of fixed nitrogen and a higher surface-water $[NO_3^-]$:$[PO_4^{3-}]$. These conditions would favour 'bloomers' (Arrigo, 2005), organisms adapted for exponential growth that contain a high proportion of growth machinery and which eventually confer a disadvantage to N_2-fixing organisms (Redfield et al., 1963; Tyrrell, 1999). However, an increase in export production due to the exponential growth of bloom-forming phytoplankton would eventually lead to an increase in denitrification, thereby reducing the amount of fixed nitrogen that reaches the surface ocean. This negative feedback loop suppresses the activity of the bloomers and the resulting lower $[NO_3^-]$:$[PO_4^{3-}]$ ratio in surface waters shifts the ecological advantage to 'survivalists' (Arrigo, 2005) and N_2-fixing organisms, which are capable of using the excess $[PO_4^{3-}]$. Survivalist phytoplankton can sustain growth when resources are low and tend to have a high cellular N:P ratio which is explained by their need for large quantities of P-poor light-harvesting pigment and proteins required to drive N_2 fixation (LaRoche and Breitbarth, 2005). What results from this picture is that the commonly accepted N:P ratio of 16 for phytoplankton cannot be applied universally to all marine systems, but instead represents an average for a different phytoplankton assemblages growing under a variety of environmental conditions, which export production N:P ratios ranging from ~8 for bloomers to N:P > 35 for diazotrophs.

As the evidence of increasing organic carbon and $\delta^{15}N$ in sediments during interstadials and reduced denitrification and export productivity during stadials has been extended to oxygen minimum zones ranging from the ETNP, the Arabian Sea, the Eastern South Pacific, to the Subarctic Pacific and western Africa (Ganeshram et al, 2000; Altabet et al., 2002; Galbraith et al., 2004; De Pol-Holz et al., 2006), we can observe that the feedback loops are integrated throughout the global marine system and are closely connected with atmospheric CO_2 and climate. In addition, records that have been recovered from areas distant from denitrification zones indicate that there was no significant change in ^{15}N /^{14}N between the Last Glacial

Maximum and Early Holocene (Kienast, 2000). Hence, we may view the nitrogen cycle as a series of processes in dynamic equilibrium, where the rate of inputs (via N_2 fixation) is equal to the rate of outputs (via water-column denitrification, benthic denitrification and anammox) so that the composition of the system remains unchanged over glacial/interglacial cycles. Indeed, no evidence of dramatic increases or decreases in global ocean productivity has yet been found in the marine sedimentary records (Blunier et al., 2002; Sigman and Haug, 2003).

The quest for the role that the nitrogen cycle has in modulating atmospheric CO_2 levels remains one of the most hotly debated topics among current biogeochemical research. Whilst it is almost universally acknowledged that variations in the carbon cycle are ultimately responsible for large changes in atmospheric CO_2, a number of authors have recently published hypotheses suggesting that the variations in the marine nitrogen inventory between stadials-interstadials may have contributed indirectly to changes in atmospheric CO_2 and directly to variations in N_2O, a secondary greenhouse gas (Altabet et al., 1995; Ganeshram et al., 1995; Falkowski et al., 1997; Broecker and Henderson, 1998; Michaels et al., 2001; Karl et al., 2002; Gruber, 2004). These hypotheses can be summarised under two separate mechanisms: one involving N_2 fixation and one involving denitrification. The N_2 fixation mechanism is based on observations relating to the timing and extent of increases in dust-derived iron deposition on the surface ocean during stadials, estimated at twice the amount deposited today. The increase in iron deposition from the increasingly desertified Asian and American continents to the ocean is thought to have increased N_2 fixation in the North Pacific and Atlantic gyres. This would have ultimately lead to a larger fixed nitrogen inventory throughout stadials achieved by means of the remineralisation of sinking particulate matter with increased N:P ratios (Arrigo, 2005). The resulting increase in primary production would have drawn down atmospheric CO_2 through the export of organic carbon to the underlying sediments. By contrast, the denitrification-based mechanism proposes that any increase in fixed nitrogen inventory throughout stadials would have occurred as a result of reduced denitrification in the oceans' OMZs, as there are agreements in timing between increases in denitrification observed in sedimentary $\delta^{15}N$ records and increases in atmospheric CO_2 as recorded in air

bubbles from various Antarctic cores (Indermuehle et al., 2000; Fluckiger et al., 2002; Monnin et al., 2002). The decrease in fixed nitrogen during interstadials through increased denitrification would reduce global oceanic productivity and cause an overall release of CO_2 into the atmosphere, predominantly through marine-atmosphere gaseous exchanges at high latitudes (Knox and McElroy, 1984). The records from Mazatlan Margin (Fig 5.3) show an increase in primary production occurring in tandem with increases in denitrification, as opposed to a global scenario in which increases in denitrification occur in concomitance with reduced primary productivity. This can be reconciled by records highlighting that primary productivity did not vary uniformly (Pedersen et al., 1991; Kohfield et al, 2005). Hence, while global productivity is likely to have decreased during interstadials, major upwelling regions experienced an increase in productivity.

The author believes that both processes (N_2 fixation and denitrification) worked in concert, regulating the nitrogen inventory and thus the carbon cycle through primary production between stadials and interstadials. However, the inferred changes in the fixed nitrogen inventory are unlikely to have been the main driver that caused the glacial-interglacial variations in atmospheric CO_2, as the marine carbon cycle is also affected by a number of externalities which include, but are not restricted to, the depth of the lysocline, sea-level change and the extent of stratification of waters at high latitudes (which represents a conduit for carbon between the atmosphere and the deep ocean). In addition, any future research into the connection between the nitrogen cycle and past climate variability should also analyse whether the near zero intercept of the $[NO_3^-]$:$[PO_4^{3-}]$ ratio of surface waters (Tyrrell, 1999), currently responsible for maintaining the negative feedback loops visible in Fig 5.7, may have changed in the past. Chapter 7 of this thesis will guide the reader through an assessment of how N:P ratios in the ETNP may have changed in the past.

5.8 Cyclical changes in detrital elements and latitudinal shifts in the Pacific mid-tropospheric subtropical ridge

Millennial-scale reorganizations of the wind systems in the areas surrounding Baja California and the Mazatlan Margin are not only highlighted in changes in upwelling and intermediate water ventilation, but are also visible in the bulk composition of detrital elements in core MD02-2518. The cores show cyclical changes in Si/Al, K/Al and Ti/Al, which are in phase with stadial/interstadial changes observed in Greenland ice-core records from 0-130kyrs BP (Fig. 5.5). The fluctuations are generally driven by changes in transport mechanisms, which the author believes to be of a predominantly fluvial origin due to the proximity of the core to the Mexican mainland and the western foothills of the Sierra Madre Occidental, where most of the Mexican monsoon rains are primarily centred throughout the summer months (Douglas et al. 1993). In addition the geochemical imprint of the sediments may be affected, to a lesser degree, by changes in direction and strength of marine currents that run along the continental shelf. High-frequency variations in the concentration of K, Si and Ti in the Mazatlan Margin occur in tandem with Greenland D-O events. Bulk concentrations of detrital elements increase by as much as 50% during stadials (Fig. 5.5), suggesting more humid conditions with increased precipitation and the concomitant fluvial transport of terrigenous material from the Mexican mainland (Fig 5.8).

The locations of upper air ridges and troughs are the main atmospheric variables that determine precipitation patterns over Mexico (Metcalfe et al., 2000). A more southerly position of the mid-tropospheric subtropical ridge, the area of high pressure associated with the descending branch of the Hadley cell situated around the latitudes of 30°N in the Northern Hemisphere, is associated with wetter conditions in the Sonoran deserts, NW Mexico and areas adjacent to the Gulf of California, while a northerly location is associated with dry periods. In addition, El Niño years are associated with high rainfall in the usually dry northwest of Mexico following a relaxation in wind-driven upwelling, weaker Hadley and Walker circulation patterns and a relaxation of the eastern equatorial Pacific sea surface temperature gradients (Koutavas et al., 2002).

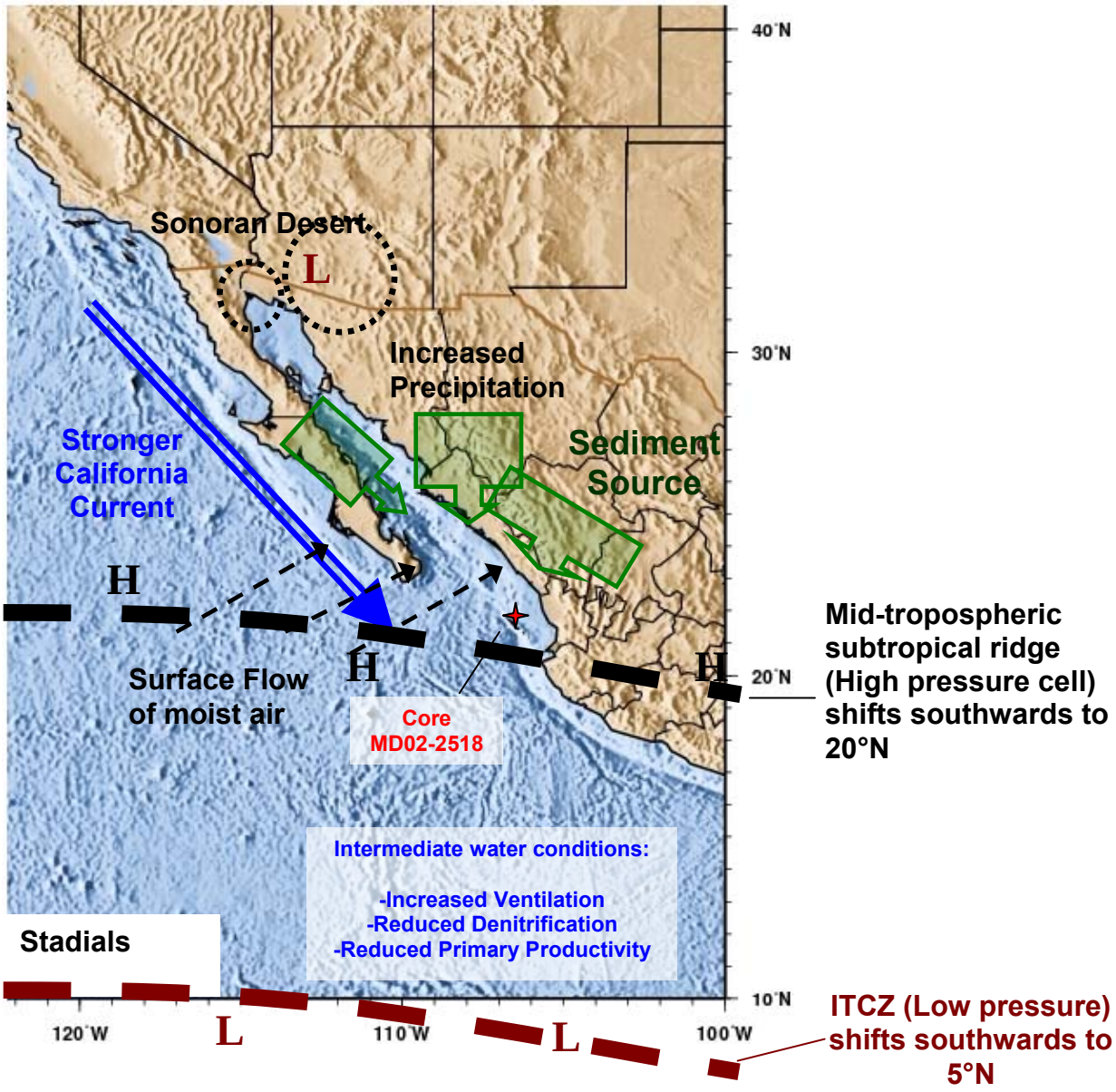

Figure 5.8: Generalised illustration of the sources of sediment which led to increased concentrations of detrital elements in core MD02-2518 during intervals that corresponded with Greenland stadials. Throughout these intervals, the author postulates that a more southerly position of the ITCZ (as proposed by Haug et al., 2001; Ivanocko et al., 2005 and Leduc et al., 2007) would have led to the mid-tropospheric subtropical ridge shifting southwards. This would in turn have increased the onshore flow of moist air, ultimately leading to increased precipitation along the western Mexican Margin, resulting in increased deposition of detrital elements in the core area. The southward shift in the ITCZ and the subtropical ridge, coupled with a relaxation in wind-driven upwelling, a weaker Hadley and Walker circulation (Koutavas et al., 2002) and a relaxation of the eastern equatorial Pacific sea surface temperature gradients are all indicative of a persistent El Niño-like pattern in the ETNP throughout stadials.

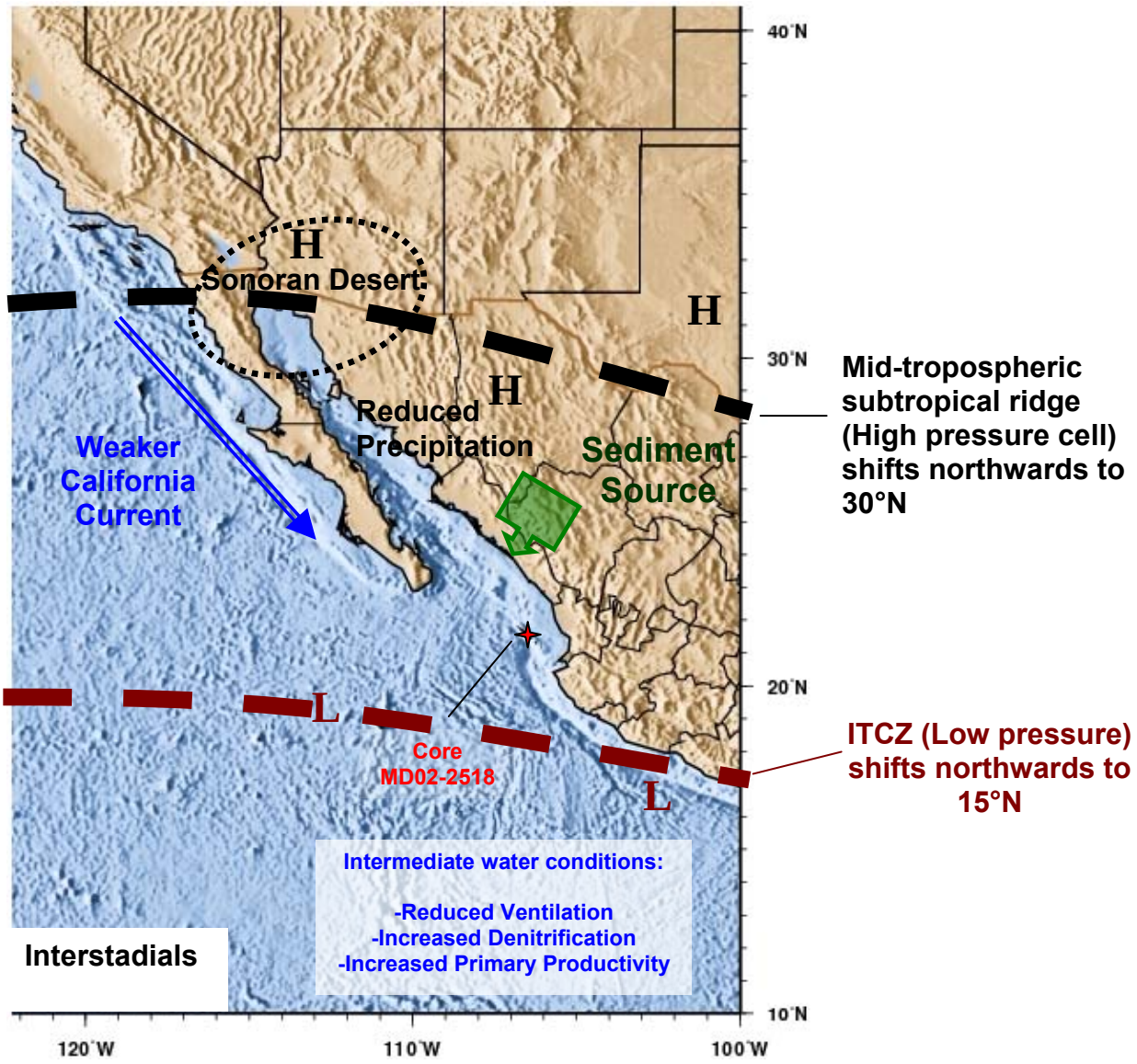

Figure 5.9: Illustration of conditions along NW Mexico during interstadials which would have resulted in the reduced deposition of detrital elements in core MD02-2518. The northward shift of the ITCZ and subtropical ridge, coupled with the retreat of the Mexican Low southward and inland would have led to arid conditions and increased upwelling in the area surrounding core MD02-2518.

The lithogenic records presented in this study (Fig. 5.5) are indicative of a southerly shift of the mid-tropospheric subtropical ridge throughout stadials, which resulted in a deepening of the Mexican Low over the head of the Gulf of California and increased precipitation throughout NW Mexico, resulting in an increase in the sedimentary input of detrital material to the core location. The southerly shift of the subtropical ridge is likely to have been a direct result of the southward movement in

the mean location of the ITCZ that has been suggested to occur during stadials (Haug et al., 2001; Ivanocko et al., 2005 and Leduc et al., 2007). This shift in tropical convection, coupled with an eastward shift in the equatorial convergence zone, a reduction in the intensity of wind-driven upwelling along the ETNP, an onshore surface flow of moist air resulting in increased precipitation over the Gulf of California and NW Mexico are all indicative of a persistent "super-ENSO" state (Stott et al., 2002) during stadials. These conditions would have been contrasted by increased upwelling, offshore winds and drier conditions along the north-western Mexican Margin throughout interstadials resulting from the strengthening of the subtropical ridge along 30°N (Fig. 5.9).

However, what remains yet unclear is how changes in the high latitudes and low latitudes interact with each other and what the driving factors for these changes are. Does climate variability originate at high latitude and propagate to the tropics or vice versa? Following the discovery of millennial-scale climate variability in many sites at low latitudes, McIntyre and Molfino (1996) suggested that rapid climate oscillations might emanate from the tropics, where they originate as unstable responses to insolation. The most likely tropical source of rapid climate variability affecting the ETNP is likely to reside in a combination of variations between persistent El Niño Southern Oscillation events affecting the eastern tropical Pacific during stadials (Clement et al., 2000; Rosenthal and Broccoli, 2004) and millennial-scale fluctuations of moisture transport from the Atlantic to the Pacific ocean across Central America, which ultimately modulates the North Atlantic freshwater budget and hence North Atlantic Deep Water formation (Leduc et al., 2007). The reconstruction of the local precipitation patterns in NW Mexico presented in this study has wider implications: the "super-ENSO" state previously documented as a relaxation of sea-surface temperature (SST) gradients in the cold tongue of the equatorial Pacific (Koutavas et al., 2002) and in Corals from Papua New Guinea (Tudhope et al., 2001) can be extended to include stadial-interstadial variations in detrital element deposition documented in the ETNP, which are most likely the result of variations in trade winds, zonal SST gradients and zonal moisture transport patterns between the Pacific and the Gulf of Mexico. Ivanochko et al. (2005) recently suggested that the global magnitude of millennial-scale signals is amplified by

modulations in the tropical hydrological cycle and tropical emissions of greenhouse gases. These variations in tropical convection are driven by latitudinal shifts in the ITCZ and would affect heat transfers to higher latitudes by atmospheric teleconnections, ultimately amplifying millennial-scale changes.

5.9 Conclusion

Coastal upwelling, productivity and intermediate water denitrification in the ETNP for the past 200,000 years and past reorganizations of wind systems off Baja California and NW Mexico over the past 130,000 years have been reconstructed by means of analysis of a giant piston core recovered from Mazatlan Margin. Millennial-scale variations observed in the ETNP are synchronous with Dansgaard-Oeschger temperature variations measured observed in Greenland ice cores. The sediments have $\delta^{15}N$ values ranging between 6-10 ‰, indicating that the intense denitrification occurring within intermediate waters of the ETNP are likely to be related to changes in local productivity as much as changes in the remote ventilation of intermediate waters.

The cyclical changes in detrital elements are in phase with stadial/interstadial changes observed in Greenland records of temperature variability, with stadials corresponding to a southerly position of the mid-tropospheric subtropical ridge (and ITCZ) and wetter conditions in the Sonoran desert and areas adjacent to the Gulf of California, while interstadials are linked to a more northerly location of the subtropical ridge leading to more arid condition along the ETNP. To summarise, during stadials the portion of the ETNP surrounding the Mazatlan Margin would have been characterised by:

- reduced upwelling and reduced primary productivity;
- a less intense OMZ leading to reduced denitrification;
- a stronger California Current (Herbert et al., 2001);
- wetter conditions in NW Mexico following a more westerly wind flow of moist air associated with the Mexican Low being situated at the head of the Gulf of California.

The data appears to reinforce a concept which implies a persistent shift in the tropical Pacific ocean/atmosphere system analogous to modern El Niño/Southern

Oscillation of an “El Niño” state (reduction in the intensity of wind-driven upwelling along the ETNP and an onshore surface flow of moist air resulting in increased precipitation over the Gulf of California and NW Mexico) during stadials, and more persistent “La Niña” conditions (intensified wind-driven upwelling along the ETNP and an offshore surface flow of dry air resulting in more arid conditions in areas surrounding the Gulf of California and NW Mexico) correlating with interstadials. These conditions are indicative of close feedback links between the atmospheric moisture zonal transfers, wind patterns, SSTs and ITCZ latitudinal variability in the eastern Pacific.

References

Altabet, M.A., Francois, R., Murray, D.W., Prell, W.L. (1995) Climate-related variations in denitrification in the Arabian Sea from sediment 15N/14N ratios. *Nature*, vol. **373**, pp. 506-509

Altabet, M.A., Higginson, M. and Murray, D.W. (2002) The effect of millennial-scale changes in Arabian Sea denitrification on atmospheric CO2. *Nature*, vol. **415**, pp. 159-162

Arrigo, K.R. (2005) Marine microorganisms and global nutrient cycles. *Nature*, vol. **437**, pp. 349-355

Beaufort, de Garidel-Thoron, T., Mix, A.C. and Pisias, N.G. (2001) ENSO-like Forcing on Oceanic Primary Production During the Late Pleistocene. *Science*, vol. **293**, pp. 2440-2444

Beckmann, B., Floegel, S., Hofmann, P., Schulz, M. and Wagner, T. (2005) Orbital forcing of Cretaceous river discharge in tropical Africa and ocean response. *Nature*, vol. **437**, pp. 241–244

Behl, R. J., and J. P. Kennett (1996) Evidence for brief interstadial events in the Santa Barbara Basin, NE Pacific during the past 60 Kyr. *Nature*, vol. **379**, pp. 243– 246.

Bender, M., Sowers, T., M.-L. Dickson, J. Orchardo, P. Grootes, P. Mayewski and D. Meese (1994) Climate correlations between Greenland and Antarctica during the past 100,000 years. Nature, vol. 372, pp. 663-666

Blunier, T., Barnett, B., Bender, M.L., and. Hendricks, M.B. (2002), Biological oxygen productivity during the last 60,000 years from triple oxygen isotope measurements. *Global Biogeochem. Cycles*, vol. **16**, doi:10.1029/2001GB001460

Brandes, J.A. and Devol, A.H. (2002) A global marine nitrogen isotopic budget: Implications for Holocene nitrogen cycling. *Global Biogem. Cycles*, vol. **16**, 1120

Broecker, W.S. and Henderson, G.M. (1998), The sequence of events surrounding Termination II and their implications for the cause of glacial-interglacial CO2 changes. *Paleoceanography*, vol. **13**, pp. 352– 364

Capone, D.G., Zehr, J.P., Paerl, H.W., Bergman, B., Carpenter, E.J. (1997) Trichodesmium, a Globally Significant Marine Cyanobacterium. *Science*, vol. **276**, pp. 1221-1229

Carleton, A.M., Carpenter D.A. and Weber, P.J. (1990) Mechanisms of interannual variability of the Southwest United States summer rainfall maximum. *Journal of Climate*, vol. **3**, pp. 99-1015

Clement, A.C., Seager, R., Cane M.A. (2000) Suppression of El Nino during the Mid-Holocene by changes in the Earth's orbit. *Paleoceanography*, vol **15**, pp. 731-737

Cline, J.D., Wisegarver, D.P. and Kelly-Hansen, K. (1987) Nitrous oxide and vertical mixing in the equatorial Pacific during the l982-1983 El Nino. *Deep-Sea Res*., vol. 34, pp. 857-873

Codispoti, L.A. and Christensen, J.P. (1985) Nitrification, denitrification and nitrous oxide cycling in the eastern tropical South Pacific Ocean. *Mar. Chem*., vol. **16** ,pp. 277-300.

Codispoti, L.A., Brandes, J.A., Christensen, J.P., Devol, A.H., Naqvi, S.W.A., Paerl, H.W., and Yoshinari, T. (2001) The oceanic fixed nitrogen and nitrous oxide budgets: Moving targets as we enter the anthropocene?, *Sci. Mar*., vol. **65**, pp. 85–105

Dalsgaard, T., Canfield, D.E., Petersen, J., Thamdrup, B. & Acuña-González, J. (2003) N_2 production by the anammox reaction in the anoxic water column of Golfo Dulce, Costa Rica. *Nature*, vol. **422**, pp. 606-608

De Pol-Holz, R., Ulloa, O., Dezileau, L., Kaiser, J., Lamy, F., Hebbeln, D. (2006) Melting of the Patagonian Ice Sheet and deglacial perturbations of the marine nitrogen cycle in the eastern South Pacific. *Geophysical Research Letters*, vol. **33**, L04704, doi:10.1029/2005GL024477

Douglas, M.W., Maddox, R., Howard K. and Reyes. S. (1993) The Mexican Monsoon. *Journal of Climate*, vol. **6**, pp.1665-1667

Elkins, J.W., Wofsy, S.C., McElroy, M.B., Kolb, C.E. and Kaplan. W.A., (1978). Aquatic sources and sinks for nitrous oxide. *Nature*, vol. **275**, pp. 602-606.

Falkowski, P. (1997) Evolution of the nitrogen cycle and its influence on the biological sequestration of CO2 in the ocean, *Nature*, vol. **387**, pp. 272-275

Fluckiger, J., Monnin, E., Stauffer, B., Schwander, J., Stocker, T.F., Raynaud, J.C.D. and Barnola, J.-M. (2002) High-resolution holocene N_2O ice core record and its relationship with CH_4 and CO_2. *Global Biogeochem. Cycles*, vol. **16(1)**, doi: 10.29/2001GB001417

Fluckiger, J. Knutti, R. White, J. W. C. (2006) Oceanic processes as potential trigger and amplifying mechanisms for Heinrich events. *Paleoceanography*, vol. **21**, PA2014, doi: 10.1029/2005PA001204
Ganeshram, R.S., Pedersen, T.F., Calvert, S.E. and Murray, J.W. (1995) Large changes in oceanic nutrient inventories from glacial to interglacial periods. *Nature*, vol. **376**, pp. 755-757

Ganeshram, R.S. and Pedersen, T.F. (1998) Glacial-interglacial variability in upwelling and bioproductivity off NW Mexico: implications for Quaternary paleoclimate. *Paleoceanography*, vol. **13**, pp. 634-635

Ganeshram, R.S., Pedersen, T.F., Calvert, S.E., McNeill G.W., Fontugne M.R. (2000) Glacial-Interglacial variability in denitrification in the world's oceans: Causes and consequences. *Paleoceanography*, vol. **15**, pp 361-376

Ganeshram, R.S., Pedersen, T.F., Calvert, S.E. and Francois, R. (2002) Reduced nitrogen fixation in the glacial ocean inferred from changes in marine nitrogen and phosphorus inventories. *Nature*, vol. **415**, pp. 156-159

Gruber, N (2004) The dynamics of the marine nitrogen cycle and its influence on atmospheric CO_2 variations. *The ocean carbon cycle and climate.* Edited by Mick Follows; Temel Oguz; North Atlantic Treaty Organization. Scientific Affairs Division. Dordrecht ; Boston : Kluwer Academic Publishers, pp 97-148.

Haug, G.H., Hughen, K.A., Sigman, D.M., Peterson, L.C. and Rohl, U. (2001) Southward migration of the intertropical convergence zone through the Holocene. *Science*, vol. **293**, pp. 1304–1308

Hendy I. and J. Kennett, 2000, Dansgaard/Oeschger cycles and the California Current System; Planktonic foraminiferal response. Paleoceanography, vol. **15**, pp. 30-42

Hendy, I.L., Pedersen T.F., Kennett J.P., and Tada R. (2004) Intermittent existence of a southern Californian upwelling cell during submillennial climate change of the last 60kyr. *Paleoceanography*, vol. **19**, PA3007, doi:10.1029/2003PA000965.

Herbert, T.D., Schuffert, J.D., Andreasen, D., Heusser, L., Lyle, M., Mix, A., Ravelo, A.C., Stott, L.D., Herguera, J.C. (2001) Collapse of the California Current during glacial maxima linked to climate change on land. *Science*, vol. **293**, pp. 71-76

Indermuehle, A., Monnin, E., Stauffer, B., Stocker, T.F. and Wahlen, M. (2000) Atmospheric CO_2 concentration from 60 to 20 kyr BP from the Taylor Dome ice core, Antarctica. *Geophys. Res. Lett.*, vol. **27(5)**, pp. 735–738

Ivanochko, T.S., Ganeshram, R.S., Brummer, G.J.A., Ganssen, G., Jung, S.J.A., Moreton, S.G.,

Kroon, D. (2005) Variations in tropical convection as an amplifier of global climate change at the millennial scale. *Earth and Planetary Science* Letters, vol. **235**, pp. 302–314

Karl, D., Michaels, A., Bergman, B., Capone, D., Carpenter, E., Letelier, R., Lipschultz, F., Paerl, H., Sigman, D. and Stal L. (2002) Dinitrogen fixation in the world's oceans. *Biogeochemistry*, vol. **57/58**, pp. 47– 98

Kienast, M. (2000), Unchanged nitrogen isotopic composition of organic matter in the South China Sea during the last climatic cycle: Global implications. *Paleoceanography*, vol. **15**, 244– 253

Knox, F., and McElroy, M. (1984) Changes in atmospheric CO_2: influence of marine biota at high latitudes. *J. Geophys. Res.*, vol. **89**, pp. 4629–4637

Kohfeld, K.E., Le Quéré, C., Harrison, S.P. and Anderson R.F. (2005) Role of Marine Biology in Glacial-Interglacial CO_2 Cycles. *Science*, vol. **308**, pp. 74-78

Koutavas, A., Lynch-Stieglitz, J., Marchitto T.M. and Sachs, J.P (2002) El Niño-Like Pattern in Ice Age Tropical Pacific Sea Surface Temperature. *Science*, vol. **297**, pp. 226-230

LaRoche, J. and Breitbarth, E. (2005) Importance of diazotrophs as a source of new nitrogen in the ocean. *J. Sea Res.*, vol. **53**, pp. 67–91

Leduc, G., Vidal, L., Tachikawa, K., Rostek, F., Sonzogni, C., Beaufort, L. and Bard, E., (2007) Moisture transport across Central America as a positive feedback on abrupt climatic changes. *Nature*, vol. **445**, pp. 908-911

McElroy, M. B. (1983) Marine biological controls on atmospheric CO_2 and climate. *Nature*, vol. **302**, pp. 328– 329

McIntyre, A., and Molfino, B. (1996) Forcing of Atlantic equatorial and subpolar millennial cycles by precession. *Science,* vol. **274**, pp.1867–1870

McManus, J., Oppo, D.W., Cullen, J.L. (1999) A 0.5-Million-Year Record of Millennial-Scale Climate Variability in the North Atlantic. *Science*, vol. **283**, pp 971- 975

Meissner, K.J., Galbraith, E.D., Volker, C. (2005) Denitrification under glacial and interglacial conditions: A physical approach. *Paleoceanography*, vol. **20**, PA3001, doi:10.1029/2004PA001083

Metcalfe S.E., O'Hara S.L., Caballero M., Davies S.J. (2000) Records of Late Pleistocene-Holocene climatic change in Mexico - a review. *Quaternary Science Reviews*, vol. **19**, pp. 699-721

Michaels, A.F., Karl, D.M. and Capone, D.G. (2001) Element stoichiometry, new production nitrogen fixation. *Oceanography*, vol. **14**, pp. 68–77

Monnin, E., Indermuhle, A., D¨allenbach, A., Fluckiger, J., Stauffer, B., Stocker, T.F., Raynaud, D., and Barnola, J.-M. (2002) Atmospheric CO_2 concentrations over the last glacial termination. *Science*, vol. **291**, pp. 112–114

Nameroff, T.J., Calvert S.E. and Murray, J.W. (2004) Glacial-interglacial variability in the eastern Tropical North Pacific oxygen minimum zone recorded by redox-sensitive trace metals. *Paleoceanography*, vol. **19**, pp. 1-19

NGRIP members (2004) High-resolution record of Northern Hemisphere climate extending into the last interglacial period, *Nature*, vol. **431**, pp 147- 151

Pedersen, T.F., Nielsen, B. and Pickering, M. (1991) The timing of Late Quaternary productivity pulses in the Panama Basin and implications for atmospheric CO_2. *Paleoceanography*, vol. **6**, pp. 657-677

Pride, C., Thunell, R., Sigman, D., Keigwin, L., Altabet, M., and Tappa, E. (1999) Nitrogen isotopic variations in the Gulf of California since the last deglaciation: Response to global climate change. *Paleoceanogr*., vol. **14**, pp. 397–409

Redfield, A.C., Ketchum, B.H. and Richards, F.A. (1963) The influence of organisms on the composition of sea-water, in The Sea, edited by M. N. Hill, vol. **2**, pp. 26–77, Wiley-Interscience, New York.

Rosenthal, Y and Broccoli A.J. (2004) In Search of Paleo-ENSO. *Science*, vol. **304**, pp. 219 - 221

Sigman, D.M., Altabet, M.A., Michener, R., McCorkle, D.C., Fry, B., Holmes, R.M. (1997) Natural abundance-level measurement of the nitrogen isotopic composition of oceanic nitrate: an adaptation of the ammonia diffusion method. *Marine Chemistry*, vol. **57**, pp. 227-242

Sigman, D.M. and Haug, G.H. (2003) Biological pump in the past, in *Treatise On Geochemistry*, edited by H. D. Holland, K. K. Turekian, and H. Elderfield, pp. 491– 528, Elsevier Sci., New York.

Stott, L., Poulsen, C., Lund, S., Thunell, R. (2002) Super ENSO and Global Climate Oscillations at Millennial Time Scales. *Science*, vol. **297**, pp. 222-226

Thunell, R.C., and Kepple A.B. (2004) Glacial-Holocene $\delta^{15}N$ record from the Gulf of Tehuantepec, Mexico: Implications for denitrification in the eastern equatorial Pacific and changes in atmospheric N2O. *Global Biogeochem. Cycles*, vol. **18,** GB1001, doi:10.1029/2002GB002028

Tudhope, A.W., Chilcott, C.P. McCulloch, M.T. Cook, E.R.. Chappell, J Ellam, R.M. Lea, D.W. Lough, J.M and Shimmield, G.B. (2001) Variability in the El Nino-Southern Oscillation through a glacial-interglacial cycle. *Science*, vol. **291**, pp. 1511-1517

Venrick, E.L. (1997) The distribution and significance of *Richelia intracellularis* in the North Pacific Central gyre. *Limnol. Oceanogr*., vol. **19**, pp. 437-444

Wedepohl K.H. (1995) The composition of the continental crust. *Geochim. Cosmochim.* Acta, vol. **59**, pp. 1217–1232

Yarincik, K.M., Murray, R.W. and Peterson, L.C. (2000) Climatically Sensitive Eolian and Hemipelagic Deposition in the Cariaco Basin, Venezuela, Over the Past 578,000 Years: Results From Al/Ti and K/Al. *Paleoceanogr.*, vol. 15, pp. 210–228.

Yoshinari T., Altabet, M.A., Naqvi, S.W.A., Codispoti, L., Jayakumar, A., Kuhland, M., Devol A. (1997) Nitrogen and oxygen isotopic composition of N_2O from suboxic waters of the eastern tropical North Pacific and the Arabian Sea - measurement by continuous-flow isotope-ratio monitoring. *Marine Chemistry*, vol. **56**, pp. 253-264

CHAPTER 6

Glacial-Holocene $\delta^{15}N$ record from the Gulf of Tehuantepec, Mexico: Implications for denitrification in the eastern equatorial Pacific

ABSTRACT

Cores collected along the NW Mexican continental shelf impinging on the OMZ have shown that the past oxygen content of intermediate waters, rates of water-column denitrification and primary productivity have varied in tandem with climate cycles. So far, cores collected from latitudes north of 20ºN have shown a "Greenland" timing, whereas cores collected south of this latitude show variations that are contemporaneous with changes in sea ice extent and temperature variations in Antarctica. Here we present high-resolution $\delta^{15}N$ records, variations in organic carbon and $\delta^{13}C$, and changes in the concentration of detrital elements from a piston core collected at 720 metres depth in the Gulf of the Tehuantepec, Mexico, that spans the last 45,000 years. The data highlights millennial-scale variations in $\delta^{15}N$ that appear to precede Greenland warming events by a few hundred to a thousand years and a decoupling from organic carbon records records. These features are most likely due to a combination of remote ventilation changes, heavy nitrate "leakage" from the Eastern Tropical South Pacific and local increases denitrification led by strengthening of the *tehuanos* blowing through the gaps in the Sierra Madre Mexican highlands during interstadials. In addition, the profile of terrigenous elements in the Gulf of Tehuantepec mirrors the sediment reflectance record from Cariaco Basin in northern Venezuela throughout the last 15,000 years. However, the detrital element records older than 15,000 years do not show any correlation with the Cariaco records. Due to the relative proximity and similar latitude of the two records, the records are interpreted to be consistent with a northern shift of the Intertropical Convergence Zone (ITCZ) during Early Holocene, with the orographic barrier of Central America imprinting a distinctive signal on east vs. west precipitation patterns. This results in maximum precipitation along the Caribbean coast and minimum precipitation along the Pacific coast of Central America. The interpretation of the detrital records is complicated by the presence of a number of patches of cold sea surface temperatures (SSTs) that develop under these wind jets as a result of enhanced mixing across the base of the ocean mixed layer. These cold patches, together with the varying strength of upwelling would have affected both precipitation patterns and the intensity of the ITCZ in areas surrounding the Gulf of Tehuantepec.

6.1 Introduction

The nitrogen isotope composition of sediments collected from regions of high primary productivity has been used in many instances as a record of spatial and temporal variations in the marine nitrogen cycle. This is a result of the isotopic fractionation that occurs during the uptake up NO_3^- by plankton: in areas of partial NO_3^- utilisation, the nitrogen isotope composition of sinking organic matter (expressed as $\delta^{15}N$ relative to atmospheric N_2) varies with the degree of nutrient utilisation in surface waters. By contrast, in areas where NO_3^- is completely utilized, the $\delta^{15}N$ of sinking organic matter is a reflection of surface and subsurface water NO_3^-, which is largely controlled by denitrification occurring at intermediate water depths, vertical transport through upwelling and lateral transport of water masses through intermediate-depth currents (Cline and Kaplan, 1975; Liu and Kaplan, 1989; Behl and Kennett, 1996; Galbraith et al., 2004). Denitrification leads to the preferential reduction of nitrate containing the light isotope of nitrogen (^{14}N), thus causing the remaining nitrate pool to become progressively enriched in the heavier isotope (^{15}N). As a consequence, any variation in the nitrogen isotope composition of source waters will leave an imprint on the $^{15}N/^{14}N$ ratio of organic N preserved within the underlying marine sediments, thus offering an opportunity to reconstruct past changes in the oceanic nitrogen budget.

At present, suboxic denitrification is a prominent oceanographic feature in three regions: the Eastern Tropical North Pacific (ETNP), the Arabian Sea and the Eastern Tropical South Pacific (Deutsch et al., 2007). A conservative estimate of oceanic suboxic denitrification occurring at intermediate depths suggests a rate of ~150Tg N yr^{-1} (Codispoti et al., 2001). Most nitrogen is lost to the atmosphere through gaseous N_2 and nitrous oxide (N_2O); while the former is an inert diatomic gas that forms 78.1% by volume of the Earth's atmosphere, the latter is a trace gas that is formed as an intermediary of denitrification and which, on a per molecule basis, is 180 times more powerful than CO_2 as a greenhouse gas (Codispoti and Richards, 1976; Yoshinari et al., 1997).

The need to better understand past variations in the marine nitrogen cycle stems from the recognition that nitrate is an essential nutrient for living organisms that is in limited supply in the oceans, but may also indirectly contribute to changes

in climate, as the by-products of denitrification contribute to variations in greenhouse gases and a loss of reactive nitrate may reduce primary productivity and consequently the biological sink for CO_2. At present, our most comprehensive understanding of the global nitrogen cycle derives from its interaction with the carbon cycle in the past. The close coupling between N_2O variations and CO_2 levels throughout the last glacial epoch was highlighted by Fluckinger et al. (1999 and 2004) and many studies have highlighted synchronicities between episodes of past climate change and variations in $^{15}N/^{14}N$ in sediments, representing changes in suboxic denitrification (Altabet et al., 1999 and 2002; Ganeshram et al., 1995; 2000 and 2002). Low-oxygen environments beneath areas of high productivity show a high degree of sensitivity to climate change (Van Geen et al., 2003) and high rates of denitrification have shown to correspond closely with high atmospheric CO_2 levels. Even though it is unlikely that changes in marine denitrification were the main driver of past climate change, it is likely that reductions in the oceanic nitrate inventories contributed to reductions in marine productivity, thus affecting both atmospheric CO_2 and N_2O levels (Gruber and Galloway, 2008).

This chapter examines high-resolution records of nitrogen isotopes, organic carbon and changes in the concentration of detrital elements in a sedimentary record collected at 720m water depth in the Gulf of Tehuantepec, SW Mexico. The comparison covers the past 45,000 years and suggests that records of past productivity, unlike other sites in NW Mexico and California, are decoupled from changes in local denitrification, indicating that the lateral supply of oxygen poor water masses may play a more important role in regulating the timing and extent of the Oxygen Minimum Zone (OMZ) than remineralisation deriving from the overlying primary productivity. The data from our core also highlights how the concentrations of total Si, Ti, and K in the Gulf of Tehuantepec compare with the sediment reflectance from Cariaco Basin in northern Venezuela, a record that monitors the latitudinal mean position of the ITCZ (Haug et al., 2001). The Cariaco record depicts a northward shift of the Intertropical Convergence Zone (ITCZ) during D/O interstadials and a southward migration during stadials, and this chapter will assess how the orographic barrier of Central America imprints a distinctive signal on the effects of precipitation and sedimentary records between the Caribbean

and the Pacific Ocean. Although detrital element concentrations in the Gulf of Tehuantepec mirror the sediment reflectance from Cariaco Basin for the past 15,000 years, there is little similarity between detrital records from 15,000-47,000 years BP, suggesting that the influence of the ITCZ may not have penetrated as far north as the Gulf of Tehuantepec throughout the last glacial.

6.2 Environmental Setting: Upwelling in the Gulf of Tehuantepec as a consequence of Central American Cold Surges

The Gulf of Tehuantepec is characterised by wind-induced coastal upwelling in winter and early spring and by a stratified water column during the summer months (Machain-Castillo et al., 2008). These conditions are influenced by the seasonal latitudinal shifts in the ITCZ and by surges of cold air that move south along the eastern slopes of the Sierra Madre during the winter months producing winds that blow perpendicular to the coastline, commonly known as *tehuanos*. These northerly winds occur during the cold season (November-April), commonly reaching 10-20m s^{-1} and tend to last for 2-6 days, though some of these occurrences have been documented to last for up to 13 days. As the *tehuanos* emerge into the Gulf of Tehuantepec, they displace surface waters away from the shoreline, thus enhancing upwelling, primary productivity and reducing sea surface temperatures by as much as 8°C (Chelton et al., 2000; Xie et al., 2005). The conditions for the development of the *tehuanos* are set by the interaction of Central American cold surges (cold anticyclones that originate at mid-latitudes in the winter) with the Sierra Madre mountain range. At 20ºN, the topography of Sierra Madre mountains acts as a natural barrier to the cold front until the anticyclone reaches the Chivela Pass, a narrow gap in the Sierra Madre extending from the Gulf of Mexico to the Pacific Ocean. This gap produces a pressure gradient leading to strong offshore winds, a phenomenon known as a "gap wind" or *tehuano* when referring to a gap wind extending into the Gulf of Tehuantepec (Fig. 6.1). The ensuing upwelling leads to nitrate concentrations in surface layers reaching above 5 μM and phytoplankton concentrations in the gulf reaching densities from 2-10 mg m^{-3} (Machain-Castillo et al., 2008).

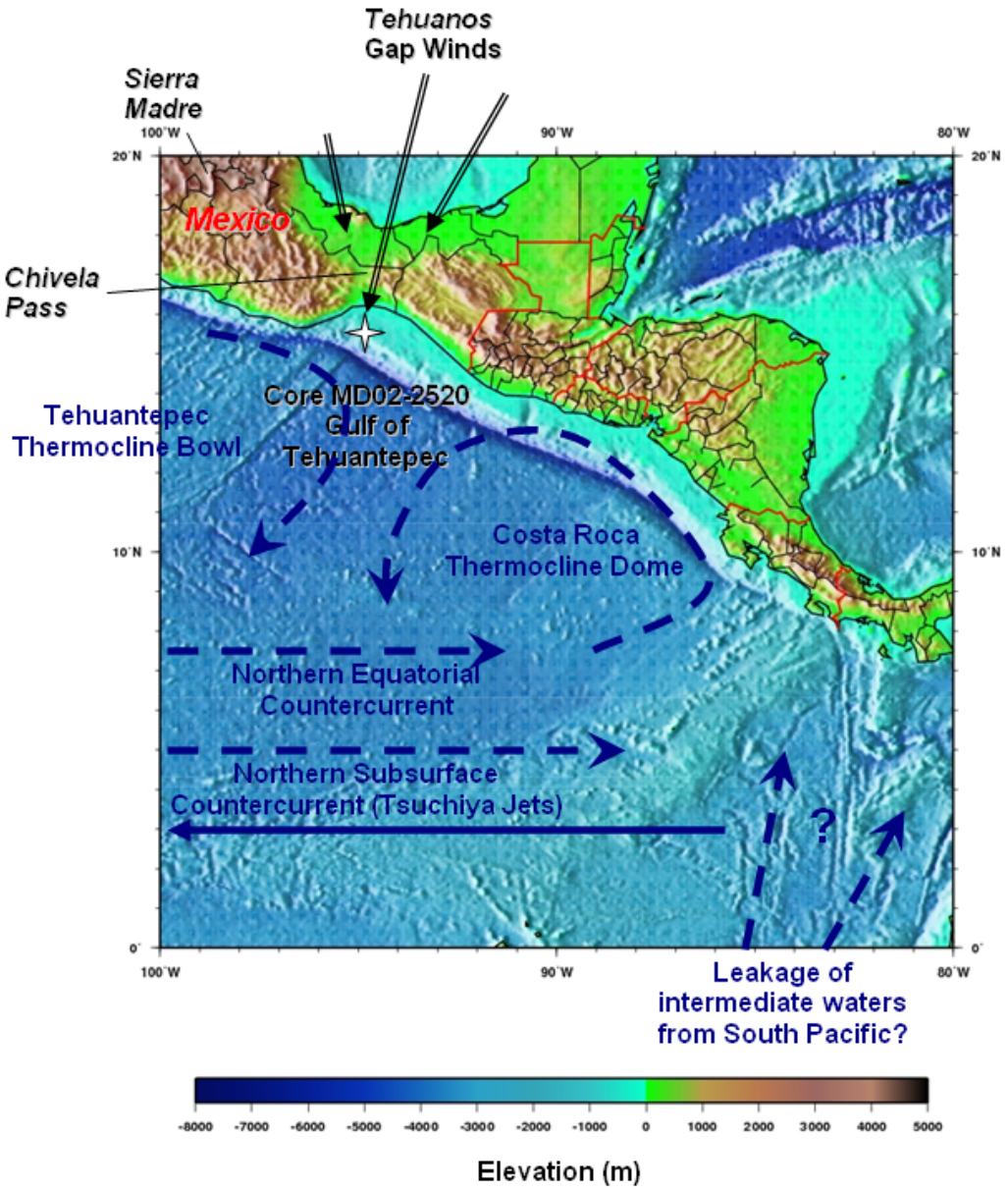

Figure 6.1: Map of Central America showing the location of core MD02-2520 in the Gulf of Tehuantepec, the direction of the winter 'gap winds', the main topographic features and shallow-to-intermediate depth ocean currents in the region. A thermocline "bowl" and "dome" are found in the ETNP, centered at 13°N, 105°W and 9°N, 90°W, respectively. In the Costa Rica Dome the 20°C isotherm (which characterises the thermocline depth in the Tropical North Pacific) rises to about 25m water depth, whereas in the Tehuantepec Bowl the 20°C isotherm is found at about 90m (Kessler, 2006).

6.3 Methods

See chapter 3 of this thesis.

6.4 Results: $\delta^{15}N$ and Organic Carbon

The particulate nitrogen isotope data recorded in samples from core MD02-2520, expressed as $\delta^{15}N$, ranges from 6 - 9.5‰, significantly higher than the mean deep ocean nitrate $\delta^{15}N$ of 5.0‰ (Brandes and Devol, 2002; Deutsch et al., 2004). The lowest values ($\delta^{15}N < 6.5$‰ in Fig. 6.4 (d)) are recorded in sediments deposited throughout the late Holocene and Last Glacial Maximum (LGM = 18-23kyr BP; Thunell and Kepple, 2004), indicating either a decrease in water-column denitrification during these periods, or by increased lateral supply of oxygen ventilation (Ganeshram et al., 2000; Kienast et al., 2002). The highest values are found between 13-15kyr BP and throughout two major symmetrical peaks occurring during MIS3 between 36-39kyr BP and 44-46kyr BP (within radiocarbon dating errors), which coincide respectively with D/O events 8 and 12 (Dansgaard et al., 1993; Grootes et al., 1993). The period from 36kyr BP to the LGM is punctuated by a series of gradual and relatively symmetrical millennial-scale increases in denitrification, which may suggest that the origin of $\delta^{15}N$ records is somehow associated with both the shorter and less pronounced climate variability found in the Antarctic EPICA Dronning Maud Land (EDML; EPICA Community Members, 2006) and the abrupt variability observed in Greenland records.

The high rates of sedimentation in the Gulf of Tehuantepec (50-90 cm kyr^{-1}) indicate that the % C_{org} record from core MD02-2520 is more likely to indicate changes in paleoproductivity than variations in organic matter preservation (Calvert et al., 1992; Calvert et al., 1995). The C_{org} content ranges between 3 - 6.5 wt.% and appears to be decoupled from variations in the nitrogen isotope record (Fig. 6.4 (d) and (e)). This decoupling is especially highlighted in sediments deposited throughout the deglaciation, where the $\delta^{15}N$ record shows a gradual increase, followed by a gradual decrease during the Holocene, in contrast to the C_{org} record that shows a more abrupt "on or off" pattern throughout the last 20kyrs. The highest C_{org} values are to be found from 16-10kyr BP and during the Late Holocene, with the latter mostly due to enhanced preservation of organic carbon in relatively "young" sediments at the top of the core. By contrast, peaks in C_{org} contents of sediments older than 20kyr BP occur with a frequency that is more similar in timing to

millennial-scale warming events observed in Greenland. There is also a remarkable synchroneity in timing between minima in organic carbon contents at 16kyr, 24kyr, 31kyr and 39kyr and Heinrich events recorded in Greenland ice cores. $\delta^{13}C$, $\delta^{15}N$ and C/N values were used to study the origin of sedimentary organic matter in the Gulf of Tehuantepec (Fig 6.5). The binary mixing equation (Thornton and McManus, 1994) for $\delta^{13}C$ and $\delta^{15}N$ values of terrigenous ($\delta^{13}C_{terrestrial}$= -28‰; $\delta^{15}N_{terrestrial}$= +1.7‰; C/N >20) and marine organic matter ($\delta^{13}C_{marine}$= -21‰; $\delta^{15}N_{marine}$= +7.1‰; C/N = 8-12) confirms that the organic matter in core MD02-2520 has a predominantly planktonic origin ($\delta^{13}C$= -19.5 - -21.5‰; $\delta^{15}N$= 6 -10‰; and C/N = 8-12; Fig 6.5).

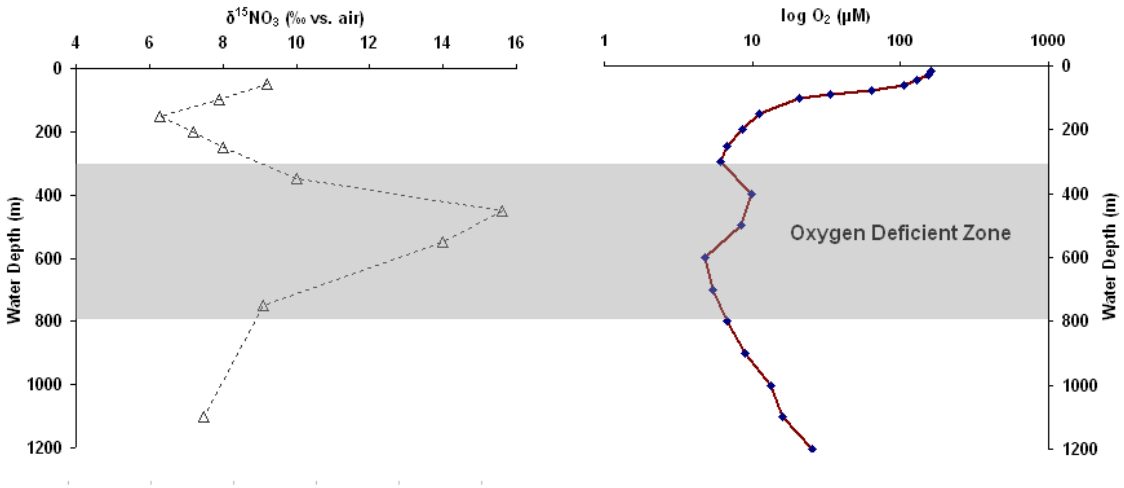

Figure 6.2: Water column profiles of $\delta^{15}NO_3$ and $[O_2]$ in the Gulf of Tehuantepec (15°39.37'N 95°16.85'W) during the upwelling season (November-March). The shaded area represents the approximate depth of the OMZ in the Gulf (Thunell and Kepple, 2004).

(*next page*) Figure 6.3: Denitrification and organic carbon millennial-scale changes in the Gulf of Tehuantepec during the last 50,000 years compared with Greenland stable isotope records of past temperature variations. a) GISP2 $\delta^{18}O$ ice core record highlighting climate fluctuations in Greenland over the past 50,000 years (Grootes et al., 1993); b) glacial-interglacial transition of marine denitrification from core GeoB 7139-2 (30°12'S, 71°59'W, 3269 m depth), collected from the Chilean margin at the southern edge of the present-day OMZ; c) $\delta^{13}C_{org}$ record from core MD02-2520, showing lighter values (~21‰) coinciding with periods of enhanced upwelling [as evidenced by higher $\delta^{15}N$ and C_{org} values in d) and e)]. The observed variations in $\delta^{13}C_{org}$ are probably produced by changes in the isotopic composition and the concentration of dissolved $CO_{2\ which}$ is welled up from intermediate depths in the Eastern Pacific; d) high resolution $\delta^{15}N$ record from core MD02-2520; e) weight percentage C_{org} record from core MD02-2520. Numbers above major Greenland interstadials (3-12) indicate the respective D/O event. B/A = Bolling / Allerod warm period. Y/D = Younger Dryas cold period. H1-H4 and the corresponding yellow shading indicate Heinrich events. The black arrows in e) highlight the position of organic C % minima in core MD02-2520 which appear to coincide with Heinrich events. The triangles indicate the position of ^{14}C radiocarbon measurements throughout the core.

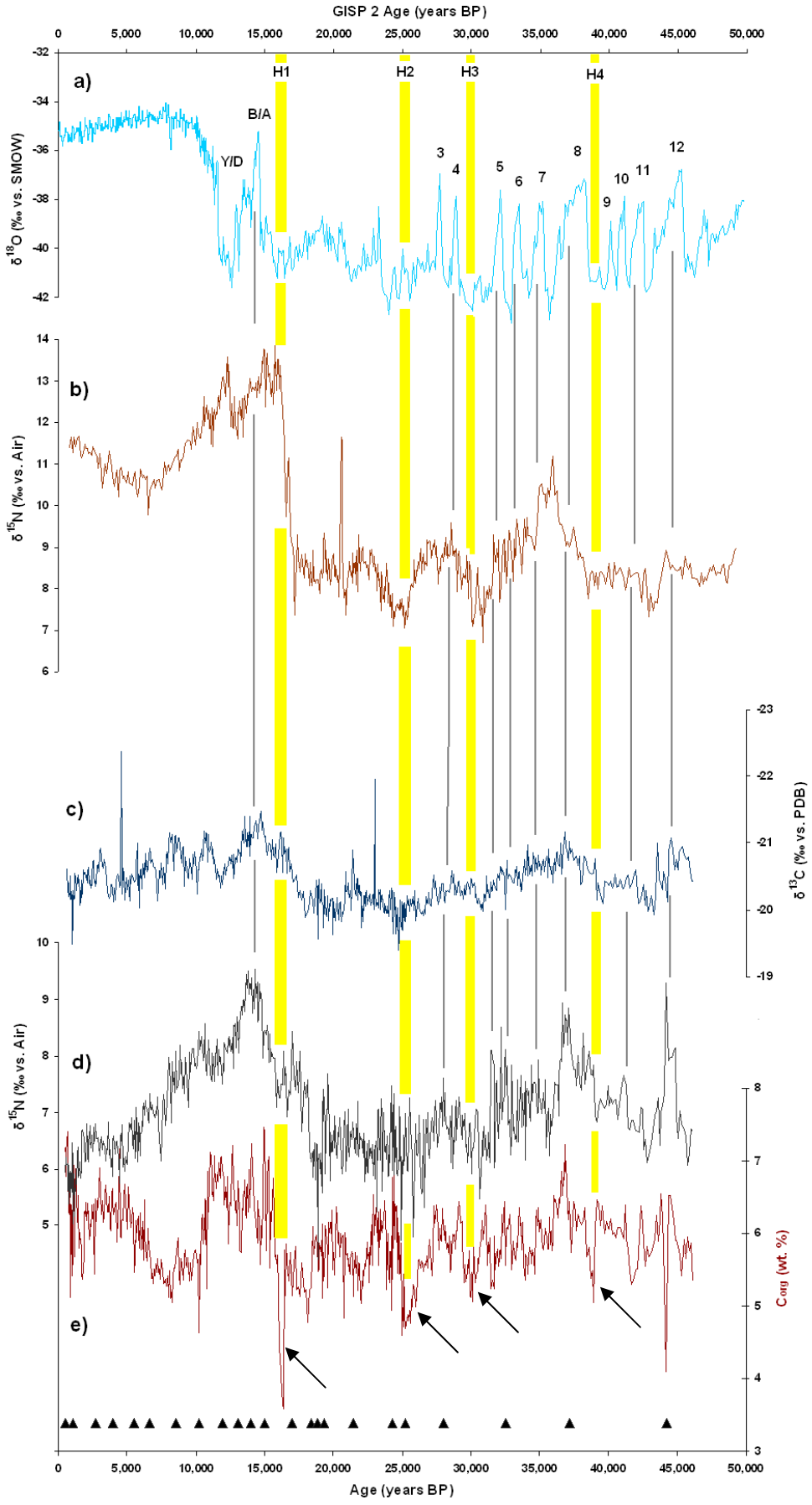
GISP 2 Age (years BP)
0
5,000
10,000
15,000
20,000
25,000
30,000
35,000
40,000
45,000
50,000
a)
H1
H2
H3
H4
B/A
Y/D
3
4
5
6
7
8
9
10
11
12
δ18O (‰ vs. SMOW)
-32
-34
-36
-38
-40
-42
b)
δ15N (‰ vs. Air)
14
13
12
11
10
9
8
7
6
c)
δ13C (‰ vs. PDB)
-23
-22
-21
-20
-19
d)
δ15N (‰ vs. Air)
10
9
8
7
6
5
e)
Corg (wt. %)
8
7
6
5
4
3
Age (years BP)

6.5 Results: Detrital elements

Si/Al variations in core MD02-2520 (Fig 6.4e) record the input of biogenic Si (opal) from diatoms and other siliceous phytoplankton as well as the lateral input of lithogenic (detrital) Si. The average Si/Al ratio of approximately 2.7-2.8 is slightly below the crustal average of 3.1 (Wedepohl, 1995) and likely reflects the input from basic (Si-poor) Mesozoic and Permian intrusive gabbros surrounding the Gulf of Tehuantepec as sediments recovered from the western portion of the Gulf of Tehuantepec are composed of up to 50% of garnets, 20-50 % amphiboles and up to 20% chlorite (Boumaggard et al., 1998 - see chapter 2.6 for a description of the surface geology surrounding the Gulf of Tehuantepec). The Si/Al ratio is highest (>2.9) during Late Holocene, from 11-16kyr BP and during a short interval at 42kyr. While the latter may represent the coarser fraction of a turbidite, the younger increases are replicated in the K/Al and Ti/Al records.

K is associated with continental siliciclastics (clay minerals and feldspars) that have experienced only moderate amounts of chemical alteration (Yarincik et al., 2000). K/Al ratios range from 0.16 – 0.28, with the highest values in Late Holocene, 11-16kyr BP, 37-39kyr BP and during a short interval at 42kyr that coincides with the Si/Al peak. Titanium minerals (ilmenite, augite, rutile and anatase) are classically considered to be very resistant to weathering in soils and Ti is generally insensitive to environmental redox variations (Haug et al., 2001). Both minerals are often transported via fluvial pathways into marine sediments and can be interpreted to reflect changes in terrigenous sediment input (Peterson et al., 2000). Ti/Al ratios range from 0.036 – 0.055, with the highest values from 11-16kyr BP. In contrast to the Si and K profiles, the short interval at 42kyr coincides with a Ti/Al minimum.

The profiles of terrigenous elements in the Gulf of Tehuantepec tend to bear a very moderate resemblance to the reflectance data for the last 15,000 years from core ODP 1002 collected in the Cariaco Basin, Venezuela. For example, the Younger Dryas cold period is marked by higher reflectance, and the concomitant interval in the Gulf of Tehuantepec shows higher concentrations of Si, K and Ti. Due to the similar latitude of the two records, this study will try to interpret the terrigenous element data in terms of precipitation and its effects on local river runoff, and the variability in the position of the ITCZ throughout the Holocene and Late Glacial.

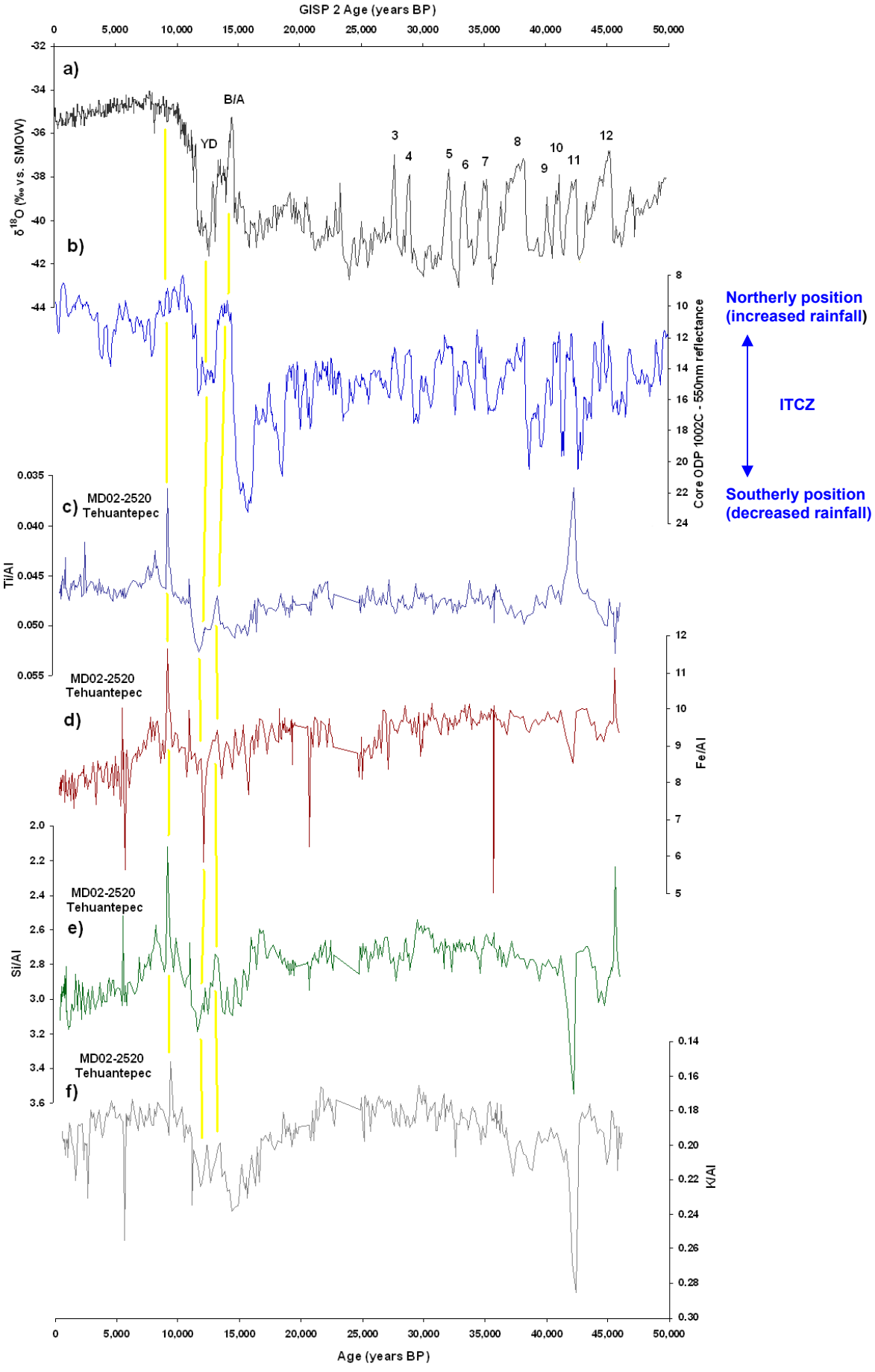
GISP 2 Age (years BP)
0
5,000
10,000
15,000
20,000
25,000
30,000
35,000
40,000
45,000
50,000
a)
B/A
YD
3
4
5
6
7
8
9
10
11
12
δ18O (‰ vs. SMOW)
-32
-34
-36
-38
-40
-42
-44
b)
Core ODP 1002C - 550nm reflectance
8
10
12
14
16
18
20
22
24
Northerly position
(increased rainfall)
ITCZ
Southerly position
(decreased rainfall)
c) MD02-2520
Tehuantepec
Ti/Al
0.035
0.040
0.045
0.050
0.055
MD02-2520
Tehuantepec
d)
Fe/Al
12
11
10
9
8
7
6
5
MD02-2520
Tehuantepec
e)
Si/Al
2.0
2.2
2.4
2.6
2.8
3.0
3.2
3.4
3.6
MD02-2520
Tehuantepec
f)
K/Al
0.14
0.16
0.18
0.20
0.22
0.24
0.26
0.28
0.30
0
5,000
10,000
15,000
20,000
25,000
30,000
35,000
40,000
45,000
50,000
Age (years BP)

(*previous page*) Figure 6.4: Changes in the concentration of detrital elements in the Gulf of Tehuantepec mirror changes in rainfall patterns in the Cariaco Basin during the last 15,000 years. a) Greenland GISP2 paleotemperature record (Stuiver and Grootes, 2000); b) Cariaco basin sediment reflectance, which provides a proxy-record for the latitudinal mean position of the ITCZ from core ODP 1002C (Peterson et al., 2000); c) record of Ti/Al; d) Fe/Al; e) Si/Al; and f) K/Al in core MD02-2520. The sharp increase in Si/Al and K/Al around 42ka may represent quartzose debris and feldspatic sand fractions of a turbidite.

6.6 Discussion: Origin of the $\delta^{15}N$ signal in the Gulf of Tehuantepec

The range of $\delta^{15}N$ values (Fig 6.2) and sedimentation rates from core MD02-2520 is very similar to the range of values published by Thunnel and Kepple (2004) and by Hendy and Pedersen (2006) for jumbo piston core ME0005A 03JC (15°65'N, 95.°28'W) collected at 740m water depth in the Gulf of Tehuantepec – in close proximity to the site of the present study. The relationship between the $\delta^{15}NO_3^-$ of the water column in a nitrate-limited region and the sedimentary record in the ETNP has been established in a number of studies (Altabet et al., 1999; Ganeshram et al., 1995; 2002), suggesting that in the case of core MD02-2520, the $\delta^{15}N$ record can be used as an indicator of the past variability in marine denitrification. The relative abundance of nitrogen isotopes ($\delta^{15}N$) preserved in sedimentary organic matter in the ETNP is a useful proxy for past changes in upwelling, increases in productivity and the associated nitrate utilisation and/or water column ventilation. At present, denitrification is a major sink of fixed nitrogen between 200-400m water depth around 15-25°N in the ETNP. The $\delta^{15}N$ of phytoplankton in the Gulf of Tehuantepec reflects the $\delta^{15}N$ of the upwelled nitrate, as no net isotopic fractionation will take place in an environment in which all nitrate is utilised (Emmer and Thunell, 2000). The sediments in core MD02-2520 collected below the highly productive, nitrate-depleted waters of the gulf have $\delta^{15}N$ values ranging from 6-10 ‰, where higher values reflect the widespread denitrification that occurred throughout the Holocene, Bolling/Allerod and major interstadials within the intermediate waters of the entire ETNP (Ganeshram et al., 1995, Kiefer and Kienast, 2005). $\delta^{15}N$ values above 8‰ recorded in core MD02-2520 are likely to be a result of the upwelling of waters from intermediate depths (200-700m) in the Gulf of Tehuantepec where nitrate $\delta^{15}N$

ranges at present from ~7.5 ‰ at 100-200m depth, increasing to 15 ‰ at 400m depth and 9 ‰ at 700m depth (Fig. 6.2)

Several studies of highly productive, continental margin upwelling areas have shown how global ocean nitrate inventories appear to have varied in synchrony on glacial-interglacial time-scales (and more recently on millennial time-scales), with major areas of water column denitrification in OMZs intensifying during interglacials and decreasing in intensity during cooler periods (Ganeshram et al., 2000, Altabet et al., 1995). The work of Altabet et al. (2002), Ganeshram et al. (2002) and Hendy et al. (2004) respectively highlighted the close correspondence of denitrification in the Arabian Sea, the Mazatlan Margin and Santa Barbara Basin with millennial-scale changes in Greenland, whereas Higginson and Altabet (2004) and De Pol-Holz (2006) highlighted the "Antarctic" timing of sub-Milankovitch shifts in $\delta^{15}N$ records from cores off Chile and Peru. This dichotomy between sedimentary $\delta^{15}N$ records from the Eastern North and South Pacific is due to a combination of local processes (i.e. the strength of gap wind regulating upwelling in the Gulf or the melting of the Patagonia ice-sheet; De Pol-Holz et al., 2006), the source of intermediate waters bathing the OMZs and climatic influences from high latitudes.

Differences between sedimentary $\delta^{15}N$ records collected within these areas of enhanced denitrification (ETNP, ESP and Arabian Sea) are most notable when analysing the timing of high frequency oscillations. Core MD02-2520 was collected 5° latitude south of Mazatlan Margin, though its $\delta^{15}N$ profile is noticeably different from that of core MD02-2518 (Fig 5.3). The most noticeable features include an early increase in the intensity of the OMZ (indicated by higher $\delta^{15}N$ values) taking place at ~17kyr BP and a more gradual and symmetric shape of $\delta^{15}N$ maxima and a timing of the record which is remarkably similar to that of temperature records from Antarctica and marine records of denitrification from the Chilean margin (Fig. 6.3). It emerges that intermediate waters in the Gulf of Tehuantepec may have a different source from that of intermediate waters in the Mazatlan Margin. The separating line between the southern and northern component of the nitrogen isotope regimes in the Eastern Pacific Ocean is yet poorly constrained and is believed to lie between 10-25°N (Hendy and Kennett, 2003; Hendy and Pedersen, 2006). At intermediate water

depths in the area surrounding the Gulf of Tehuantepec, water mass properties of the Pacific Ocean are highly asymmetric and water mass exchanges across the Equator are poorly understood. The interaction between the Pacific Intermediate Water (NPIW), which contains abundant nutrients but is relatively low in oxygen (Talley, 1993), and eastward-flowing Equatorial Undercurrents and Tsuchiya Jets affected by the high oxygen, low salinity signature of the Antarctic Intermediate Water (AAIW) create a steep property gradient at depths of 200–800m where the southern-source and northern-source intermediate water masses meet in the eastern Pacific.

Hendy and Pedersen (2006) have reconstructed the history of the northern and southern component waters based on differences in sediment redox chemistry between the Gulf of Tehuantepec and the Santa Barbara Basin. Their results show that the concentration of trace metals (Mo, Re and Cd) and C_{org} in sediments collected at 574m and 740m depth in the Gulf of Tehuantepec remained constant throughout the LGM and the Holocene, with the exception of a sharp increase above background levels between 16.5-12kyr. This data suggests that from ~17kyr BP, the concomitant increase in trace metal concentrations (Hendy and Pedersen, 2006) and marine C_{org} (this study), coupled with pronounced laminations and heavier $\delta^{15}N$ values (this study and Thunell and Kepple, 2004) indicate a strong depletion in O_2 concentrations in intermediate waters bathing the Gulf of Tehuantepec, while high O_2 concentrations were present in the Santa Barbara Basin (Ivanochko and Pedersen, 2004), along Baja California (van Geen et al., 2003), and along the Mazatlan Margin (this study; Ganeshram et al., 1995; 2002; Ganeshram and Pedersen, 1998).

The unique character imprinted on nitrogen isotope records preserved in the Gulf of Tehuantepec is marked by quasi-symmetrical peaks and a timing that, unlike records from the Arabian Sea and Mazatlan, appears to precede Greenland warming events by a few hundred years to a thousand years. These features are most likely due to a combination of remote ventilation changes, heavy nitrate "leakage" from the Eastern Tropical South Pacific (ETSP) (Pichevin et al., *in press*) and local increases denitrification led by strengthening of the *tehuanos* blowing through the Chivela Pass (and the associated upwelling) during interstadials. However, one important question remains unanswered: how could denitrification regimes that occurred in the ETSP have affected the Gulf of Tehuantepec?

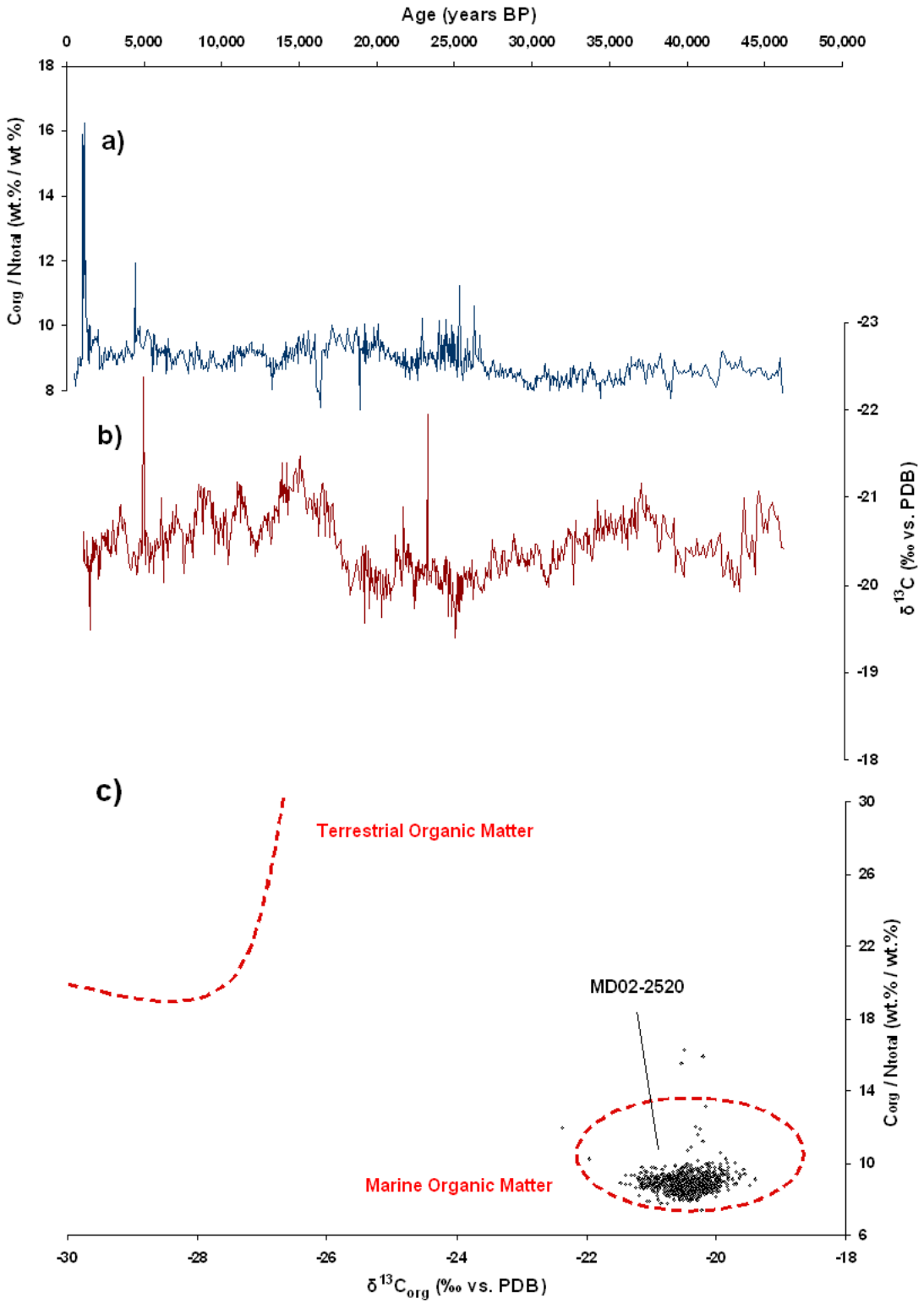

Figure 6.5: a) C_{org} / N_{total} in core MD02-2520; b) δ^{13}Corg record from core MD02-2520; and c) relationship between C_{org} / N_{total} ratio and δ^{13}Corg values in core MD02-2520, highlighting the dichotomy between marine and terrestrial organic matter. Some samples from sediments younger than 1,000 yrs BP display C/N ratios may be as high as 16 due to the small levels of N_{total} in organic matter. This could be due to the presence of small amounts of terrestrial organic matter with a relatively higher Corg content.

6.7 Advection of heavy nitrate from the southern OMZ

Chapter 2.1 introduced the oceanographic settings of the ETNP, and highlighted how the intermediate waters in the Gulf of Tehuantepec have a rather complex origin, being influenced by temperature shifts at upstream sources and the duration of isolation from the atmosphere (Kessler, 2006). The temperature, salinity and density properties of intermediate water masses in the ETNP south of ~20ºN appear to coincide with those of the "equatorial 13ºC water", a water mass that lies at depths of 75-300m east of 150°W that is thought to originate between the northeast of New Zealand and the Tasman Sea during the southern winter mixing (Tsuchiya, 1981). At intermediate depths within the Equatorial Pacific, the 13ºC water flows eastward next to the Equatorial Undercurrent and the subsurface North and South Equatorial Counter-currents as a Tsuchiya Jet (Fig. 6.6). Pahnke and Zahn (2005) observed that millennial-scale mid-depth variability in the ventilation of Antarctic Intermediate Water (AAIW) and the Subantarctic Mode Water (SAMW) - two important sources of the 13ºC water mass - varied in synchrony with the Antarctic temperature history. The authors found that warmings in Antarctica coincided with departures from low glacial benthic $\delta^{13}C$ levels and preceded the onset of Greenland warmings by 1500 to 3000 years, in a similar fashion to the marine denitrification from core GeoB 7139-2 collected from the Chilean margin (De Pol-Holz et al., 2006 and Fig. 6.2-b) and the increases in $\delta^{15}N$ at 17.5 ka in the Gulf of Tehuantepec (Fig. 6.2-d). It is thought that ~15 Sverdrups of SAMW and AAIW may leak into the eastward-flowing Equatorial Undercurrents and Tsuchiya Jets (Tsuchiya and Talley, 1996; Reid, 1997; Hendy and Pedersen, 2006) and the speed of these tongues (50-100cm s^{-1}) is high enough to allow the water mass to maintain their properties against the action of lateral mixing from westward-flowing low-oxygen equatorial currents, thus conferring a "quasi-Antarctic" character to the denitrification patterns in the OMZ within the Gulf of Tehuantepec.

An alternative proposition to the leakage of heavy nitrate across the Equator via Tsuchiya jets to explain the Antarctic timing of $\delta^{15}N$ enrichments in the ETNP may derive from the northward advection of heavy nitrate generated in the Peru Margin (Pichevin et al., *in press*). The analysis of N* (a tracer that eliminates all processes occurring with a N:P ratio of 16:1; Gruber and Sarmiento, 1997) in the

Eastern Tropical Pacific shows a severe nitrate deficit in the ETNP between 200-350m water depth and between 100-200m depth off the Peruvian coast. This may imply that a pool of denitrified waters at 50-100m depth may extend from the Eastern Tropical South Pacific, via the subduction of high-salinity surface waters at around 25-12°S, into the Equatorial Undercurrent system, the Costa Rica Dome and eventually into the Gulf of Tehuantepec. The advection signal of heavy nitrate from the denitrifying zones off Peru and northern Chile would link the ETNP to the water-column denitrification processes occurring in the southern Hemisphere. However it is worth noting that, although the early increases in $\delta^{15}N$ in the Gulf of Tehuantepec led Greenland interstadials by 1-2kyrs, peak denitrification only occurred during Greenland interstadials (see peaks at 14.5ka, 37ka and 45ka in Fig 6.3). This would suggest that the strength of the *tehuanos* and Northern Hemisphere climate pacing are the main drivers of denitrification in the Gulf of Tehuantepec.

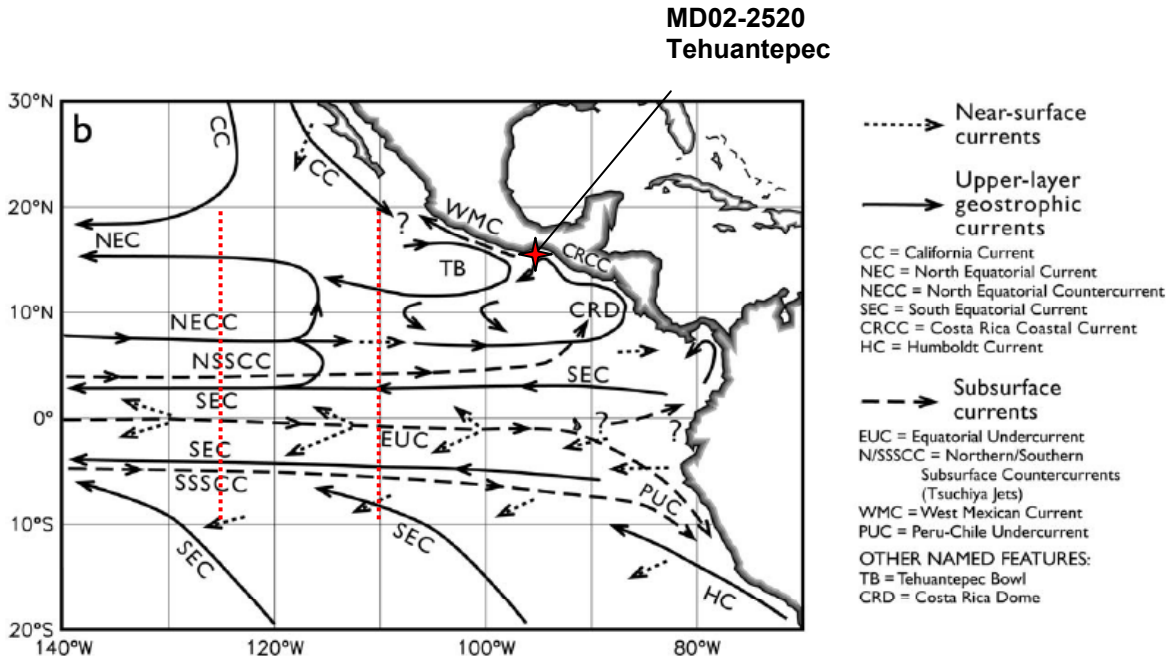

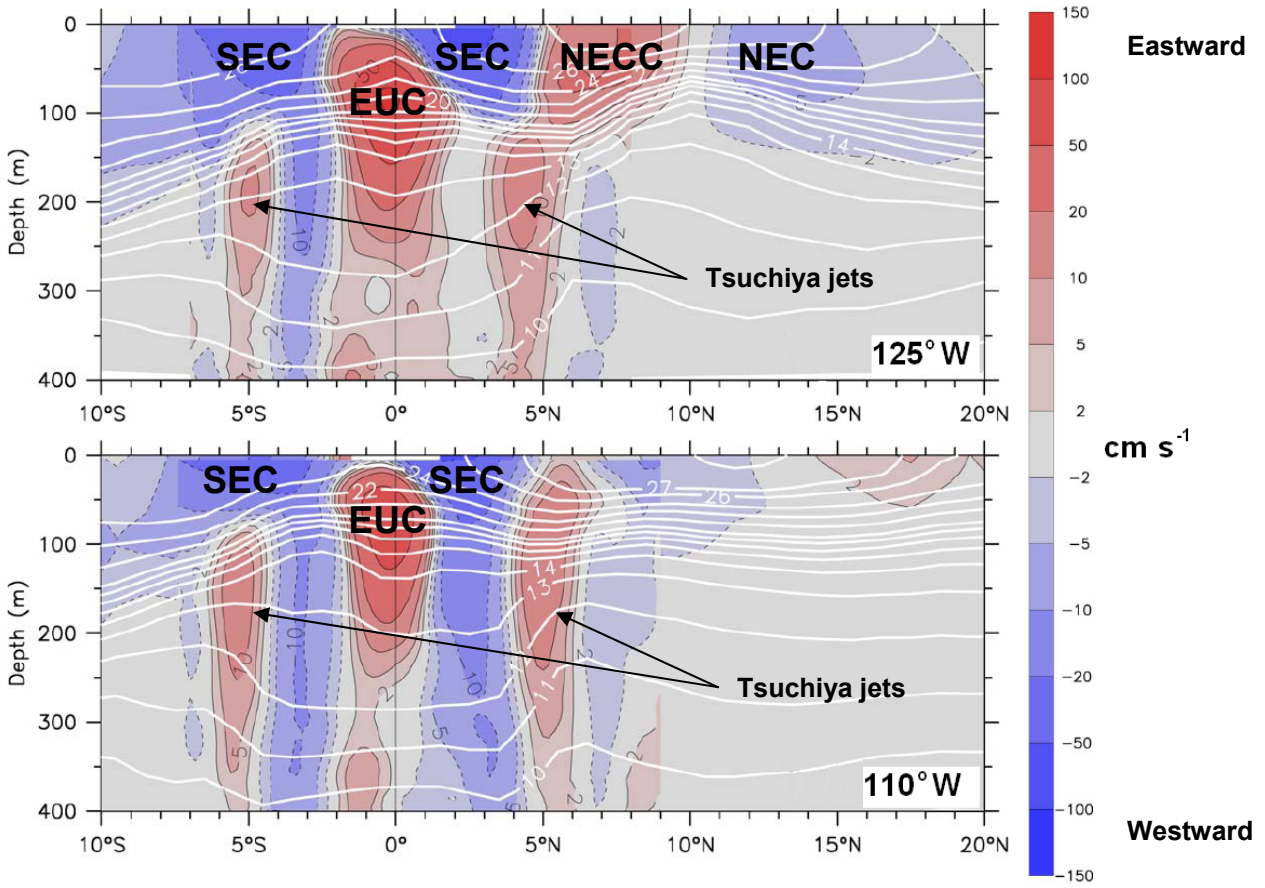

Figure 6.6: Mean meridional sections of temperature (white contours) and zonal current in the Eastern Pacific at 125ºW and 110ºW (colour shading, where red is eastward and blue westward; current speeds are in cm s^{-1}). The red dashed lines indicates the position of the zonal current profiles. From Kessler (2006). SEC = South Equatorial Current; EUC = Equatorial Undercurrent; NECC = North Equatorial Counter-Current; NEC = North Equatorial Current. The Tsuchiya jet north of the Equator is visible as an eastward-flowing current below thermocline at about 125–400 m depth near ±4–5º latitude that originate in the far western Pacific (Rowe et al, 2000).

6.8 Gap winds and moisture transport across Central America as a positive feedback on denitrification and abrupt climate change

The planktonic foraminiferal records of core MD02-2520 also show variations in the dominant assemblages throughout the last 40kyr (Machain-Castillo, M L, *pers. comm*), with *G. glutinata* and *G. bulloides* (indicating upwelling conditions) dominating during Greenland warm periods and coinciding with peaks in the $\delta^{15}N$ record. By contrast, planktonic foraminiferal assemblages deposited in the gulf during stadials are dominated by *G. menardii* and *N. dutertrei*, which generally suggest warmer and more stratified oceans and reduced or absent upwelling. The increase in productivity at the end of the LGM in core MD02-2520 lags the increase in $\delta^{15}N$ intensification of the OMZ by ~1,500 years, suggesting that either the reorganization of the intermediate OMZ in the Gulf of Tehuantepec or the onset of advection of heavy nitrate from the ETSP was independent of upwelling patterns and the Northern Hemisphere atmospheric influence on the development of *Tehuanos*.

But how do correlation between the $\delta^{15}N$ and C_{org} records and the succession of planktonic foraminiferal assemblages in core MD02-2520 support the idea of changes in the ocean-atmosphere system? It is very likely that the evolving topography and extent of the Laurentide Ice Sheet affected the wind patterns in the western northern hemisphere throughout the transitions from stadials to interstadials and throughout the LGM. At present, the seasonal upwelling is primarily due to strong northerly winds impact the gulf during winter-spring (Chelton et al., 2000; Xie et al., 2005). These winds originate from cold, high-pressure weather systems moving southward from North America over the Gulf of Mexico, eventually affecting the tropical atmosphere and ocean, by contributing to the strengthening of the northeast trade winds over the eastern Pacific Ocean and by inducing local cooling of the sea surface temperatures (Schultz et al., 1997). It is possible that during stadials and during the four Heinrich events recorded in core MD02-2520 (Fig 6.3), a combination of factors reduced the frequency and intensity of cold air surges entering the Gulf of Mexico, thus reducing primary productivity in the Gulf of Tehuantepec. These factors include:

- a more southerly jet stream in the northern hemisphere;

- a reduction of cold-air damming following a change in topography to the east of the Rockies with the establishment of the Laurentide ice sheet; and
- the establishment of low pressure system over the Gulf of Mexico, which would have reduced the southward movement of cold, high-pressure weather systems from the North American plains (Schultz et al., 1997). core ODP 1002C

Proxy records of upwelling from planktonic foraminiferal assemblages (Machain-Castello, M., *pers. comm.*) and primary productivity (C_{org}) from core MD02-2520 suggest that the intensity and frequency of cold surges penetrating into Central America was at its highest from the Bolling-Allerod to Early Holocene and has gradually decreased during the last 10,000 years (Machain-Castello, M., *pers. comm.*). The role of Central American gap winds as important modulators of the global climate system was first suggested by Leduc et al. (2007). Moisture transport from the Gulf of Mexico to the Pacific is thought to regulate the high salinities in the North Atlantic Ocean, which in turn is the main driver in the formation of North Atlantic Deep Water. Leduc et al. (2007) reconstructed sea surface salinities in the eastern equatorial Pacific and found high salinities to be associated with the southward migration of the ITCZ during Heinrich events and Greenland stadials. By contrast, interstadials were characterised by a more northern position of the ITCZ and increased precipitation in the eastern equatorial Pacific. This reaffirms results presented by Stott et al. (2002), who found that the pattern and magnitude of the salinity variations in the equatorial Pacific imply shifts in the tropical Pacific ocean/atmosphere system analogous to modern El Niño-Southern Oscillation (ENSO). El Niño conditions correlate with stadials at high latitudes, whereas La Niña conditions correlate with interstadials. If El Niño conditions were a persistent feature in the eastern equatorial Pacific during stadials, the ensuing adiabatic warming and drying through atmospheric subsidence over Northeast Brazil and the tropical Atlantic would have reduced precipitation and river runoff from the Amazon catchment area and increased evaporation from the tropical Atlantic. The application of these models to past climate patterns would suggest that during stadials and Heinrich events, the central equatorial Pacific and the Mexican Pacific margin lying south of 10°N are more likely to have experienced lower precipitation, and the

Cariaco Basin at the northern edge of the Amazon catchment area, would have experienced drier conditions (Fig. 6.4). Past variability in the latitudinal position of the ITCZ over the Eastern Pacific has also been observed from Titanium and Iron deposited in the anoxic Cariaco basin during the past 14kyr (Haug et al., 2001).

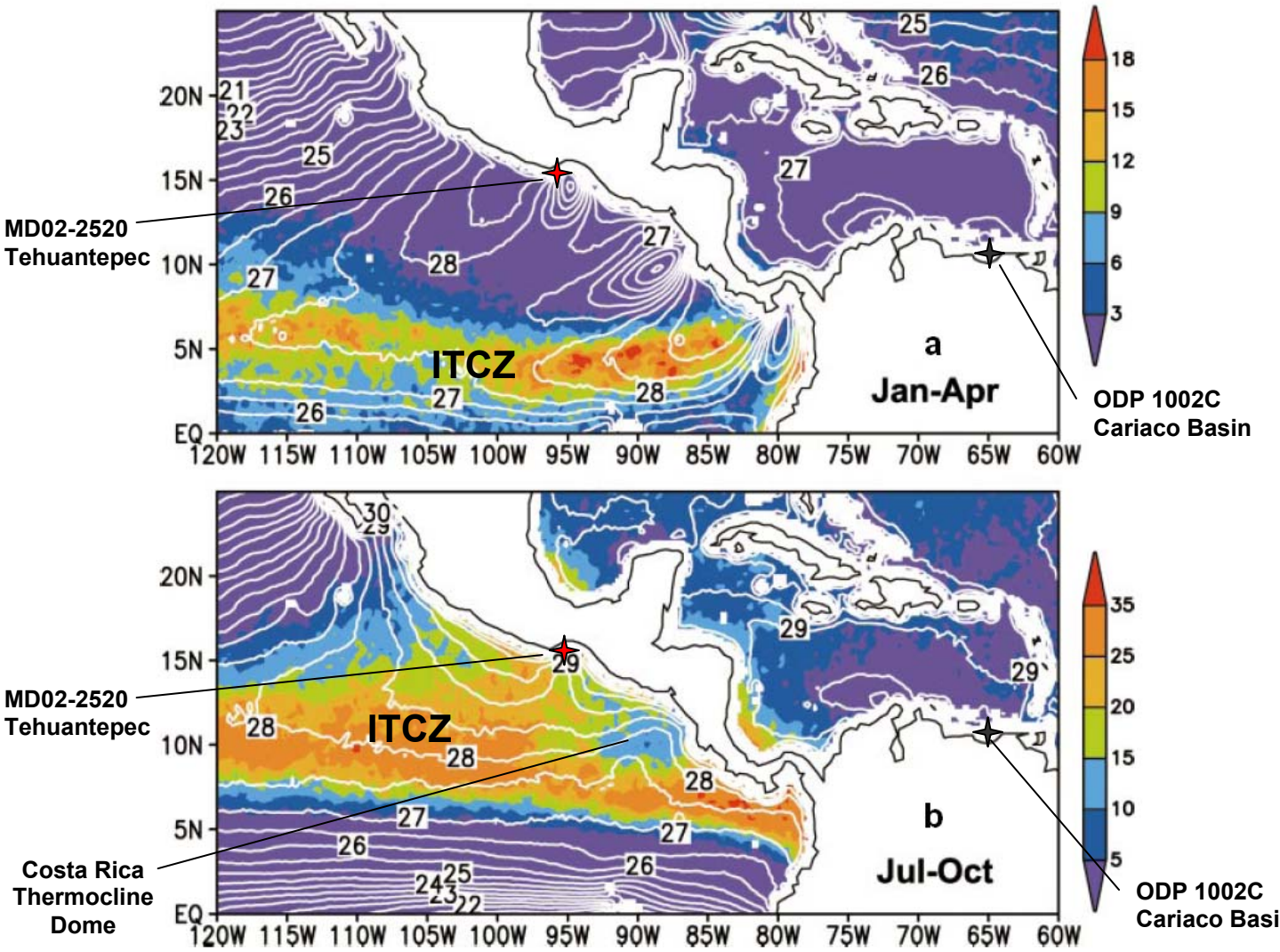

Figure 6.7: Sea Surface Temperature (SST - contours; °C) and precipitation (shade; mm day^{-1}) in the ETNP: (a) Jan–Apr, and (b) Jul–Oct. In (b), note the different colour scale for summer. Notice the decrease in SSTs associated with the Tehuantepec and Papagayo wind jets in winter, the southern position (along 5°N) of the ITCZ in winter and a more northerly position throughout the summer months (7-15°N). The precipitation pattern in the summer months also highlights the cold patch over the Costa Rica Dome, where a 50% drop in precipitation occurs as the shallow thermocline (at 10-30m water depth) allows cold water to suppress atmospheric convection. From Xie et al. (2005).

The general trend observed in the Cariaco basin (Fig. 6.4) is that of higher reflectance in sediments deposited during Greenland stadials, the Last Glacial Maximum and the Younger Dryas cold period between 12.6 and 11.5 ka. A change in the mean position of the ITCZ has been attributed as the main parameter controlling precipitation and, by proxy, sediment deposition in the Cariaco basin (Petersen et al., 2000). As Fig. 6.7 shows, a more northerly ITCZ, as is assumed for the early Holocene, corresponds to increased rainfall and increased Ti deposition in the Cariaco Basin basin. In Tehuantepec, present-day conditions during July and August (when the ITCZ is at its most northerly position) result in the orographic forcing of trade winds over the mountains of most of Central America, which results in maximum precipitation along the Caribbean coast and minimum precipitation along the Pacific coast of Central America (Magana et al., 1999). This results from precipitation deficits over cold spots on top of the Costa Rica Dome and over the weak summer jet off Tehuantepec, which leaves small but visible signatures in SST (Fig. 6.6 and Fig. 6.7; Xie et al., 2005). The interaction between SSTs and the atmosphere would suggest that identifying any clear trends in the mean position of the ITCZ from sediments deposited in the Gulf of Tehuantepec will be compounded by cold patches (thermocline domes) and the strength of upwelling.

Throughout the past 45ka, as the ITCZ shifted north during the summer season, the orographic barrier of Central America is likely to have imprinted a distinctive signal on precipitation patterns between western and eastern areas (Metcalfe et al., 2000). During interstadials, strong trade winds combined with the orographic barrier led to enhanced ascending motion and intense convective activity and precipitation over the Caribbean side and around the Cariaco Basin. However, on the western side of the Mexican mainland, strong atmospheric subsidence over the colder patches of the ETNP, caused by increased upwelling in the Gulf of Tehuantepec and the Costa Rica Dome, resulted in a decrease in both convective activity and precipitation. The combined effect of a northerly ITCZ (conducing to increased precipitation) during episodes of increased upwelling in the Gulf of Tehuantepec (reduced SSTs and reduced atmospheric convection) would have resulted in rather complex precipitation patterns at 10-15°N and between 85-100°W (Fig 6.7). Throughout stadials, decreased upwelling, warmer SSTs leading to wetter

conditions along the Pacific would have been matched by drier conditions in the Gulf of Mexico, as the ITCZ assumed a more southerly mean latitudinal position. In addition to the southerly shift in the ITCZ during stadials, the Eastern Tropical Pacific is likely to have been influenced by a weakened Hadley and Walker circulation and what is generally believed to be a persistent El Niño-like pattern (Koutavas et al., 2002). The interplay of the two negative feedback loops (atmospheric convection vs. upwelling) has resulted in records of detrital elements from core MD02-2520 that do not bear much relation to records of stadial-interstadial variability that have been observed in the Cariaco Basin (Fig 6.4) The main exception is top section of the core, spanning the last 15,000 years, where the profile of terrigenous elements in the Gulf of Tehuantepec appears to mirror the sediment reflectance record from the Cariaco Basin. Detrital element records from the Gulf of Tehuantepec indicate high concentrations of Si, Ti and K in sediments deposited during the Younger Dryas cold period, followed by a sharp decrease during the Mid Holocene 'thermal maximum' and a gradual increase throughout the Late Holocene (Fig 6.4). This observation would suggest that movements in the ITCZ may have not only directly impacted precipitation patterns in the Gulf of Tehuantepec, but also the strength of gap winds, the ensuing upwelling and primary productivity between stadials and interstadials.

The cause of the meridional movement of the ITCZ may lie in changes in insolation associated with the precession component of the Milankovitch forcing: Southern Hemisphere insolation has become more seasonal during Mid to Late Holocene, whereas Northern Hemisphere insolation has become less seasonal, decreasing the capacity of boreal regions to pull the ITCZ off the Equator (Berger and Loutre, 1991). Xie (1999) proposed a mechanism for the transfer of temperature changes from high latitudes to the marine ITCZ during stadials. The increased extent of ice cover at northern high latitudes glacial maxima cools and dries the atmosphere above it, which in turn initiates cooling of the entire northern high- and mid-latitudes through advection. Eventually, wind-evaporation acting on SSTs in the region of the northeasterly trades of the North Pacific and Atlantic oceans initiates further movement of the cold SSTs to the tropical latitudes. Once the cold SST front reaches the ITCZ latitudes, the meridional SST gradient initiates a southward shift of the

ITCZ, which eventually increases precipitation, wind and upwelling in Tehuantepec. What results is a complex interplay between high and low latitudes linking atmospheric processes to the strength of gap winds in the ETNP, local production and denitrification patterns and ultimately the waxing and waning of the largest OMZ in the world.

6.9 Conclusion

The multiproxy study of sediments from core MD02-2520 provides new evidence on the dichotomy of water masses present in the ETNP during the last glacial-interglacial cycle. The complex interplay of remote ventilation changes, variations in the strength of gap winds, upwelling and the resulting primary productivity has led to nitrogen isotope records in the Gulf of Tehuantepec that are decoupled from local records of primary productivity. This provides evidence that the "supply" mechanism from the Southern Hemisphere complements changes in regional productivity in modulating the intensity of the OMZ and water-column denitrification in the portion of the ETNP that lies to the south of 15ºN. Detrital element records from the Gulf of Tehuantepec do not show such clear stadial-interstadial variability as the denitrification and organic carbon records, as the combined effect of latitudinal movements in the ITCZ coupled with varying upwelling intensity and SSTs resulted in rather complex precipitation patterns around the Gulf of Tehuantepec. A comparison between core MD02-2520 and records from the Cariaco Basin suggests that when the ITCZ is in its most northerly position (as was the case in the Early Holocene and throughout stadials), precipitation is highest in regions that drain into the Cariaco basin and a "rain-shadow" is created in the ETNP. By contrast, the Younger Dryas and Greenland stadials were characterised by:

- a southward migration of the ITCZ;
- wetter conditions along the Pacific associated with drier conditions in the Gulf of Mexico; and
- increases in sea surface temperatures of the eastern tropical Pacific associated with reduced wind-induced upwelling and El Niño-like conditions.

The marine record from the Gulf of Tehuantepec highlights new correlations with climate records from distant regions and provides a new bridge in understanding atmospheric and marine teleconnections across Central America. In addition, the denitrification record from the Gulf of Tehuantepec bears influence to climate variations observed in high-latitude records from both Greenland and Antarctica, suggesting that the denitrification changes and OMZ variability in the ETNP are linked to processes in high latitudes within the boreal and austral hemispheres.

References

Altabet, M.A., Francois, R., Murray, D.W., Prell, W.L. (1995) Climate-related variations in denitrification in the Arabian Sea from sediment 15N/14N ratios. *Nature*, vol. **373**, pp. 506-509

Altabet, M.A., Higginson, M. and Murray, D.W. (2002) The effect of millennial-scale changes in Arabian Sea denitrification on atmospheric CO2. *Nature*, vol. **415**, pp. 159-162

Behl, R. J., and J. P. Kennett (1996) Evidence for brief interstadial events in the Santa Barbara Basin, NE Pacific during the past 60 Kyr. *Nature*, vol. **379**, pp. 243– 246.

Berger, A. and Loutre, M.F. (1991) Insolation values for the climate of the last 10 million years. *Quat. Sci. Rev.*, vol. **10**,pp. 297-317

Boumaggard, El H., Gayet, J., Bobier, C., Machain-Castillo, M.L., Aguayo_Camargo, E. (1998) Distribution des sediments sur la marge du golfe de Tehuantepec (Pacifique Oriental). Exemple d'interaction tectonique-eustatisme. *Oceanologica Acta*, vol. **21**, pp. 21-31

Brandes, J.A., Devol, A.H, Yoshinari, T., Jayakumar, D.A. and Naqvi, S.W.A. (1998) Isotopic composition of nitrate in the central Arabian Sea and western Tropical North Pacific: a tracer for mixing and nitrogen cycles. *Limnol. Oceanogr.*, vol. **43**, pp. 1680-1689

Brandes, J.A. and Devol, A.H. (2002) A global marine nitrogen isotopic budget: Implications for Holocene nitrogen cycling. *Global Biogem. Cycles*, vol. **16**, 1120

Calvert, S.E., Bustin, R.M. and Pedersen, T.F., (1992) Lack of evidence for enhanced preservation of sedimentary organic matter in the oxygen minimum of the Gulf of California. *Geology*, vol. **20**, pp. 757-760

Calvert, S.E., Pedersen, T.F., Naidu, P.D. and von Stackelberg, U. (1995) On the organic carbon maximum on the continental slope of the eastern Arabian Sea. *Journal of Marine Research*, vol. **53**, pp. 269-296

Chelton, D.B., Freilich, M.H. and Esbensen, S.K. (2000) *Satellite Observations of the Wind Jets off the Pacific Coast of Central America. Part I: Case Studies and Statistical Characteristics.* Monthly Weather Review, **128**, pp.1993-2018

Cline, J.D. and Kaplan, I.R. (1975) Isotopic fractionation of dissolved nitrate during denitrification in the eastern tropical North Pacific Ocean. *Mar. Chem.*, vol. **3**, pp. 271-299.

Codispoti, L. A. and Richards R. A. (1976) An analysis of the horizontal regime of denitrification in the eastern tropical North Pacific. *Limnol. Oceanogr*., vol. **21**, pp. 379−388

Codispoti, L.A., Brandes, J.A., Christensen, J.P., Devol, A.H., Naqvi, S.W.A., Paerl, H.W., and Yoshinari, T. (2001) The oceanic fixed nitrogen and nitrous oxide budgets: Moving targets as we enter the anthropocene?, *Sci. Mar*., vol. **65**, pp. 85–105

De Pol-Holz, R., Ulloa, O., Dezileau, L., Kaiser, J., Lamy, F. and Hebbeln, D. (2006) Melting of the Patagonian Ice Sheet and deglacial perturbations of the marine nitrogen cycle in the eastern South Pacific. *Geophysical Research Letters*, vol. **33**, L04704, doi:10.1029/2005GL024477

Dansgaard, W., Johnsen, S.J., Clausen, H.B., Dahl-Jensen, D., Gundestrup, N.S., Hammer, C.U., Hvidberg, C.S., Steffensen, J.P., Sveinbjörnsdottir, A.E., Jouzel, J. et al. (1993) Evidence for general instability of past climate from a 250-kyr ice-core record. *Nature*, vol. **364**, 218-220

Deutsch, C., Sigman, D.M., Thunell, R.C., Meckler, A.N. and Haug, G.H. (2004) Isotopic constraints on glacial/interglacial changes in the oceanic nitrogen budget. Global Biogeochem. Cycles, vol. **18**, doi:10.1029/2003GB002189

Deutsch, C., Sarmiento, J.L., Sigman, D.M., Gruber, N. And Dunne, J.P (2007) Spatial coupling of nitrogen inputs and losses in the ocean, *Nature*, vol. **445**, pp. 163-167

Emmer, E. and Thunell R.C. (2000) Nitrogen isotope variations in Santa Barbara Basin sediments: Implications for denitrification in the eastern tropical North Pacific during the last 50000 years. *Paleoceanography*, vol. **15**, pp. 377– 387

Fluckiger, J., Dallenbach, A., Blunier, T., Stauffer, B., Stocker, T.F., Raynaud, D. Barnola, J.M. (1999) Variations in atmospheric N_2O concentration during abrupt climatic changes. *Science*, vol. **285**, pp. 227–230

Fluckiger, J., Blunier, T., Stauffer, B., Chappellaz, J., Spahni, R., Kawamura, K., Schwander, J., Stocker, T., Dahl-Jensen, D. (2004) N_2O and CH_4 Variations during the last glacial epoch: insight into global processes, *Glob. Biogeochem. Cycles*, vol. **18,**

Fontugne, M.R., Calvert, S.E. (1992) Late Pleistocene Variability of the Carbon Isotopic Composition of Organic Matter in the Eastern Mediterranean: Monitor of Changes in Carbon Sources and Atmospheric CO_2 Concentrations. *Paleoceanography*, vol. **7**, pp. 1-20

Galbraith, E.D., Kienast, M., Pedersen, T.F., Calvert, S.E. (2004) Glacial-interglacial modulation of the marine nitrogen cycle by high-latitude O2 supply to the global thermocline. *Paleoceanography*, vol. **19**, PA4007, doi:10.1029/2003PA001000

Ganeshram, R.S., Pedersen, T.F., Calvert, S.E. and Murray, J.W. (1995) Large changes in oceanic nutrient inventories from glacial to interglacial periods. *Nature*, vol. **376**, pp. 755-757

Ganeshram, R.S., Pedersen, T.F., Calvert, S.E., McNeill G.W., Fontugne M.R. (2000) Glacial-Interglacial variability in denitrification in the world's oceans: Causes and consequences. *Paleoceanography*, vol. **15**, pp 361-376

Ganeshram, R.S., Pedersen, T.F., Calvert, S.E. and Francois, R. (2002) Reduced nitrogen fixation in the glacial ocean inferred from changes in marine nitrogen and phosphorus inventories. *Nature*, vol. **415**, pp. 156-159

Grootes, P.M., Stuiver, M., White J.W.C., Johnsen, S., and Jouzel, J. (1993) Comparison of Oxygen Isotope Records from the GISP2 and GRIP Greenland Ice Cores. *Nature*, vol. **366**, pp. 552-554

Gruber, N. and Sarmiento, J.L. (1997) Global Patters of marine nitrogen fixation and denitrification. *Global Biogeochem. Cycles*, vol. **11**, pp. 235-266

Gruber, N. and Galloway, J.N. (2008) An Earth-system perspective of the global nitrogen cycle. *Nature*, vol. **451**, pp. 293-296

Haug, G.H., Hughen, K.A., Sigman, D.M., Peterson, L.C. and Rohl, U. (2001) Southward migration of the intertropical convergence zone through the Holocene. *Science*, vol. **293**, pp. 1304–1308

Hendy, I.L., Pedersen T.F., Kennett J.P., and Tada R. (2004) Intermittent existence of a southern Californian upwelling cell during submillennial climate change of the last 60kyr. *Paleoceanography*, vol. **19**, PA3007, doi:10.1029/2003PA000965.

Hendy, I.L. and Kennett J.P. (2003) Tropical forcing of North Pacific intermediate water distribution during Late Quaternary rapid climate change. *Quat. Sci. Reviews*, vol. **22**, Issues 5-7, pp. 673-689

Hendy, I. L. and Pedersen, T. F. (2006) Oxygen minimum zone expansion in the eastern Tropical North pacific during deglaciation. *Geophys. Res. Lett.*, vol. **33**, L20602, doi:10.1029/2006GL025975

Higgins, R.W., Mo, K.C., Yao, Y. (1998) Interannual variability in the US summer precipitation regime with emphasis on the southwestern monsoon. *Journal of Climate*, vol. **11**, pp. 2582-2606

Higginson, M.J. and Altabet, M.A. (2004) Initial test of the silicic acid leakage hypothesis using sedimentary biomarkers. *Geophys. Res. Lett*.,vol. **31**, L18303, doi:10.1029/2004GL020511

Ivanochko, T.S. and Pedersen, T.F. (2004) Detrmining the influences of Late Quaternary ventilation and productivity variations on Santa Barbara Basin sedimentary oxygenation: A multi-proxy approach. *Quat. Sci. Rev.*, vol. **23**, pp 467-480

Ivanochko, T.S., Ganeshram, R.S., Brummer, G.J.A., Ganssen, G., Jung, S.J.A., Moreton, S.G., Kroon, D. (2005) Variations in tropical convection as an amplifier of global climate change at the millennial scale. *Earth and Planetary Science* Letters, vol. **235**, pp. 302–314

Kienast, S.S., Calvert, S.E., Pedersen, T.F. (2002) Nitrogen isotope and productivity variations along the northeast Pacific margin over the last 120 kyr: Surface and subsurface paleoceanography. *Paleoceanography*, vol. **17**, doi:10.1029/2001PA000650

Kessler, W. S. (2006) The circulation of the eastern tropical Pacific: A review. *Prog. Oceanogr.*, vol. **18**, pp. 181-217

Kiefer, T. and Kienast, M. (2005) Patterns of deglacial warming in the Pacific Ocean: a review with emphasis on the time interval of Heinrich event 1. *Quat. Sci. Reviews*, vol. **24**, pp. 1063-1081

Koutavas, A., Lynch-Stieglitz, J., Marchitto T.M. and Sachs, J.P (2002) El Niño-Like Pattern in Ice Age Tropical Pacific Sea Surface Temperature. *Science*, vol. **297**, pp. 226-230

Leduc, G., Vidal, L., Tachikawa, K., Rostek, F., Sonzogni, C., Beaufort, L. and Bard, E. (2007) Moisture transport across Central America as a positive feedback on abrupt climatic changes. *Nature*, vol. **445**, pp. 908-911

Liu, K.-K. and Kaplan, I.R. (1989) The eastern tropical Pacific as a source of ^{15}N-enriched nitrate in seawater off southern California. *Limnol. Oceanogr*., vol. **34**, pp. 820-830

Machain-Castillo, M.L., Monreal-Gomez, M.A., Arellano-Torres, E., Merino-Ibarra, M., Gonzalez-Chavez, G (2008) Recent Planktonic foraminiferal distribution patterns and their relation to hydrographic conditions in the Gulf of Tehuantepec, Mexican Pacific. *Marine Micropaleontology*, vol. **66**, pp. 103-119

Magana, V., Amador, J.A., Medina, S. (1999) The Midsummer Drought over Mexico and Central America. *Journal of Climate*, vol. **12**, pp 1577-1588

Metcalfe S.E., O'Hara S.L., Caballero M., Davies S.J. (2000) Records of Late Pleistocene-Holocene climatic change in Mexico - a review. *Quaternary Science Reviews*, vol. **19**, pp. 699-721

Peterson, L.C., Haug, G.H., Hughen, K.A., and Rohl, U. (2000) Rapid Changes in the Hydrological Cycle of the Tropical Atlantic During the Last Glacial. *Science*, vol. **290**, pp. 1947-1951

Pichevin, L., Ganeshram, R.S., Francavilla, S., Arellano-Torres, E., Pedersen, T.F., and Beaufort, L. Inter-hemispheric Leakage of Heavy Nitrate in the Eastern Tropical Pacific? Implications for the Timing of Denitrification Changes at Millennial Scale. Submitted to *Paleoceanography*.

Rowe, G.D., Firing, E., Johnson, G.C., 2000. Pacific equatorial subsurface countercurrent velocity, transport and potential vorticity. *Journal of Physical* Oceanography, vol. **30**, pp. 1172–1187

Schultz, D.M., Bracken, W.E. and Bosart, L.F, Hakim, G.J., Bedrick, M.A., Dickinson M.J. and Tyle, K.R. (1997) The 1993 Superstorm Cold Surge: Frontal Structure, Gap Flow, and Tropical Impact. *Monthly Weather Review*, vol. **125**, pp. 5-39

Stott, L., Poulsen, C., Lund, S. and Thunell, R. (2002) Super ENSO and global climate oscillations at millennial time scales. *Science*, vol. **297**, pp. 222–226

Stuiver, M. and Grootes, P.M. (2000) GISP2 oxygen isotope ratios. *Quat. Res.*, vol. **53**, pp277-284

Thornton, S. F., and McManus, J. (1994) Application of organic carbon and nitrogen stable isotope and C/N ratios as source indicators of organic matter provenance in estuarine systems: evidence from the Tay Estuary, Scotland. Estuarine. *Coastal and Shelf Science*, vol. **38**, pp. 219-233

Talley, L.D., (1993) Distribution and formation of North Pacific intermediate water. *J. Phys. Oceanogr.*, vol. **23**, pp. 517–537

Thunell, R.C. and Kepple A.B. (2004) Glacial-Holocene $\delta^{15}N$ record from the Gulf of Tehuantepec, Mexico: Implications for denitrification in the eastern equatorial Pacific and changes in atmospheric N2O. *Global Biogeochem. Cycles*, vol. **18,** GB1001, doi:10.1029/2002GB002028

Tsuchiya, M. (1981) The Origin of the Pacific 13°C Water. *J. Phys. Oceanogr*, vol. **11**, pp. 794-812.

Tsuchiya, M., and Talley, L.D., (1998) A Pacific hydrographic section at 88°W: water-property distribution. *J. Geophys. Res.,* vol. **103**, pp. 12899–12918

van Geen, A., Zheng, Y., Bernhard, J.M., Cannariato, K.G., Carriquiry, J., Dean, W.E., Eakins, B.W., Ortiz, J.D. and Pike J. (2003) On the preservation of laminated sediments along the western margin of North America. *Paleoceanography*, vol. **18**(4), 1098, doi:10.1029/2003PA000911

Wedepohl K.H. (1995) The composition of the continental crust. *Geochim. Cosmochim.* Acta, vol. **59**, pp. 1217–1232

Xie, S.P. (1999) A dynamic ocean-atmosphere model of the tropical Atlantic decadal variability. *Journal of Climate*, vol. **12**, pp. 64–70

Xie, S.P, Xu, H., Kessler, W.S., Monaka, M. (2005) Air–Sea Interaction over the Eastern Pacific Warm Pool: Gap Winds, Thermocline Dome, and Atmospheric Convection. *Journal of Climate*, vol. **18**, pp. 5-20

Yarincik, K.M., Murray, R.W. and Peterson, L.C. (2000) Climatically Sensitive Eolian and Hemipelagic Deposition in the Cariaco Basin, Venezuela, Over the Past 578,000 Years: Results From Al/Ti and K/Al. *Paleoceanogr.*, vol. 15, pp. 210–228.

Yoshinari T., Altabet, M.A., Naqvi, S.W.A., Codispoti, L., Jayakumar, A., Kuhland, M., Devol A. (1997) Nitrogen and oxygen isotopic composition of N_2O from suboxic waters of the eastern tropical North Pacific and the Arabian Sea - measurement by continuous-flow isotope-ratio monitoring. *Marine Chemistry*, vol. **56**, pp. 253-264

CHAPTER 7

Millennial-scale variations in phosphorite deposition in the Eastern Tropical North Pacific

ABSTRACT

The deposition of phosphatic horizons and phosphorites - large accumulations of P-rich sediments on continental margins in the ETNP, ESP, Arabian Sea and Namibian Shelf- represents a particularly important sink in the marine P cycle. Late-Quaternary sedimentary records from NW Mexican Margin have shown phosphorite deposition to occur predominantly during interglacials, which normally coincide with higher rates of export productivity than those observed in stadials, and an increase in intensity of the oxygen minimum zone impinging on the continental shelf. Here we present new data from two cores from the Eastern Tropical North Pacific documenting high-frequency (centennial-to-millennial-scale) phosphorites deposition occurring in tandem with millennial-scale variations in denitrification in the area. In addition, total-P accumulation rates from the two sites are compared with accumulation rates for a variety of marine environments. Our data suggests that P accumulation rates throughout the Holocene (4 -10 mmol P $cm^{-2}kyr^{-1}$) in the ETNP are about 4-5 times higher than what has been previously inferred for this region. This leads to the assumption that N and P cycles during stadial-interstadial excursions are more closely coupled than was previously through and that the N:P ratios during stadials are less likely to depart from the canonical value of 16.

7.1. Introduction

Modern phosphorites are formed in laminated, organic-rich sediments underlying highly productive western boundary currents and their formation and burial in the sedimentary record is thought to contribute to the long-term regulation of PO_3^{-4} in seawater (Froelich et al., 1982; Ganeshram et al., 2002). The origin of phosphorites and their precursory lenses of unconsolidated phosphatic deposits has been attributed to the supersaturation of interstitial pore waters (Price and Calvert., 1978; Jahnke et al., 1983), dissolution of fish remains (Suess, 1981) and phosphate mineralisation mediated by benthic sulphur-oxidising bacteria (Reimers et al., 1990).

At present, phosphorite deposition has been documented in laminated sediments retrieved from suboxic continental slopes in the ETNP (Ganeshram et al., 2002), in the Gulf of California (Williams & Reimers, 1983), along the Peru-Chile margin (Gallardo, 1977; Baturin and Bezrukov, 1979; Suess, 1981), Arabian Sea (Babu and Nath, 2005), SW African Margin (Gallardo; 1977; Price and Calvert, 1978; Kuypers et al., 2005; Schultz & Schultz, 2005) and the eastern coastal margin of Australia (Kress and Veeh, 1980; O'Brien and Veeh, 1980).

The exclusive occurrence of phosphorite deposits in black shales and organic-rich, finely laminated sediments deposited beneath areas of suboxic denitrification led Piper and Codispoti (1975) to suggest the existence of a link between increased water-column denitrification and increased phosphate sequestration within phosphorites. The first evidence of a direct coupling between enhanced periods of denitrification and phosphogenesis in the ETNP during interglacial periods was observed by Ganeshram et al. (2002) in a core collected at 400m depth in the NW Mexican margin. The authors estimated the global phosphogenic P deposition

through CFA formation in sediments during interglacials was relatively small when compared to global P sinks (1.2 x 10^{10} mol yr^{-1}, compared to global P sedimentary sink of 11-34 x 10^{10} mol yr^{-1}; Delaney, 1998). This finding would ultimately suggest that: *a*) phosphorus sequestration during interglacials would contribute to a certain degree to stabilise the oceanic N:P ratios and *b*) any increase in nitrogen fixation during stadials would be limited by the reduced phosphate availability and by increased N/P ratios in the oceans.

The objective of this study is to present the existence of high-frequency (centennial-to-millennial-scale) phosphorite deposition in finely laminated sediments from two cores collected in the ETNP. All phosphorites documented in this study are found in horizons that coincide with episodes of enhanced water-column denitrification - as indicated by $\delta^{15}N$ records. The weight-percent records of phosphorus are compared with high-resolution records of $\delta^{15}N$ and organic carbon in sediments from two cores collected in the Mazatlan Margin (MD02-2518) and Gulf of Tehuantepec (MD02-2520) (Fig. 7.1). In addition, the total-P accumulation rates from the two sites are compared with P accumulation rates compiled from different oceanographic settings. This work provides a follow-up to the initial investigative work by Ganeshram et al. (2002) and suggests an upward revision of P-sinks during interstadials, which would contribute to stabilising N:P ratios following variations in the intensity of suboxic denitrification. Finally, this study further explores how the marine microbial community inhabiting suboxic sediments on continental margins may provide a source of phosphorus for phosphogenesis. This is accomplished by comparing P enrichments in the two cores with recent observations of the role of large sulphur bacteria in phosphorite deposition.

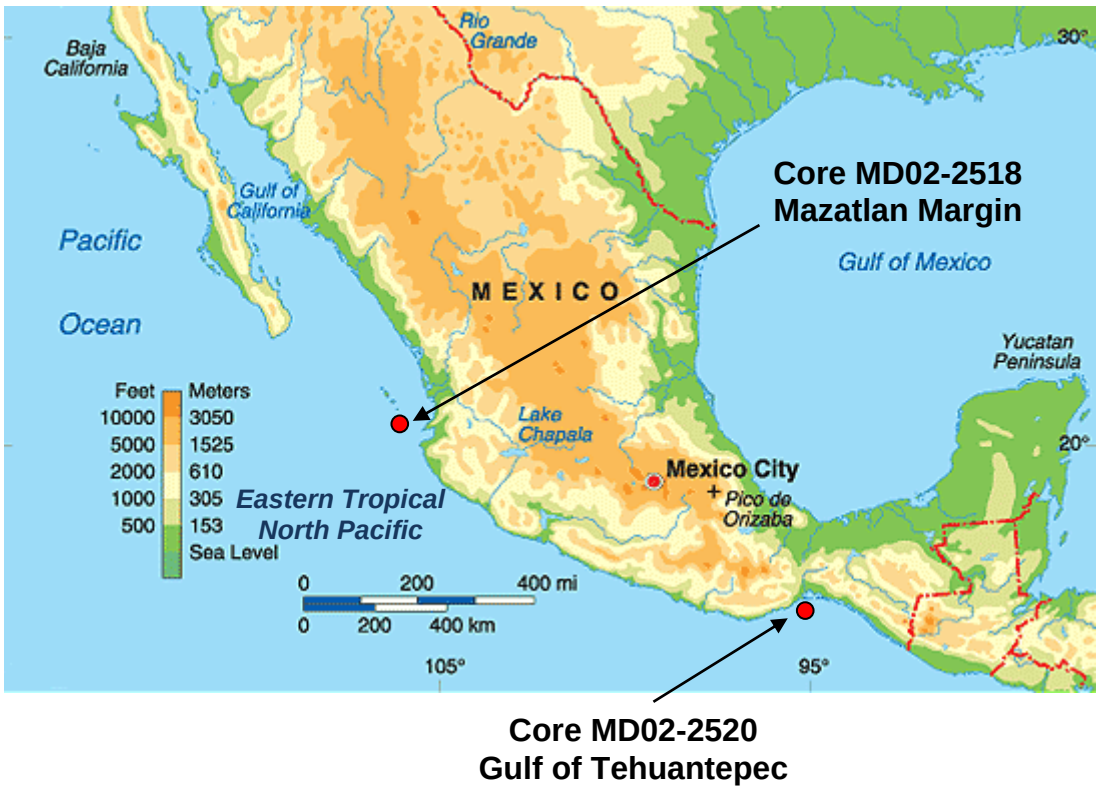

Figure 7.1: Map showing locations of core MD02-2518 collected at 454m water depth on the upper slope of NW Mexico (22º40.39N, 106º29.19W) and core MD02-2520 collected at 719m water depth in the Gulf of Tehuantepec (15º40.14 N, 95º18.00W).

7.2. Methods

(See chapter 3 of this thesis)

7.3. Results: Phosphorus burial in total P concentrations in cores MD02-2518 and MD02-2520

Phosphorus concentration in seawater exerts a primary control on biological productivity in the surface layer of the ocean. Average P concentrations in seawater have been found to range from 0.1 to 2.5 µM l^{-1} with vertical water column profiles reflecting surface uptake and a concomitant release at intermediate water depths (Broecker and Peng, 1982; Delaney, 1998). Marine P concentrations represent a balance between inputs from rivers, atmospheric deposition and removal of P to sediments on the sea bed by means of sinking organic carbon, biogenic apatite (fish scales and bones),

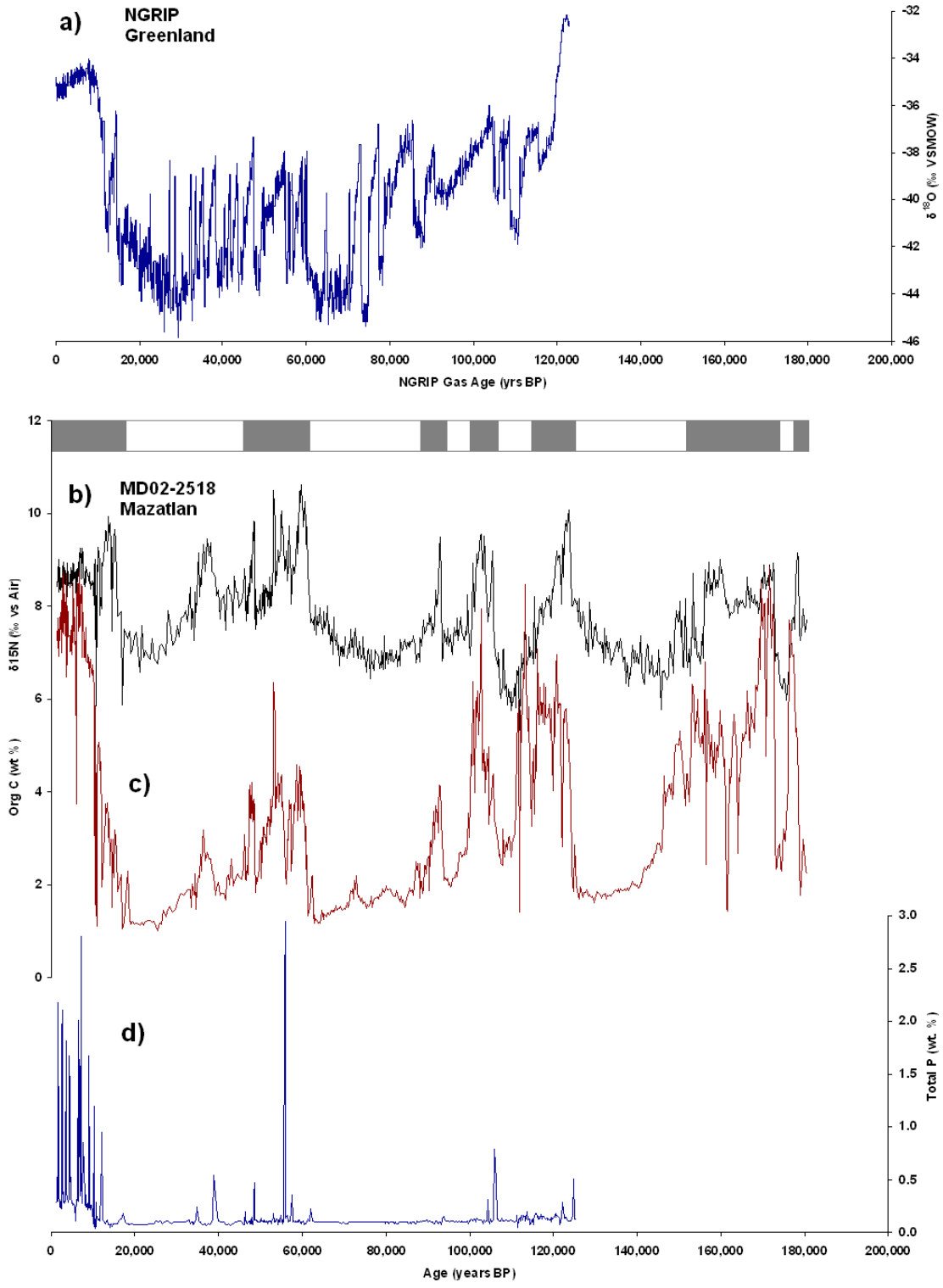

Figure 7.2: a) records of $\delta^{18}O$, a proxy for atmospheric temperature, from the NGRIP ice core, Greenland (NGRIP Members, 2004); b) $\delta^{15}N$ variations, c) organic C weight %, and d) weight percent phosphorus, based on a 2-cm sampling interval, in core MD02-2518 from Mazatlan, Mexico. The grey and white bars above the Mazatlan core records represent laminated/bioturbated intervals in core MD02-2518. The majority of P enrichments in Holocene sediments are due to reactive P as carbonate fluorapatite (CFA)-free and organic-free sediments have P/Al values of ~0.0088 compared to

observed Holocene P/Al values ranging from 0.05 - 0.3 wt. %. The enrichments observed from 100 – 130kyr are due to the presence of dispersed CFA grains, whereas the interval at 57kyr (Total P = 3%) is a hard layer containing up to 25% CFA (pure CFA contains ~13% P; Price & Calvert, 1978). Additional measurements in laminated sediments from MIS 7 between 200-210kyrs BP (or 18.1-19m depth) yield Total P concentrations between 0.08-0.14%, suggesting that either the preservation or sequestration of P was reduced in sediments older than MIS 6.

adsorption onto Fe-oxyhydroxides and precipitation as carbonate fluorapatite (Froelich, 1982). Sedimentary P concentrations in non-phosphogenic continental margins and deep sea sediments range from 10-100 μmol P g^{-1}, however, the higher sedimentation rates commonly observed in continental margins lead to P accumulation rates that exceed by far those observed in deep sea sediments (see Table 1 and data in Filippelli, 1997). The average P/Al value of shales is 0.008 (Wedepohl, 1995) and it may be inferred that P/Al ratios above this value are likely to be due to the mineralisation of biogenic P sources and CFA formation.

Phosphorus concentrations in core MD02-2518, retrieved from the continental shelf offshore Mazatlan, Mexico, were calculated at 2cm intervals (Fig. 7.2). All P enrichments observed in the core occur in organic-rich, finely-laminated intervals deposited during MIS 1, 3 and 5. By contrast, total P concentrations in bioturbated sections are noticeably lower, ranging from 0.07 to 0.1%. The highest P concentrations are found in Holocene sediments and the range of background P concentrations in this section of the core (0.2-0.5%) is very similar to values reported by Jahnke et al. (1983) from (their) Station 15 (21º34.1'N, 113º50.0'W; 388m water depth) and Ganeshram et al. (2002) from core NH15P (22º41.09'N, 106º28.89'W; 425m water depth). A hard phosphorite horizon of 2.5cm was found at 600cm depth, where the surrounding sediments are thought to have been deposited approximately 55,000 years BP. Depth profiles of molar ratios for N_{total}:P_{total}, C_{org}:P_{total}, C_{org}:N_{total}

and P_{total} weight percentage for core MD02-2518 are shown in Figure 7.3. Both N_{total}:P_{total} and C_{org}:P_{total} ratios are interdependent with the organic content of the core, with a trend of higher values in interstadial intervals and lower ratios throughout stadials. The mean molar organic C:P ratio of marine phytoplankton is 106:1, with a mean molar C:N ratio of 6.6:1 and a mean molar N:P ratio of 16:1 (Redfield et al., 1963). In contrast, terrestrial organic matter is relatively impoverished in P and N, with C:P ratios ranging up to or exceeding 800, C:N ratios ranging up to or exceeding 1000 and N:P ratios ranging between 5-40 (Likens et al., 1981). The N_{total}:P_{total} ratios in core MD02-2518 fall into two distinct populations: interstadial intervals are characterised by N_{total}:P_{total} ratios ranging between 5-10, as opposed to values ranging between 1-4 found in sediments deposited during Greenland stadials. C_{org}:N_{total} molar ratios are relatively constant, ranging throughout the core between 10-15, with the exception of three samples deposited around 10ka that appear to be depleted in N. The highest P values show a high degree of interdependence with total Ca percentage in the core and the weight percentage ratio between Ca and P in samples with the highest P wt% values is approximately 3:1 (Fig. 7.4), broadly similar to the ratio of Ca : P in the theoretical composition of carbonate fluorapatite [$Ca_{10}(PO_4)_6F_2$]. Total P molar concentrations range from 0.3 to 1 mmol P g^{-1} in Holocene sediments, with peaks of up to 2 mmol P g^{-1} in phosphorite horizons. Concentrations in bioturbated sediments are much lower, ranging between 45-70 µmol P g^{-1}, of which up to 10-15 µmol P $g^{-1}$is likely to be of detrital origin (if it is assumed that the average detrital P/Al values of sediments to be 0.008), which suggests that any P enrichment is independent of the presence of aluminosiliocates.

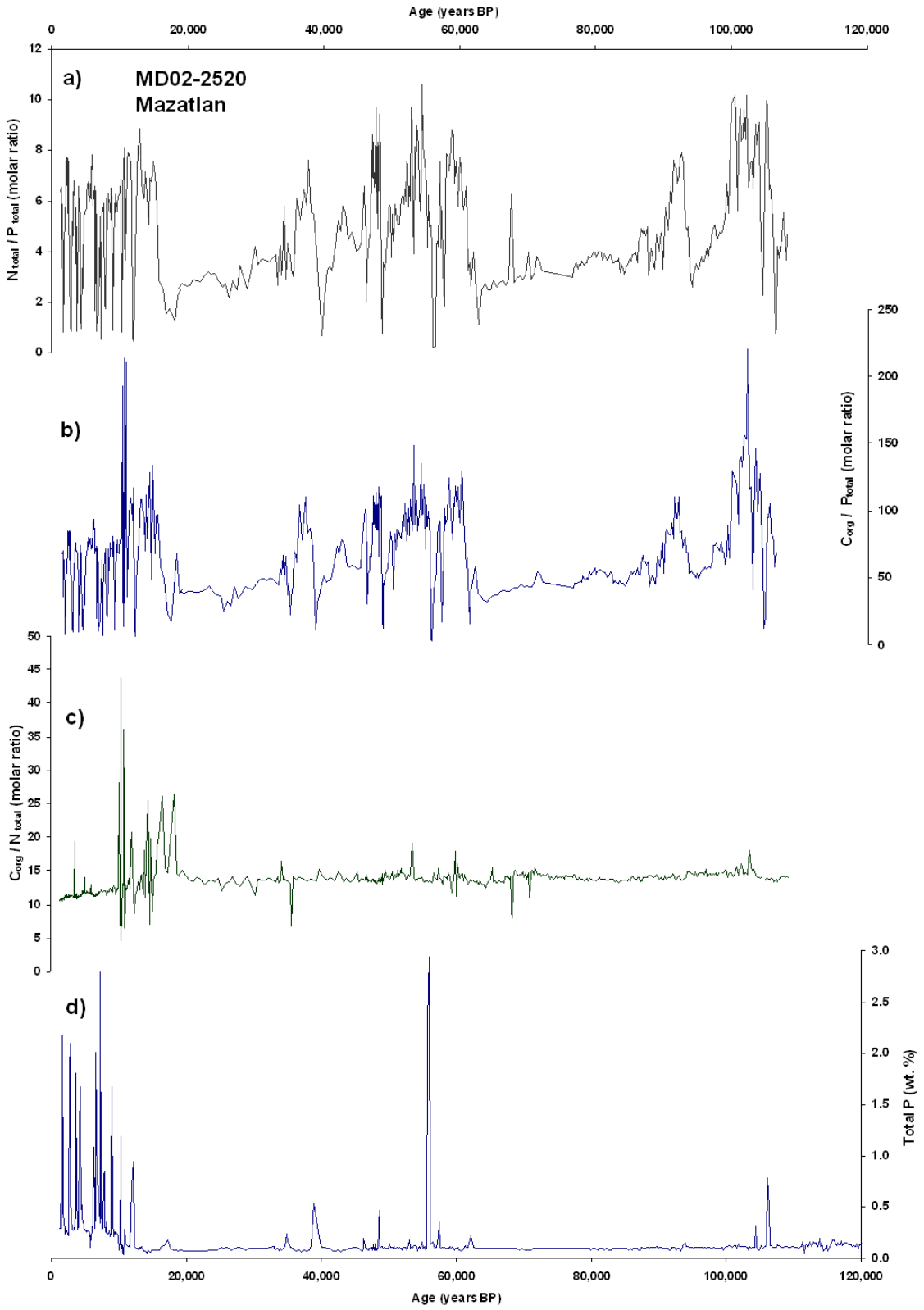

Figure 7.3: age profiles of elemental C:N:P ratios for core MD02-2518 from Mazatlan, Mexico. a) N_{total}:P_{total} molar ratio; b) C_{org}:P_{total} molar ratio; c) C_{org}:N_{total} molar ratio; and d) weight percent phosphorus, based on a 2-cm sampling interval.

Total phosphorus concentrations, $\delta^{15}N$ and C_{org} in core MD02-2520 were calculated at 5cm intervals (Fig. 7.5). The 37-metre piston core, retrieved from 720m depth in the Gulf of Tehuantepec, Mexico, spans the last 45,000 years and the majority of it consists of organic-rich, laminated sediments, with the exception of a faintly bioturbated interval between 12-14,000 yrs BP. The $\delta^{15}N$ and C_{org} records in the core are decoupled and total P is found to vary in close correspondence with organic matter concentrations in the core. Average total P concentrations in core MD02-2520 vary between 0.1 % (in sediments with organic contents of 3-4%) to 0.2% (in sediments with higher organic contents of 5-6%). Within the higher C_{org} intervals, there are a number of sections containing up to 0.3% P, which are confined to what appear to be major Dansgaard-Oeschger (D-O) episodes of rapid climate warming observed in Greenland ice cores (in particular D-O events 1, 2, 6, 8 and 12).

Depth profiles of molar ratios for N_{total}:P_{total}, C_{org}:P_{total}, C_{org}:N_{total} and P_{total} weight percentage for core MD02-2520 are shown in Figure 7.6. The N_{total}:P_{total} ratio ranges between 5-10, however, it does not show the level of variability between Greenland stadials and interstadials as can be seen in the core from Mazatlan Margin. C_{org}:P_{total} ratios range between 100-200, whereas C_{org}:N_{total} ratios range between 10-25 with one sample deposited around 16.5ka reaching a ratio of 40. Both C_{org}:P_{total} and C_{org}:N_{total} show an inverse correlation with C_{org} weight percentage throughout the core that is opposite to that seen in core MD02-2518 (Mazatlan Margin), with higher C_{org} values (found to correlate with Greenland interstadials) resulting in lower C_{org}:P_{total} and C_{org}:N_{total} molar ratios. This is likely to be due to preferential regeneration of N- and P-rich compounds under high sedimentation rates found in the Gulf of Tehuantepec (>60cm ka^{-1}) and within sediments containing higher levels

of refractory organic carbon.

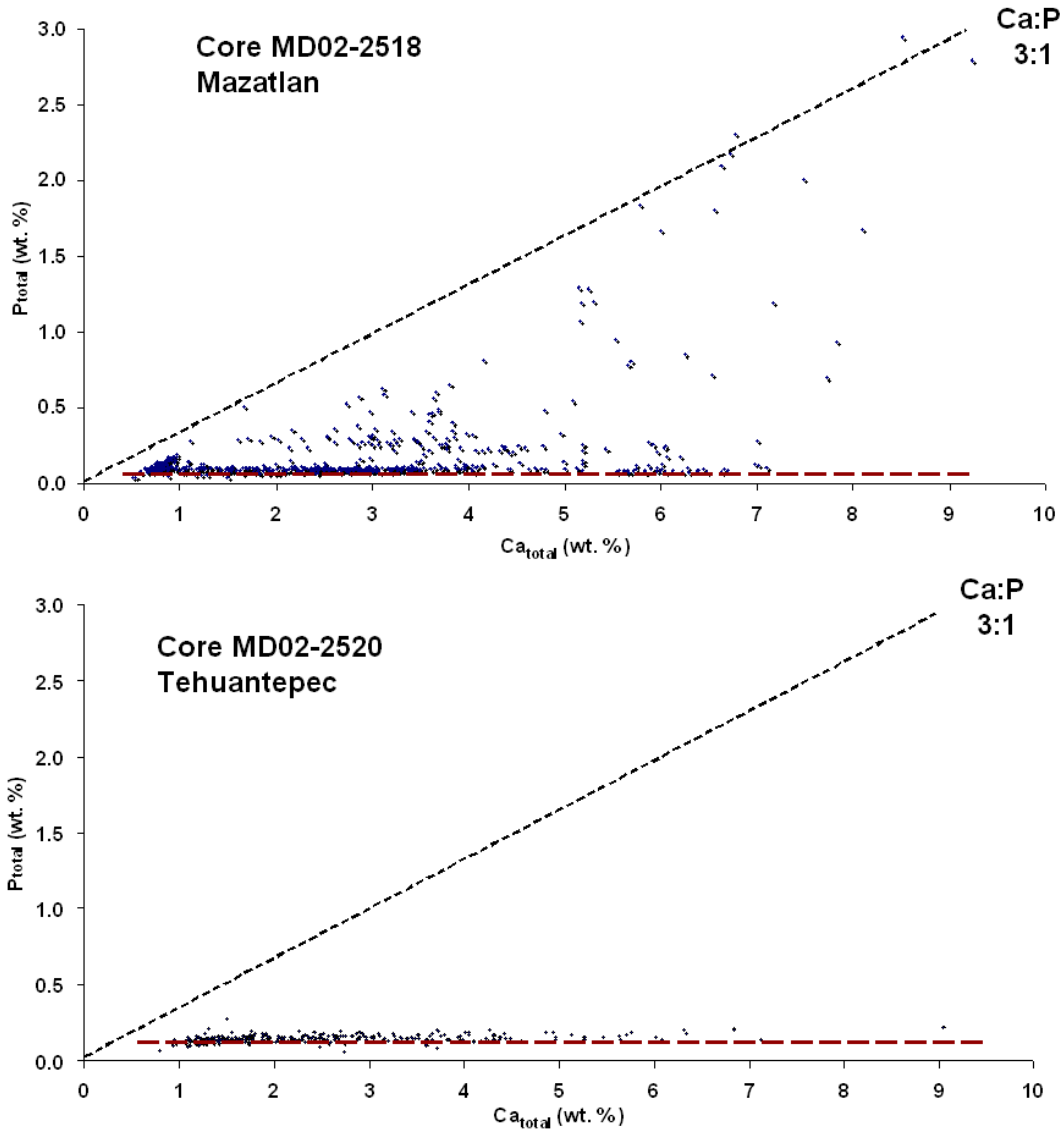

Figure 7.4: (a) Plot of Total P% versus total Ca% in core MD02-2518. The stippled ellipse highlights sediments with Ca:P = 3:1 ratio typical of phosphorite layers in laminated sections of the core, which are composed largely of calcium phosphate minerals. (b) Plot of total P% versus Total Ca% in core MD02-2520 from the Gulf of Tehuantepec. Total phosphorus concentrations in core MD02-2520 (Fig. 7.5) were calculated at 10cm intervals, corresponding to an average age of 120-150 years per interval. The total P concentration profile approximately matches that of C_{org} content of the core. The weight percentage concentrations are lower than those found in laminated sections of core MD02-2518 and range from 0.1 - 0.2%, with the exception of four peaks that have total P contents of up to 0.3%, with the peaks at 25 and 36kyr BP coinciding with peaks in total Ca exceeding 10%.

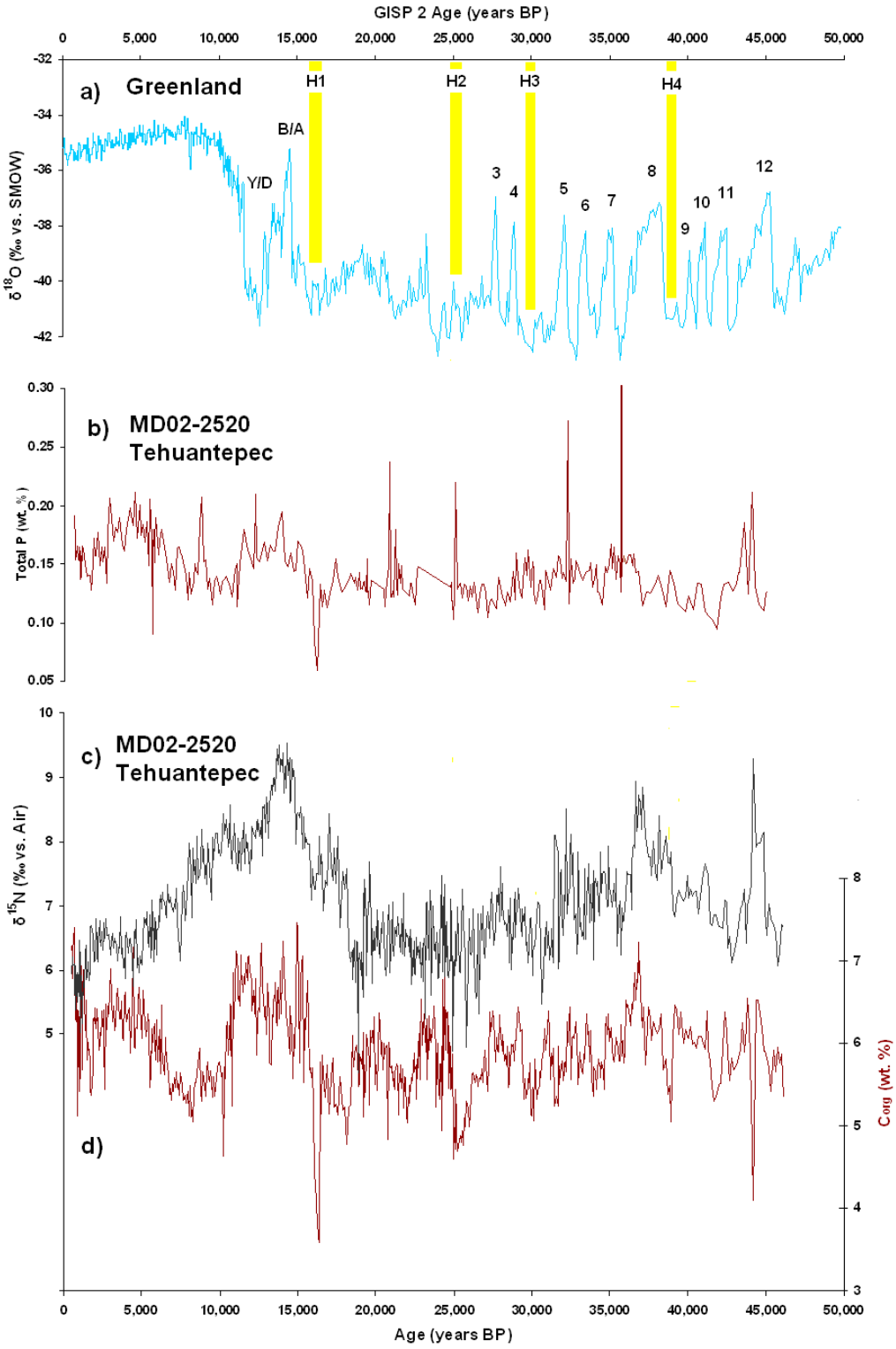

Figure 7.5: Age profile of weight percentage of A) total phosphorus measured at 10cm intervals, B) δ15N and organic carbon in core MD02-2520 from the Gulf of Tehuantepec. Numbers indicate peaks in C_{org} and total P percentage correlated to Greenland Dangaard Oeschger events.

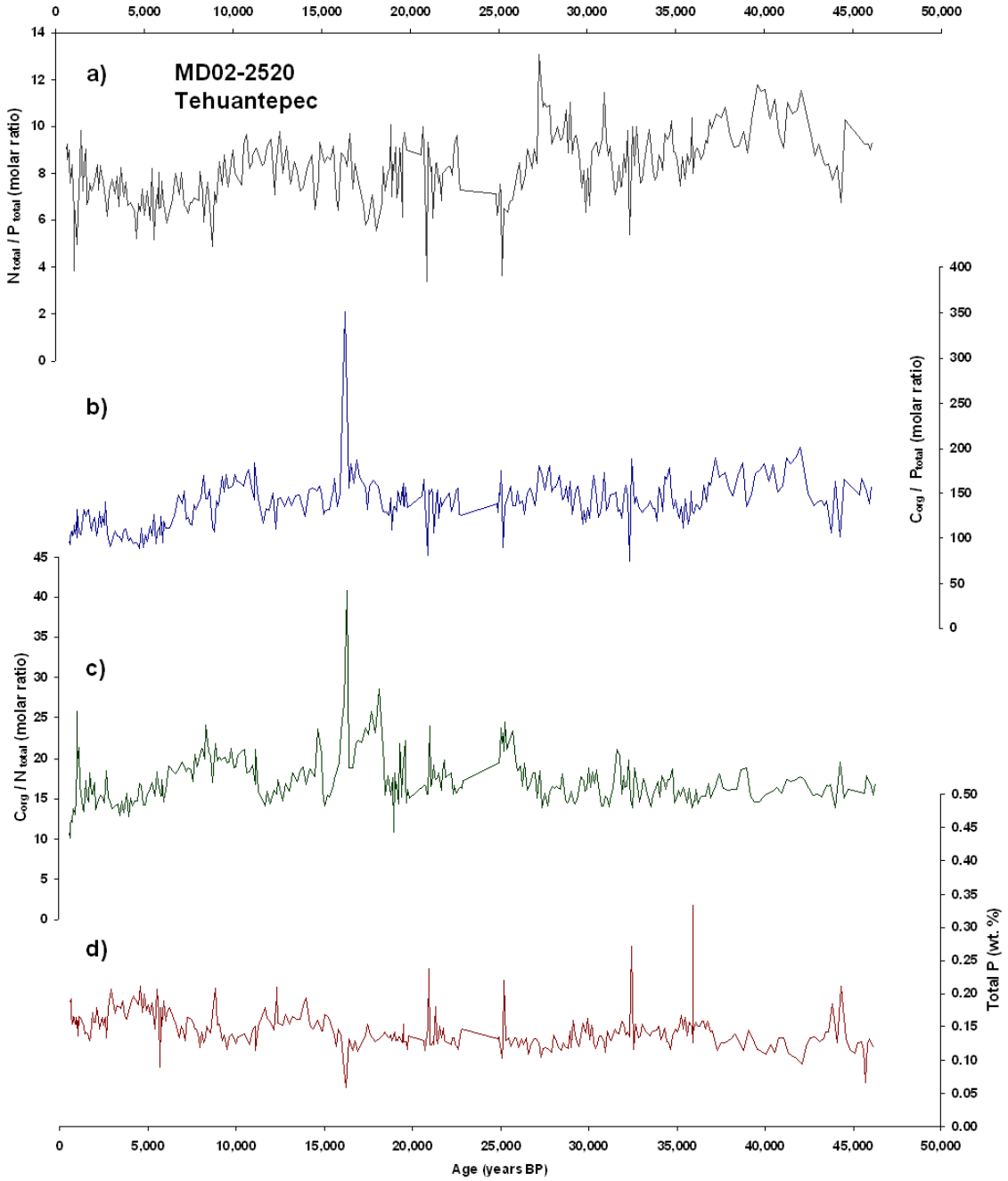

Figure 7.6: age profiles of elemental C:N:P ratios for core MD02-2518 from Mazatlan, Mexico. a) N_{total}:P_{total} molar ratio; b) C_{org}:P_{total} molar ratio; c) C_{org}:N_{total} molar ratio; and d) weight percent phosphorus, based on a 2-cm sampling interval.

7.4 Discussion

Sediments on continental margins where P concentrations may exceed 1000 μmol P g^{-1} are an exception and have only been described from settings underlying areas of high export productivity, which leads to an oxygen minimum zone impinging on the continental shelf. *Phosphogenesis* (the authigenic formation of carbonate fluorapatite - CFA) and *phosphorite* deposition (large accumulations of P-rich sediments on continental margins) are common features in sediments where the porewater HPO_4^{2-} concentrations exceed CFA saturation (Price & Calvert, 1978). Van Cappellen and Berner (1991) found that nucleation of octacalcium phosphate [$Ca_4H(PO_4)_3 \cdot xH_2O$], a likely precursor to CFA, can occur under the conditions of phosphate concentrations exceeding about 290 μmol l^{-1}. Phosphorite deposition represents a particularly important sink in the marine P cycle and has been found to occur in continental margins predominantly during interglacials (Ganeshram et al., 2002), which normally coincide with higher rates of export productivity and an increase in intensity of the oxygen minimum zone in continental margins in the ETNP, ESP and Arabian Sea. Hence, it was argued that relatively small areas of the ocean may account for an estimated removal of 10-15% of biologically available P from the ocean during interstadials (Delaney, 1998). Any increase in burial efficiency in phosphogenic regions during interstadials will remove a fraction of biologically available P from the oceans and may have potentially perturbed canonical N:P ratios in seawater. Nevertheless, the ratio of phosphate removal to the total oceanic reservoir of P occurring during interstadials is likely to have been smaller than the ratio of interglacial decrease in fixed nitrogen to the total oceanic reservoir of fixed nitrate (10-15% reduction in P compared to ~50% reduction in fixed N; Ganeshram et al., 2000). The existence of different removal rates between N and P may have led to changes in N:P ratios and productivity in the ocean between stadials and interstadials, which may have favoured organisms thriving on lower N:P ratios during interstadials and higher N:P ratios during stadials.

Filippelli (1997) compiled a synopsis of data on sedimentary P concentration and sedimentation rates from continental margins, phosphogenic continental margins and open ocean settings with the purpose of quantifying the major sinks in the marine P cycle (see Table 7.1). The results of his paper showed that ranges in

sedimentary P concentrations are relatively similar in both continental margin and deep sea settings, though higher sedimentation rates in continental margins led to P accumulation rates that exceed by far those observed in deep sea sediments. Areas of significant phosphogenesis are an exception: the high P concentrations in these sedimentary settings are not reflected in their P accumulation rates due to low sedimentation rates and their P accumulation rates thus are comparable to generic continental margins.

However, new results from two cores collected from the Mexican Margin highlight that laminated sediments in the ETNP may constitute a larger sink for phosphorus than has been previously observed. It emerges from Table 7.1 that sediment accumulation rate is the most important factor affecting P accumulation rates. Lower sedimentation rates in the Mazatlan Margin, ranging from 5.5-18 cm kyr^{-1}, led to good preservation conditions for phosphatic laminae with total P concentrations >0.3%. By contrast, the lower total P concentrations and lack of visual observation of phosphorites in core MD02-2520 suggests that any phosphatic horizons formed in the Gulf of Tehuantepec are likely to have been diluted by the extremely high sedimentation rates in the area. This study highlights the remarkable similarity between P accumulation rates in sediments from the Gulf of Tehuantepec and from Mazatlan Margin, despite the noticeably different sedimentation rates in the two settings. The similarity in P accumulation rates (4,000-10,000 μmol P $cm^{-2}kyr^{-1}$) in these two settings highlight how high sedimentation rates are just an important contributor to the P burial flux as is the formation of laminated, P-rich sediments deposited on the Mazatlan Margin.

Location	P concentration (µmol P g^{-1})	Sedimentation rate (cm kyr^{-1})	P accumulation rate (µmol P $cm^{-2}kyr^{-1}$)
Open ocean regions			
Indo-Pacific	17-23	2.5-5.0	28-75
Equatorial Pacific	7-36	0.9-4.5	7-35
Equatorial Atlantic	21-23	0.9-2.8	9-52
Southern Ocean	9-13	2.8-3.2	16-19
Pacific Red Clay province	26-119	0.3-0.6	6-17
North Pacific Gyre	16	0.2	2
Central equatorial Pacific	307	0.2	16
Continental margin regions			
Non-phosphogenic			
West Africa (Namibia)	92-108	260	2,800-3,300
St. Lawrence Seaway	26-32	200	1,100-8,000
Long Island Sound	8	100-300	400-1,200
Mississippi Delta	16	800	6,400
Peru Margin	35-80	160-360	770-1,800
California margin	23-33	8-21	90-120
North Carolina margin	23-24	60	810-830
Phosphogenic			
Baja California	580	2-31	80-1,250
Peru Margin	2,800-3,700	1.7-1.8	5,000-6,300
Arabian Sea *(cores BC451 & BC 455)*	60-130	9-24	76-1000
Core MD02-2518 Mazatlan	300-2000 (laminated) 45-70 (bioturbated)	5.5-18	5,000-10,000 * (laminated) 800-1600 § (bioturbated)
Core MD02-2520 Gulf of Tehuantepec	80-140	50-90	4,000-10,000 †

Table 7.1. Phosphorus concentrations, bulk sedimentation rates and P accumulation rates for several marine environments, modified from Table 1 in Filippelli, 1997. Total P concentration in sediments represents a combination of detrital P, which comprises all forms of apatite which do not undergo any geochemical reactions with seawater, and reactive P which was once in bioavailable form and may be deposited in a variety of forms (Ruttenberg, 1992, 1993). The sources in this table mostly report total P concentration, with the exception of values reported for the Equatorial Pacific, Equatorial Atlantic and Mississippi Delta, where P concentrations refer to the reactive fraction. Hence, P accumulation rates calculated for the continental margin sites, where sediments can have detrital P contents ranging from 10-50%, are maximum values for reactive P. Values for the Arabian Sea are an addition to Filippelli's original table and are taken from Schenau et al, 2000.

* The values in the laminated sections of the Mazatlan Margin core were calculated as an average of the top two and a half metres of the core as follows: Mean porosity (16.6%); mean Wet Bulk Density (2.46g cm^{-3}); average density of sediments (2.051 g cm^{-3}). The physical properties of core MD02-2518 can be found on the PANGAEA Network for Geoscientific & Environmental Data at: http://doi.pangaea.de/10.1594/PANGAEA.95610

(*Continued from previous page*)
§ The values in the bioturbated sections of the Mazatlan Margin core were calculated as an average of the first bioturbated section of the core (2.8 – 4m depth) as follows: Mean porosity (7.1%); mean Wet Bulk Density (2.62g cm^{-3}); average density of sediments (2.43 g cm^{-3})

† The values in the Gulf of Tehuantepec core were calculated as an average of top six metre of the core as follows: Mean porosity (47.7%); mean Wet Bulk Density (1.927 g cm^{-3}); average density of sediments (1.008 g cm^{-3}). The physical properties of core MD02-2520 can be found on the PANGAEA Network for Geoscientific & Environmental Data at: http://doi.pangaea.de/10.1594/PANGAEA.95612

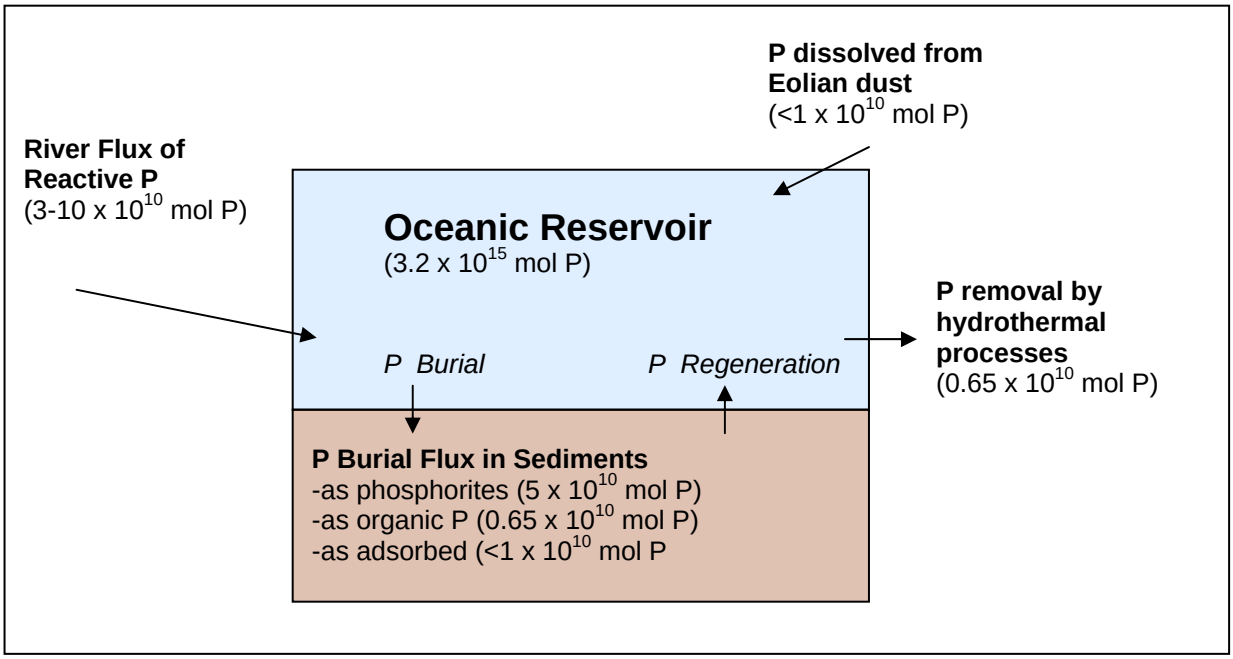

	Area (km^2)	mol P km^2 yr^{-1}	P Burial as phosphorite (10^{10} mol P)
ETNP	500,000	75000	3.75
ETSP	200,000	60000	1.2
Arabian Sea	400,000	5000	0.2
Namibian Shelf	30,000	30000	0.09
Total	1,130,000		~5

Figure 7.7: A reassessment of the oceanic P mass balance, modified from Figure 1 in Delaney (1998).

The remarkable similarity between P concentrations in sediments retrieved from open ocean cores and those observed in continental margin regions is also surprising, considering that rates of surface productivity and export production above continental margins are generally several times higher than those for open ocean regions. In addition, water depths can be up to 5 times greater in the pelagic open

ocean settings than in continental margins, which would result in a greater degree of organic matter degradation through the deeper water column and a remineralisation of organic P. Based on these reasons, Filippelli (1997) concluded that phosphorite deposits in phosphogenic regions do not represent particularly important sinks in the marine P cycle. This assumption did not take into account the extremely high sedimentation rates in some phosphogenic areas along the Mexican Margin where total P accumulation rates can be as high as 10,000 μmol P cm^{-2} kyr^{-1} in laminated sediments.

Ganeshram et al. (2002) speculated that the global phosphogenic P burial is in the order of 1.2 x 10^{10} mol yr^{-1} by extrapolating a median P burial of 1000 μmol P $cm^{-2}kyr^{-1}$1 over a total phosphogenic sediment area of 1.2 x 10^6 km^2. The ETNP covers around 0.5 x 10^6 km^2 or 40-45% of the total modern phosphogenic sediment area. This study shows that the estimated P accumulation rate throughout the Holocene (4,000-10,000 μmol P $cm^{-2}kyr^{-1}$) is about 4-5 times higher than what had been estimated by Ganeshram et al (2002), suggesting that the ETNP may play a more important role in regulating modern global P budgets than was previously thought (Fig. 7.7), although the mechanisms of P removal in continental margins are more complex than the mere phosphorite deposition through the reworking of phosphatic layers, and involve additional pathways such adsorption onto Fe-oxides, consequent desorption in a reducing environment and eventual uptake through vacuoles within giant sulphur bacterial 'mats' (Reimers et al. 1990; Schulz et al.; 1999 and Schulz & Schulz 2005).

Benthic P fluxes in the ETNP upwelling region and N_{total}:P_{total}, C_{org}:P_{total} ratios in underlying sediments (Figs. 7.3 and 7.6) are regulated by regeneration processes occurring shortly after deposition of organic matter on the continental shelf and slope. Both N_{total}:P_{total} and C_{org}:P_{total} molar ratios in the Mazatlan core (Fig 7.3) are higher during interstadials than in sediments deposited during stadials, with the exception of P-rich intervals. It is likely that these P-rich intervals are reworked layers, which have much lower C_{org} content due to shelf current winnowing and the consequent amalgamation of phosphatic horizons near the sediment/water interface. The higher N_{total}:P_{total} and C_{org}:P_{total} ratios in interstadials are likely to be due to organic matter in the sediments maintaining a stoichiometry that bears a closer

relation to the Redfield ratio of C:N:P = 106:16:1. Bioturbated intervals deposited during stadials show preferential loss of C_{org} due to organic matter decomposition, while the P is retained in authigenic phases, thus giving lower molar ratios. In core MD02-2520 (Gulf of Tehuantepec), N_{total}:P_{total} and C_{org}:P_{total} ratios do not show the same level of variability between Greenland stadials and interstadials that is as large as that seen in the Mazatlan core. Ingall and van Cappellen (1990) found that organic C/P ratios tend to be lower than the Redfield ratio at low sedimentation rates. An average C_{org}:P_{total} ratio of 140 (Fig 7.6) suggests that the high productivity and high sedimentation rates within the Gulf of Tehuantepec lead to preferential recycling of P, which results in the high C_{org}:P_{total} ratios. Deposition of organic matter and fish debris are the primary means of transport of reactive P from the water column to the sediment (Suess, 1981). The hard parts of fish (scales, bones and teeth) consist of 60-70% hydroxyapatite and will sink to the seafloor relatively intact, with any dissolution of biogenic apatite occurring after burial. Average export productivity in the northern ETNP is circa 200-300g C m^{-2} y^{-1} (see chapter 2.1) which, based on a C:P ratio of 106:1, would gives rise to an annual P export flux of ~15-20μmol P cm^{-2} y^{-1}. Assuming that 90% of export productivity is recycled within the water column (Schenau and De Lange, 2001), the flux of organic P reaching the sediment surface in the ETNP is 1.5-2.0 μmol P cm^{-2} y^{-1}. However, the data in table 7.1 suggests that there is more P buried in sediments relative to supply by export of organic carbon (up to 5-10 μmol P cm^{-2} y^{-1} in laminated sediments compared to 1.5-2.0 μmol P cm^{-2} y^{-1} from organic carbon). This suggests that there must be another source of 'authigenic' phosphorus burial, which the author believes to be found in the mechanism of phosphate uptake from the surrounding water column and from the release under anoxic conditions by giant sulphur bacteria (Reimers et al. 1990; Schulz and Schulz, 2005).

Fig. 7.2 shows that phosphorus-enriched layers in the Mazatlan Margin are confined to finely laminated C_{org}-rich sediments deposited during warm interstadials. The laminated intervals in the core also coincide with higher N_{total}:P_{total}, C_{org}:P_{total} molar ratios (Fig 7.3), suggesting that the organic carbon in these sediments may be of a more refractory nature or that P remineralisation rates from organic matter may have been higher throughout interstadials. However, core MD02-2518 contains only

one P-rich horizon (>1% total P) in sediments older than the LGM, which is in contrast to the eight CFA laminae identified in core NH15P in laminated sediments dating from MIS 3 & 5 (see Fig. 2 in Ganeshram et al., 2002). Hence, it is likely that phosphorites form localised deposits, each with a variable thickness and geographical extent. This was recently confirmed by new evidence from Schulz and Schulz (2005), who suggests that phosphorites are formed as large, inhomogeneous bacterial mats developing where the OMZ impinges on the continental shelf and pore water gradients of O_2 and H_2S overlap. The deposition of phosphorites in the ETNP has been attributed to the giant sulphur bacteria *Thioploca* and *Beggiatoa* (Gallardo, 1977), a genetic cousins of the microbe *Thiomargarita*, or "Sulfur pearl". These bacteria bear similar characteristics to sulphur-oxidising bacteria belonging to the *Beggiatoaceae* family and can grow up to three-quarters of a millimeter in diameter by storing sulfur within the cell wall as well as nitrate and polyphosphates in globules within a huge central sac (Schulz et al., 1999). The appreciation of the large degree of complexity within the marine microbial community lead Reimers et al. (1990) and Schulz & Schulz (2005) to suggest an active bacterial role in phosphorite formation within laminated sediments. These bacteria gain energy by oxidising sulphide, which accumulates in anoxic sediments as a by-product of the decomposition of organic matter, and accumulate polyphosphates. The release of phosphate by these bacteria has been observed to occur only episodically in the presence of acetate, which may indicate why the distribution of porewater phosphate levels exceeding CFA saturation and phosphorite layers in laminated sediments from the Mazatlan Margin is rather sporadic.

The flux of particulate P that reaches the sediment-water interface consists of a detrital and a reactive fraction (Ruttenberg and Berner 1993). Detrital P comprises all forms apatite that do not undergo any geochemical reactions with seawater, whereas reactive P was once in bioavailable form and may be sedimented in a variety of forms. Reactive P is defined as the sum of organic, Fe-bound, authigenic and biogenic P (Ruttenberg, 1992; 1993). Recent studies suggest that P may exhibit preferential regeneration compared to C during diagenesis of organic matter in low oxygen continental margin sediments (Compton et al., 1993; Ingall and Jahnke, 1994; 1997). Ingall et al. (1993) and Ingall and Jahnke (1994) suggested that P

exhibits a preferential regeneration compared to C during diagenesis of organic matter in low-oxygen continental margin sediments, which may lead to decoupling of these elements in their long-term biogeochemical cycles. Organic P concentrations in sediments decrease dramatically with depth and age and may reach less than 10% of original near-surface values (Filippelli and Delaney, 1996). The observed decrease is most likely due to microbial regeneration of organic matter and the release of P from its organic form.

Laminated sediments deposited during MIS 3 and 5 in core MD02-2518 from Mazatlan show lower P concentrations compared to Holocene sediments. This is likely to be due to phosphate being deposited in Holocene sediments as numerous layers of amorphous precipitates following the early diagenesis of bacterial mats, which release phosphate into porewaters leading to the growth of phosphatic phases in nucleation sites (Reimers et al., 1990). The organic fraction of reactive P is remineralised in marine sediments during diagenesis but it is not immediately lost as it is normally redistributed to other burial pools. Reducible sedimentary components, mostly in the form of Fe-oxyhydroxides, act as temporary shuttles in the remobilisation of P. During later stages of diagenesis (as found in MIS 3 and 5), the presence of nucleation sites in the form of calcite, skeletal material, feldspars and fish debris (Guldbrandsen et al., 1984) may help to 'kick-start' the precipitation of apatite as discrete horizons. However, Jahnke et al. (1983) found that organic matter may act as an inhibitor to the formation of apatite by reducing the sedimentary pH and reducing presence of calcite-rich nucleation sites. This is confirmed by the very poor preservation of foraminifera in organic-rich horizons within both cores. It also explains why in sediments older than MIS 2 phosphorite precipitation is reduced, suggesting that the majority of P-rich layers in Holocene sediments are likely to be amorphous precursors to apatite formation (i.e. octacalcium phosphate [$Ca_4H(PO_4)_3 \cdot xH_2O$] Van Cappellen and Berner, 1991). The P-rich interval at 57kyr in core MD02-2518 (Total P = 3%) is a hard layer containing up to 25% CFA coinciding with a C_{org} values of 2% against values of surrounding sediments of 4% (Fig. 7.2). This would confirm the theory proposed by Jahnke et al. (1983) that where C_{org} is low within laminated sediments, apatite nucleation and precipitation occur more rapidly. The formation of authigenic carbonate fluorapatite CFA limits the remobilisation and loss

of P from sediments, and explains why sporadic peaks in total P in both cores occur in concomitance with high levels of calcium in core MD02-2518 (Fig. 7.4).

In order to evaluate P cycling in the ETNP, it is important to further research the life cycle of large sulphur bacteria and the environmental conditions influencing the formation of authigenic apatite. Burial in non-reactive and authigenic sediments is the only sink for P, hence changes in the burial rate can affect the P inventory of bottom waters on stadial-interstadial time-scales. This may, in turn, affect surface water productivity on regional and global scales through changes in the marine C:N:P stoichiometry on the scale of ocean overturning (~1,500 yrs) provided that there is sufficient vertical mixing and diffusion rates to allow transport of nutrients from bottom waters to the euphotic layer (Van Cappellen and Ingall, 1994, 1996; Arrigo, 2005). The lack of P-enrichments in bioturbated, organic-poor (stadial) sections of core MD02-2518 is likely due to a combination of reduced P fluxes to sediments and benthic oxic conditions inhibiting the establishment of *Beggiatoa*, *Thioploca* and *Thiomargarita*. At the same time, reduced denitrification and a less intense OMZ in the ETNP would have affected nutrient ratios in the oceans, raising inorganic NO_3:PO_4 ratios of intermediate waters and determining the activity and composition of phytoplankton in the Equatorial Pacific.

During interstadials, denitrification causes a degree of nitrogen deficit relative to P for upwelled waters, theoretically favouring N_2-fixers in nutrient-poor waters. However, reviews of field studies of blooms of *E. huxlei* in cold waters indicate that low NO_3:PO_4 ratios in surface waters are not necessarily limiting conditions (Lessard et al., 2005). If the same principles are found to apply to taxa living in warm tropical waters in the ETNP, it may be possible that the high rates of productivity observed in cores MD02-2518 and MD02-2520 that occurred during interstadials were driven by plankton able to use amino acids, amides, urea and purines such as hypoxanthine (Berman and Bronk, 2003) rather than the limiting inorganic nitrate. If plankton in the ETNP are found to utilise an increasing amount of regenerated nitrogen (recycled nitrogen in the form of ammonia) compared to new sources such as nitrate from deep water, it is reasonable to postulate that the limiting factor for productivity in the ETNP during interstadials is the rate of wind-induced upwelling. The influence of increases in productivity along upwelling margins on the

partial pressure of CO_2 is likely to have been limited and partially offset by increased degasification of CO_2 from upwelled waters. In addition, as plankton took up regenerated nitrogen and inorganic phosphorus along continental margins during interstadials, it is likely that the nitrogen fixation in subtropical gyres may have been less dependent on inorganic P from continental margins than previously thought. Future work will have to take into account taxa-specific, non-Redfield stoichiometry of plankton and the role of microbial metabolism in low oxygen environments, which mediates N and P inventories through newly discovered metabolic pathways.

7.5 Conclusion

Modern phosphorites are formed in laminated, organic-rich sediments underlying highly productive western boundary currents and are thought to contribute to the regulation of PO^{3-}_4 in seawater (Froelich et al., 1982). The origin of these lenses of unconsolidated phosphatic deposits has been attributed to the supersaturation of interstitial pore waters and reworking of sediments (Price and Calvert., 1978; Jahnke et al., 1983; Van Cappellen and Berner, 1991), dissolution of fish remains (Suess, 1981) and phosphate mineralisation mediated by benthic sulphur-oxidising bacteria (Reimers et al., 1990). Total phosphorus measurements from two piston cores collected at intermediate water depths in the ETNP indicate that a substantial increase in phosphorite deposition occurred during interstadials. The increases in P sequestration from the marine inventory occurred in tandem with periods of enhanced suboxic denitrification, suggesting a coupling between phosphogenesis and the loss of fixed N on millennial time-scales. This study estimated P accumulation rates throughout the Holocene in the ETNP ranging between 4,000-10,000 μmol P $cm^{-2}kyr^{-1}$, which is around 4-5 times higher than previously suggested. Hence, it emerges that the ETNP may play a more important role in regulating modern global P budgets than was previously thought. This reassessment of P burial on millennial has two important consequences: on the one hand it suggests that global N:P ratios may be more closely tied to the canonical value of 16 during transitions from stadials to interstadials. On the other hand, the enhanced sequestration of P into suboxic sediments during interstadials agrees with

the recent discovery of the role of large sulphur bacteria in phosphorite formation, suggesting that sediments in the ETNP may switch from being a net importer of phosphate during interstadials to a net exporter during stadials.

References

Arrigo, K.R. (2005) Marine microorganisms and global nutrient cycles. *Nature*, vol. **437**, pp. 349-355

Babu, C. P. and Nath, B. N. (2005) Processes controlling forms of phosphorus in surficial sediments from the eastern Arabian Sea impinged by varying bottom water oxygenation conditions, *Deep-Sea Res*. II, vol. **52**, pp. 1965–1980

Baturin, G.N. and Bezrukov P.L. (1979) Phosphorites on the sea floor and their origin. *Marine Geology*, Vol. **31**, pp. 317-332

Berman, T. and Bronk, D.A. (1993) Dissolved organic nitrogen: a dynamic participant in aquatic ecosystems. *Aquat. Microb. Ecol*., vol. **31**, pp. 279-305

Broecker, W. S. and Peng, T.-H (1982) Tracers in the Sea. Lamont-Doherty Geological Observatory, Eldigio Press, Palisades, N.Y.

Calvert, S.E., Bustin, M., Pedersen, T.F., 1985. An X-ray fluorescence spectrometric method for the determination of major and minor elements in ferromanganese nodules. *Chem. Geol*., vol. **51**, 9-18.

Compton, J.S., D.A. Hodell, J.R. Garrido and D. J. Mallison (1993) Origin and age of phosphorite from the south-central Florida Platform: relation of phosphogenesis to sea-level fluctuations and δ13C excursions, *Geochim. Cosmoc. Acta*, vol. **57**, pp. 131-146

Delaney, M.L. (1998) Phosphorus accumulation in marine sediments and the oceanic phosphorus cycle. *Glob. Biogeoc. Cycles*, vol. **12**, pp. 563-572

EPICA Community Members (2006) One-to-one coupling of glacial climate variability in Greenland and Antarctica. *Nature*, vol. **444**, pp. 195-198

Filippelli, G.M., (1997) Controls on phosphorus concentration and accumulation in oceanic sediments. *Marine Geology*, vol. **139**, pp. 231-240

Filippelli, G.M. and Delaney, M.L. (1992) Similar Phosphorus fluxes in ancient phosphorite deposits and a modern phosphogenic environment. *Geology*, vol. **20**, pp. 709-712

Froelich P.N., Bender, M.L., Luedtke, N.A., Heath G.R., and DeVries, T. (1982) The marine phosphorus cycle. *Amer. J. Sci*., vol. **282**, pp. 474-511

Gallardo, V.A. (1977) Large benthic microbial communities in sulfide biota under Peru-Chile subsurface countercurrent. *Nature*, vol. **268**, pp. 331-332

Ganeshram, R.S., Pedersen, T.F., Calvert, S.E. and Murray, J.W. (1995) Large changes in oceanic nutrient inventories from glacial to interglacial periods. *Nature*, vol. **376**, pp. 755-757

Ganeshram, R.S. and Pedersen, T.F. (1998) Glacial-interglacial variability in upwelling and bioproductivity off NW Mexico: implications for Quaternary paleoclimate. *Paleoceanography*, vol. **13**, pp. 634-635

Ganeshram, R.S., Pedersen, T.F., Calvert, S.E., McNeill G.W., Fontugne, M.R. (2000) Glacial-Interglacial variability in denitrification in the world's oceans: Causes and consequences. *Paleoceanography*, vol. **15**, pp. 361-376

Ganeshram, R.S., Pedersen, T.F., Calvert, S.E. and Francois, R. (2002) Reduced nitrogen fixation in the glacial ocean inferred from changes in marine nitrogen and phosphorus inventories. *Nature*, vol. **415**, pp. 156-159

Gulbrandsen, R. A., Roberson, C. E. and Neil, S. T. (1984) Time and the crystallization of apatite in seawater. *Geochim. Cosmochim. Acta*, vol. **48**, pp. 213–218

Jahnke, R.A., Emerson, S.R., Roe, K.K. and Burnett, W.C. (1983) The present day formation of apatite in Mexican continental margin sediments, *Geochim. Cosmochim. Acta*, vol. **47**, pp. 259-266

Kress, A.G. and Veeh, H.H. (1980) Geochemistry of radiometric ages of phosphatic nodules from the continental margin of northern New South Wales, Australia. *Mar. Geol*., vol. **36**, pp. 143-157

Kuypers, M.M.M., Lavik, G., Woebken, D., Schmid, M., Fuchs, B.M., Amann, R., Jørgensen and Jetten, M.S.M. (2005) Massive nitrogen loss from the Benguela upwelling system through anaerobic ammonium oxidation, *Proc. Nat. Acad. Sci*., vol. **102**, pp. 6478–6483

Ingall, E.D. and Van Cappellen, P. (1990) Relation between sedimentation rate and burial of organic phosphorus and organic carbon in marine sediments. *Geochim. Cosmochim. Acta*, vol. **54**, pp. 1219-1234

Ingall, E. and Jahnke, R. (1994) Evidence for enhanced phosphorus regeneration from sediments overlain by oxygen depleted waters. *Geochim. Cosmochim. Acta*, vol. **58**, pp. 2571-2575

Ingall, E. and Jahnke, R. (1997) Influence of water column anoxia on the elemental fractionation of carbon and phosphorus during sediment diagenesis. *Mar. Geol*., vol. **139**, pp. 219-229.

Lessard, E.J., Merico, A., Tyrrell, T. (2005) Nitrate : Phosphate ratios and Emiliana huxlei blooms. *Limnol. Oceanogr*., vol. **50**, pp. 1020- 1024

Likens, G.E., Bormann, F.H., and Johnson, N.M. (1981) Interaction between major biogeochemical cycles in terrestrial ecosystems. In Likens, G.E., (Ed.), Some Perspectives of the Major Biogeochemical Cycles-SCOPE 17: New York (Wiley), pp. 93–112

Longhurst, A.R., Sathyendranath, S., Platt, T. and Caverhill, C. (1995) An estimate of global primary production in the ocean from satellite radiometer data. *Journal of Plankton Research*, vol. **17**, pp1245-1271

McManus, J., Oppo, D.W., Cullen, J.L. (1999) A 0.5-Million-Year Record of Millennial-Scale Climate Variability in the North Atlantic. *Science*, vol. **283**, pp 971- 975

NGRIP members (2004) High-resolution record of Northern Hemisphere climate extending into the last interglacial period, *Nature*, vol. **431**, pp 147- 151

O'Brien C.W. and Veeh, H.H. (1980) Holocene phosphorite on the east Australian continental margin. *Nature*, vol. **288**, pp. 690-692

Piper, D.Z. and Codispoti, L.A. (1975) Marine phosphorite deposits and the nitrogen cycle. *Science*, vol. **188**, pp. 15–18

Price, N.B. and Calvert, S.E. (1978) The geochemistry of phosphorites from the Namibian shelf. *Chem. Geol*., Vol. **23**, pp. 151-170

Redfield, A.C., Ketchum, B.H., and Richards, F.A. (1963) The influence of organisms on the composition of seawater. In Hill, M.N. (Ed.), *The Sea* (Vol. 2): New York (Wiley), pp. 26–77

Reimers, C.E., Kastner, M. and Garrison R.E. (1990) The role of bacterial mats in phosphate mineralization with particular reference to the Monterey Formation, in Burnett, W.C. and Riggs, S.R. (eds.), Phosphate Deposits of the World, Vol. **3**, Neogene to Modern Phosphorites: Cambridge University Press, Ch. 24, p. 300-311

Ruttenberg, K.C. (1992). Development of a sequential extraction method for different forms of phosphorus in marine sediments. *Limnol. Oceanogr*., vol. **37**, 1460-1482.

Ruttenberg, K.C., (1993) Reassessment of the oceanic residence time of phosphorus. *Chem. Geol*., vol. **107**, pp. 405-409

Ruttenberg, K.C. and Berner, R.A. (1993). Authigenic apatite formation and burial in sediments from non-upwelling, continental margin environments. *Geochim. Cosmochim. Acta.*, vol. **57**, pp. 991-1007.

Schenau, S.J. and De Lange G.J. (2001) Phosphorus regeneration vs. burial in sediments of the Arabian Sea. Mar. Chem., vol. **75**, pp. 201-217

Schulz, H.N., Brinkhoff, T., Ferdelman, T.G., Hernández Mariné, M., Teske, A. and Jørgensen B.B. (1999) Dense Populations of a Giant Sulfur Bacterium in Namibian Shelf Sediments. *Science*, vol. **284**, pp. 493-495

Schulz H.N. and Schulz H.D. (2005) Large Sulfur Bacteria and the Formation of Phosphorite. *Science*, vol. **307**, pp. 416-418

Suess E. (1981) Phosphate regeneration from sediments of the Peru continental margin by dissolution of fish debris. *Geochim. Cosmochim. Acta*, vol. **45**, pp. 577-588

Thunell, R.C., and Kepple A.B. (2004), Glacial-Holocene $\delta^{15}N$ record from the Gulf of Tehuantepec, Mexico: Implications for denitrification in the eastern equatorial Pacific and changes in atmospheric N2O. *Glob. Biogeochem. Cycles*, vol. **18** GB1001, doi:10.1029/2002GB002028

Van Cappellen, P. and R. Berner. 1991. Fluorapatite crystal growth from modified seawater solutions. *Geochim. Cosmochim. Acta*, vol. **55**, pp. 1219-1234

Van Cappellen, P. and Ingall, E. (1994) Benthic phosphorus regeneration, net primary production, and ocean anoxia: A model of the coupled marine biogeochemical cycles of carbon and phosphorus. *Paleoceanography*, vol. **9**, pp. 677-692

Verardo, D.J., Froelich, P.N., McIntyre, A., (1990) Determination of organic carbon and nitrogen in marine sediments using the Carlo Erba NA-1500 Analyzer. *Deep Sea Res*., vol. **37**, pp. 157-165.

Wedepohl K.H. (1995) The composition of the continental crust. *Geochim. Cosmochim.* Acta, vol. **59**, pp. 1217–1232

Williams, L.A. and Reimers, C. (1983) Role of bacterial mats in oxygen-deficient marine basins and coastal upwelling regimes: preliminary report. *Geology*, vol. **11**, pp. 267-269

Appendix A
Core MD02-2518 (Mazatlan) – Carbon & Nitrogen

Depth (cm)	Age (yrs BP)	Corg %	N %	$\delta^{15}N$ ‰	Depth (cm)	Age (yrs BP)	Corg %	N %	$\delta^{15}N$ ‰
9	1,242	7.26	0.81	8.44	76	4,145	7.36	0.77	8.53
10	1,286	7.42	0.82	8.52	77	4,188	7.13	0.74	8.41
11	1,329	7.54	0.83	8.56	78	4,232	7.00	0.72	8.46
12	1,373	7.76	0.85	8.85	79	4,275	7.06	0.74	8.69
13	1,416	7.10	0.77	8.55	80	4,318	7.05	0.72	8.64
14	1,459	7.30	0.80	8.62	81	4,362	7.05	0.72	8.66
15	1,503	7.31	0.80	8.58	82	4,405	7.04	0.72	8.82
16	1,546	7.16	0.78	8.49	83	4,448	7.19	0.75	8.66
17	1,589	7.52	0.81	8.30	84	4,492	7.03	0.72	8.58
18	1,633	7.33	0.79	8.59	85	4,535	7.30	0.74	8.50
19	1,676	7.50	0.80	8.59	86	4,578	7.42	0.76	8.84
20	1,719	6.89	0.77	8.75	87	4,622	7.57	0.76	8.74
21	1,763	7.31	0.79	9.03	88	4,665	6.95	0.68	8.45
22	1,806	7.26	0.78	8.37	89	4,708	7.31	0.74	8.77
23	1,849	7.71	0.83	8.65	90	4,752	7.20	0.71	8.60
24	1,892	7.76	0.83	8.75	91	4,795	7.33	0.71	8.63
25	1,936	7.51	0.83	8.84	92	4,838	7.28	0.71	8.55
26	1,979	7.60	0.80	8.54	93	4,882	7.45	0.74	8.95
27	2,022	7.63	0.82	8.63	94	4,925	7.32	0.71	8.88
28	2,066	7.51	0.80	8.53	95	4,968	7.20	0.71	8.68
29	2,109	7.87	0.82	8.59	96	5,012	8.53	0.71	8.59
30	2,152	7.85	0.81	8.35	97	5,055	7.44	0.74	8.64
31	2,196	7.73	0.82	8.51	98	5,098	7.50	0.74	8.61
32	2,239	7.85	0.84	8.56	99	5,141	7.65	0.76	8.74
33	2,282	7.22	0.77	8.58	100	5,185	7.67	0.77	8.92
34	2,326	6.99	0.71	8.51	101	5,228	7.79	0.77	8.87
35	2,369	7.92	0.84	8.62	102	5,271	8.18	0.81	8.61
36	2,412	8.14	0.85	8.59	103	5,315	7.42	0.72	8.65
37	2,456	8.01	0.84	8.50	104	5,358	7.72	0.76	8.68
38	2,499	7.45	0.77	8.31	105	5,401	7.58	0.75	8.63
39	2,542	7.45	0.78	8.56	106	5,445	7.30	0.72	8.73
40	2,586	8.12	0.85	8.71	107	5,488	7.18	0.70	8.68
41	2,629	8.68	0.88	8.78	108	5,531	7.16	0.72	8.75
42	2,672	8.16	0.84	8.88	109	5,575	7.23	0.71	8.71
43	2,716	7.42	0.76	8.79	110	5,618	7.19	0.71	8.62
44	2,759	7.75	0.80	8.81	111	5,661	6.91	0.69	8.60
45	2,802	8.35	0.87	8.86	112	5,705	6.76	0.66	8.55
46	2,846	8.75	0.92	8.96	113	5,748	6.10	0.60	8.41
47	2,889	8.65	0.90	8.96	114	5,791	5.16	0.50	8.17
48	2,932	8.31	0.86	8.77	115	5,835	3.75	0.34	7.75
49	2,975	7.82	0.80	8.75	116	5,878	8.24	0.83	8.80
50	3,019	7.77	0.80	8.63	117	5,921	8.30	0.84	8.60
51	3,062	8.28	0.86	8.63	118	5,965	7.90	0.79	8.77
52	3,105	7.64	0.79	8.49	120	6,008	8.25	0.81	8.58
53	3,149	8.14	0.85	8.83	121	6,051	8.23	0.84	8.60
54	3,192	7.92	0.83	8.74	122	6,095	8.01	0.81	8.69
55	3,235	8.02	0.84	8.77	123	6,138	8.33	0.84	8.65
56	3,279	7.38	0.77	8.48	124	6,181	8.27	0.85	8.82
57	3,322	7.61	0.79	8.63	125	6,224	8.49	0.86	8.53
58	3,365	7.55	0.78	8.52	126	6,268	8.50	0.89	8.73
59	3,409	8.09	0.85	8.53	127	6,311	8.33	0.87	8.76
60	3,452	7.86	0.47	8.51	128	6,354	7.98	0.81	8.67
61	3,495	7.32	0.77	8.56	129	6,398	7.48	0.77	8.97
62	3,539	7.27	0.74	8.28	130	6,441	8.16	0.83	8.74
63	3,582	6.46	0.67	8.47	134	6,484	8.10	0.84	9.06
64	3,625	8.72	0.92	8.65	135	6,528	8.06	0.80	8.71
65	3,669	7.34	0.76	8.67	136	6,571	8.23	0.85	8.85
66	3,712	6.74	0.67	8.21	137	6,614	8.72	0.89	8.90
67	3,755	7.03	0.76	8.34	138	6,658	7.60	0.76	9.09
68	3,799	7.23	0.77	8.75	139	6,701	7.55	0.76	9.05
69	3,842	8.00	0.85	8.95	140	6,744	7.89	0.81	9.26
70	3,885	7.76	0.81	8.61	141	6,794	7.78	0.80	9.21
71	3,929	7.81	0.81	8.56	142	6,844	7.59	0.76	9.06
72	3,972	7.90	0.82	8.45	143	6,894	8.26	0.84	9.19
73	4,015	7.55	0.79	8.72	144	6,944	8.07	0.82	9.11
74	4,058	7.45	0.78	8.58	145	6,995	8.45	0.86	9.10
75	4,102	7.36	0.76	8.46	146	7,045	8.20	0.81	8.76

Appendix A
Core MD02-2518 (Mazatlan) – Carbon & Nitrogen

Depth (cm)	Age (yrs BP)	Corg %	N %	$\delta^{15}N$ ‰	Depth (cm)	Age (yrs BP)	Corg %	N %	$\delta^{15}N$ ‰
147	7,095	8.39	0.82	8.61	262	14,248	2.42	0.11	7.48
148	7,145	8.46	0.85	8.88	263	14,460	1.51	0.25	9.28
149	7,195	8.44	0.82	8.97	264	14,672	2.98	0.18	8.39
150	7,245	6.89	0.67	8.99	265	14,884	2.15	0.28	9.48
152	7,345	7.17	0.69	9.27	266	15,096	3.16	0.27	9.67
154	7,445	7.88	0.75	9.14	267	15,308	3.00	0.24	9.41
156	7,546	7.57	0.73	8.95	268	15,520	2.70	0.17	8.57
158	7,646	7.61	0.74	8.73	269	15,732	1.86	0.11	7.80
160	7,746	7.30	0.71	8.48	272	16,368	2.21	0.10	7.90
162	7,846	6.89	0.67	8.50	274	16,792	1.05	0.08	5.86
164	7,946	6.88	0.67	8.44	276	17,216	1.20	0.10	7.53
166	8,047	7.00	0.70	8.74	280	18,064	2.29	0.10	7.32
168	8,147	7.56	0.77	8.51	282	18,488	1.20	0.10	7.49
170	8,247	7.29	0.71	8.86	284	18,916	1.21	0.10	7.20
172	8,347	6.81	0.66	8.84	286	18,724	1.16	0.09	6.97
174	8,447	6.77	0.66	8.68	288	19,253	1.21	0.09	7.06
176	8,548	6.94	0.68	8.68	290	19,782	1.14	0.09	7.36
178	8,648	6.84	0.64	8.67	292	20,311	1.17	0.10	7.46
180	8,748	6.66	0.63	8.60	294	20,840	1.13	0.10	6.57
182	8,848	6.62	0.62	8.50	296	21,369	1.18	0.10	7.57
184	8,948	6.47	0.65	8.56	298	21,898	1.13	0.10	6.87
186	9,049	6.73	0.65	8.74	300	22,427	1.21	0.11	7.03
188	9,149	6.84	0.65	8.36	302	22,956	1.23	0.11	6.87
190	9,249	6.74	0.62	8.37	304	23,485	1.23	0.11	6.83
192	9,349	6.59	0.62	8.49	306	24,014	1.19	0.10	7.31
194	9,449	6.58	0.62	8.46	308	24,543	1.21	0.10	6.86
196	9,550	6.51	0.66	8.54	310	25,072	1.00	0.10	6.75
198	9,650	6.72	0.64	8.47	312	25,601	1.16	0.10	7.14
200	9,750	6.67	0.64	8.56	314	26,130	1.14	0.10	7.18
202	9,850	6.58	0.61	8.52	316	26,659	1.45	0.12	7.11
204	9,950	6.43	0.60	8.43	318	27,188	1.29	0.12	6.92
206	10,051	6.32	0.26	8.03	320	27,717	1.48	0.14	7.93
208	10,151	3.06	0.52	8.82	322	28,246	1.53	0.13	7.66
210	10,251	5.61	0.54	9.03	324	28,775	1.40	0.12	7.16
211	10,301	5.83	0.43	8.69	326	29,304	1.46	0.13	7.24
212	10,351	4.62	0.12	7.29	328	29,833	1.60	0.16	7.59
213	10,401	1.57	0.40	7.79	330	30,362	1.72	0.15	7.35
214	10,451	4.37	0.39	8.01	332	30,891	1.81	0.15	7.74
215	10,502	4.24	0.40	8.24	334	31,420	1.77	0.15	7.80
216	10,552	4.41	0.39	7.99	336	31,949	1.84	0.15	7.93
217	10,602	4.23	0.34	7.59	338	32,478	1.90	0.16	7.66
218	10,652	3.83	0.12	7.46	340	33,005	1.89	0.17	8.42
219	10,702	1.55	0.07	5.85	342	33,209	1.50	0.12	7.51
220	10,752	1.10	0.18	8.36	344	33,412	2.02	0.18	7.94
221	10,802	2.14	0.38	8.90	346	33,616	1.94	0.17	7.85
222	10,852	4.17	0.46	8.90	348	33,820	1.81	0.13	7.25
224	10,952	4.99	0.45	8.92	350	34,024	1.76	0.15	7.84
226	11,053	4.89	0.47	8.75	352	34,227	2.22	0.19	8.30
228	11,153	4.97	0.47	9.28	354	34,431	1.46	0.13	7.87
230	11,253	5.05	0.45	9.16	356	34,635	1.98	0.17	8.16
232	11,424	4.87	0.41	8.97	358	34,838	2.09	0.18	8.74
234	11,595	4.46	0.42	7.81	360	35,042	2.19	0.20	9.16
236	11,767	4.62	0.29	8.21	362	35,246	2.15	0.37	8.23
238	11,938	3.28	0.18	7.95	364	35,449	2.66	0.22	8.63
240	12,110	1.96	0.20	8.95	366	35,653	2.35	0.20	8.48
242	12,281	2.23	0.30	8.88	368	35,857	2.30	0.20	8.66
244	12,453	3.13	0.32	9.27	370	36,061	2.91	0.25	8.95
246	12,624	3.42	0.34	9.55	372	36,264	3.16	0.26	9.35
248	12,796	3.74	0.32	9.64	374	36,652	2.50	0.21	8.75
250	12,967	3.54	0.34	9.61	376	37,039	2.70	0.23	9.45
252	13,139	3.75	0.30	9.19	378	37,427	2.55	0.22	9.08
254	13,310	3.38	0.27	9.61	380	37,815	2.55	0.22	9.38
256	13,482	3.02	0.31	9.93	382	38,203	2.34	0.20	8.75
258	13,653	3.41	0.22	9.59	384	38,590	2.18	0.19	8.70
260	13,824	2.40	0.25	9.80	386	38,978	1.77	0.15	8.64
261	14,036	2.98	0.20	9.28	388	39,366	1.93	0.15	8.25

Appendix A
Core MD02-2518 (Mazatlan) – Carbon & Nitrogen

Depth (cm)	Age (yrs BP)	Corg %	N %	$\delta^{15}N$ ‰	Depth (cm)	Age (yrs BP)	Corg %	N %	$\delta^{15}N$ ‰
390	39,753	2.03	0.17	8.34	522	50,250	3.23	0.27	8.48
392	40,141	1.77	0.15	7.72	524	50,386	2.86	0.23	8.00
394	40,529	1.80	0.15	8.12	526	50,523	3.22	0.27	8.36
396	40,916	1.81	0.15	8.27	528	50,659	3.16	0.26	7.80
398	41,304	1.66	0.14	7.49	530	50,795	3.02	0.23	7.91
400	41,692	2.11	0.18	8.34	532	50,932	3.08	0.25	8.45
402	42,080	2.21	0.17	8.44	536	51,204	2.85	0.22	8.25
404	42,467	2.00	0.16	8.29	538	51,341	3.20	0.24	8.39
406	42,855	2.54	0.22	8.26	540	51,477	3.47	0.28	8.01
408	43,243	1.97	0.17	7.64	542	51,614	3.26	0.26	8.33
410	43,630	2.05	0.18	8.66	544	51,750	3.46	0.28	8.31
412	44,018	2.14	0.19	8.31	546	51,886	3.38	0.27	7.96
414	44,406	2.23	0.19	8.30	548	52,023	3.07	0.26	8.64
416	44,793	2.17	0.17	7.98	550	52,159	3.41	0.29	8.00
418	45,181	2.11	0.18	8.09	552	52,295	3.85	0.32	8.14
420	45,569	2.35	0.20	8.35	554	52,432	3.33	0.27	8.01
422	45,956	3.07	0.26	8.80	556	52,568	3.67	0.30	8.46
424	46,028	2.59	0.22	8.53	558	52,704	3.67	0.30	8.23
426	46,099	2.68	0.23	8.28	559	52,841	4.14	0.29	9.20
428	46,171	2.11	0.17	8.12	560	52,977	6.34	0.39	10.51
430	46,243	2.21	0.19	7.70	562	53,114	5.57	0.38	9.79
432	46,314	2.08	0.18	7.76	564	53,250	3.63	0.30	8.44
434	46,386	2.09	0.17	7.80	566	53,386	3.66	0.31	8.75
436	46,457	2.24	0.19	7.99	568	53,523	4.11	0.36	8.54
438	46,529	2.33	0.20	8.24	570	53,659	3.87	0.33	8.78
440	46,601	2.41	0.21	7.88	572	53,795	4.39	0.37	9.19
442	46,672	2.29	0.20	7.86	574	53,932	4.36	0.36	9.22
444	46,744	2.20	0.19	8.05	576	54,068	3.99	0.34	8.95
446	46,816	2.28	0.20	7.86	578	54,204	3.78	0.31	9.02
448	46,887	2.49	0.22	8.34	580	54,341	4.08	0.34	9.12
450	46,959	3.13	0.27	8.50	582	54,477	4.29	0.37	9.26
452	47,031	3.23	0.27	8.24	584	54,613	4.28	0.37	9.93
454	47,102	4.04	0.35	8.35	586	54,750	4.35	0.38	10.05
456	47,174	3.45	0.29	8.37	588	54,929	3.68	0.32	9.70
458	47,246	4.13	0.35	8.37	590	55,107	3.78	0.33	9.73
460	47,317	3.72	0.32	8.30	592	55,286	3.39	0.30	9.39
462	47,389	3.47	0.30	8.89	594	55,464	2.95	0.26	8.82
464	47,460	3.42	0.30	8.80	596	55,643	2.90	0.25	8.78
466	47,532	3.73	0.33	9.00	598	55,821	2.26	0.20	8.83
468	47,604	3.63	0.31	8.70	600	56,000	2.02	0.17	9.19
470	47,675	4.20	0.37	8.52	602	56,179	2.57	0.20	8.55
472	47,747	3.54	0.32	8.95	604	56,357	3.39	0.28	8.84
474	47,819	3.52	0.31	9.08	606	56,536	2.94	0.25	9.11
476	47,890	3.65	0.32	9.16	608	56,714	3.83	0.29	9.74
478	47,962	3.76	0.33	9.60	610	56,893	3.64	0.30	8.95
480	48,034	3.80	0.32	9.35	612	57,071	3.74	0.32	8.70
482	48,105	3.36	0.29	9.26	614	57,250	2.29	0.20	8.06
484	48,177	3.39	0.30	9.53	616	57,429	2.90	0.26	8.89
486	48,248	3.78	0.33	9.51	618	57,607	3.71	0.31	8.80
488	48,320	3.85	0.34	9.82	620	57,786	3.59	0.30	8.73
490	48,392	3.64	0.31	9.82	622	57,964	3.61	0.30	8.70
492	48,463	2.65	0.22	8.61	624	58,143	3.92	0.34	9.00
494	48,535	2.23	0.19	7.74	626	58,321	4.59	0.36	9.50
496	48,607	2.16	0.17	8.00	628	58,500	3.89	0.32	9.74
498	48,678	1.93	0.17	8.37	630	58,679	3.37	0.30	9.13
500	48,750	1.83	0.15	7.53	632	58,857	3.81	0.38	9.59
502	48,886	2.14	0.18	7.66	634	59,036	4.55	0.35	10.48
504	49,023	2.03	0.16	8.01	636	59,214	4.39	0.29	10.50
506	49,159	2.21	0.18	7.86	638	59,393	3.47	0.36	10.25
508	49,295	2.35	0.19	7.97	640	59,571	4.35	0.32	10.61
510	49,432	2.57	0.21	8.00	642	59,750	3.65	0.30	10.17
512	49,568	2.91	0.25	8.27	644	59,929	3.58	0.30	9.96
514	49,705	2.93	0.24	8.06	646	60,107	3.79	0.31	9.73
516	49,841	2.87	0.23	7.78	648	60,286	3.73	0.30	9.98
518	49,977	2.11	0.17	7.74	650	60,464	2.94	0.25	10.27
520	50,114	2.79	0.24	8.14	652	60,643	3.25	0.26	9.74

Appendix A
Core MD02-2518 (Mazatlan) – Carbon & Nitrogen

Depth (cm)	Age (yrs BP)	Corg %	N %	$\delta^{15}N$ ‰	Depth (cm)	Age (yrs BP)	Corg %	N %	$\delta^{15}N$ ‰
653	60,821	2.33	0.20	9.35	784	74,858	1.57	0.13	6.81
654	61,000	2.63	0.23	9.72	786	75,071	1.48	0.12	6.57
656	61,213	1.31	0.12	8.74	788	75,284	1.56	0.13	7.02
658	61,426	1.51	0.13	8.07	790	75,497	1.53	0.12	7.08
660	61,640	1.67	0.14	7.65	792	75,711	1.55	0.13	6.85
662	61,853	2.14	0.18	7.73	794	75,924	1.59	0.13	6.44
664	62,066	2.19	0.19	7.64	796	76,137	1.73	0.14	7.04
666	62,279	1.28	0.11	7.71	798	76,350	1.75	0.15	6.76
668	62,492	1.33	0.12	7.49	800	76,563	1.51	0.12	6.79
670	62,706	1.18	0.11	7.55	802	76,777	1.63	0.13	6.70
672	62,919	1.28	0.11	8.03	804	76,990	1.65	0.14	6.60
674	63,132	1.25	0.11	7.39	806	77,203	1.70	0.15	7.04
676	63,345	1.22	0.11	7.80	808	77,416	1.70	0.14	6.98
678	63,558	1.17	0.11	7.59	810	77,629	1.73	0.15	6.95
680	63,772	1.18	0.11	7.69	812	77,843	1.68	0.14	6.89
682	63,985	1.17	0.10	7.96	814	78,056	1.79	0.15	6.65
684	64,198	1.25	0.11	7.65	816	78,269	1.73	0.15	6.80
686	64,411	1.45	0.12	7.61	818	78,482	1.77	0.15	6.68
688	64,624	1.36	0.10	7.41	820	78,695	1.76	0.15	7.02
690	64,838	1.26	0.11	7.65	822	78,909	1.92	0.16	6.87
692	65,051	1.36	0.12	7.91	824	79,122	1.85	0.16	6.63
694	65,264	1.34	0.12	7.55	826	79,335	1.84	0.16	7.36
696	65,477	1.29	0.11	7.71	828	79,548	1.87	0.16	6.64
698	65,690	1.39	0.12	8.01	830	79,761	1.99	0.17	6.98
700	65,904	1.38	0.12	7.41	832	79,975	1.89	0.16	6.99
702	66,117	1.34	0.12	7.59	834	80,188	1.88	0.16	6.76
704	66,330	1.37	0.12	7.18	836	80,401	1.89	0.16	6.91
706	66,543	1.44	0.12	7.34	838	80,614	1.92	0.16	7.05
708	66,756	1.40	0.12	7.53	840	80,827	1.89	0.16	6.82
710	66,970	1.44	0.12	6.95	842	81,041	1.85	0.16	6.88
712	67,183	1.41	0.12	7.77	844	81,254	1.82	0.16	7.06
714	67,396	1.44	0.12	7.37	846	81,467	1.79	0.15	6.82
716	67,609	1.44	0.25	7.34	848	81,680	1.74	0.15	6.80
718	67,822	1.55	0.13	7.16	850	81,893	1.75	0.15	6.86
720	68,036	1.45	0.11	7.41	852	82,107	1.86	0.16	7.02
722	68,249	1.47	0.12	7.05	854	82,320	1.80	0.15	6.69
724	68,462	1.48	0.12	7.16	856	82,533	1.72	0.15	6.88
726	68,675	1.48	0.12	6.71	858	82,746	1.67	0.15	6.93
728	68,888	1.53	0.12	7.11	860	82,959	1.64	0.14	6.71
730	69,102	1.47	0.12	7.12	866	83,173	1.63	0.14	7.29
732	69,315	1.45	0.12	6.90	868	83,386	1.73	0.15	7.15
734	69,528	1.45	0.12	7.15	870	83,599	1.61	0.14	7.04
736	69,741	1.48	0.13	6.90	872	83,812	1.65	0.14	7.07
738	69,954	1.47	0.12	7.36	874	84,025	1.61	0.14	7.22
740	70,168	1.51	0.16		876	84,239	1.50	0.13	7.29
742	70,381	1.62	0.13	6.86	878	84,452	1.57	0.14	7.18
744	70,594	1.50	0.12	7.01	880	84,665	1.71	0.15	7.07
746	70,807	1.56	0.13	7.18	882	84,878	1.74	0.15	7.21
748	71,020	1.69	0.13	6.98	884	85,091	1.86	0.15	7.14
750	71,234	1.87	0.15	7.52	886	85,305	1.87	0.15	7.25
752	71,447	1.84	0.15	7.12	888	85,518	1.94	0.16	7.12
754	71,660	1.82	0.15	7.32	890	85,731	1.85	0.16	7.21
756	71,873	1.92	0.16	7.32	892	85,944	1.90	0.16	7.22
758	72,086	1.67	0.13	6.89	894	86,157	1.77	0.15	7.37
760	72,299	2.08	0.17	7.39	896	86,371	1.99	0.17	7.24
762	72,513	1.88	0.15	7.55	898	86,584	2.16	0.19	7.16
764	72,726	2.18	0.18	7.19	900	86,797	2.48	0.21	6.78
766	72,939	1.85	0.15	6.99	902	87,010	2.31	0.19	6.88
768	73,152	1.72	0.15	6.87	904	87,223	2.45	0.20	6.98
770	73,365	1.75	0.14	7.23	906	87,437	2.15	0.18	6.96
772	73,579	1.64	0.14	6.84	908	87,650	2.44	0.20	6.80
774	73,792	1.70	0.14	6.91	910	87,863	1.70	0.14	7.34
776	74,005	1.63	0.13	6.94	912	88,076	2.06	0.17	7.26
778	74,218	1.60	0.13	7.36	914	88,289	2.07	0.17	7.14
780	74,431	1.62	0.13	6.84	916	88,503	1.81	0.15	7.46
782	74,645	1.64	0.13	6.90	918	88,716	1.90	0.15	7.72

Appendix A
Core MD02-2518 (Mazatlan) – Carbon & Nitrogen

Depth (cm)	Age (yrs BP)	Corg %	N %	$\delta^{15}N$ ‰	Depth (cm)	Age (yrs BP)	Corg %	N %	$\delta^{15}N$ ‰
920	88,929	2.40	0.20	7.41	1048	103,000	4.91	0.38	9.52
922	89,142	2.40	0.20	7.48	1049	103,192	3.97	0.32	9.10
924	89,355	2.23	0.19	7.50	1050	103,385	4.62	0.38	8.86
926	89,569	2.55	0.22	7.65	1052	103,577	4.24	0.35	8.51
928	89,782	2.62	0.22	7.61	1054	103,769	4.81	0.4	8.06
930	89,995	1.87	0.15	7.87	1056	103,962	4.43	0.37	7.66
932	90,208	2.88	0.25	7.67	1058	104,154	4.97	0.41	7.90
934	90,421	2.95	0.25	7.79	1060	104,346	3.29	0.27	7.97
936	90,635	2.66	0.22	7.38	1062	104,538	3.65		7.98
938	90,848	3.11	0.26	7.62	1064	104,731	3.75	0.32	8.22
940	91,061	3.58	0.29	7.44	1066	104,923	3.87	0.33	8.78
942	91,274	2.98	0.24	7.68	1068	105,115	4.32	0.37	9.19
944	91,487	3.70	0.32	8.35	1070	105,308	4.38	0.38	8.49
945	91,701	3.55	0.30	7.98	1072	105,500	4.31	0.36	7.71
946	91,914	3.55	0.29	8.09	1074	105,692	3.39	0.29	7.23
948	92,127	3.12	0.25	8.43	1076	105,885	3.31	0.29	6.95
950	92,340	3.63	0.31	8.39	1078	106,077	3.03	0.26	6.79
952	92,553	4.14	0.35	9.25	1080	106,269	2.92	0.25	6.68
954	92,766	4.12	0.35	9.50	1082	106,462	2.93	0.26	6.98
956	92,980	3.51	0.29	8.47	1084	106,654	2.61	0.22	6.75
958	93,193	2.83	0.22	6.82	1086	106,846	2.65	0.22	6.13
960	93,406	2.69	0.21	6.91	1088	107,038	2.46	0.20	6.01
962	93,619	2.09	0.16	7.49	1090	107,231	2.43	0.20	6.21
964	93,832	2.15	0.17	7.38	1092	107,423	2.39	0.20	6.21
966	94,046	2.07	0.17	7.19	1094	107,615	3.20	0.26	7.06
968	94,259	2.13	0.17	7.55	1096	107,808	2.74	0.23	7.06
970	94,472	2.03	0.16	7.13	1098	108,000	2.59	0.22	6.18
972	94,685	1.99	0.16	7.32	1100	108,192	2.78	0.23	6.23
974	94,898	2.02	0.16	7.19	1102	108,385	2.90	0.24	6.31
976	95,112	1.95	0.15	7.4	1104	108,577	2.85	0.23	6.21
978	95,325	1.97	0.16	7.05	1106	108,769	2.77	0.23	5.87
980	95,538	2.12	0.17	6.95	1108	108,962	3.01	0.24	6.21
982	95,751	2.11	0.17	7.33	1110	109,154	3.03	0.26	6.13
984	95,964	2.14	0.17	7.57	1112	109,346	2.85		5.92
986	96,178	2.14	0.18	7.37	1114	109,538	2.61		6.13
988	96,391	2.26	0.18	7.5	1116	109,731	2.6		5.74
990	96,604	2.17	0.17	7.4	1118	109,923	2.85		5.93
992	96,817	2.28	0.19	7.74	1120	110,115	2.98		5.93
994	97,030	2.29	0.18	7.27	1122	110,308	3.09		6.33
996	97,244	2.67	0.22	7.44	1124	110,500	3.67		5.79
998	97,457	2.69	0.21	7.6	1126	110,692	3.61		6.04
1000	97,670	2.7	0.22	7.78	1128	110,885	5.10		6.61
1002	97,883	2.6	0.2	7.45	1130	111,077	5.42		6.49
1004	98,096	2.65		7.34	1131	111,269	5.97		6.70
1006	98,310	2.62	0.21	7.24	1132	111,462	1.40		5.34
1008	98,523	2.79	0.22	7.48	1134	111,654	5.73		6.34
1010	98,736	2.65	0.21	7.39	1136	111,846	4.71		6.32
1012	98,949	2.81	0.22	7.76	1138	112,038	5.35		6.96
1014	99,162	2.87	0.24	8.25	1140	112,231	5.95		6.60
1016	99,376	3.52	0.28	7.61	1142	112,423	6.48		6.86
1018	99,589	3.01	0.24	7.23	1144	112,615	6.64		6.75
1020	99,802	3.88	0.31	6.93	1146	112,808	6.43		7.05
1022	100,015	4.81	0.39	7.28	1148	113,000	8.47		7.66
1024	100,228	4.57	0.37	7.71	1150	113,192	6.33		6.91
1026	100,442	6.36	0.48	8.95	1152	113,385	5.83		6.73
1028	100,655	5.19	0.42	8.07	1154	113,577	5.30		6.88
1030	100,868	3.96	0.31	7.90	1156	113,769	5.82		6.91
1032	101,081	5.88	0.43	8.72	1158	113,962	5.38		7.34
1034	101,294	6.03	0.45	8.97	1160	114,154	4.73		6.89
1036	101,508	5.60	0.46	9.14	1161	114,346	3.25		7.04
1038	101,721	6.15	0.48	8.93	1162	114,538	4.38		6.99
1040	101,934	5.22	0.42	9.06	1164	114,731	4.92		6.76
1042	102,147	6.41	0.52	9.54	1166	114,923	4.88		7.12
1044	102,360	7.94	0.51	9.57	1167	115,115	3.50		8.23
1046	102,574	4.45	0.34	8.87	1168	115,308	5.00		6.87
1047	102,787	4.76	0.37	8.76	1170	115,500	4.44		7.07

Appendix A
Core MD02-2518 (Mazatlan) – Carbon & Nitrogen

Depth (cm)	Age (yrs BP)	Corg %	N %	$\delta^{15}N$ ‰	Depth (cm)	Age (yrs BP)	Corg %	N %	$\delta^{15}N$ ‰
1172	115,692	7.07		7.51	1302	130,221	1.85	0.17	7.29
1174	115,885	6.08		7.58	1304	130,479	1.79	0.16	7.17
1176	116,077	5.89		7.42	1306	130,737	1.76	0.16	7.21
1178	116,269	5.44		7.89	1308	130,995	1.69	0.15	7.10
1180	116,462	6.25		7.98	1310	131,253	1.75	0.15	7.20
1182	116,654	5.66		7.85	1312	131,511	1.78	0.16	6.78
1184	116,846	5.72		8.08	1314	131,768	1.79	0.16	7.55
1186	117,038	5.91		7.94	1316	132,026	1.80	0.16	6.86
1188	117,231	5.48		7.60	1318	132,284	1.68	0.15	7.37
1190	117,423	6.34		7.93	1320	132,542	1.76	0.16	7.14
1192	117,615	5.44		7.96	1322	132,800	1.74	0.15	6.99
1194	117,808	6.25		7.99	1324	133,058	1.75	0.16	7.21
1196	118,000	5.60		8.03	1326	133,316	1.74	0.16	6.74
1198	118,192	5.58		8.20	1328	133,574	1.78	0.15	6.86
1200	118,385	5.71		8.10	1330	133,832	1.81	0.15	6.85
1204	118,577	5.89		8.25	1332	134,089	1.83	0.15	6.95
1206	118,769	5.28		7.82	1334	134,347	1.86	0.15	7.05
1208	118,962	5.77		7.75	1336	134,605	1.89	0.16	7.10
1210	119,154	5.50		7.92	1338	134,863	1.85	0.15	7.25
1212	119,346	4.67		8.37	1340	135,121	1.91	0.16	7.02
1214	119,538	4.02		8.31	1342	135,379	1.82	0.15	7.16
1216	119,731	6.04		8.57	1344	135,637	1.91	0.15	7.30
1218	119,923	5.44		8.64	1346	135,895	1.88	0.16	7.00
1220	120,115	5.18		8.79	1348	136,153	1.86	0.15	6.80
1222	120,308	6.68		8.98	1350	136,411	1.88	0.16	6.89
1224	120,500	6.94		9.20	1352	136,668	1.92	0.16	6.89
1226	120,692	5.70		9.00	1354	136,926	1.86	0.16	6.33
1228	120,885	5.87		9.09	1356	137,184	1.90	0.16	6.77
1230	121,077	5.91		9.10	1360	137,700	1.87	0.16	6.27
1232	121,269	5.85	0.48	8.96	1362	137,958	1.93	0.16	6.54
1234	121,462	5.88	0.48	8.88	1364	138,216	1.96	0.17	6.49
1235	121,654	3.20	0.26	8.04	1366	138,474	2.06	0.17	7.15
1236	121,846	2.80	0.24	9.35	1370	138,732	2.00	0.17	6.78
1238	122,038	5.57	0.46	9.21	1372	138,989	2.01	0.17	7.04
1240	122,231	5.22	0.45	8.63	1374	139,247	1.98	0.16	6.79
1242	122,423	5.71	0.47	9.55	1376	139,505	2.00	0.16	6.96
1244	122,615	5.78	0.48	9.85	1378	139,763	1.92	0.16	6.78
1246	122,808	5.23	0.43	9.62	1380	140,021	1.94	0.16	6.75
1248	123,000	5.04	0.42	9.93	1382	140,279	1.96	0.16	7.05
1250	123,258	5.12	0.42	10.10	1384	140,537	2.04	0.17	7.38
1252	123,516	4.16	0.35	9.58	1386	140,795	2.05	0.17	6.60
1253	123,774	3.96	0.33	8.76	1388	141,053	2.23	0.19	6.45
1254	124,032	2.31	0.19	8.01	1390	141,311	2.38	0.20	6.31
1256	124,289	2.02	0.17	8.02	1392	141,568	2.33	0.20	6.79
1258	124,547	1.85	0.16	8.05	1394	141,826	2.32	0.19	6.99
1260	124,805	2.84	0.25	8.17	1396	142,084	2.38	0.20	7.19
1262	125,063	1.95	0.17	8.06	1398	142,342	2.40	0.20	7.11
1264	125,321	1.89	0.17	8.12	1400	142,600	2.35	0.20	6.53
1266	125,579	1.77	0.16	7.66	1402	142,858	2.46	0.20	6.66
1268	125,837	1.68	0.15	8.18	1404	143,116	2.55	0.21	6.92
1270	126,095	1.95	0.17	7.61	1406	143,374	2.43	0.19	6.51
1272	126,353	1.89	0.16	7.53	1408	143,632	2.65	0.22	6.46
1274	126,611	1.73	0.14	7.89	1410	143,889	2.67	0.22	6.51
1276	126,868	1.84	0.15	7.71	1412	144,147	2.81	0.23	6.61
1278	127,126	1.83	0.16	7.66	1414	144,405	2.89	0.24	6.51
1280	127,384	1.82	0.15	7.06	1416	144,663	2.88	0.22	7.04
1282	127,642	1.88	0.16	7.28	1418	144,921	2.89	0.23	6.71
1284	127,900	1.74	0.15	6.90	1420	145,179	2.78	0.22	6.28
1286	128,158	1.79	0.15	8.10	1422	145,437	2.70	0.20	5.77
1288	128,416	1.74	0.15	7.82	1424	145,695	2.80	0.23	6.58
1290	128,674	1.71	0.15	7.56	1426	145,953	3.54	0.28	6.56
1292	128,932	1.74	0.15	7.07	1428	146,211	4.32	0.34	6.60
1294	129,189	1.71	0.15	7.18	1430	146,468	3.70	0.30	6.51
1296	129,447	1.61	0.14	7.57	1432	146,726	3.92	0.32	6.42
1298	129,705	1.70	0.15	7.52	1434	146,984	4.11	0.33	6.49
1300	129,963	1.74	0.16	7.62	1436	147,242	4.16	0.34	7.24

Appendix A
Core MD02-2518 (Mazatlan) – Carbon & Nitrogen

Depth (cm)	Age (yrs BP)	Corg %	N %	$\delta^{15}N$ ‰	Depth (cm)	Age (yrs BP)	Corg %	N %	$\delta^{15}N$ ‰
1438	147,500	3.94	0.32	7.14	1574	164,779	5.25	0.44	8.14
1440	147,758	4.19	0.34	6.88	1576	165,037	5.10	0.43	8.06
1442	148,016	3.85	0.31	6.84	1578	165,295	5.30	0.45	7.98
1444	148,274	4.00	0.33	6.54	1580	165,553	5.25	0.44	8.03
1446	148,532	4.67	0.39	7.37	1582	165,811	6.15	0.51	8.65
1448	148,789	5.00	0.41	7.60	1584	166,068	5.70	0.46	8.26
1450	149,047	5.00	0.41	7.92	1586	166,326	5.25	0.43	8.32
1452	149,305	4.98	0.44	7.68	1588	166,584	4.95	0.40	7.97
1454	149,563	4.98	0.41	7.68	1590	166,842	5.82	0.48	8.38
1456	149,821	5.31		8.11	1592	167,100	5.58	0.46	8.11
1458	150,079	4.91		7.36	1594	167,358	5.44	0.45	8.08
1460	150,337	4.88		7.69	1596	167,616	5.28	0.43	8.27
1462	150,595	4.48		6.72	1598	167,874	6.28	0.51	8.03
1464	150,853	4.28		6.67	1600	168,132	6.16	0.51	8.11
1466	151,111	3.69		8.18	1602	168,389	6.43	0.53	7.87
1468	151,368	4.37		6.95	1604	168,647	7.30	0.59	7.96
1470	151,626	4.37		6.67	1606	168,905	6.63	0.53	8.20
1472	151,884	3.77		7.07	1608	169,163	8.54	0.65	8.56
1474	152,142	4.38		6.47	1610	169,421	7.86	0.60	8.62
1476	152,400	5.07		7.34	1612	169,679	7.51	0.60	8.40
1478	152,658	6.31		7.34	1614	169,937	8.03	0.63	8.90
1480	152,916	6.26	0.53	8.70	1616	170,195	8.07	0.65	8.61
1482	153,174	5.95	0.50	7.51	1618	170,453	4.75	0.37	8.37
1484	153,432	5.06	0.43	7.10	1620	170,711	8.17	0.63	8.62
1486	153,689	5.52	0.46	7.55	1622	170,968	7.85	0.63	8.46
1488	153,947	5.45		6.99	1624	171,226	8.86	0.71	8.89
1490	154,205	6.00		6.88	1626	171,484	7.10	0.55	8.58
1492	154,463	5.23		6.99	1628	171,742	7.60	0.59	8.55
1494	154,721	4.96		6.76	1630	172,000	8.06	0.63	8.95
1496	154,979	5.26		7.42	1632	172,258	7.33	0.60	8.68
1500	155,495	5.59	0.46	8.28	1656	172,516	2.93	0.23	6.82
1502	155,753	6.79	0.53	8.78	1660	172,774	2.34	0.20	6.97
1504	156,011	2.43	0.21	8.20	1664	173,032	2.39	0.19	6.93
1506	156,268	5.99	0.49	8.43	1668	173,289	2.77	0.22	6.99
1508	156,526	5.48	0.44	8.51	1672	173,547	2.87	0.23	6.37
1510	156,784	5.41	0.44	8.96	1676	173,805	2.35	0.20	6.32
1512	157,042	4.61	0.39	8.28	1680	174,063	2.30	0.19	6.25
1514	157,300	5.22	0.43	8.51	1684	174,321	2.71	0.22	6.20
1516	157,558	4.56	0.38	8.25	1688	174,579	3.19	0.26	6.44
1518	157,816	4.41	0.37	8.79	1692	174,837	3.02	0.25	6.43
1520	158,074	5.06	0.42	8.77	1696	175,095	2.92	0.24	6.27
1522	158,332	4.29	0.35	8.40	1700	175,353	3.39	0.28	5.97
1524	158,589	4.91	0.40	8.45	1704	175,611	4.15	0.35	6.41
1526	158,847	5.00	0.40	8.58	1708	175,868	7.72	0.62	6.76
1528	159,105	4.74	0.39	8.41	1712	176,126	7.43	0.59	7.28
1530	159,363	5.73	0.45	9.04	1716	176,384	6.99	0.57	7.66
1532	159,621	5.18	0.43	8.70	1720	176,642	6.91	0.57	7.76
1534	159,879	5.41	0.43	8.79	1724	176,900	6.94	0.55	7.77
1536	160,137	4.54	0.37	8.42	1728	177,158	6.14	0.49	7.52
1538	160,395	4.69	0.39	8.34	1732	177,416	5.28	0.44	8.56
1540	160,653	3.56	0.29	8.06	1736	177,674	5.34	0.46	8.84
1542	160,911	1.48	0.13	8.14	1740	177,932	4.99	0.42	9.15
1544	161,168	1.42	0.13	7.97	1744	178,189	4.16	0.36	9.02
1546	161,426	3.02	0.25	8.05	1748	178,447	2.40	0.23	7.45
1548	161,684	4.49	0.38	7.74	1752	178,705	1.76	0.16	7.26
1550	161,942	4.19	0.34	7.86	1756	178,963	2.46	0.22	7.62
1552	162,200	4.41	0.37	7.89	1760	179,221	2.96	0.27	7.94
1554	162,458	5.01	0.42	7.85	1764	179,479	2.52	0.23	7.45
1556	162,716	5.68	0.46	7.91	1768	179,737	2.31	0.20	7.55
1558	162,974	5.35	0.45	8.14	1772	179,995	2.23	0.21	7.74
1560	163,232	4.86	0.40	8.19					
1562	163,489	2.68	0.22	7.86					
1566	163,747	4.29	0.35	8.12					
1568	164,005	4.22	0.35	8.02					
1570	164,263	4.55	0.38	8.13					
1572	164,521	4.91	0.39	8.08					

Appendix B
Core MD02-2520 (Gulf of Tehuantepec) – Carbon & Nitrogen

Depth (cm)	Age (yrs BP)	C_{org} wt. %	N_{org} wt. %	$\delta^{13}C$ ‰ vs.PDB	$\delta^{15}N$ ‰ vs. Air	C/N_{org}
8	560	6.36	0.75	-20.61	6.84	8.5
11	573	6.24	0.77	-20.27	7.05	8.14
13	582	5.86	0.71	-20.34	6.95	8.27
16	594	6.32	0.77	-20.25	6.93	8.18
21	615	6.65	0.80	-20.40	6.96	8.28
26	636	6.17	0.73	-20.25	6.78	8.44
31	656	5.65	0.66	-20.20	6.60	8.58
36	677	5.54	0.66	-20.27	6.93	8.45
41	698	5.22	0.61	-20.49	6.40	8.58
46	719	5.35	0.63	-20.50	6.64	8.5
51	740	5.73	0.65	-20.16	6.64	8.87
56	761	5.57	0.62	-20.20	6.83	9.02
61	781	5.64	0.64	-20.26	6.57	8.82
66	802	5.27	0.60	-20.15	6.61	8.76
71	823	5.11	0.57	-20.22	6.60	9.05
76	844	5.37	0.60	-19.99	6.49	8.94
81	865	5.05	0.57	-20.03	6.51	8.93
86	885	3.72	0.43	-19.48	6.86	8.76
91	906	5.23	0.58	-19.88	6.84	8.98
96	927	4.93	0.55	-19.91	6.67	8.98
101	948	5.36	0.60	-20.29	6.66	8.96
106	969	5.20	0.58	-20.16	6.57	8.97
111	990	4.91	0.54	-20.22	7.00	9.03
116	1,010	4.10	0.26	-20.22	7.25	15.9
121	1,031	5.01	0.38	-20.17	6.54	13.11
126	1,052	4.31	0.28	-20.54	6.12	15.53
131	1,073	5.05	0.42	-20.25	7.11	11.9
136	1,093	4.87	0.45	-20.39	6.68	10.86
141	1,138	6.05	0.37	-20.51	6.82	16.22
146	1,182	4.44	0.38	-20.28	6.24	11.58
151	1,227	5.63	0.47	-20.32	6.62	11.99
151	1,227	6.00	0.56	-20.44	6.58	10.71
156	1,272	5.52	0.56	-20.51	6.89	9.78
161	1,317	5.57	0.57	-20.41	6.68	9.86
166	1,361	5.05	0.56	-20.46	7.10	9.02
171	1,406	5.52	0.62	-20.24	7.18	8.84
176	1,451	5.29	0.53	-20.07	6.78	10.01
181	1,495	4.60	0.46	-20.14	6.81	9.98
186	1,540	4.89	0.52	-20.44	6.98	9.33
191	1,585	4.86	0.53	-20.19	6.96	9.16
196	1,630	4.71	0.49	-20.27	6.76	9.57
201	1,674	4.64	0.49	-20.50	6.89	9.42
206	1,719	4.14	0.43	-20.60	7.39	9.57
211	1,764	4.05	0.43	-20.52	7.43	9.47
216	1,809	4.43	0.46	-20.56	7.31	9.66
221	1,853	5.22	0.54	-20.56	7.23	9.67
226	1,898	5.25	0.55	-20.44	6.99	9.56
231	1,943	5.17	0.54	-20.59	7.21	9.58
236	1,987	5.41	0.57	-20.40	6.99	9.49
241	2,032	5.08	0.52	-20.64	7.51	9.85
246	2,077	5.32	0.54	-20.62	7.20	9.83
251	2,122	5.40	0.60	-20.42	7.05	8.94
256	2,166	5.16	0.60	-20.36	6.99	8.64
261	2,211	5.12	0.59	-20.45	7.28	8.75
266	2,256	4.75	0.52	-20.32	7.34	9.1
271	2,300	4.87	0.56	-20.38	7.49	8.63
276	2,345	5.02	0.55	-20.51	7.27	9.07
281	2,390	4.98	0.54	-20.72	7.17	9.15
286	2,435	5.24	0.57	-20.73	7.32	9.2
291	2,479	5.36	0.58	-20.52	7.36	9.33
296	2,524	5.12	0.57	-20.40	7.14	8.95
301	2,569	5.38	0.59	-20.43	7.34	9.06
306	2,614	4.84	0.54	-20.35	7.46	8.93
311	2,658	4.14	0.46	-20.41	7.28	8.96
316	2,703	5.48	0.60	-20.66	7.51	9.19
321	2,769	5.07	0.56	-20.68	7.31	9.04
326	2,835	5.44	0.58	-20.58	7.31	9.34

Appendix B
Core MD02-2520 (Gulf of Tehuantepec) – Carbon & Nitrogen

Depth (cm)	Age (yrs BP)	C_{org} wt. %	N_{org} wt. %	$\delta^{13}C$ ‰ vs.PDB	$\delta^{15}N$ ‰ vs. Air	C/N_{org}
331	2,901	5.31	0.58	-20.87	7.33	9.15
336	2,967	6.03	0.66	-20.92	7.07	9.13
341	3,032	5.54	0.62	-20.67	7.26	8.94
346	3,098	5.20	0.58	-20.62	7.33	9.02
351	3,164	5.45	0.60	-20.75	7.15	9.12
356	3,230	5.06	0.58	-20.69	7.27	8.80
361	3,296	5.15	0.59	-20.63	7.22	8.79
366	3,362	5.57	0.61	-20.43	7.19	9.12
371	3,428	5.71	0.63	-20.28	7.00	9.06
376	3,494	5.48	0.61	-20.22	7.16	9.02
381	3,560	5.24	0.57	-20.18	7.15	9.26
386	3,626	5.24	0.58	-20.22	7.54	8.98
391	3,691	5.51	0.62	-20.26	7.08	8.86
396	3,757	4.94	0.54	-20.38	7.15	9.13
401	3,823	4.91	0.52	-20.38	6.92	9.53
406	3,889	5.58	0.60	-20.32	7.03	9.23
411	3,955	5.66	0.62	-20.12	6.79	9.13
416	4,015	5.45	0.59	-20.33	7.28	9.27
421	4,075	5.19	0.57	-20.15	7.35	9.18
426	4,134	5.36	0.59	-20.45	7.10	9.11
431	4,194	5.41	0.60	-20.53	7.25	8.98
436	4,254	4.71	0.52	-20.50	7.27	9.12
441	4,314	5.17	0.57	-20.34	7.15	9.10
446	4,374	5.38	0.59	-20.38	7.06	9.13
451	4,433	6.34	0.53	-22.38	6.70	11.92
456	4,493	4.82	0.51	-20.68	7.37	9.49
461	4,553	4.78	0.50	-20.25	7.27	9.55
466	4,613	5.07	0.51	-20.63	7.27	9.90
471	4,673	5.10	0.53	-20.52	7.50	9.72
476	4,733	5.09	0.51	-20.15	6.92	9.99
481	4,792	5.53	0.58	-20.37	7.03	9.57
486	4,852	5.73	0.61	-20.49	6.85	9.35
491	4,912	5.39	0.58	-20.30	7.06	9.28
496	4,972	5.20	0.55	-20.44	6.98	9.45
501	5,032	4.93	0.52	-20.26	6.95	9.48
506	5,091	5.69	0.60	-20.13	7.29	9.55
511	5,151	5.44	0.55	-20.50	7.51	9.82
516	5,211	5.39	0.55	-20.39	7.52	9.87
521	5,271	4.96	0.51	-20.52	7.43	9.75
526	5,331	5.09	0.52	-20.47	7.59	9.77
531	5,390	5.32	0.55	-20.42	7.27	9.64
536	5,450	5.16	0.54	-20.43	7.16	9.52
541	5,510	4.16	0.48	-20.47	7.57	8.59
546	5,550	4.73	0.51	-20.75	7.04	9.33
551	5,591	4.30	0.49	-20.76	7.07	8.79
556	5,631	5.09	0.52	-21.00	7.74	9.76
561	5,672	5.05	0.52	-20.37	7.14	9.71
566	5,712	4.88	0.52	-20.53	7.59	9.44
571	5,753	5.13	0.55	-20.02	7.21	9.39
576	5,793	5.02	0.54	-20.43	6.99	9.25
581	5,834	5.17	0.55	-20.60	7.28	9.42
586	5,874	4.86	0.55	-20.48	7.52	8.79
591	5,915	4.60	0.50	-20.62	7.43	9.21
596	5,955	5.22	0.57	-20.31	7.08	9.23
601	5,996	5.08	0.55	-20.48	7.38	9.20
606	6,036	4.57	0.49	-20.55	7.37	9.27
611	6,077	4.93	0.54	-20.70	7.39	9.09
616	6,117	4.88	0.52	-20.57	7.54	9.32
621	6,158	5.07	0.56	-20.49	7.47	9.12
626	6,198	4.76	0.52	-20.70	7.71	9.24
631	6,239	4.37	0.48	-20.60	7.80	9.14
636	6,279	5.45	0.58	-20.84	7.63	9.38
641	6,320	4.82	0.53	-20.65	7.67	9.09
646	6,360	4.63	0.50	-20.65	7.82	9.33
651	6,401	4.59	0.54	-20.57	7.77	8.51
656	6,441	4.36	0.50	-20.61	7.71	8.67
661	6,482	4.94	0.53	-20.68	7.62	9.28

Appendix B
Core MD02-2520 (Gulf of Tehuantepec) – Carbon & Nitrogen

Depth (cm)	Age (yrs BP)	C_{org} wt. %	N_{org} wt. %	$\delta^{13}C$ ‰ vs.PDB	$\delta^{15}N$ ‰ vs. Air	C/N_{org}
666	6,522	4.80	0.52	-20.93	7.59	9.16
671	6,563	4.67	0.49	-20.84	7.53	9.61
676	6,613	4.45	0.49	-20.71	7.93	9.05
681	6,780	4.43	0.49	-20.75	7.72	9.12
696	6,948	4.07	0.47	-20.67	7.70	8.67
701	7,004	4.15	0.46	-20.63	7.77	8.98
706	7,060	3.97	0.45	-20.64	7.66	8.80
711	7,115	4.24	0.47	-20.59	7.64	9.03
716	7,171	4.10	0.45	-20.36	7.59	9.06
721	7,227	4.33	0.49	-20.13	7.69	8.81
726	7,283	4.17	0.46	-20.34	7.63	9.11
731	7,339	4.41	0.49	-20.58	7.88	9.02
736	7,395	4.17	0.46	-20.48	7.53	9.16
741	7,450	4.24	0.46	-20.71	7.26	9.25
746	7,506	4.05	0.44	-20.57	7.20	9.13
751	7,562	4.40	0.48	-20.38	7.00	9.21
756	7,618	4.22	0.48	-20.63	7.75	8.89
761	7,674	3.98	0.45	-20.31	7.91	8.84
766	7,730	3.98	0.45	-20.79	7.80	8.77
771	7,785	4.05	0.46	-20.87	7.49	8.74
776	7,841	3.93	0.46	-20.69	7.61	8.52
801	8,065	4.10	0.44	-21.00	8.08	9.24
806	8,120	3.73	0.41	-21.16	8.43	9.10
811	8,176	4.20	0.46	-21.01	8.27	9.18
816	8,232	3.72	0.42	-21.12	8.06	8.92
821	8,288	3.81	0.44	-20.87	7.52	8.63
831	8,344	3.63	0.40	-20.59	8.36	8.98
836	8,400	4.11	0.43	-21.09	8.10	9.49
841	8,455	4.24	0.46	-21.11	8.14	9.28
846	8,511	4.25	0.46	-20.88	7.94	9.19
851	8,567	4.38	0.49	-20.95	8.50	8.96
856	8,633	4.56	0.49	-21.07	7.99	9.25
861	8,698	4.79	0.55	-21.07	8.04	8.71
866	8,764	4.11	0.46	-20.83	8.17	8.95
871	8,830	3.96	0.46	-20.71	8.59	8.64
876	8,895	4.42	0.51	-20.94	8.20	8.73
881	8,961	4.31	0.50	-20.95	8.36	8.69
886	9,026	4.21	0.47	-20.34	8.01	8.88
891	9,092	4.03	0.47	-20.79	8.15	8.58
896	9,158	4.45	0.51	-20.68	7.93	8.76
901	9,223	4.57	0.50	-20.64	8.43	9.20
906	9,289	4.32	0.49	-20.49	8.29	8.87
911	9,355	4.26	0.47	-20.47	8.11	9.10
916	9,420	4.42	0.49	-20.76	7.92	9.01
921	9,486	4.27	0.46	-20.65	7.74	9.20
926	9,552	4.03	0.45	-20.64	8.49	8.89
931	9,617	4.35	0.49	-20.46	8.23	8.84
936	9,683	4.04	0.47	-20.82	8.42	8.69
941	9,749	4.16	0.47	-20.69	8.54	8.85
946	9,814	4.48	0.51	-20.86	8.55	8.80
951	9,880	4.56	0.52	-20.58	8.30	8.84
956	9,945	4.57	0.52	-20.24	8.34	8.77
961	10,011	4.48	0.51	-20.59	8.26	8.80
966	10,077	4.35	0.51	-20.59	8.31	8.57
971	10,142	4.39	0.49	-20.69	8.55	8.97
976	10,208	3.10	0.35	-20.83	8.79	8.92
981	10,291	4.29	0.48	-20.79	8.56	8.91
986	10,373	4.50	0.52	-20.91	8.53	8.66
991	10,456	4.31	0.48	-20.73	8.60	9.08
996	10,538	5.13	0.57	-20.85	8.71	8.97
1001	10,621	4.92	0.55	-20.92	8.52	8.98
1006	10,704	5.20	0.57	-21.18	8.58	9.17
1011	10,786	4.66	0.53	-21.00	8.39	8.73
1016	10,869	5.13	0.57	-21.15	8.46	8.94
1021	10,952	4.75	0.54	-21.03	8.90	8.77
1026	11,034	5.48	0.60	-21.14	8.65	9.10
1031	11,117	5.45	0.58	-20.72	8.30	9.39

Appendix B
Core MD02-2520 (Gulf of Tehuantepec) – Carbon & Nitrogen

Depth (cm)	Age (yrs BP)	C_{org} wt. %	N_{org} wt. %	$\delta^{13}C$ ‰ vs.PDB	$\delta^{15}N$ ‰ vs. Air	C/N_{org}
1032	11,133	3.88	0.45	-21.12	8.18	8.57
1036	11,199	5.97	0.66	-20.93	8.48	9.01
1041	11,282	5.64	0.62	-20.86	8.37	9.15
1046	11,365	5.24	0.57	-20.90	8.66	9.20
1051	11,447	6.29	0.67	-21.01	8.21	9.34
1053	11,480	6.22	0.68	-20.76	8.14	9.15
1054	11,497	5.95	0.64	-20.90	8.08	9.28
1056	11,530	5.54	0.61	-20.70	8.48	9.11
1058	11,563	5.59	0.60	-20.74	8.19	9.36
1059	11,579	5.45	0.62	-20.62	8.44	8.74
1061	11,613	6.23	0.68	-20.66	8.18	9.19
1063	11,646	5.97	0.66	-20.46	8.09	9.08
1064	11,662	5.88	0.64	-20.61	8.48	9.22
1066	11,695	5.65	0.63	-20.54	8.48	9.04
1068	11,728	5.90	0.65	-20.49	8.68	9.06
1069	11,745	5.86	0.64	-20.51	8.46	9.21
1071	11,778	5.76	0.62	-20.51	8.18	9.36
1073	11,811	6.11	0.67	-20.32	8.53	9.14
1074	11,827	5.91	0.64	-20.49	8.37	9.26
1076	11,860	5.83	0.62	-20.51	8.42	9.40
1078	11,893	6.21	0.66	-20.38	8.36	9.45
1079	11,910	6.22	0.65	-20.52	8.29	9.51
1081	11,943	5.98	0.65	-20.64	8.05	9.16
1083	11,987	5.95	0.64	-20.53	8.34	9.24
1086	12,054	5.82	0.63	-20.69	8.24	9.22
1088	12,098	5.36	0.59	-20.52	8.63	9.17
1091	12,165	5.69	0.63	-20.63	8.54	9.10
1093	12,209	5.31	0.58	-20.66	8.52	9.16
1096	12,275	5.86	0.63	-20.79	8.48	9.25
1098	12,320	4.66	0.51	-20.76	8.68	9.09
1101	12,386	5.32	0.58	-20.77	8.71	9.13
1103	12,431	5.33	0.58	-20.69	8.57	9.24
1106	12,497	5.42	0.59	-20.81	8.67	9.18
1108	12,541	5.34	0.59	-20.63	8.51	9.13
1111	12,608	6.13	0.68	-20.83	8.54	9.06
1113	12,652	6.41	0.68	-20.48	8.69	9.41
1116	12,719	5.72	0.63	-20.58	8.27	9.07
1118	12,763	5.65	0.62	-20.78	8.87	9.10
1121	12,829	5.60	0.61	-20.78	8.86	9.15
1123	12,874	5.26	0.58	-20.72	8.89	9.09
1126	12,940	5.44	0.62	-20.91	8.56	8.74
1128	12,985	4.99	0.57	-20.86	8.98	8.79
1131	13,051	5.54	0.64	-20.90	8.67	8.72
1133	13,089	5.78	0.64	-20.84	8.91	9.01
1136	13,145	5.52	0.63	-20.85	8.48	8.76
1138	13,183	5.30	0.60	-20.71	8.88	8.88
1141	13,239	4.56	0.57	-20.89	8.88	8.01
1143	13,277	4.52	0.50	-21.19	9.12	9.02
1146	13,333	5.30	0.63	-20.99	9.12	8.43
1148	13,371	4.99	0.58	-21.00	9.00	8.57
1151	13,427	5.51	0.63	-21.40	9.21	8.82
1153	13,465	5.57	0.62	-21.02	9.22	8.94
1156	13,522	5.65	0.65	-21.15	9.05	8.67
1158	13,559	5.80	0.66	-20.95	9.08	8.82
1161	13,616	5.21	0.59	-21.16	9.34	8.79
1163	13,653	5.14	0.59	-20.96	9.56	8.70
1166	13,710	5.66	0.65	-21.12	9.47	8.66
1168	13,747	5.73	0.65	-20.95	9.37	8.78
1171	13,804	5.23	0.59	-21.40	9.62	8.83
1173	13,841	5.82	0.65	-20.81	9.30	8.91
1176	13,898	5.99	0.69	-21.13	9.31	8.67
1178	13,936	5.32	0.60	-21.13	9.43	8.93
1181	13,992	5.92	0.65	-21.11	9.35	9.11
1183	14,034	6.45	0.72	-21.08	9.52	8.93
1186	14,096	5.99	0.63	-21.07	9.03	9.48
1188	14,138	5.75	0.66	-21.25	9.34	8.67
1191	14,200	5.29	0.57	-21.26	9.10	9.34

Appendix B
Core MD02-2520 (Gulf of Tehuantepec) – Carbon & Nitrogen

Depth (cm)	Age (yrs BP)	C_{org} wt. %	N_{org} wt. %	$\delta^{13}C$ ‰ vs.PDB	$\delta^{15}N$ ‰ vs. Air	C/N_{org}
1193	14,242	5.20	0.59	-21.33	9.63	8.88
1196	14,305	5.06	0.54	-21.25	9.24	9.33
1198	14,346	4.68	0.52	-21.06	9.46	8.97
1201	14,409	5.44	0.59	-21.25	8.91	9.29
1206	14,513	5.16	0.56	-21.41	8.95	9.30
1208	14,555	5.17	0.58	-21.47	9.44	8.91
1211	14,617	4.31	0.47	-21.20	9.23	9.20
1216	14,721	4.99	0.54	-21.31	9.31	9.33
1221	14,826	4.77	0.51	-21.16	9.16	9.45
1225	14,909	5.42	0.61	-21.09	8.41	8.83
1226	14,930	6.73	0.70	-21.10	8.75	9.59
1231	15,034	6.66	0.69	-20.92	8.79	9.69
1236	15,112	4.56	0.49	-20.82	8.73	9.35
1241	15,190	5.83	0.64	-20.94	8.87	9.13
1246	15,268	6.09	0.64	-20.99	8.70	9.45
1251	15,346	6.23	0.64	-20.96	8.35	9.76
1256	15,424	4.25	0.47	-20.75	8.74	9.09
1261	15,501	5.23	0.57	-21.05	8.36	9.11
1264	15,548	5.07	0.55	-20.83	8.50	9.29
1266	15,579	5.83	0.59	-20.79	8.41	9.84
1271	15,657	4.44	0.50	-20.98	8.42	8.82
1276	15,735	4.48	0.49	-20.56	8.03	9.14
1281	15,813	4.33	0.47	-20.83	7.74	9.32
1286	15,891	4.47	0.48	-20.96	8.11	9.25
1291	15,969	3.87	0.40	-21.15	7.95	9.74
1296	16,047	2.76	0.34	-21.18	7.86	8.20
1301	16,125	2.73	0.34	-21.03	7.86	7.93
1306	16,203	2.35	0.29	-20.55	8.06	7.98
1311	16,280	1.82	0.23	-21.07	8.04	7.93
1316	16,358	1.76	0.24	-20.84	8.51	7.47
1321	16,436	4.57	0.50	-20.92	8.04	9.15
1326	16,514	3.76	0.41	-20.54	8.29	9.26
1331	16,592	4.67	0.51	-20.89	8.11	9.25
1336	16,670	4.36	0.48	-20.94	7.60	9.08
1341	16,748	4.03	0.43	-20.58	7.98	9.48
1346	16,826	4.52	0.50	-20.69	7.92	9.02
1351	16,904	4.10	0.43	-20.52	8.28	9.44
1356	16,982	3.77	0.40	-20.42	8.78	9.41
1361	17,108	4.33	0.43	-20.46	8.17	10.00
1366	17,235	4.63	0.48	-20.52	7.98	9.71
1371	17,362	3.86	0.41	-20.19	8.36	9.39
1376	17,489	3.91	0.41	-20.29	7.93	9.65
1381	17,616	3.75	0.38	-20.14	8.50	9.77
1386	17,743	4.34	0.46	-20.26	7.40	9.42
1391	17,870	3.81	0.41	-19.89	8.07	9.39
1396	17,997	3.86	0.42	-19.97	7.86	9.22
1401	18,124	3.28	0.33	-20.11	8.11	9.91
1406	18,251	3.86	0.40	-20.28	7.15	9.56
1411	18,378	3.89	0.42	-20.17	6.98	9.22
1416	18,425	4.46	0.49	-20.16	7.08	9.14
1421	18,472	4.97	0.54	-19.95	7.13	9.26
1426	18,519	4.79	0.49	-20.13	6.77	9.77
1431	18,566	4.49	0.46	-20.22	7.08	9.75
1436	18,614	4.68	0.47	-20.45	7.24	9.94
1451	18,755	4.78	0.51	-20.27	6.74	9.42
1456	18,802	4.83	0.52	-19.56	7.23	9.38
1461	18,849	4.62	0.48	-20.28	7.23	9.69
1466	18,882	4.45	0.50	-20.46	7.10	8.93
1471	18,915	4.49	0.61	-20.23	5.64	7.40
1476	18,949	4.19	0.45	-20.10	6.97	9.26
1481	18,982	4.22	0.46	-20.13	7.10	9.25
1486	19,015	4.69	0.51	-20.22	7.08	9.29
1491	19,048	4.53	0.49	-20.40	6.82	9.25
1496	19,082	4.62	0.51	-20.13	7.11	9.11
1501	19,115	4.57	0.48	-20.05	6.87	9.53
1506	19,148	4.46	0.49	-19.74	6.75	9.13
1511	19,181	5.03	0.54	-20.13	6.55	9.39

Appendix B
Core MD02-2520 (Gulf of Tehuantepec) – Carbon & Nitrogen

Depth (cm)	Age (yrs BP)	C_{org} wt. %	N_{org} wt. %	$\delta^{13}C$ ‰ vs.PDB	$\delta^{15}N$ ‰ vs. Air	C/N_{org}
1516	19,214	3.71	0.42	-20.30	7.65	8.91
1521	19,248	4.29	0.43	-20.12	7.98	10.06
1526	19,281	4.52	0.47	-20.03	7.55	9.56
1531	19,314	4.09	0.46	-20.14	7.88	8.85
1536	19,353	4.74	0.51	-19.94	7.39	9.31
1541	19,391	4.99	0.52	-19.90	6.82	9.54
1546	19,430	4.89	0.54	-20.14	7.37	9.04
1551	19,469	4.71	0.50	-20.21	7.71	9.45
1556	19,507	4.62	0.49	-19.84	7.72	9.47
1559	19,530	3.89	0.43	-20.10	8.20	9.06
1561	19,546	5.06	0.54	-20.04	7.90	9.43
1566	19,584	4.88	0.51	-20.16	7.39	9.51
1571	19,623	5.00	0.54	-20.13	6.72	9.23
1576	19,662	5.05	0.51	-20.17	7.38	9.94
1581	19,700	4.86	0.51	-20.17	7.12	9.45
1586	19,739	5.26	0.56	-19.63	7.37	9.32
1591	19,778	5.21	0.55	-20.11	7.13	9.41
1596	19,816	4.21	0.44	-19.94	7.14	9.66
1666	20,357	4.53	0.45	-19.84	7.42	10.04
1671	20,396	4.31	0.44	-19.94	7.17	9.87
1676	20,435	4.12	0.46	-20.00	7.61	8.92
1681	20,473	5.33	0.56	-20.18	7.13	9.51
1686	20,512	5.13	0.54	-19.85	7.03	9.57
1691	20,551	4.69	0.50	-19.91	7.39	9.45
1696	20,589	4.83	0.52	-20.10	7.32	9.25
1701	20,628	4.88	0.51	-20.11	7.34	9.49
1706	20,667	4.45	0.48	-19.96	7.59	9.33
1711	20,705	4.86	0.52	-19.81	7.35	9.37
1716	20,744	4.63	0.51	-19.97	7.33	9.00
1721	20,782	4.76	0.52	-19.94	6.96	9.11
1726	20,821	4.82	0.53	-19.96	6.82	9.09
1731	20,860	4.84	0.52	-20.00	7.02	9.23
1736	20,898	4.64	0.50	-20.16	7.17	9.23
1741	20,937	3.37	0.36	-20.57	7.45	9.30
1746	20,976	4.87	0.54	-20.27	7.68	9.04
1751	21,014	4.71	0.52	-20.26	7.32	9.09
1756	21,053	4.51	0.50	-20.31	6.85	8.94
1761	21,092	4.47	0.50	-20.40	7.12	9.03
1766	21,130	4.51	0.50	-20.27	7.28	9.00
1771	21,169	4.27	0.47	-20.19	7.71	9.13
1776	21,208	4.41	0.50	-20.28	7.16	8.89
1781	21,246	4.21	0.46	-20.10	7.06	9.15
1786	21,285	4.13	0.47	-19.99	7.31	8.77
1791	21,323	4.40	0.50	-20.33	7.40	8.85
1796	21,362	4.55	0.50	-20.90	7.29	9.17
1801	21,401	4.49	0.50	-20.41	7.53	9.00
1806	21,439	3.75	0.41	-20.34	7.38	9.05
1811	21,478	4.21	0.48	-20.25	7.41	8.83
1816	21,523	4.26	0.48	-20.21	7.22	8.82
1821	21,568	4.53	0.52	-20.31	7.11	8.74
1826	21,613	4.36	0.49	-20.48	7.13	8.90
1831	21,658	4.15	0.48	-20.15	7.51	8.70
1836	21,703	4.46	0.49	-20.48	7.09	9.15
1841	21,748	4.03	0.46	-20.27	7.82	8.74
1846	21,793	3.84	0.44	-20.24	7.40	8.79
1851	21,838	4.34	0.47	-20.37	7.06	9.28
1856	21,883	4.32	0.51	-20.22	7.24	8.42
1861	21,928	4.32	0.49	-20.26	7.37	8.86
1866	21,973	3.74	0.42	-19.73	7.30	8.83
1871	22,018	3.61	0.41	-20.05	7.29	8.92
1876	22,063	3.71	0.44	-19.82	7.31	8.54
1881	22,108	4.03	0.46	-20.22	7.24	8.74
1886	22,153	3.93	0.47	-19.99	7.11	8.36
1891	22,198	4.20	0.46	-20.17	7.23	9.06
1896	22,243	4.11	0.47	-20.26	7.38	8.77
1901	22,288	4.33	0.50	-20.05	6.71	8.62
1906	22,333	4.28	0.47	-20.28	7.28	9.06

Appendix B
Core MD02-2520 (Gulf of Tehuantepec) – Carbon & Nitrogen

Depth (cm)	Age (yrs BP)	C_{org} wt. %	N_{org} wt. %	$\delta^{13}C$ ‰ vs.PDB	$\delta^{15}N$ ‰ vs. Air	C/N_{org}
1911	22,378	4.28	0.48	-20.08	6.82	8.96
1916	22,423	4.70	0.53	-20.18	7.23	8.90
1921	22,468	4.41	0.51	-20.13	6.86	8.69
1926	22,513	4.48	0.48	-20.23	6.84	9.26
1931	22,558	4.52	0.52	-20.16	7.21	8.72
1936	22,603	3.99	0.48	-20.06	7.28	8.32
1941	22,648	4.61	0.51	-20.13	7.08	9.12
1946	22,693	4.47	0.51	-20.10	7.17	8.69
1951	22,738	4.78	0.51	-20.22	7.17	9.32
1956	22,783	5.02	0.55	-20.24	7.04	9.13
1961	22,828	4.30	0.49	-20.17	7.22	8.80
1966	22,873	4.86	0.53	-20.00	7.13	9.11
1971	22,918	5.53	0.54	-21.95	6.80	10.23
1976	22,963	4.83	0.54	-20.27	7.15	8.90
1981	23,008	5.14	0.56	-20.05	6.75	9.24
1986	23,053	5.08	0.55	-20.10	7.15	9.17
1991	23,098	5.32	0.59	-20.11	7.27	9.01
1996	23,143	4.88	0.54	-20.10	7.11	9.07
2001	23,188	5.05	0.56	-20.02	6.29	8.98
2006	23,233	5.14	0.59	-20.30	7.70	8.76
2011	23,278	4.30	0.49	-20.24	7.72	8.80
2016	23,323	5.24	0.57	-20.30	7.35	9.14
2021	23,368	4.61	0.51	-20.01	7.30	9.14
2026	23,413	4.87	0.54	-20.22	7.01	9.00
2031	23,458	5.28	0.57	-20.17	7.36	9.24
2036	23,503	4.90	0.54	-20.23	7.85	9.01
2041	23,548	4.99	0.55	-20.10	7.60	9.15
2046	23,593	4.87	0.53	-19.99	6.58	9.16
2051	23,638	5.15	0.57	-19.95	7.67	8.98
2056	23,683	5.33	0.59	-20.09	7.17	8.97
2061	23,728	5.45	0.60	-19.95	7.14	9.08
2066	23,773	5.10	0.58	-20.05	7.19	8.73
2071	23,818	4.75	0.52	-19.96	7.02	9.17
2076	23,863	3.87	0.45	-20.00	7.11	8.59
2081	23,908	4.55	0.49	-19.90	7.35	9.30
2086	23,953	4.86	0.52	-20.17	7.10	9.42
2091	23,998	4.51	0.45	-20.28	6.78	10.14
2096	24,043	4.08	0.47	-20.07	6.79	8.65
2101	24,088	4.00	0.45	-20.00	7.38	8.82
2106	24,133	4.54	0.47	-20.33	6.97	9.73
2111	24,178	4.26	0.48	-20.25	7.80	8.82
2116	24,223	4.81	0.53	-20.00	7.40	9.10
2121	24,268	3.50	0.38	-19.64	8.02	9.19
2126	24,302	4.57	0.48	-20.13	7.31	9.55
2131	24,330	5.85	0.64	-20.12	6.87	9.13
2136	24,357	5.02	0.58	-20.26	7.50	8.61
2141	24,385	4.61	0.53	-20.00	7.62	8.76
2146	24,412	5.38	0.57	-20.18	7.93	9.37
2151	24,440	5.67	0.57	-19.93	7.65	10.00
2156	24,467	5.94	0.58	-19.87	6.81	10.20
2161	24,495	4.75	0.51	-19.64	7.15	9.40
2166	24,522	5.38	0.55	-19.81	7.38	9.76
2171	24,550	5.25	0.57	-19.82	7.48	9.16
2176	24,577	5.33	0.56	-20.03	7.05	9.44
2181	24,605	5.35	0.57	-19.86	7.15	9.37
2186	24,632	5.21	0.58	-19.69	7.17	8.91
2191	24,660	5.25	0.55	-19.69	6.82	9.50
2196	24,687	4.15	0.46	-19.39	6.85	9.10
2201	24,715	5.14	0.54	-19.57	6.79	9.61
2206	24,742	4.14	0.44	-19.85	7.09	9.32
2211	24,770	4.35	0.50	-19.94	7.75	8.72
2216	24,797	4.82	0.54	-20.14	7.00	8.90
2221	24,825	4.15	0.47	-19.84	7.60	8.86
2226	24,852	4.24	0.42	-19.70	7.00	10.02
2231	24,880	4.20	0.42	-20.12	7.07	9.91
2236	24,907	4.69	0.48	-20.02	5.91	9.77
2241	24,935	3.37	0.38	-19.69	6.75	8.86

Appendix B
Core MD02-2520 (Gulf of Tehuantepec) – Carbon & Nitrogen

Depth (cm)	Age (yrs BP)	C_{org} wt. %	N_{org} wt. %	$\delta^{13}C$ ‰ vs.PDB	$\delta^{15}N$ ‰ vs. Air	C/N_{org}
2246	24,962	3.06	0.35	-19.83	6.90	8.84
2251	24,990	3.34	0.34	-20.09	6.95	9.76
2256	25,017	3.32	0.38	-19.94	7.01	8.75
2261	25,045	3.31	0.37	-19.82	6.82	9.08
2266	25,072	3.78	0.40	-20.10	7.04	9.43
2271	25,100	3.22	0.35	-20.10	7.00	9.13
2276	25,127	4.14	0.49	-19.95	7.36	8.43
2281	25,155	3.69	0.40	-19.82	7.14	9.21
2286	25,182	3.44	0.36	-19.96	7.00	9.69
2291	25,209	3.18	0.36	-19.95	7.65	8.73
2296	25,279	3.25	0.29	-20.21	7.26	11.22
2301	25,349	3.34	0.38	-20.07	6.87	8.78
2306	25,419	3.42	0.37	-20.16	6.86	9.15
2311	25,489	3.31	0.38	-19.98	7.36	8.64
2316	25,559	3.50	0.42	-20.15	7.86	8.33
2321	25,629	3.27	0.37	-20.05	7.47	8.76
2326	25,699	3.70	0.40	-20.20	7.25	9.27
2331	25,769	3.56	0.42	-20.00	7.08	8.57
2336	25,839	3.95	0.41	-20.29	5.95	9.61
2341	25,909	3.85	0.44	-19.83	6.97	8.74
2346	25,979	3.55	0.39	-20.06	7.51	9.22
2351	26,049	3.76	0.44	-20.17	7.09	8.64
2356	26,119	4.05	0.46	-20.04	7.08	8.79
2361	26,189	4.38	0.51	-19.99	7.12	8.68
2366	26,259	4.40	0.51	-19.97	7.62	8.71
2371	26,329	4.26	0.40	-19.94	6.68	10.58
2376	26,399	4.36	0.48	-19.98	6.55	9.14
2381	26,469	4.33	0.48	-19.91	6.58	9.03
2386	26,539	4.18	0.47	-20.01	7.57	8.89
2391	26,609	4.31	0.44	-19.94	6.35	9.70
2396	26,679	4.33	0.49	-20.20	7.18	8.93
2401	26,749	4.30	0.49	-20.11	7.57	8.85
2406	26,819	4.45	0.50	-20.09	7.24	8.91
2411	26,889	4.24	0.49	-20.26	7.67	8.63
2416	26,959	4.56	0.53	-20.10	7.13	8.56
2421	27,029	4.74	0.54	-20.05	7.04	8.73
2426	27,099	4.33	0.51	-20.27	7.51	8.46
2431	27,169	4.11	0.48	-20.52	7.59	8.56
2436	27,239	4.57	0.55	-20.31	7.51	8.37
2441	27,309	5.35	0.62	-20.43	7.27	8.67
2446	27,379	5.05	0.59	-20.23	7.67	8.58
2451	27,449	5.16	0.58	-20.19	7.82	8.90
2456	27,519	5.37	0.60	-20.08	7.58	8.93
2461	27,589	5.21	0.60	-20.14	7.19	8.73
2466	27,659	4.57	0.54	-20.34	7.37	8.44
2471	27,729	4.94	0.58	-20.17	7.81	8.59
2476	27,799	4.74	0.55	-20.39	7.71	8.60
2481	27,869	4.71	0.56	-20.39	7.88	8.44
2486	27,939	5.30	0.60	-20.39	7.47	8.83
2491	28,012	4.93	0.58	-20.14	8.14	8.46
2496	28,069	4.91	0.56	-20.10	7.55	8.70
2501	28,126	4.73	0.56	-20.28	7.94	8.40
2506	28,182	4.99	0.58	-20.27	7.67	8.54
2511	28,239	4.59	0.53	-20.29	7.43	8.60
2516	28,296	4.68	0.54	-20.25	7.46	8.64
2521	28,353	4.53	0.54	-20.30	7.44	8.43
2526	28,409	4.82	0.57	-20.31	7.30	8.48
2531	28,466	4.17	0.49	-20.45	7.62	8.47
2536	28,523	4.23	0.49	-20.58	7.49	8.62
2541	28,580	4.71	0.54	-20.40	6.98	8.68
2546	28,636	4.51	0.53	-20.52	7.76	8.55
2551	28,693	4.84	0.56	-20.26	6.90	8.69
2556	28,750	4.81	0.57	-20.23	7.28	8.41
2561	28,807	4.84	0.57	-20.37	7.27	8.50
2566	28,863	4.59	0.54	-20.23	7.66	8.44
2571	28,920	4.92	0.58	-20.26	7.83	8.51
2576	28,977	4.85	0.58	-20.42	7.28	8.33

Appendix B
Core MD02-2520 (Gulf of Tehuantepec) – Carbon & Nitrogen

Depth (cm)	Age (yrs BP)	C_{org} wt. %	N_{org} wt. %	$\delta^{13}C$ ‰ vs.PDB	$\delta^{15}N$ ‰ vs. Air	C/N_{org}
2581	29,034	4.94	0.60	-20.44	7.57	8.28
2586	29,090	5.23	0.61	-20.30	7.58	8.54
2591	29,147	5.43	0.64	-20.30	7.87	8.47
2596	29,204	5.30	0.61	-20.21	7.75	8.63
2601	29,261	5.04	0.59	-20.28	7.54	8.48
2606	29,317	5.07	0.60	-20.27	7.29	8.44
2611	29,374	4.59	0.55	-20.16	7.62	8.31
2616	29,431	4.49	0.54	-20.37	7.47	8.34
2621	29,488	3.98	0.49	-20.25	7.49	8.10
2626	29,544	4.31	0.52	-20.23	7.65	8.32
2631	29,601	4.01	0.49	-20.36	7.18	8.27
2636	29,658	4.10	0.50	-20.41	7.23	8.29
2641	29,715	4.15	0.52	-20.38	7.00	8.02
2646	29,771	4.32	0.54	-20.31	6.98	8.01
2651	29,828	4.26	0.52	-20.32	7.15	8.21
2656	29,885	4.55	0.55	-20.24	7.49	8.24
2661	29,942	3.76	0.47	-20.47	7.53	8.07
2666	29,998	3.73	0.47	-20.46	7.27	8.02
2671	30,055	3.95	0.49	-20.33	6.82	8.11
2676	30,112	4.17	0.52	-20.37	7.10	8.08
2681	30,169	3.64	0.46	-20.41	7.17	7.97
2686	30,225	4.64	0.55	-20.32	7.17	8.37
2701	30,282	4.30	0.51	-20.18	7.34	8.48
2706	30,339	3.99	0.49	-20.24	7.56	8.10
2711	30,396	4.11	0.49	-20.12	7.71	8.46
2716	30,452	4.18	0.50	-20.09	7.67	8.40
2721	30,509	4.41	0.52	-20.17	7.46	8.41
2726	30,566	4.32	0.52	-20.07	7.34	8.28
2731	30,623	4.56	0.54	-20.01	6.48	8.48
2736	30,679	4.66	0.55	-20.07	6.75	8.48
2741	30,736	4.74	0.56	-20.08	6.81	8.42
2746	30,793	5.08	0.59	-19.98	7.29	8.69
2751	30,850	4.75	0.54	-20.24	7.08	8.82
2756	30,906	4.81	0.58	-20.23	7.34	8.34
2761	30,963	4.88	0.58	-20.13	7.47	8.43
2766	31,020	5.09	0.61	-20.33	7.15	8.42
2771	31,077	5.36	0.62	-20.50	7.37	8.67
2776	31,133	5.01	0.60	-20.27	7.00	8.30
2781	31,190	4.29	0.54	-20.29	7.12	7.99
2786	31,247	4.69	0.57	-20.18	7.19	8.26
2791	31,304	4.51	0.53	-20.18	7.38	8.48
2796	31,360	4.54	0.54	-20.41	7.12	8.45
2801	31,417	4.78	0.59	-20.28	6.98	8.16
2806	31,474	3.88	0.46	-20.27	8.52	8.44
2811	31,531	3.94	0.47	-20.28	8.52	8.38
2816	31,587	4.04	0.49	-20.44	8.41	8.29
2821	31,644	3.87	0.48	-20.39	8.32	8.14
2826	31,701	4.82	0.56	-20.34	6.91	8.56
2831	31,758	4.21	0.53	-20.28	7.04	8.00
2836	31,814	4.39	0.53	-20.40	8.03	8.32
2841	31,871	4.49	0.53	-20.52	8.10	8.47
2846	31,928	4.59	0.54	-20.50	7.50	8.44
2851	31,985	4.28	0.52	-20.44	7.31	8.18
2856	32,041	4.39	0.53	-20.65	7.69	8.26
2861	32,098	4.54	0.55	-20.64	7.80	8.24
2866	32,155	4.57	0.54	-20.52	7.73	8.44
2871	32,212	4.41	0.52	-20.61	8.84	8.50
2876	32,268	5.21	0.61	-20.58	7.58	8.48
2881	32,325	4.87	0.60	-20.55	7.77	8.07
2886	32,382	5.22	0.63	-20.47	7.84	8.33
2891	32,439	5.42	0.67	-20.01	7.90	8.13
2896	32,495	5.36	0.62	-20.49	8.33	8.70
2901	32,554	4.29	0.53	-20.73	8.52	8.10
2906	32,613	4.93	0.57	-20.56	8.04	8.68
2911	32,671	4.97	0.58	-20.48	8.31	8.50
2916	32,730	4.93	0.56	-20.53	7.50	8.78
2921	32,788	5.21	0.61	-20.52	7.58	8.59

Appendix B
Core MD02-2520 (Gulf of Tehuantepec) – Carbon & Nitrogen

Depth (cm)	Age (yrs BP)	C_{org} wt. %	N_{org} wt. %	$\delta^{13}C$ ‰ vs.PDB	$\delta^{15}N$ ‰ vs. Air	C/N_{org}
2926	32,847	4.86	0.58	-20.50	7.09	8.46
2931	32,905	4.47	0.54	-20.43	7.29	8.24
2936	32,964	4.21	0.49	-20.41	8.32	8.52
2941	33,022	4.40	0.53	-20.40	7.88	8.36
2946	33,081	4.72	0.55	-20.53	7.41	8.55
2951	33,139	4.50	0.52	-20.59	7.47	8.63
2956	33,198	4.45	0.51	-20.56	7.30	8.67
2961	33,256	4.38	0.55	-20.66	7.35	7.95
2966	33,315	4.69	0.56	-20.36	7.26	8.36
2971	33,373	4.65	0.56	-20.54	8.11	8.30
2976	33,432	4.61	0.56	-20.57	7.85	8.20
2981	33,490	5.02	0.61	-20.34	7.26	8.22
2986	33,549	5.31	0.62	-20.40	7.84	8.62
2991	33,607	5.00	0.59	-20.27	7.85	8.44
2996	33,666	5.04	0.58	-20.32	8.18	8.69
3001	33,724	4.58	0.53	-20.53	7.46	8.62
3006	33,783	5.06	0.57	-20.56	7.92	8.85
3011	33,841	4.32	0.51	-20.74	7.49	8.50
3016	33,900	4.04	0.47	-20.52	8.09	8.66
3021	33,958	4.49	0.54	-20.65	7.01	8.37
3026	34,017	4.45	0.52	-20.97	7.93	8.56
3031	34,075	4.42	0.52	-20.50	8.00	8.51
3036	34,134	4.14	0.51	-20.79	7.91	8.15
3041	34,192	4.44	0.54	-20.53	7.97	8.29
3046	34,251	4.62	0.56	-20.60	7.63	8.21
3051	34,309	4.51	0.55	-20.67	7.55	8.21
3056	34,368	4.51	0.55	-20.50	8.09	8.26
3061	34,426	4.34	0.56	-20.85	8.32	7.78
3066	34,485	4.58	0.56	-20.77	7.81	8.25
3071	34,543	4.49	0.54	-20.73	8.03	8.36
3076	34,602	4.44	0.53	-20.57	8.07	8.32
3081	34,660	4.14	0.51	-20.77	8.08	8.18
3086	34,719	5.06	0.61	-20.63	8.04	8.27
3091	34,777	5.26	0.63	-20.60	7.82	8.32
3096	34,836	4.99	0.60	-20.82	7.65	8.32
3101	34,894	5.13	0.60	-20.65	7.66	8.61
3106	34,953	5.32	0.63	-20.70	8.39	8.50
3111	35,011	4.90	0.57	-20.64	7.88	8.53
3116	35,070	5.10	0.62	-20.52	7.78	8.28
3121	35,128	4.78	0.58	-20.66	7.65	8.23
3126	35,187	4.63	0.56	-20.75	7.77	8.31
3131	35,245	4.58	0.57	-20.57	7.94	8.10
3136	35,304	4.73	0.58	-20.72	7.72	8.22
3141	35,362	4.93	0.58	-20.75	7.72	8.51
3146	35,421	4.94	0.59	-20.80	8.12	8.35
3151	35,479	4.86	0.58	-20.76	7.18	8.40
3156	35,538	4.78	0.58	-20.49	7.48	8.21
3161	35,596	4.59	0.55	-20.91	7.64	8.35
3166	35,655	4.58	0.55	-20.66	7.73	8.30
3171	35,713	5.16	0.60	-20.65	7.07	8.65
3176	35,772	4.66	0.57	-20.52	7.64	8.17
3181	35,830	4.91	0.59	-20.66	7.48	8.29
3186	35,889	4.86	0.59	-20.41	7.49	8.18
3201	35,947	4.56	0.54	-20.68	7.49	8.43
3206	36,006	4.72	0.56	-20.74	7.68	8.43
3211	36,064	5.52	0.63	-20.77	7.76	8.73
3216	36,123	5.43	0.62	-20.59	8.07	8.73
3221	36,181	5.47	0.62	-20.84	8.04	8.82
3226	36,240	5.25	0.61	-20.87	8.04	8.60
3231	36,298	5.14	0.61	-20.69	8.05	8.37
3236	36,357	5.47	0.60	-20.65	7.62	9.06
3241	36,415	5.45	0.62	-20.99	8.15	8.82
3246	36,474	5.40	0.62	-20.70	8.36	8.75
3251	36,532	5.63	0.64	-20.52	8.41	8.80
3256	36,591	5.95	0.68	-20.71	8.37	8.79
3261	36,649	5.53	0.63	-20.94	9.17	8.75
3266	36,708	5.84	0.66	-21.00	8.56	8.88

Appendix B
Core MD02-2520 (Gulf of Tehuantepec) – Carbon & Nitrogen

Depth (cm)	Age (yrs BP)	C_{org} wt. %	N_{org} wt. %	$\delta^{13}C$ ‰ vs.PDB	$\delta^{15}N$ ‰ vs. Air	C/N_{org}
3271	36,766	5.80	0.67	-21.17	8.66	8.64
3276	36,825	6.44	0.73	-20.94	8.87	8.77
3281	36,883	5.96	0.67	-20.90	9.01	8.92
3286	36,942	6.14	0.69	-20.84	8.93	8.97
3291	37,000	5.70	0.65	-20.80	8.93	8.82
3296	37,059	5.30	0.61	-20.73	8.59	8.69
3301	37,117	5.10	0.58	-21.02	9.11	8.76
3306	37,174	5.43	0.61	-20.84	8.93	8.94
3311	37,300	4.53	0.55	-20.91	8.50	8.20
3316	37,426	5.42	0.62	-20.73	8.26	8.79
3321	37,552	5.25	0.59	-20.80	8.25	8.85
3326	37,678	4.91	0.57	-20.67	8.03	8.57
3331	37,804	5.21	0.62	-20.80	8.46	8.43
3336	37,930	5.09	0.58	-20.38	8.07	8.83
3341	38,056	5.00	0.58	-20.42	7.98	8.67
3346	38,182	5.06	0.57	-20.80	8.75	8.82
3351	38,308	5.31	0.58	-20.76	8.05	9.12
3356	38,434	4.45	0.52	-20.63	8.26	8.5
3361	38,560	4.61	0.54	-20.55	8.50	8.61
3366	38,686	4.08	0.51	-20.53	8.19	8.01
3371	38,812	4.21	0.51	-20.54	8.18	8.28
3376	38,938	3.64	0.47	-20.76	8.31	7.77
3381	39,064	4.94	0.58	-20.15	7.63	8.49
3386	39,190	5.47	0.61	-20.41	7.54	8.95
3391	39,316	5.39	0.62	-20.28	7.75	8.70
3396	39,442	4.99	0.59	-20.18	7.85	8.49
3401	39,568	5.35	0.62	-20.09	7.79	8.58
3406	39,694	4.87	0.57	-20.43	7.72	8.51
3411	39,820	5.07	0.59	-20.40	7.77	8.60
3416	39,946	4.95	0.58	-20.37	8.03	8.55
3421	40,072	4.92	0.57	-20.44	7.76	8.57
3426	40,198	5.11	0.58	-20.32	7.86	8.85
3431	40,324	4.85	0.58	-20.35	7.78	8.44
3436	40,450	4.87	0.57	-20.53	7.83	8.59
3441	40,576	4.78	0.56	-20.34	7.84	8.51
3446	40,702	4.96	0.58	-20.34	7.58	8.56
3451	40,828	4.96	0.59	-20.46	7.88	8.48
3456	40,954	4.86	0.58	-20.31	8.05	8.46
3461	41,080	4.76	0.55	-20.35	8.18	8.70
3466	41,206	5.36	0.61	-20.48	8.08	8.81
3471	41,332	4.75	0.55	-20.51	8.06	8.66
3476	41,458	4.59	0.55	-20.33	7.45	8.39
3481	41,584	4.18	0.50	-20.35	7.42	8.35
3486	41,710	3.96	0.48	-20.42	7.57	8.27
3491	41,836	4.02	0.50	-20.52	7.56	8.09
3496	41,962	4.22	0.51	-20.60	7.41	8.35
3501	42,088	4.23	0.50	-20.10	7.39	8.51
3516	42,214	4.80	0.52	-20.11	7.39	9.17
3521	42,340	5.35	0.58	-20.23	7.74	9.20
3526	42,466	5.02	0.56	-20.38	7.71	9.05
3531	42,592	4.69	0.53	-20.06	7.15	8.78
3536	42,718	4.28	0.48	-20.28	7.29	8.92
3541	42,844	4.63	0.54	-19.98	6.97	8.65
3546	42,970	4.44	0.51	-20.06	7.08	8.67
3551	43,096	4.52	0.51	-20.22	7.25	8.86
3556	43,222	4.63	0.53	-19.92	7.42	8.70
3561	43,348	4.77	0.54	-20.22	7.62	8.85
3566	43,474	5.19	0.57	-20.99	7.68	9.07
3571	43,600	4.72	0.55	-20.45	7.87	8.62
3576	43,726	5.10	0.59	-20.41	7.22	8.61
3581	43,852	5.55	0.65	-20.29	7.66	8.55
3586	43,978	5.15	0.60	-20.56	7.76	8.63
3591	44,104	4.01	0.47	-20.45	7.93	8.48
3596	44,256	2.40	0.28	-20.12	9.45	8.56
3604	44,356	5.52	0.65	-20.88	8.37	8.53
3607	44,482	5.52	0.64	-21.08	8.43	8.66
3611	44,608	5.31	0.61	-20.90	8.43	8.68

Appendix B
Core MD02-2520 (Gulf of Tehuantepec) – Carbon & Nitrogen

Depth (cm)	Age (yrs BP)	C_{org} wt. %	N_{org} wt. %	$\delta^{13}C$ ‰ vs.PDB	$\delta^{15}N$ ‰ vs. Air	C/N_{org}
3616	44,734	5.09	0.59	-20.60	8.50	8.68
3626	44,860	4.74	0.56	-20.74	8.56	8.52
3636	44,986	4.74	0.56	-20.59	7.60	8.46
3661	45,112	4.64	0.54	-20.87	7.31	8.57
3666	45,238	4.47	0.53	-20.91	7.68	8.37
3671	45,364	4.10	0.49	-20.95	7.51	8.38
3676	45,490	4.74	0.56	-20.82	7.42	8.51
3681	45,616	4.41	0.52	-20.75	7.35	8.48
3686	45,742	4.79	0.56	-20.79	6.93	8.62
3691	45,868	4.56	0.54	-20.58	7.11	8.48
3696	45,994	4.69	0.52	-20.43	7.44	9.01
3701	46,120	4.02	0.51	-20.42	7.39	7.89

Appendix C
Core MD02-2518 (Mazatlan) - Major Elements

Depth (cm)	Age (yrs BP)	Si wt. %	Al wt. %	Fe wt. %	Mg wt. %	Ca wt. %	Na wt. %	K wt. %	Ti wt. %	Mn wt. %	P wt. %
10	1286	24.33	9.07	3.32	1.89	1.82	6.90	2.71	0.352	0.032	0.284
12	1373	24.56	9.10	3.33	1.93	1.59	6.49	2.51	0.359	0.031	0.288
14	1459	23.51	8.71	3.24	1.90	2.72	5.73	2.36	0.344	0.031	0.528
16	1546	24.69	9.02	3.34	1.89	2.02	5.56	2.47	0.360	0.032	0.293
18	1633	23.48	8.56	3.25	1.91	2.87	5.72	2.31	0.339	0.029	0.568
20	1719	21.14	7.71	2.94	1.85	6.72	5.41	2.09	0.302	0.028	2.182
22	1806	23.56	8.52	3.21	1.89	3.12	5.89	2.36	0.338	0.031	0.584
24	1892	23.54	8.53	3.19	1.95	2.97	5.91	2.30	0.338	0.031	0.474
26	1979	24.05	8.71	3.25	1.94	2.53	5.85	2.37	0.347	0.032	0.313
28	2066	24.29	8.68	3.22	1.90	2.52	5.76	2.38	0.340	0.032	0.304
30	2152	24.52	8.90	3.33	2.00	2.13	5.94	2.42	0.355	0.031	0.239
32	2239	25.31	9.25	3.37	2.09	2.33	6.29	2.44	0.354	0.034	0.241
34	2326	24.43	8.50	3.17	1.79	3.05	5.45	2.41	0.337	0.031	0.286
36	2412	23.96	8.71	3.16	2.00	3.18	6.17	2.35	0.330	0.031	0.245
38	2499	22.98	8.93	3.00	1.83	3.78	6.07	2.27	0.317	0.032	0.228
40	2586	23.54	8.82	3.05	1.89	3.00	5.75	2.35	0.336	0.032	0.324
42	2672	21.62	7.83	2.84	1.90	5.78	6.02	2.16	0.304	0.029	1.837
44	2759	21.61	7.87	2.76	1.86	6.63	5.68	2.21	0.304	0.028	2.100
46	2846	23.39	8.44	3.02	1.95	3.11	6.18	2.30	0.331	0.031	0.631
48	2932	24.10	8.84	3.14	1.99	2.61	6.63	2.35	0.331	0.031	0.368
50	3019	23.39	8.72	3.18	1.85	2.85	5.92	2.32	0.330	0.032	0.380
52	3105	23.43	8.53	3.16	1.84	2.77	5.73	2.31	0.334	0.028	0.292
54	3192	23.43	8.48	3.15	1.90	2.89	5.85	2.31	0.328	0.030	0.271
56	3279	23.40	8.32	3.05	1.83	3.14	5.62	2.31	0.329	0.029	0.272
58	3365	23.66	8.45	3.06	1.85	2.78	5.68	2.34	0.334	0.028	0.280
60	3452	23.19	8.31	3.00	1.80	3.27	5.75	2.27	0.326	0.030	0.296
62	3539	23.14	8.27	2.97	1.83	3.42	5.76	2.30	0.318	0.030	0.288
64	3625	22.85	8.22	2.97	1.83	3.68	5.68	2.28	0.322	0.028	0.477
66	3712	20.73	7.58	2.70	1.81	6.56	5.36	2.03	0.298	0.027	1.811
68	3799	22.97	8.37	3.02	1.86	3.63	5.71	2.27	0.329	0.028	0.562
70	3885	23.13	8.42	3.05	1.86	3.02	5.88	2.34	0.334	0.030	0.370
72	3972	23.77	8.69	3.17	1.91	2.60	5.73	2.37	0.347	0.031	0.276
74	4058	23.47	8.40	3.12	1.79	3.43	5.43	2.34	0.331	0.029	0.302
76	4145	23.08	8.29	3.10	1.80	3.85	5.42	2.28	0.326	0.031	0.310
78	4232	21.90	7.71	2.91	1.74	5.29	5.50	2.15	0.302	0.029	1.199
80	4318	22.02	7.81	2.91	1.75	6.00	5.44	2.16	0.301	0.025	1.673
82	4405	21.86	7.77	2.91	1.74	5.15	5.67	2.18	0.305	0.025	1.298
84	4492	22.99	8.80	3.09	1.67	3.40	7.71	3.07	0.326	0.028	0.478
86	4578	22.69	8.11	3.08	1.89	3.80	6.16	2.21	0.319	0.030	0.655
88	4665	23.88	8.38	3.26	1.85	3.83	5.97	2.28	0.331	0.031	0.405
90	4752	23.36	8.10	3.09	1.74	4.05	5.45	2.24	0.316	0.028	0.323
92	4838	23.17	8.16	3.01	1.83	3.78	6.47	2.21	0.316	0.028	0.294
94	4925	23.19	8.23	3.03	1.80	3.47	5.93	2.40	0.318	0.028	0.283
96	5012	24.24	8.63	3.13	1.86	3.47	5.67	2.43	0.330	0.029	0.275
98	5098	23.38	8.31	3.00	1.83	3.77	5.72	2.33	0.318	0.028	0.262
100	5185	23.57	8.49	3.02	1.88	3.73	5.93	2.33	0.321	0.032	0.256
102	5271	23.11	9.22	3.06	1.77	3.18	9.85	3.64	0.335	0.028	0.266
104	5358	24.09	8.72	3.07	1.89	2.85	6.23	2.40	0.334	0.029	0.259
106	5445	23.89	8.56	3.17	1.82	3.25	5.70	2.38	0.340	0.031	0.265
108	5531	23.89	8.54	3.13	1.81	3.78	5.61	2.37	0.333	0.032	0.258
110	5618	24.22	8.81	3.15	1.88	3.70	5.85	2.33	0.336	0.029	0.255
111	5661	23.60	8.52	3.09	1.73	4.21	4.97	2.33	0.335	0.031	0.228
112	5705	23.48	8.59	3.13	1.74	4.07	5.09	2.30	0.334	0.032	0.218
113	5748	24.00	8.62	3.15	1.71	4.14	4.98	2.35	0.341	0.029	0.220
114	5791	24.28	9.72	3.51	1.69	3.51	4.61	2.47	0.384	0.035	0.150
115	5835	24.75	10.80	3.89	1.64	1.79	3.76	2.60	0.443	0.041	0.103
116	5878	23.27	8.43	3.33	1.88	3.51	5.73	2.31	0.335	0.032	0.247
118	5965	23.26	8.66	3.22	1.89	3.22	5.58	2.31	0.329	0.030	0.224
120	6008	23.17	8.38	3.09	1.83	3.07	5.36	2.27	0.328	0.031	0.258
122	6095	23.62	8.64	3.14	1.86	2.99	5.36	2.32	0.343	0.030	0.306
124	6181	24.75	9.07	3.30	1.98	1.70	5.74	2.47	0.370	0.032	0.300
126	6268	24.33	8.90	3.28	1.98	2.25	5.62	2.46	0.362	0.032	0.298
128	6354	22.50	8.20	3.02	1.92	5.16	5.59	2.21	0.332	0.032	1.077
130	6398	23.08	8.41	3.14	1.89	3.68	5.48	2.31	0.344	0.029	0.491
132	6441	23.62	8.63	3.27	1.94	2.95	5.64	2.40	0.350	0.032	0.317
134	6484	23.62	8.59	3.26	1.92	3.23	5.62	2.39	0.343	0.029	0.290
136	6571	23.48	8.45	3.14	1.88	3.59	5.46	2.36	0.340	0.029	0.407
138	6658	20.08	7.27	2.72	1.82	7.49	5.52	2.08	0.293	0.028	2.013
140	6744	22.31	8.03	2.93	1.86	5.24	6.08	2.28	0.326	0.028	1.284
142	6844	22.50	7.94	2.95	1.79	5.18	5.23	2.24	0.323	0.028	1.192

Appendix C
Core MD02-2518 (Mazatlan) - Major Elements

Depth (cm)	Age (yrs BP)	Si wt. %	Al wt. %	Fe wt. %	Mg wt. %	Ca wt. %	Na wt. %	K wt. %	Ti wt. %	Mn wt. %	P wt. %
144	6944	23.00	8.20	3.03	1.85	4.15	5.59	2.31	0.337	0.028	0.817
146	7045	23.51	8.40	3.11	1.89	3.66	5.51	2.35	0.343	0.027	0.606
148	7145	23.85	8.52	3.22	1.88	3.20	5.50	2.39	0.353	0.028	0.349
150	7245	19.66	7.00	2.60	1.69	9.23	4.85	1.94	0.295	0.024	2.800
152	7345	24.31	9.04	3.25	1.86	3.59	5.02	2.50	0.367	0.036	0.460
154	7445	23.08	8.15	3.15	1.83	3.63	5.51	2.25	0.350	0.028	0.307
156	7546	24.06	8.56	3.24	1.86	2.95	5.29	2.34	0.374	0.030	0.275
158	7646	24.37	8.44	3.23	1.87	2.75	5.36	2.38	0.370	0.031	0.297
160	7746	22.30	7.82	2.98	1.85	5.69	5.36	2.10	0.339	0.031	0.811
162	7846	22.07	7.52	2.91	1.75	6.26	5.37	2.07	0.324	0.028	0.850
164	7946	23.97	8.18	3.23	1.77	3.98	5.17	2.29	0.350	0.031	0.336
166	8047	24.16	8.79	3.34	1.84	3.00	5.63	2.60	0.379	0.032	0.253
168	8147	23.81	8.19	3.19	1.86	3.57	5.36	2.31	0.374	0.032	0.354
170	8247	23.30	8.02	3.09	1.88	4.52	5.66	2.21	0.368	0.028	0.249
172	8347	23.83	8.24	3.17	1.88	4.58	5.41	2.27	0.383	0.032	0.240
174	8447	23.67	8.10	3.07	1.80	4.37	5.29	2.29	0.368	0.032	0.243
176	8548	23.30	8.03	3.08	1.88	5.19	6.11	2.21	0.376	0.035	0.258
178	8648	23.13	7.91	3.06	1.80	5.88	5.15	2.08	0.362	0.030	0.269
180	8748	23.34	8.68	3.15	1.76	4.46	5.42	2.24	0.373	0.031	0.213
182	8848	22.75	7.98	3.01	1.75	5.43	5.27	2.16	0.357	0.032	0.232
184	8948	22.33	7.97	3.06	1.73	6.54	4.75	2.13	0.334	0.030	0.714
186	9049	20.22	8.09	2.74	1.66	8.09	5.67	2.02	0.293	0.028	1.677
188	9149	22.85	8.15	3.09	1.75	4.96	5.02	2.20	0.334	0.032	0.334
190	9249	22.01	7.79	3.11	1.68	6.05	4.84	2.14	0.320	0.030	0.244
192	9349	22.95	8.00	3.07	1.69	5.19	4.71	2.26	0.334	0.032	0.219
194	9449	23.73	8.27	3.05	1.73	4.35	4.88	2.31	0.337	0.032	0.249
196	9550	23.14	8.12	3.04	1.76	4.77	4.95	2.25	0.332	0.032	0.245
198	9650	22.91	8.02	2.95	1.72	5.92	4.62	2.25	0.330	0.032	0.256
200	9750	22.28	7.78	2.95	1.68	6.03	4.76	2.19	0.318	0.030	0.240
202	9850	24.42	8.41	3.12	1.69	4.32	4.81	2.40	0.342	0.033	0.220
204	9950	22.91	8.01	2.91	1.65	5.96	4.81	2.23	0.324	0.030	0.212
206	10051	26.95	10.16	2.97	1.39	1.51	3.45	2.89	0.370	0.035	0.085
208	10151	25.28	8.98	3.07	1.65	2.97	4.56	2.58	0.349	0.032	0.172
210	10251	22.67	8.08	2.95	1.63	5.52	4.56	2.25	0.328	0.033	0.956
211	10301	21.95	7.86	2.74	1.48	7.16	4.12	2.25	0.308	0.031	1.193
212	10351	27.59	10.25	2.81	1.13	1.27	2.79	3.10	0.328	0.037	0.056
213	10401	23.30	8.51	3.40	1.50	5.18	4.01	2.37	0.337	0.036	0.131
214	10451	23.72	8.78	3.43	1.50	6.01	4.26	2.40	0.338	0.035	0.131
215	10502	22.44	8.31	3.50	1.53	6.97	4.24	2.27	0.326	0.037	0.126
216	10552	21.64	8.02	3.48	1.47	7.02	4.13	2.18	0.311	0.032	0.119
217	10602	22.01	8.23	3.70	1.44	6.65	3.69	2.25	0.316	0.034	0.094
218	10652	26.09	10.71	3.46	1.23	1.49	2.86	2.80	0.385	0.040	0.047
219	10702	27.70	11.34	3.42	1.22	0.54	2.65	3.02	0.405	0.042	0.040
220	10752	26.32	10.16	3.43	1.28	1.82	3.00	2.75	0.377	0.042	0.067
221	10802	23.30	8.49	3.53	1.48	5.19	4.08	2.28	0.337	0.032	0.156
222	10852	21.97	7.72	3.49	1.54	7.00	4.20	2.22	0.312	0.032	0.280
224	10952	22.60	7.97	3.49	1.53	6.06	4.11	2.26	0.320	0.030	0.175
226	11053	23.30	8.26	3.49	1.54	4.99	4.21	2.36	0.326	0.032	0.144
228	11153	23.97	8.47	3.26	1.56	4.53	4.31	2.45	0.339	0.032	0.135
230	11253	24.03	8.39	3.09	1.54	4.26	4.26	2.43	0.338	0.034	0.125
232	11424	24.88	8.50	3.05	1.50	3.95	4.16	2.51	0.343	0.031	0.114
234	11595	25.21	8.62	3.02	1.47	3.68	4.22	2.56	0.343	0.031	0.124
236	11767	23.87	7.34	2.52	1.14	7.09	3.62	2.34	0.299	0.029	0.102
238	11938	24.58	6.97	2.36	0.97	7.72	3.08	2.30	0.308	0.030	0.699
240	12110	23.75	7.10	2.52	1.03	7.83	3.05	2.27	0.312	0.029	0.941
242	12281	25.71	8.46	3.26	1.31	3.70	3.73	2.57	0.359	0.032	0.122
244	12453	26.02	8.74	3.49	1.37	3.15	3.86	2.62	0.360	0.035	0.103
246	12624	25.97	9.06	3.47	1.45	3.05	4.16	2.65	0.362	0.035	0.093
248	12796	26.57	9.27	3.34	1.44	2.41	4.00	2.75	0.373	0.032	0.089
250	12967	26.57	9.44	3.33	1.47	1.94	4.16	2.85	0.371	0.034	0.084
252	13139	26.74	9.46	3.35	1.45	2.36	3.80	2.84	0.371	0.035	0.100
254	13310	26.41	9.19	3.30	1.39	2.60	3.88	2.82	0.365	0.032	0.092
256	13482	25.74	9.24	3.22	1.42	2.83	3.83	2.77	0.353	0.035	0.112
258	13653	27.53	8.85	2.98	1.21	2.95	3.46	2.81	0.339	0.034	0.079
260	13824	26.42	9.26	3.22	1.39	2.76	3.73	2.83	0.361	0.033	0.078
261	14036	27.10	9.48	3.07	1.30	1.92	3.47	2.99	0.347	0.039	0.071
262	14248	28.39	9.97	2.79	1.15	0.88	3.02	3.26	0.331	0.042	0.049
263	14460	26.93	9.62	3.28	1.39	1.79	4.07	2.97	0.363	0.038	0.080
264	14672	27.41	10.19	3.30	1.33	1.15	3.22	3.07	0.382	0.039	0.058
265	14884	26.61	9.42	3.26	1.37	2.23	3.77	2.88	0.365	0.034	0.082

Appendix C
Core MD02-2518 (Mazatlan) - Major Elements

Depth (cm)	Age (yrs BP)	Si wt. %	Al wt. %	Fe wt. %	Mg wt. %	Ca wt. %	Na wt. %	K wt. %	Ti wt. %	Mn wt. %	P wt. %
266	15096	26.09	9.00	3.19	1.33	2.90	3.82	2.76	0.350	0.034	0.085
267	15308	25.81	8.78	3.09	1.28	4.05	3.59	2.73	0.335	0.032	0.080
268	15520	25.44	7.52	2.58	0.94	6.38	2.93	2.56	0.301	0.029	0.082
269	15732	27.03	7.06	2.30	0.80	6.13	2.76	2.59	0.295	0.028	0.083
270	15935	27.85	7.70	2.18	0.72	5.57	3.21	2.62	0.286	0.027	0.087
272	16368	27.69	6.97	2.23	0.70	5.74	2.79	2.60	0.284	0.025	0.116
274	16792	27.67	6.74	2.32	0.71	5.88	2.71	2.59	0.286	0.024	0.122
276	17216	27.67	6.89	2.47	0.77	6.19	2.79	2.60	0.292	0.026	0.178
278	17623	27.47	6.87	2.49	0.76	5.90	2.70	2.64	0.299	0.027	0.095
280	18064	26.50	6.55	2.33	0.74	5.95	2.65	2.53	0.281	0.027	0.088
282	18488	26.92	7.58	2.51	0.76	5.66	2.78	2.61	0.296	0.026	0.082
284	18916	27.28	7.10	2.54	0.78	5.64	2.76	2.62	0.297	0.027	0.077
286	18724	27.18	6.96	2.56	0.78	5.54	2.82	2.63	0.299	0.028	0.078
288	19253	27.25	6.93	2.46	0.76	5.83	2.65	2.61	0.297	0.028	0.082
290	19782	27.14	6.80	2.45	0.75	5.84	2.54	2.60	0.293	0.023	0.075
292	20311	27.52	6.92	2.48	0.76	5.83	2.62	2.63	0.299	0.024	0.077
294	20840	27.54	6.86	2.49	0.74	6.05	2.62	2.63	0.292	0.023	0.076
296	21369	27.11	6.70	2.39	0.74	6.22	2.57	2.58	0.286	0.026	0.079
298	21898	26.72	6.65	2.42	0.73	6.48	2.56	2.52	0.289	0.028	0.075
301	22427	27.43	6.97	2.46	0.77	5.68	2.76	2.60	0.302	0.025	0.075
302	22956	26.96	6.87	2.46	0.77	6.28	2.64	2.58	0.295	0.025	0.074
304	23485	26.87	6.78	2.42	0.76	6.63	2.89	2.55	0.295	0.025	0.080
306	24014	26.67	6.70	2.37	0.75	6.70	2.57	2.52	0.287	0.025	0.082
308	24543	27.04	6.78	2.40	0.76	5.99	2.65	2.58	0.289	0.025	0.085
310	25072	27.59	6.46	2.26	0.69	6.27	2.62	2.53	0.272	0.026	0.102
312	25601	26.98	6.67	2.40	0.74	6.44	2.61	2.53	0.284	0.023	0.094
314	26130	27.57	6.68	2.42	0.74	5.96	2.70	2.56	0.280	0.025	0.102
316	26659	27.31	7.17	2.76	0.84	5.18	2.81	2.63	0.310	0.025	0.088
318	27188	26.92	6.81	2.50	0.77	5.74	2.84	2.60	0.290	0.025	0.098
320	27717	27.21	7.11	2.70	0.84	5.12	2.91	2.64	0.309	0.028	0.102
322	28246	27.18	7.16	2.65	0.86	5.13	2.85	2.59	0.305	0.026	0.092
324	28775	27.08	7.04	2.46	0.79	5.71	2.85	2.63	0.305	0.027	0.087
326	29304	26.57	6.88	2.49	0.80	6.01	2.76	2.52	0.296	0.025	0.093
328	29833	26.71	7.45	3.05	0.93	4.62	2.82	2.60	0.323	0.030	0.092
330	30362	27.22	7.41	2.73	0.87	4.70	3.12	2.75	0.318	0.027	0.092
332	30891	26.81	7.44	2.70	0.89	5.00	2.94	2.62	0.317	0.028	0.095
334	31420	27.14	7.50	2.75	0.90	4.76	3.00	2.63	0.323	0.026	0.096
336	31949	27.41	7.62	2.87	0.90	4.40	2.92	2.67	0.323	0.027	0.095
338	32478	27.18	7.71	2.93	0.89	4.07	3.52	2.89	0.325	0.026	0.102
340	33005	27.37	8.18	2.82	0.89	4.09	2.87	2.70	0.326	0.025	0.108
342	33209	26.40	7.32	2.53	0.83	5.62	2.71	2.53	0.304	0.028	0.088
344	33412	27.03	7.85	3.12	0.98	3.71	3.02	2.64	0.340	0.027	0.093
346	33616	28.00	7.94	2.86	0.95	3.88	3.08	2.74	0.334	0.029	0.097
348	33820	28.01	8.87	2.91	1.02	2.42	2.93	2.86	0.346	0.031	0.071
350	34024	27.85	7.70	2.62	0.87	3.78	2.92	2.69	0.311	0.029	0.096
352	34227	27.15	8.33	3.01	1.06	3.18	3.18	2.72	0.341	0.028	0.088
354	34431	28.16	7.15	2.44	0.77	4.70	2.82	2.63	0.297	0.026	0.102
356	34635	28.07	8.04	2.95	0.97	4.14	2.91	2.72	0.338	0.029	0.111
358	34838	26.80	7.64	3.13	0.93	4.38	2.84	2.61	0.332	0.028	0.241
360	35042	26.99	7.90	3.19	0.97	3.89	2.88	2.66	0.339	0.031	0.160
362	35246	27.26	7.82	3.09	0.95	3.95	2.90	2.65	0.337	0.031	0.129
364	35449	27.67	8.65	3.20	1.09	2.57	3.11	2.78	0.363	0.031	0.099
366	35653	27.75	8.38	3.03	1.03	3.32	2.98	2.76	0.344	0.028	0.091
368	35857	27.53	8.20	2.95	1.03	3.04	2.99	2.72	0.344	0.025	0.097
370	36061	27.61	8.83	3.19	1.14	1.87	3.24	2.83	0.358	0.029	0.087
372	36264	27.75	9.21	3.25	1.18	1.20	3.30	2.93	0.367	0.030	0.078
374	36652	28.30	8.87	3.12	1.09	2.12	3.25	2.86	0.356	0.028	0.083
376	37039	28.04	9.27	3.13	1.16	1.23	3.27	3.05	0.355	0.030	0.063
378	37427	27.59	8.80	3.05	1.10	2.07	3.21	2.83	0.347	0.030	0.080
380	37815	27.69	8.98	3.10	1.08	2.25	3.08	2.90	0.343	0.028	0.075
382	38203	27.53	8.82	3.05	1.09	3.26	3.08	2.89	0.334	0.030	0.084
384	38590	26.96	8.11	3.00	1.00	3.98	2.96	2.74	0.325	0.028	0.117
386	38978	26.93	7.48	2.93	0.90	5.08	2.91	2.62	0.318	0.028	0.544
390	39753	27.27	7.82	2.93	0.93	3.45	2.86	2.67	0.323	0.028	0.149
392	40141	27.72	7.71	2.93	0.90	3.77	2.83	2.74	0.332	0.028	0.104
394	40529	27.53	7.68	2.94	0.90	3.86	2.79	2.71	0.333	0.025	0.098
396	40916	27.58	7.75	2.88	0.91	3.89	2.89	2.73	0.335	0.028	0.097
398	41304	27.58	7.51	2.74	0.86	4.80	2.73	2.70	0.318	0.028	0.096
400	41692	27.89	8.44	3.11	1.00	3.18	2.96	2.87	0.346	0.029	0.074
402	42080	28.63	8.82	3.09	1.06	2.27	3.07	2.94	0.350	0.031	0.075

Appendix C
Core MD02-2518 (Mazatlan) - Major Elements

Depth (cm)	Age (yrs BP)	Si wt. %	Al wt. %	Fe wt. %	Mg wt. %	Ca wt. %	Na wt. %	K wt. %	Ti wt. %	Mn wt. %	P wt. %
404	42467	28.23	8.24	2.98	0.98	2.65	2.91	2.86	0.340	0.028	0.085
406	42855	27.33	8.98	3.26	1.13	1.97	3.09	2.90	0.349	0.028	0.066
408	43243	28.26	8.16	3.00	0.97	3.00	2.85	2.81	0.353	0.030	0.088
410	43630	27.43	7.96	3.56	0.96	3.04	2.74	2.73	0.349	0.030	0.087
412	44018	27.56	8.42	3.13	0.96	3.30	2.88	2.76	0.346	0.029	0.091
414	44406	27.25	8.37	3.07	0.99	3.31	2.95	2.73	0.350	0.028	0.094
416	44793	27.42	8.13	2.99	0.98	3.42	2.86	2.73	0.344	0.028	0.100
418	45181	27.91	8.09	2.99	0.98	2.95	2.86	2.77	0.349	0.028	0.099
420	45569	28.10	8.42	3.05	1.04	2.20	2.97	2.84	0.349	0.028	0.095
422	45956	27.47	9.16	3.33	1.21	1.48	3.08	2.93	0.364	0.028	0.075
424	46028	27.45	8.61	3.16	1.07	2.65	3.00	2.82	0.359	0.031	0.079
426	46099	27.89	9.12	3.27	1.14	1.65	3.05	2.95	0.364	0.032	0.071
428	46171	28.67	8.47	3.02	1.02	2.02	2.91	2.89	0.343	0.032	0.072
430	46243	28.31	8.27	2.74	0.97	3.01	2.93	2.83	0.314	0.028	0.092
432	46314	27.82	8.02	3.06	0.97	3.53	2.89	2.73	0.346	0.031	0.192
434	46386	27.41	8.05	3.29	0.99	3.40	2.99	2.72	0.351	0.030	0.123
436	46457	26.94	8.95	3.17	1.01	3.72	3.37	2.75	0.352	0.031	0.103
438	46529	27.31	8.37	3.02	1.03	3.46	3.10	2.73	0.347	0.030	0.103
440	46601	26.89	8.16	3.00	1.04	3.92	2.97	2.68	0.350	0.028	0.094
442	46672	26.94	8.04	2.95	1.03	3.96	2.93	2.67	0.347	0.028	0.092
444	46744	26.75	7.86	2.83	0.98	4.43	2.89	2.63	0.345	0.028	0.092
446	46816	26.88	8.01	2.86	1.00	4.05	3.08	2.67	0.348	0.030	0.088
448	46887	27.42	8.54	3.09	1.13	2.56	3.47	2.75	0.364	0.029	0.085
450	46959	27.71	8.97	3.38	1.15	1.62	3.04	2.88	0.368	0.028	0.082
452	47031	27.67	9.00	3.07	1.16	1.58	3.18	2.94	0.361	0.028	0.089
454	47102	28.09	9.57	3.16	1.30	0.83	3.43	3.09	0.374	0.031	0.093
456	47174	28.32	9.64	3.23	1.33	0.73	3.36	3.04	0.389	0.029	0.094
458	47246	27.93	9.55	3.16	1.33	0.77	3.56	3.03	0.370	0.028	0.099
460	47317	27.12	9.28	3.28	1.33	1.75	3.39	2.87	0.363	0.031	0.100
462	47389	28.42	9.43	3.35	1.29	0.73	3.62	3.03	0.385	0.031	0.094
464	47460	28.23	9.34	3.36	1.28	0.72	3.29	3.03	0.386	0.028	0.100
466	47532	28.00	9.33	3.28	1.29	0.96	3.30	2.98	0.380	0.028	0.103
468	47604	28.18	9.56	3.32	1.33	0.68	3.36	3.02	0.385	0.029	0.085
470	47675	27.81	9.63	3.39	1.36	0.72	3.44	3.03	0.374	0.032	0.098
472	47747	27.05	8.96	3.19	1.23	1.99	3.29	2.80	0.348	0.028	0.126
474	47819	27.42	9.11	3.23	1.25	1.43	3.26	2.89	0.367	0.030	0.088
476	47890	27.61	9.51	3.28	1.28	0.75	3.28	2.99	0.376	0.032	0.088
478	47962	27.32	9.34	3.31	1.31	1.07	3.22	2.94	0.371	0.033	0.143
480	48034	27.46	9.41	3.26	1.31	0.88	3.30	2.96	0.373	0.028	0.082
482	48105	27.76	9.23	3.15	1.24	1.17	3.28	2.94	0.364	0.027	0.090
484	48177	28.16	9.35	3.16	1.24	1.01	3.13	3.06	0.359	0.030	0.080
486	48248	27.48	9.57	3.26	1.32	0.79	3.28	3.01	0.371	0.031	0.079
488	48320	27.56	9.43	3.14	1.28	1.17	3.25	2.98	0.362	0.030	0.095
490	48392	27.11	9.40	3.20	1.31	1.54	3.26	2.99	0.354	0.033	0.089
492	48463	27.70	8.98	3.10	1.21	1.87	2.99	2.96	0.359	0.032	0.123
494	48535	27.31	8.05	2.72	1.03	3.91	2.99	2.70	0.338	0.027	0.243
496	48607	27.34	7.75	3.03	0.99	3.83	2.88	2.69	0.335	0.028	0.354
498	48678	28.00	7.69	2.86	0.93	3.62	2.89	2.70	0.341	0.025	0.467
500	48750	28.75	7.90	3.02	0.94	2.95	2.80	2.76	0.351	0.028	0.109
502	48886	27.89	8.06	2.98	1.01	3.37	2.87	2.72	0.350	0.028	0.106
504	49023	28.11	7.99	2.93	0.98	3.25	2.84	2.75	0.349	0.028	0.108
506	49159	27.92	8.24	2.93	1.03	3.26	2.90	2.80	0.353	0.028	0.097
508	49295	28.04	8.46	3.07	1.06	2.74	2.96	2.80	0.365	0.029	0.100
510	49432	27.91	8.60	3.06	1.10	2.58	3.11	2.80	0.362	0.028	0.095
512	49568	28.54	9.19	3.23	1.25	1.90	3.22	2.88	0.375	0.031	0.092
514	49705	27.74	9.04	3.21	1.22	2.50	3.11	2.86	0.374	0.030	0.089
516	49841	28.07	8.95	3.19	1.19	2.17	3.05	2.87	0.382	0.030	0.097
518	49977	28.86	8.55	3.00	1.09	1.78	2.89	2.90	0.375	0.031	0.096
520	50114	27.61	8.65	3.10	1.16	2.50	3.02	2.78	0.389	0.033	0.135
522	50250	27.64	9.18	3.26	1.28	1.79	3.14	2.86	0.387	0.029	0.104
524	50386	27.87	8.76	3.16	1.15	2.20	3.03	2.84	0.371	0.031	0.101
526	50523	28.64	9.40	3.30	1.34	1.69	3.35	2.89	0.385	0.029	0.105
528	50659	28.44	9.39	3.35	1.33	1.04	3.32	2.98	0.401	0.033	0.096
530	50795	30.25	9.89	3.35	1.38	1.09	3.50	3.04	0.406	0.034	0.111
532	50932	28.21	9.06	3.23	1.27	1.26	3.16	2.89	0.383	0.030	0.097
534	51068	28.39	9.43	3.32	1.31	0.77	3.25	3.02	0.392	0.029	0.093
536	51204	28.32	8.92	3.16	1.21	1.38	3.05	2.91	0.382	0.032	0.099
538	51341	28.52	9.19	3.23	1.26	0.97	3.13	2.98	0.384	0.032	0.092
540	51477	28.18	9.54	3.29	1.35	0.89	3.20	3.01	0.397	0.030	0.104
542	51614	28.06	9.40	3.29	1.34	0.96	3.26	2.92	0.396	0.032	0.092

Appendix C
Core MD02-2518 (Mazatlan) - Major Elements

Depth (cm)	Age (yrs BP)	Si wt. %	Al wt. %	Fe wt. %	Mg wt. %	Ca wt. %	Na wt. %	K wt. %	Ti wt. %	Mn wt. %	P wt. %
544	51750	28.27	9.52	3.4	1.35	1.07	3.37	2.95	0.403	0.032	0.096
546	51886	28.16	9.53	3.42	1.36	0.7	3.33	2.99	0.398	0.032	0.085
548	52023	28.68	9.13	3.21	1.2	1.12	3.27	2.93	0.379	0.029	0.096
550	52159	28.4	9.48	3.37	1.33	0.75	3.32	2.96	0.393	0.03	0.103
552	52295	28.04	9.56	3.36	1.35	0.71	3.43	3	0.391	0.032	0.102
554	52432	28.29	9.46	3.4	1.36	0.73	3.25	2.97	0.415	0.033	0.098
556	52568	28.22	9.65	3.37	1.42	0.77	3.05	2.98	0.393	0.035	0.106
558	52704	28.17	9.56	3.21	1.32	0.66	3.33	3.04	0.38	0.033	0.088
559	52841	28.1	9.47	3.2	1.33	0.69	3.39	3.02	0.376	0.033	0.096
560	52977	27.17	9.61	3.44	1.42	0.74	3.61	3.02	0.372	0.031	0.126
562	53114	27.21	9.5	3.47	1.44	0.87	3.64	2.96	0.379	0.032	0.177
564	53250	28.56	9.91	3.49	1.44	0.67	3.39	3.04	0.4	0.032	0.097
566	53386	27.86	9.54	3.34	1.4	0.7	3.36	3.01	0.396	0.033	0.106
568	53523	27.64	9.7	3.37	1.44	0.65	3.4	2.99	0.39	0.032	0.092
570	53659	28.08	9.57	3.31	1.41	0.74	3.39	3	0.396	0.031	0.099
572	53795	27.83	9.71	3.3	1.44	0.75	3.46	2.99	0.398	0.032	0.117
574	53932	27.69	9.73	3.38	1.44	0.74	3.54	2.96	0.4	0.032	0.124
576	54068	27.83	9.63	3.33	1.44	0.71	3.42	2.98	0.399	0.031	0.109
578	54204	27.84	9.96	3.16	1.36	0.58	3.22	3.06	0.379	0.035	0.076
580	54341	28.32	9.74	3.4	1.42	0.7	3.48	3.02	0.394	0.029	0.1
582	54477	27.51	9.51	3.33	1.42	0.74	3.45	2.97	0.385	0.032	0.108
584	54613	27.5	9.66	3.31	1.44	0.69	3.5	3.01	0.389	0.033	0.092
586	54750	27.41	9.61	3.35	1.43	0.77	3.52	2.97	0.387	0.031	0.109
588	54929	27.89	9.46	3.3	1.39	0.95	3.5	3.01	0.385	0.032	0.157
590	55107	28.12	9.29	3.3	1.34	1.06	3.34	2.97	0.384	0.03	0.091
592	55286	28.04	9.19	3.31	1.28	1.07	3.34	3	0.38	0.032	0.112
594	55464	28.99	9.11	3.31	1.16	0.77	3.22	3.07	0.383	0.035	0.088
596	55643	28.82	9.1	3.32	1.21	0.79	3.28	3.07	0.384	0.033	0.095
598	55821	24.46	7.2	2.85	0.98	6.77	3.05	2.44	0.308	0.024	2.308
599	56000	23.55	6.38	2.78	0.87	8.51	2.64	2.25	0.285	0.024	2.947
602	56179	29.09	8.55	3.22	1.1	0.94	2.65	2.83	0.367	0.03	0.133
604	56357	28.07	9.09	3.21	1.33	1.09	3.05	2.8	0.389	0.032	0.147
606	56536	26.84	8.41	3.09	1.21	2.88	2.74	2.58	0.385	0.032	0.162
608	56714	27.73	9.48	3.49	1.4	0.77	2.85	2.88	0.399	0.035	0.093
610	56893	27.72	9.48	3.39	1.4	0.8	2.97	2.94	0.394	0.033	0.106
612	57071	27.27	9.31	3.21	1.37	1.37	2.81	2.86	0.374	0.033	0.103
614	57250	26.84	7.86	2.7	1.06	4.42	2.53	2.56	0.353	0.03	0.204
616	57429	27.27	8.38	4.17	1.19	2.16	2.7	2.71	0.382	0.031	0.358
618	57607	27.67	9.07	3.34	1.34	0.97	2.9	2.86	0.399	0.031	0.112
620	57786	27.95	9.28	3.28	1.37	0.77	2.9	2.91	0.394	0.033	0.095
622	57964	28.17	9.34	3.13	1.37	0.75	2.88	2.92	0.39	0.03	0.104
624	58143	27.76	9.37	3.02	1.38	0.71	2.96	2.97	0.372	0.032	0.09
626	58321	27.55	9.47	3.23	1.42	0.7	3.01	2.97	0.383	0.032	0.099
627	58411	27.89	9.6	3.09	1.36	0.67	2.77	3.07	0.383	0.033	0.089
628	58500	27.88	9.53	3.16	1.4	0.72	2.93	2.96	0.395	0.032	0.095
630	58679	27.3	9.26	3.72	1.37	0.69	2.79	2.86	0.387	0.032	0.091
632	58857	27.63	9.68	3.26	1.42	0.66	2.95	2.9	0.385	0.031	0.094
634	59036	27.86	9.53	3.42	1.42	0.74	2.93	2.92	0.388	0.03	0.112
636	59214	27.95	9.53	3.4	1.41	0.72	2.85	2.96	0.391	0.03	0.093
638	59393	27.23	9.41	3.22	1.43	1.22	3.09	2.93	0.371	0.032	0.114
640	59571	25.12	8.42	3.15	1.31	4.03	2.83	2.52	0.342	0.028	0.096
642	59750	26.7	9.09	3.37	1.37	2.36	3.2	2.82	0.376	0.032	0.088
644	59929	26.8	8.91	3.35	1.35	2.45	3.25	2.78	0.381	0.032	0.095
646	60107	27.01	9.03	3.33	1.37	2	3.3	2.82	0.384	0.03	0.096
648	60286	27.4	9.07	3.14	1.32	2.04	3.34	2.9	0.373	0.03	0.102
650	60464	27.95	8.87	3.33	1.22	1.81	3.14	2.9	0.377	0.028	0.084
652	60643	27.96	9.34	3.47	1.31	1.04	3.22	3	0.384	0.031	0.076
653	60821	28.89	8.44	2.95	1.06	1.77	2.94	2.92	0.345	0.028	0.08
654	61000	27.56	8.31	2.88	1.1	3.07	3.02	2.81	0.34	0.029	0.08
656	61213	28.92	7.41	2.6	0.85	3.86	2.77	2.74	0.332	0.025	0.12
658	61426	28.67	7.71	2.84	0.93	3.64	2.79	2.76	0.338	0.028	0.106
660	61640	28.05	7.83	2.93	0.98	3.54	2.89	2.74	0.343	0.028	0.105
664	62066	28.69	7.6	2.79	0.92	3.58	2.93	2.75	0.337	0.028	0.221
668	62492	29.04	7.54	2.7	0.88	3.31	2.92	2.76	0.332	0.026	0.099
672	62919	29.39	7.55	2.65	0.88	3.05	2.95	2.84	0.33	0.027	0.091
676	63345	29.22	7.47	2.53	0.9	3.2	2.44	2.74	0.328	0.026	0.095
680	63772	29.19	7.4	2.55	0.87	3.16	2.45	2.71	0.322	0.028	0.091
684	64198	28.66	7.36	2.54	0.9	3.45	2.41	2.7	0.32	0.03	0.092
688	64624	28.9	7.51	2.59	0.92	3.19	2.5	2.71	0.326	0.027	0.097
692	65051	29.16	7.64	2.71	0.93	3.19	2.45	2.74	0.336	0.026	0.097

Appendix C
Core MD02-2518 (Mazatlan) - Major Elements

Depth (cm)	Age (yrs BP)	Si wt. %	Al wt. %	Fe wt. %	Mg wt. %	Ca wt. %	Na wt. %	K wt. %	Ti wt. %	Mn wt. %	P wt. %
696	65477	28.99	7.47	2.58	0.91	3.26	2.45	2.72	0.323	0.028	0.095
700	65904	28.93	7.63	2.66	0.96	3.16	2.52	2.73	0.335	0.028	0.096
704	66330	28.76	7.64	2.67	0.96	3.28	2.53	2.75	0.335	0.031	0.094
708	66756	29.01	7.67	2.74	0.90	3.49	2.79	2.80	0.337	0.029	0.090
712	67183	29.16	7.66	2.67	0.89	3.46	2.79	2.81	0.338	0.026	0.092
716	67609	28.98	7.74	2.71	0.93	3.42	2.74	2.81	0.340	0.028	0.089
720	68036	29.24	7.85	2.76	0.93	3.40	2.79	2.82	0.339	0.025	0.092
724	68462	29.04	7.83	2.80	0.97	3.37	2.79	2.82	0.343	0.025	0.093
728	68888	28.82	7.84	2.81	0.96	3.31	2.88	2.81	0.345	0.026	0.089
732	69315	28.71	7.70	2.81	0.92	3.39	2.78	2.78	0.341	0.029	0.089
736	69741	28.81	7.79	2.84	0.96	3.49	2.73	2.80	0.350	0.028	0.090
740	70168	28.32	7.82	2.86	0.99	3.37	2.76	2.77	0.347	0.029	0.088
744	70594	28.51	7.76	2.77	0.97	3.50	2.70	2.78	0.346	0.028	0.088
748	71020	28.64	8.00	2.95	1.01	3.41	2.85	2.84	0.354	0.027	0.089
750	71234	28.11	8.09	3.12	1.04	3.19	2.79	2.76	0.361	0.030	0.092
754	71660	28.27	7.97	2.97	1.03	3.27	2.78	2.75	0.359	0.025	0.090
758	72086	28.72	7.94	2.85	1.00	3.20	2.89	2.84	0.354	0.029	0.089
800	76563	28.48	7.68	2.74	0.95	3.60	2.70	2.75	0.347	0.030	0.090
802	76777	28.22	7.80	2.86	0.98	3.43	2.79	2.77	0.356	0.028	0.090
804	76990	27.79	7.78	2.84	1.04	3.44	2.42	2.68	0.348	0.028	0.094
806	77203	27.73	7.88	2.90	1.09	3.38	2.50	2.71	0.358	0.030	0.093
808	77416	27.96	7.92	2.91	1.07	3.40	2.45	2.70	0.359	0.030	0.092
810	77629	28.07	7.97	2.91	1.08	3.30	2.52	2.68	0.359	0.030	0.094
812	77843	28.06	7.97	2.94	1.08	3.22	2.39	2.71	0.358	0.032	0.096
814	78056	28.20	8.09	2.98	1.12	2.76	2.45	2.75	0.365	0.032	0.094
816	78269	28.28	8.00	2.94	1.09	2.84	2.53	2.75	0.362	0.027	0.095
818	78482	28.45	8.16	2.96	1.13	2.85	2.59	2.76	0.368	0.030	0.093
820	78695	28.42	8.10	2.98	1.12	2.52	2.54	2.74	0.365	0.032	0.092
822	78909	28.25	8.21	3.02	1.12	2.69	2.53	2.77	0.368	0.030	0.092
824	79122	28.14	8.20	3.03	1.15	2.92	2.56	2.74	0.371	0.032	0.091
826	79335	28.18	8.10	2.98	1.13	2.70	2.60	2.74	0.365	0.030	0.094
828	79548	28.35	8.23	3.02	1.15	2.93	2.59	2.75	0.370	0.032	0.092
830	79761	27.99	8.14	3.01	1.13	2.53	2.56	2.75	0.369	0.031	0.093
832	79975	27.64	8.08	3.02	1.13	2.92	2.42	2.72	0.369	0.032	0.089
834	80188	27.55	8.08	3.00	1.13	2.90	2.52	2.69	0.367	0.032	0.089
836	80401	27.84	8.14	3.01	1.15	2.98	2.52	2.74	0.367	0.032	0.089
838	80614	27.64	8.11	3.05	1.17	3.04	2.56	2.73	0.368	0.032	0.094
840	80827	27.80	8.10	3.05	1.13	3.00	2.53	2.71	0.367	0.032	0.088
842	81041	27.73	8.15	3.00	1.13	3.00	2.48	2.69	0.364	0.032	0.089
844	81254	27.99	8.10	3.02	1.13	3.05	2.54	2.71	0.364	0.032	0.089
846	81467	27.77	8.01	2.99	1.10	3.02	2.61	2.69	0.362	0.030	0.090
848	81680	27.70	9.43	2.97	1.07	3.01	2.57	2.72	0.362	0.030	0.089
850	81893	27.18	8.18	2.91	1.04	2.77	2.47	2.63	0.349	0.031	0.088
852	82107	27.76	8.23	3.00	1.10	2.92	2.56	2.70	0.365	0.030	0.092
854	82320	28.23	8.08	3.01	1.12	2.99	2.57	2.72	0.365	0.033	0.090
856	82533	28.53	8.04	3.05	1.07	2.90	2.79	2.81	0.368	0.029	0.087
858	82746	28.48	7.95	3.03	1.03	3.01	2.76	2.77	0.362	0.030	0.086
860	82959	28.67	7.93	2.99	1.01	2.86	2.81	2.78	0.358	0.028	0.087
862	83030	28.73	7.92	3.01	1.02	2.72	2.79	2.79	0.362	0.028	0.089
864	83101	28.92	7.92	3.00	1.01	2.80	2.79	2.82	0.364	0.031	0.089
866	83173	28.95	7.91	2.96	1.01	2.77	2.79	2.79	0.359	0.028	0.097
868	83386	28.96	8.00	2.98	1.04	2.61	2.78	2.82	0.367	0.029	0.091
870	83599	29.35	7.99	2.94	1.01	2.40	2.82	2.84	0.365	0.032	0.091
872	83812	29.06	7.80	2.93	0.99	2.76	2.79	2.84	0.361	0.031	0.092
874	84025	29.25	7.89	2.93	0.98	2.58	2.88	2.83	0.360	0.029	0.091
876	84239	29.30	7.77	2.81	0.97	2.52	2.81	2.84	0.355	0.028	0.094
878	84452	28.82	7.77	2.96	0.99	2.94	2.82	2.81	0.359	0.027	0.094
880	84665	29.04	7.99	3.02	1.04	2.68	2.88	2.84	0.371	0.031	0.092
882	84878	28.94	7.96	3.01	1.03	2.45	2.83	2.81	0.368	0.029	0.094
884	85091	28.83	8.02	3.12	1.05	2.32	2.83	2.82	0.373	0.030	0.092
886	85305	28.47	7.97	3.15	1.05	2.73	2.80	2.77	0.370	0.032	0.089
888	85518	28.79	8.05	3.07	1.09	2.38	2.91	2.81	0.372	0.032	0.089
890	85731	29.02	8.13	3.07	1.06	2.01	2.82	2.84	0.373	0.030	0.092
892	85944	28.99	8.18	3.04	1.06	1.96	2.93	2.84	0.374	0.028	0.089
894	86157	28.59	8.02	2.90	1.04	2.43	2.87	2.78	0.365	0.028	0.089
896	86371	29.43	8.46	3.26	1.13	2.21	3.00	2.85	0.385	0.032	0.092
898	86584	28.29	8.21	3.15	1.12	2.36	2.85	2.78	0.378	0.032	0.091
900	86797	27.50	8.30	3.08	1.20	3.00	2.59	2.69	0.380	0.033	0.092
902	87010	27.51	8.35	3.11	1.24	2.96	2.64	2.72	0.383	0.034	0.086
904	87223	28.02	8.52	3.28	1.29	2.22	2.68	2.78	0.392	0.035	0.088

Appendix C
Core MD02-2518 (Mazatlan) - Major Elements

Depth (cm)	Age (yrs BP)	Si wt. %	Al wt. %	Fe wt. %	Mg wt. %	Ca wt. %	Na wt. %	K wt. %	Ti wt. %	Mn wt. %	P wt. %
906	87437	29.97	8.77	3.18	1.22	1.93	2.76	2.87	0.388	0.034	0.101
908	87650	28.65	8.67	3.38	1.25	1.55	2.66	2.84	0.394	0.034	0.092
910	87863	29.00	8.00	2.77	1.03	2.79	2.53	2.76	0.350	0.029	0.097
912	88076	29.25	8.40	3.01	1.15	2.09	2.67	2.84	0.379	0.031	0.097
914	88289	29.51	8.44	3.14	1.16	1.89	2.70	2.85	0.388	0.032	0.102
916	88503	29.16	8.13	2.91	1.06	2.47	2.63	2.78	0.359	0.032	0.094
918	88716	29.17	8.24	2.95	1.07	2.30	2.62	2.78	0.364	0.030	0.102
920	88929	29.03	8.54	3.40	1.24	1.41	2.68	2.84	0.403	0.035	0.102
922	89142	28.95	8.50	3.40	1.25	1.52	2.71	2.83	0.401	0.035	0.105
924	89355	29.55	8.60	3.18	1.19	1.65	2.73	2.90	0.391	0.035	0.103
926	89569	28.32	8.47	3.28	1.23	2.17	2.68	2.76	0.395	0.035	0.102
928	89782	28.26	8.45	3.31	1.23	2.26	2.70	2.78	0.399	0.035	0.109
930	89995	29.02	8.11	2.98	1.09	2.72	2.56	2.76	0.370	0.033	0.094
932	90208	28.34	8.71	3.34	1.31	1.68	2.70	2.83	0.406	0.036	0.102
934	90421	28.38	8.74	3.34	1.30	1.72	2.77	2.84	0.405	0.036	0.100
936	90635	28.42	8.55	3.26	1.25	2.00	2.98	2.81	0.401	0.036	0.096
938	90848	28.02	8.81	3.33	1.35	1.47	2.66	2.81	0.406	0.034	0.090
940	91061	28.40	9.32	3.44	1.44	1.24	2.87	2.94	0.413	0.035	0.092
942	91274	28.53	8.89	3.35	1.33	1.25	2.76	2.88	0.406	0.035	0.090
944	91487	28.24	9.36	3.53	1.48	0.80	2.85	2.95	0.418	0.036	0.088
945	91701	27.91	9.54	3.35	1.42	0.74	2.75	2.93	0.391	0.035	0.084
946	91914	28.39	9.68	3.33	1.40	0.79	2.77	3.06	0.394	0.038	0.099
948	92127	28.71	8.91	3.28	1.29	1.04	2.69	2.92	0.397	0.035	0.102
950	92340	28.58	9.38	3.44	1.44	0.86	2.78	2.96	0.415	0.033	0.098
952	92553	27.98	9.82	3.47	1.53	0.71	2.85	2.94	0.408	0.035	0.086
954	92766	27.99	9.54	3.41	1.51	0.78	2.86	2.95	0.407	0.033	0.098
956	92980	28.25	9.17	3.40	1.42	1.02	2.74	2.88	0.402	0.037	0.097
958	93193	27.27	9.48	3.36	1.47	1.43	2.59	2.91	0.391	0.035	0.073
960	93406	27.85	8.34	3.07	1.31	3.03	2.63	2.71	0.391	0.035	0.112
962	93619	29.08	8.37	3.37	1.18	2.41	2.61	2.76	0.395	0.036	0.126
964	93832	27.68	7.90	3.07	1.15	3.49	2.53	2.62	0.379	0.030	0.148
966	94046	28.82	8.28	3.09	1.18	2.43	2.65	2.78	0.394	0.034	0.113
968	94259	29.37	8.46	3.24	1.19	1.54	2.61	2.86	0.403	0.035	0.107
970	94472	28.55	8.16	3.18	1.15	2.18	2.56	2.76	0.392	0.033	0.102
972	94685	28.59	8.13	3.19	1.15	2.87	2.59	2.74	0.391	0.036	0.102
974	94898	28.40	7.96	3.14	1.13	2.82	2.58	2.74	0.384	0.034	0.104
976	95112	26.75	7.59	3.01	1.11	2.81	2.53	2.65	0.372	0.034	0.098
978	95325	27.75	7.78	2.94	1.10	2.84	4.59	2.76	0.379	0.035	0.106
980	95538	28.21	8.02	3.03	1.14	2.55	2.59	2.75	0.389	0.035	0.101
982	95751	27.89	7.95	3.14	1.15	2.48	2.52	2.70	0.387	0.035	0.102
984	95964	27.60	7.90	3.14	1.14	2.80	2.62	2.66	0.383	0.035	0.099
986	96178	28.59	8.23	3.17	1.15	2.81	2.57	2.71	0.388	0.035	0.104
988	96391	27.20	7.81	3.05	1.14	2.92	2.46	2.65	0.380	0.034	0.098
990	96604	27.39	7.87	3.03	1.10	2.85	2.44	2.63	0.382	0.033	0.098
992	96817	28.58	8.22	3.23	1.16	1.23	2.53	2.80	0.400	0.035	0.099
994	97030	28.99	8.37	3.26	1.18	1.23	2.58	2.87	0.404	0.033	0.096
996	97244	28.60	8.52	3.17	1.19	1.19	2.59	2.85	0.398	0.035	0.098
998	97457	28.64	8.52	3.26	1.24	1.31	2.62	2.83	0.400	0.032	0.102
1000	97670	29.11	8.63	3.24	1.21	1.04	2.62	2.89	0.398	0.035	0.095
1002	97883	28.24	8.37	3.26	1.22	1.71	2.56	2.77	0.400	0.033	0.097
1004	98096	28.59	8.55	3.32	1.22	1.32	2.56	2.80	0.408	0.035	0.103
1006	98310	27.86	8.29	3.17	1.19	2.29	2.55	2.69	0.395	0.033	0.095
1008	98523	27.59	8.30	3.33	1.20	2.14	2.50	2.68	0.401	0.034	0.093
1010	98736	27.35	8.21	3.21	1.17	2.56	2.52	2.65	0.395	0.035	0.093
1012	98949	27.22	8.35	3.24	1.22	2.59	2.58	2.63	0.398	0.032	0.093
1014	99162	27.46	8.38	3.30	1.22	2.71	2.57	2.70	0.394	0.034	0.095
1016	99376	27.46	8.68	3.30	1.27	2.07	2.65	2.70	0.400	0.034	0.099
1018	99589	27.24	8.61	3.35	1.30	2.67	2.56	2.60	0.395	0.035	0.089
1020	99802	27.30	8.87	3.54	1.39	1.49	2.76	2.77	0.412	0.036	0.104
1022	100015	27.36	9.37	3.43	1.49	0.79	3.02	2.90	0.406	0.035	0.100
1026	100442	27.02	9.41	3.23	1.51	0.81	3.00	2.90	0.397	0.031	0.122
1028	100655	27.57	9.47	3.30	1.45	0.82	2.84	2.93	0.408	0.034	0.112
1030	100868	29.18	9.32	3.37	1.37	0.92	2.76	2.94	0.408	0.035	0.103
1032	101081	27.46	9.47	3.34	1.47	0.82	2.88	2.90	0.400	0.035	0.122
1034	101294	27.44	9.53	3.33	1.47	0.87	2.96	2.94	0.401	0.032	0.126
1036	101508	27.31	9.58	3.31	1.48	0.73	2.82	2.88	0.400	0.028	0.096
1038	101721	27.23	9.51	3.22	1.47	0.82	2.85	2.87	0.396	0.032	0.135
1040	101934	27.50	9.33	3.23	1.45	0.87	2.77	2.88	0.397	0.033	0.112
1042	102147	27.16	9.41	3.28	1.50	0.82	2.92	2.91	0.393	0.031	0.114
1044	102360	27.33	9.61	3.35	1.54	0.78	3.08	2.97	0.389	0.032	0.111

Appendix C
Core MD02-2518 (Mazatlan) - Major Elements

Depth (cm)	Age (yrs BP)	Si wt. %	Al wt. %	Fe wt. %	Mg wt. %	Ca wt. %	Na wt. %	K wt. %	Ti wt. %	Mn wt. %	P wt. %
1046	102574	28.61	9.18	3.44	1.37	0.92	2.78	2.94	0.410	0.035	0.111
1047	102787	28.12	9.15	3.35	1.41	0.90	2.84	2.92	0.406	0.036	0.109
1048	103000	27.74	9.42	3.36	1.43	0.79	2.82	2.85	0.406	0.035	0.104
1049	103192	27.51	9.72	3.42	1.39	0.71	2.63	2.81	0.412	0.035	0.086
1050	103385	27.27	9.49	3.40	1.44	0.74	2.70	2.86	0.399	0.033	0.108
1052	103577	27.59	9.40	3.43	1.42	0.76	2.67	2.87	0.400	0.038	0.093
1054	103769	27.50	9.55	3.45	1.48	0.78	2.78	2.89	0.395	0.035	0.100
1056	103962	27.61	9.42	3.43	1.45	0.83	2.69	2.88	0.400	0.036	0.105
1058	104154	27.26	9.52	3.46	1.47	0.79	2.82	2.88	0.394	0.033	0.104
1060	104346	27.59	8.53	3.41	1.30	1.95	2.61	2.73	0.393	0.033	0.313
1062	104538	27.44	9.64	3.38	1.47	0.81	2.73	2.88	0.410	0.035	0.108
1064	104731	27.30	9.96	3.47	1.45	0.76	2.58	2.88	0.416	0.035	0.082
1066	104923	27.63	10.03	3.48	1.47	0.76	2.67	2.91	0.418	0.035	0.085
1068	105115	27.70	9.40	3.40	1.46	0.87	2.78	2.92	0.401	0.035	0.124
1070	105308	27.50	9.43	3.40	1.46	0.79	2.78	2.90	0.392	0.034	0.095
1072	105500	27.36	9.09	3.41	1.42	1.38	2.74	2.84	0.392	0.036	0.101
1074	105692	27.05	8.67	3.25	1.35	2.16	2.63	2.73	0.395	0.032	0.111
1076	105885	27.02	8.44	3.19	1.29	2.83	2.62	2.65	0.385	0.035	0.139
1078	106077	25.16	7.72	2.97	1.21	5.66	2.53	2.45	0.356	0.029	0.782
1080	106269	25.92	7.95	3.24	1.24	4.78	2.54	2.50	0.361	0.031	0.489
1082	106462	26.95	8.31	3.21	1.24	4.14	2.57	2.64	0.379	0.035	0.118
1084	106654	26.94	7.95	3.07	1.14	4.05	2.63	2.61	0.374	0.035	0.119
1086	106846	28.10	8.25	3.16	1.18	2.42	2.66	2.70	0.394	0.035	0.106
1088	107038	28.37	8.24	3.16	1.15	2.50	2.59	2.73	0.391	0.035	0.105
1090	107231	28.13	8.20	3.18	1.16	2.40	2.59	2.69	0.388	0.035	0.106
1092	107423	28.31	8.22	3.28	1.16	2.29	2.63	2.72	0.396	0.036	0.102
1094	107615	28.73	8.85	3.37	1.30	1.25	2.76	2.85	0.415	0.035	0.131
1096	107808	29.22	8.71	3.29	1.21	1.24	2.68	2.86	0.407	0.034	0.109
1098	108000	28.67	8.54	3.21	1.19	2.04	2.68	2.75	0.400	0.034	0.103
1100	108192	28.82	8.80	3.36	1.27	2.55	2.70	2.76	0.402	0.037	0.104
1102	108385	27.60	8.46	3.37	1.22	2.67	2.66	2.67	0.390	0.035	0.106
1104	108577	29.46	8.87	3.38	1.27	1.54	2.76	2.81	0.409	0.034	0.110
1106	108769	27.74	8.42	3.32	1.21	2.97	2.59	2.68	0.390	0.035	0.111
1108	108962	26.86	8.25	3.25	1.21	3.33	2.54	2.58	0.389	0.032	0.107
1110	109154	27.06	8.41	3.27	1.23	3.40	2.64	2.60	0.383	0.032	0.104
1112	109346	27.97	8.44	3.28	1.21	3.24	2.59	2.67	0.388	0.033	0.105
1114	109538	27.67	8.27	3.33	1.16	3.10	2.56	2.63	0.395	0.033	0.099
1116	109731	29.20	8.78	3.33	1.25	3.41	2.70	2.71	0.400	0.035	0.114
1126	110692	26.52	8.73	3.33	1.34	2.96	2.61	2.53	0.398	0.036	0.097
1128	110885	27.15	9.41	3.42	1.48	1.32	2.83	2.77	0.397	0.033	0.102
1130	111077	27.14	9.46	3.29	1.49	1.07	2.93	2.80	0.391	0.035	0.114
1131	111269	27.20	9.59	3.25	1.53	0.94	3.08	2.82	0.392	0.032	0.155
1132	111462	27.61	10.91	3.20	1.40	0.51	2.22	2.96	0.389	0.042	0.044
1134	111654	27.60	9.73	3.32	1.51	0.79	2.98	2.83	0.406	0.034	0.119
1136	111846	26.34	8.85	5.28	1.39	1.22	2.72	2.71	0.378	0.036	0.127
1138	112038	27.43	9.44	3.61	1.45	0.79	2.89	2.80	0.395	0.035	0.105
1140	112231	27.39	9.64	3.35	1.52	0.82	3.03	2.83	0.392	0.031	0.132
1142	112423	27.26	9.59	3.30	1.53	0.85	3.04	2.80	0.394	0.033	0.154
1144	112615	27.56	9.62	3.28	1.57	0.79	3.16	2.86	0.392	0.032	0.114
1146	112808	27.47	9.45	3.25	1.51	0.96	3.02	2.85	0.389	0.035	0.157
1148	113000	28.14	9.95	3.28	1.66	0.86	3.50	2.97	0.389	0.032	0.153
1150	113192	27.52	9.48	3.24	1.53	0.89	3.02	2.83	0.389	0.031	0.152
1152	113385	23.05	7.90	2.79	1.22	0.69	2.42	2.33	0.313	0.023	0.107
1154	113577	27.98	9.42	3.77	1.48	0.85	2.94	2.90	0.399	0.039	0.129
1156	113769	27.37	9.38	3.28	1.53	0.97	2.93	2.87	0.388	0.033	0.192
1158	113962	28.11	9.46	3.33	1.51	0.79	2.96	2.93	0.398	0.037	0.114
1160	114154	27.92	9.27	3.41	1.49	0.86	2.88	2.88	0.397	0.035	0.125
1161	114346	28.13	9.82	3.36	1.45	0.66	2.65	3.12	0.387	0.043	0.075
1162	114538	28.10	9.38	3.51	1.46	0.72	2.77	2.93	0.398	0.041	0.085
1164	114731	27.98	9.28	3.48	1.50	0.78	2.85	2.91	0.398	0.037	0.105
1166	114923	28.05	9.37	3.38	1.51	0.82	2.85	2.95	0.399	0.038	0.117
1167	115115	27.16	10.43	3.54	1.51	0.72	2.62	2.89	0.423	0.040	0.076
1168	115308	27.99	9.39	3.44	1.48	0.83	2.91	2.91	0.398	0.038	0.126
1170	115500	28.02	9.63	3.28	1.45	0.84	2.79	2.98	0.382	0.039	0.142
1172	115692	27.42	9.39	3.42	1.58	0.94	3.13	2.86	0.386	0.033	0.177
1174	115885	27.82	9.30	3.34	1.52	0.97	3.05	2.88	0.392	0.035	0.175
1176	116077	27.73	9.24	3.29	1.51	0.92	3.02	2.88	0.392	0.034	0.157
1178	116269	28.01	9.32	3.28	1.47	0.83	2.95	2.88	0.394	0.031	0.121
1180	116462	28.64	9.73	3.27	1.58	0.89	3.19	2.91	0.384	0.033	0.153
1182	116654	27.77	9.31	3.35	1.53	0.84	2.94	2.92	0.388	0.034	0.126

Appendix C
Core MD02-2518 (Mazatlan) - Major Elements

Depth (cm)	Age (yrs BP)	Si wt. %	Al wt. %	Fe wt. %	Mg wt. %	Ca wt. %	Na wt. %	K wt. %	Ti wt. %	Mn wt. %	P wt. %
1184	121195	27.71	9.35	3.28	1.52	0.82	2.99	2.91	0.382	0.035	0.130
1186	121439	27.36	9.27	3.19	1.51	0.90	2.98	2.92	0.372	0.032	0.168
1188	121683	27.86	9.29	3.24	1.49	0.80	2.93	2.92	0.379	0.032	0.123
1190	121927	27.68	9.26	3.19	1.47	0.84	3.01	2.93	0.368	0.035	0.147
1194	122415	27.47	9.33	3.27	1.50	0.84	3.01	2.90	0.374	0.032	0.147
1196	122658	27.65	9.20	3.23	1.43	0.79	2.93	2.87	0.376	0.032	0.133
1198	122902	27.50	9.17	3.19	1.43	0.74	2.94	2.87	0.370	0.033	0.126
1202	123146	27.98	9.31	3.20	1.46	0.76	3.00	2.94	0.372	0.033	0.135
1204	123390	27.99	9.32	3.16	1.47	0.79	3.02	2.97	0.367	0.035	0.115
1206	123634	27.87	9.28	3.17	1.45	0.78	2.88	2.96	0.368	0.033	0.119
1208	123878	27.99	9.31	3.16	1.49	0.75	3.07	3.01	0.358	0.033	0.109
1210	124122	28.13	9.24	3.19	1.47	0.74	2.98	3.02	0.359	0.031	0.110
1212	124366	28.67	8.95	3.11	1.37	0.82	3.01	3.12	0.346	0.033	0.139
1214	124610	29.34	8.42	2.86	1.13	0.64	3.07	3.28	0.301	0.032	0.092
1216	124854	27.74	9.75	3.63	1.62	0.84	2.93	2.85	0.422	0.033	0.129
1218	125097	27.20	9.63	3.63	1.61	0.81	2.82	2.77	0.427	0.032	0.128
1220	125341	27.15	9.64	3.44	1.57	0.86	2.78	2.84	0.406	0.033	0.142
1222	125585	27.29	9.84	3.58	1.68	0.89	2.96	2.82	0.418	0.034	0.172
1224	125829	27.24	9.79	3.61	1.69	0.93	3.04	2.87	0.419	0.034	0.180
1226	126073	27.39	9.71	3.66	1.62	0.84	2.88	2.84	0.433	0.035	0.138
1228	126317	27.25	9.79	3.58	1.65	0.87	2.90	2.86	0.424	0.035	0.159
1234	127049	27.71	9.79	3.61	1.62	0.83	2.87	2.90	0.419	0.032	0.135
1235	127293	27.91	10.25	3.19	1.47	0.59	2.49	3.12	0.384	0.037	0.079
1236	127536	27.78	10.20	3.16	1.43	0.64	2.45	3.09	0.380	0.035	0.098
1238	127780	26.46	9.31	3.55	1.62	0.74	2.76	2.74	0.403	0.031	0.130
1240	128024	26.33	9.34	3.58	1.59	1.10	2.86	2.82	0.394	0.033	0.279
1242	128268	26.64	9.35	3.65	1.60	0.75	2.85	2.79	0.412	0.027	0.128
1244	128512	26.49	9.29	3.55	1.58	0.77	2.88	2.79	0.404	0.029	0.141
1246	128756	26.81	9.57	3.56	1.57	0.76	2.76	2.82	0.406	0.031	0.130
1248	129000	27.03	9.44	3.63	1.56	0.80	2.80	2.86	0.404	0.029	0.138
1250	129330	27.21	9.48	3.46	1.55	0.74	2.85	2.91	0.398	0.028	0.113
1252	129659	27.19	9.27	3.49	1.51	0.81	2.68	2.89	0.403	0.032	0.107
1254	130318	27.74	8.36	3.12	1.18	2.55	2.55	2.70	0.394	0.035	0.101
1258	130977	28.44	8.11	3.27	1.10	2.15	2.56	2.73	0.397	0.035	0.155
1260	131307	26.60	9.33	3.28	1.51	1.67	2.68	2.90	0.394	0.029	0.508
1262	131636	28.20	7.99	3.16	1.04	2.52	2.56	2.74	0.347	0.033	0.122
1266	132295	28.81	8.22	3.14	1.08	2.19	2.67	2.76	0.395	0.033	0.111
1814	n/a	27.59	9.60	3.85	1.43	0.89	2.49	2.98	0.427	0.035	0.083
1848	n/a	26.85	9.65	3.77	1.65	0.74	2.75	3.03	0.419	0.038	0.110
1870	n/a	26.74	9.88	3.59	1.63	0.75	2.67	3.06	0.409	0.039	0.128
1873	n/a	26.76	9.68	3.60	1.67	0.70	2.75	3.06	0.423	0.035	0.117
1874	n/a	26.94	10.49	3.40	1.59	0.57	2.46	3.01	0.392	0.037	0.083
1888	n/a	27.10	9.98	3.21	1.50	0.67	2.42	3.15	0.370	0.037	0.132
1901	n/a	26.26	10.61	3.80	1.62	0.64	2.45	2.98	0.437	0.039	0.103
1908	n/a	27.01	10.06	3.35	1.31	0.69	2.25	3.02	0.397	0.035	0.142
1910	n/a	25.43	11.73	4.10	1.56	0.56	2.07	2.82	0.467	0.041	0.061

Appendix D
Core MD02-2520 (Gulf of Tehuantepec) - Major Elements

Depth (cm)	Age (yrs BP)	Si wt. %	Al wt. %	Fe wt. %	Mg wt. %	Ca wt. %	Na wt. %	K wt. %	Ti wt. %	Mn wt. %	P wt. %
11	573	23.44	7.67	3.30	2.13	2.42	5.85	1.48	0.358	0.036	0.187
21	615	24.23	7.76	3.23	2.15	2.26	5.45	1.52	0.361	0.039	0.192
31	656	23.79	8.01	3.24	2.06	3.52	5.26	1.58	0.374	0.039	0.169
41	698	23.08	7.66	3.37	1.98	3.33	5.04	1.52	0.352	0.037	0.153
51	740	23.84	8.15	3.40	2.17	2.66	5.15	1.60	0.385	0.037	0.158
61	782	23.98	8.04	3.37	2.09	2.65	4.89	1.58	0.376	0.039	0.166
71	823	22.64	7.78	3.30	1.98	3.76	4.74	1.54	0.358	0.039	0.164
81	865	24.43	8.21	3.32	2.13	2.11	5.01	1.69	0.370	0.035	0.154
91	907	23.46	8.19	3.58	2.06	3.02	4.89	1.61	0.378	0.039	0.153
101	949	24.24	8.10	3.32	2.00	2.82	4.77	1.63	0.374	0.037	0.164
111	991	22.10	7.47	3.32	1.83	4.31	4.74	1.48	0.340	0.037	0.159
121	1,031	22.52	8.02	3.29	1.89	3.82	4.30	1.58	0.346	0.037	0.137
126	1,052	24.92	8.11	3.16	1.78	2.94	4.13	1.64	0.375	0.039	0.158
131	1,073	25.24	8.34	3.33	1.98	1.69	4.56	1.73	0.385	0.036	0.139
141	1,138	23.94	7.73	3.16	1.95	3.12	4.76	1.44	0.358	0.036	0.166
151	1,227	24.20	7.63	3.14	2.08	2.72	4.99	1.46	0.357	0.039	0.164
161	1,317	25.23	7.99	3.30	2.11	1.87	4.87	1.59	0.377	0.038	0.150
171	1,406	25.71	8.15	3.34	1.97	1.59	4.51	1.63	0.386	0.039	0.140
181	1,495	22.79	7.52	3.35	1.88	4.23	4.00	1.53	0.344	0.037	0.141
191	1,585	24.76	8.17	3.45	1.94	2.47	4.21	1.69	0.379	0.039	0.140
201	1,674	25.35	8.26	3.42	1.94	1.87	4.25	1.82	0.377	0.036	0.128
211	1,764	22.20	7.29	3.08	1.71	5.27	3.63	1.52	0.332	0.036	0.136
221	1,853	23.17	8.11	3.51	1.98	3.80	4.24	1.54	0.377	0.039	0.172
231	1,943	23.23	7.57	3.33	1.80	3.96	4.11	1.42	0.347	0.035	0.157
241	2,032	22.48	7.78	3.37	1.89	4.36	4.05	1.47	0.359	0.039	0.157
251	2,122	24.08	8.20	3.35	1.88	3.10	4.25	1.54	0.376	0.037	0.178
261	2,211	24.63	8.20	3.25	2.02	2.82	4.52	1.54	0.368	0.035	0.164
271	2,300	25.58	8.20	3.23	1.99	1.76	4.36	1.71	0.370	0.036	0.148
281	2,390	24.09	8.29	3.47	1.94	3.05	4.05	1.65	0.391	0.040	0.164
291	2,479	24.90	8.28	3.58	2.00	2.49	4.17	1.66	0.388	0.041	0.152
301	2,569	25.89	8.47	3.50	1.92	1.89	4.18	1.69	0.396	0.041	0.164
311	2,658	24.35	7.89	3.06	1.63	3.95	3.87	1.82	0.328	0.045	0.133
321	2,769	24.74	8.24	3.43	1.89	2.93	4.02	1.63	0.385	0.040	0.177
331	2,901	23.06	7.83	3.30	1.92	4.27	3.89	1.41	0.361	0.037	0.207
341	3,032	24.86	8.06	3.33	1.92	2.90	4.37	1.49	0.370	0.041	0.190
351	3,164	23.41	7.99	3.29	1.85	4.06	4.07	1.45	0.364	0.041	0.170
361	3,296	25.81	8.55	3.43	1.94	1.92	4.16	1.64	0.391	0.039	0.181
371	3,426	25.20	8.24	3.37	1.94	2.52	4.32	1.51	0.383	0.039	0.177
381	3,560	22.39	7.42	3.34	1.88	4.86	3.98	1.33	0.341	0.035	0.190
391	3,691	25.78	8.59	3.54	1.89	1.74	4.17	1.63	0.403	0.039	0.166
401	3,823	24.20	8.34	3.60	1.89	3.27	3.95	1.63	0.377	0.039	0.162
411	3,955	25.72	8.45	3.56	1.98	1.80	4.25	1.62	0.395	0.040	0.179
421	4,075	23.79	8.02	3.35	1.85	4.05	3.99	1.48	0.368	0.039	0.189
431	4,194	24.12	8.00	3.33	1.88	3.73	3.96	1.45	0.373	0.039	0.198
441	4,314	25.14	8.34	3.49	1.93	2.70	3.99	1.53	0.389	0.040	0.191
451	4,433	25.07	8.58	3.58	1.93	2.87	3.99	1.55	0.401	0.042	0.183
461	4,553	22.61	7.85	3.51	1.97	6.84	3.68	1.37	0.362	0.042	0.211
471	4,673	23.65	7.95	3.37	1.85	4.31	3.78	1.42	0.374	0.038	0.172
481	4,792	24.07	8.33	3.65	1.91	3.72	3.63	1.48	0.394	0.042	0.201
491	4,912	24.51	8.48	3.72	1.94	3.25	3.71	1.56	0.403	0.040	0.175
501	5,031	22.82	7.65	3.56	1.89	5.75	3.59	1.41	0.355	0.039	0.184
511	5,151	25.66	8.72	3.71	1.92	2.48	3.76	1.60	0.406	0.040	0.169
521	5,270	23.28	7.92	3.47	1.85	4.93	3.61	1.44	0.374	0.039	0.187
531	5,390	24.85	8.45	3.65	1.88	3.16	3.92	1.57	0.395	0.043	0.148
541	5,510	22.02	7.37	3.44	1.71	6.85	3.28	1.37	0.342	0.038	0.206
551	5,591	23.50	7.73	3.49	1.75	5.13	3.49	1.55	0.364	0.036	0.172
555	5,672	25.23	10.02	4.63	1.94	2.47	2.46	2.56	0.469	0.035	0.090
561	5,712	24.66	8.36	3.60	1.85	3.64	3.68	1.53	0.387	0.039	0.163
571	5,753	24.96	8.51	3.67	1.88	3.65	3.88	1.55	0.398	0.040	0.179
581	5,793	26.59	8.82	3.74	1.88	1.95	3.88	1.67	0.416	0.042	0.151
591	5,834	23.45	8.02	3.54	1.84	5.72	3.52	1.47	0.371	0.041	0.170
595	5,915	16.83	5.63	2.51	1.85	15.51	2.85	1.05	0.266	0.032	0.190
601	5,996	26.37	8.68	3.64	1.83	2.30	3.79	1.59	0.408	0.041	0.159
611	6,077	25.84	8.88	3.74	1.88	2.49	3.68	1.67	0.415	0.044	0.170
631	6,239	22.83	7.88	3.54	1.75	6.33	3.23	1.37	0.363	0.039	0.179
671	6,563	25.67	8.65	3.82	1.79	2.90	3.57	1.59	0.393	0.042	0.155
681	6,780	25.95	8.80	3.58	1.75	2.52	3.40	1.69	0.401	0.041	0.134
691	6,891	24.82	8.58	3.68	1.73	3.44	3.38	1.53	0.393	0.039	0.150
701	7,004	24.77	8.98	3.80	1.75	3.38	3.36	1.62	0.414	0.045	0.144
711	7,115	25.04	8.70	3.84	1.71	3.14	3.40	1.62	0.398	0.039	0.129

Appendix D
Core MD02-2520 (Gulf of Tehuantepec) - Major Elements

Depth (cm)	Age (yrs BP)	Si wt. %	Al wt. %	Fe wt. %	Mg wt. %	Ca wt. %	Na wt. %	K wt. %	Ti wt. %	Mn wt. %	P wt. %
721	7,227	25.53	8.82	3.79	1.73	2.70	3.54	1.67	0.408	0.040	0.164
731	7,339	25.30	8.85	3.79	1.69	3.05	3.36	1.62	0.405	0.044	0.165
741	7,450	25.64	9.15	3.80	1.68	2.75	3.33	1.70	0.419	0.042	0.161
751	7,562	25.29	8.99	3.89	1.70	2.65	3.43	1.66	0.410	0.041	0.157
761	7,674	24.72	8.91	3.80	1.70	3.45	3.43	1.57	0.401	0.044	0.147
771	7,785	25.78	9.41	3.82	1.70	2.37	3.36	1.74	0.414	0.045	0.146
781	7,896	26.85	9.49	3.91	1.71	1.27	3.43	1.79	0.430	0.037	0.132
791	7,954	26.82	9.79	3.93	1.72	1.58	3.28	1.85	0.436	0.043	0.119
801	8,065	24.77	9.11	4.09	1.70	3.45	3.25	1.63	0.411	0.042	0.143
811	8,176	26.14	9.65	3.91	1.70	2.07	3.36	1.77	0.430	0.040	0.125
821	8,288	24.39	9.30	4.10	1.63	3.66	3.23	1.64	0.404	0.043	0.135
831	8,344	23.51	9.14	3.76	1.71	5.47	3.09	1.60	0.388	0.043	0.150
841	8,427	25.56	9.61	4.12	1.74	2.88	3.30	1.70	0.425	0.041	0.146
851	8,567	25.84	9.66	4.07	1.71	2.67	3.33	1.73	0.425	0.039	0.142
861	8,698	24.88	9.25	3.98	1.74	4.01	3.31	1.66	0.418	0.041	0.184
871	8,830	23.76	8.54	3.68	1.81	6.31	3.22	1.54	0.392	0.040	0.208
881	8,961	25.53	9.15	4.00	1.69	3.05	3.34	1.69	0.422	0.042	0.152
891	9,092	24.63	8.66	3.96	1.67	3.93	3.60	1.63	0.400	0.039	0.153
901	9,223	26.00	9.31	3.95	1.71	2.22	3.51	1.81	0.431	0.039	0.129
911	9,355	24.71	11.65	3.93	1.62	1.88	3.24	1.77	0.422	0.039	0.138
921	9,486	24.78	10.02	4.09	1.68	1.64	3.24	1.67	0.442	0.039	0.116
931	9,617	26.61	9.87	3.96	1.76	1.09	3.31	1.82	0.436	0.038	0.136
941	9,749	24.59	8.98	3.90	1.67	2.56	3.17	1.63	0.417	0.037	0.140
951	9,880	25.68	9.04	3.91	1.63	0.96	3.34	1.71	0.425	0.032	0.134
961	10,011	24.79	9.37	4.19	1.68	1.40	3.21	1.75	0.437	0.036	0.125
971	10,142	25.31	9.29	4.07	1.66	1.26	3.18	1.71	0.438	0.035	0.136
981	10,291	24.43	8.83	4.07	1.59	2.30	3.32	1.57	0.416	0.035	0.137
991	10,456	25.53	8.97	4.07	1.63	1.37	3.21	1.78	0.428	0.033	0.140
1001	10,621	25.78	8.95	3.96	1.62	1.06	3.65	1.68	0.421	0.033	0.131
1011	10,786	26.24	8.96	3.91	1.57	1.00	3.25	1.73	0.428	0.032	0.122
1021	10,952	23.49	8.16	3.75	1.66	3.39	3.24	1.54	0.386	0.031	0.146
1031	11,117	25.65	8.98	4.03	1.62	1.37	3.17	1.76	0.429	0.031	0.150
1032	11,133	26.65	9.96	4.26	1.77	1.27	2.81	2.34	0.451	0.035	0.115
1041	11,282	26.25	8.64	3.78	1.62	1.09	3.47	1.76	0.422	0.030	0.150
1061	11,613	27.06	8.79	4.01	1.62	1.27	3.51	1.87	0.453	0.032	0.179
1071	11,778	26.30	8.25	3.75	1.61	2.35	3.19	1.85	0.429	0.032	0.163
1081	11,943	26.87	8.58	3.79	1.62	1.41	3.40	1.90	0.451	0.033	0.158
1091	12,165	26.16	8.65	3.98	1.60	1.93	3.32	1.85	0.449	0.035	0.146
1098	12,320	20.86	6.80	3.08	1.69	10.50	3.05	1.38	0.342	0.036	0.198
1099	12,332	17.80	5.85	2.61	1.81	14.39	2.82	1.17	0.296	0.035	0.210
1101	12,386	23.02	7.84	3.70	1.57	4.96	3.12	1.57	0.393	0.032	0.156
1111	12,608	26.34	8.53	3.90	1.59	1.73	3.42	1.89	0.430	0.031	0.152
1121	12,829	25.45	8.77	4.25	1.56	2.32	3.20	1.88	0.442	0.032	0.169
1131	13,051	26.76	9.14	4.10	1.53	1.21	3.29	1.91	0.453	0.031	0.153
1141	13,239	25.01	9.14	4.20	1.45	3.50	3.02	1.84	0.439	0.035	0.167
1151	13,427	26.05	9.43	4.05	1.47	2.04	3.19	1.87	0.443	0.032	0.162
1161	13,616	25.49	8.71	4.19	1.53	2.57	3.07	1.90	0.434	0.035	0.162
1171	13,804	24.91	8.11	3.64	1.57	4.42	3.21	1.75	0.403	0.033	0.181
1181	13,992	27.13	8.79	3.74	1.51	1.75	3.19	2.00	0.442	0.030	0.194
1191	14,200	26.70	9.10	3.83	1.54	1.35	3.13	2.06	0.455	0.034	0.153
1201	14,409	27.59	8.98	3.77	1.59	1.10	3.09	2.14	0.452	0.032	0.147
1211	14,617	25.88	8.36	3.65	1.50	3.64	2.74	1.98	0.426	0.035	0.160
1221	14,826	27.18	9.45	3.88	1.60	1.22	2.83	2.23	0.484	0.037	0.144
1225	14,909	26.97	9.32	3.95	1.62	1.27	3.02	2.18	0.469	0.036	0.145
1231	15,034	26.85	8.88	3.77	1.52	1.89	3.35	1.95	0.442	0.036	0.170
1241	15,190	26.40	8.72	3.69	1.47	2.62	3.19	1.85	0.437	0.037	0.167
1251	15,334	27.12	8.91	3.75	1.45	1.94	3.20	1.96	0.452	0.039	0.162
1261	15,484	26.96	9.31	3.85	1.51	1.47	2.87	2.10	0.468	0.038	0.147
1264	15,548	27.04	9.55	3.91	1.53	1.27	2.94	2.09	0.481	0.035	0.138
1271	15,657	26.12	9.09	3.77	1.52	2.48	2.90	2.10	0.454	0.036	0.121
1281	15,813	24.17	8.19	3.62	1.30	4.44	2.65	1.78	0.417	0.035	0.147
1291	15,969	21.81	7.68	3.41	1.33	7.14	2.47	1.58	0.388	0.032	0.136
1301	16,125	23.86	9.04	4.07	1.34	3.71	2.25	1.94	0.437	0.036	0.085
1311	16,280	25.17	9.28	4.00	1.21	2.74	1.99	2.08	0.461	0.032	0.059
1321	16,436	23.63	8.77	3.66	1.43	4.31	2.72	1.76	0.416	0.033	0.133
1331	16,592	27.06	9.57	3.79	1.43	1.18	2.85	2.12	0.484	0.032	0.115
1341	16,748	23.29	8.98	3.94	1.44	4.18	2.52	1.76	0.424	0.032	0.128
1351	16,904	25.52	9.74	4.06	1.42	2.58	2.62	1.92	0.468	0.035	0.114
1361	17,108	25.23	9.68	4.05	1.44	2.68	2.75	1.88	0.464	0.032	0.126
1371	17,362	25.35	9.18	3.86	1.34	3.28	2.64	1.82	0.449	0.035	0.136

Appendix D
Core MD02-2520 (Gulf of Tehuantepec) - Major Elements

Depth (cm)	Age (yrs BP)	Si wt. %	Al wt. %	Fe wt. %	Mg wt. %	Ca wt. %	Na wt. %	K wt. %	Ti wt. %	Mn wt. %	P wt. %
1376	17,489	24.22	8.77	3.91	1.38	5.27	2.53	1.69	0.424	0.035	0.154
1381	17,616	25.06	9.20	3.79	1.37	3.60	2.65	1.83	0.443	0.035	0.139
1391	17,870	25.87	9.62	3.93	1.39	2.04	2.63	1.95	0.463	0.033	0.127
1401	18,124	24.85	9.14	4.03	1.34	3.85	2.71	1.81	0.443	0.035	0.132
1411	18,378	25.12	9.09	3.82	1.31	3.98	2.60	1.81	0.436	0.032	0.138
1421	18,472	27.17	10.00	4.11	1.40	1.77	3.06	1.89	0.475	0.034	0.143
1431	18,566	25.54	9.24	3.92	1.31	3.38	2.88	1.67	0.432	0.037	0.140
1441	18,661	25.68	9.17	3.84	1.34	2.89	2.88	1.71	0.436	0.032	0.134
1451	18,755	26.82	9.67	3.87	1.36	1.60	2.91	1.88	0.466	0.035	0.139
1461	18,849	26.10	9.44	3.75	1.34	2.56	2.90	1.78	0.449	0.035	0.128
1471	18,915	27.33	9.77	3.83	1.39	1.44	2.98	1.88	0.469	0.035	0.133
1481	18,982	26.41	9.36	3.82	1.34	2.40	2.85	1.80	0.458	0.038	0.143
1491	19,048	26.07	9.37	3.84	1.37	2.09	2.80	1.76	0.451	0.034	0.129
1501	19,115	26.67	9.49	3.85	1.42	1.94	3.11	1.85	0.457	0.033	0.130
1511	19,181	26.79	9.37	3.75	1.48	1.52	3.48	1.81	0.452	0.032	0.129
1521	19,248	26.47	9.47	4.05	1.40	2.26	2.96	1.90	0.466	0.032	0.135
1531	19,314	26.54	9.30	3.63	1.34	2.64	2.86	1.85	0.448	0.033	0.136
1541	19,391	27.13	9.64	3.84	1.39	1.32	3.02	1.84	0.462	0.034	0.127
1551	19,469	27.00	9.72	3.77	1.40	1.27	2.95	1.90	0.470	0.032	0.126
1559	19,530	23.55	8.48	3.69	1.49	6.01	2.88	1.63	0.398	0.032	0.154
1561	19,546	26.91	9.60	3.85	1.39	1.28	3.05	1.80	0.457	0.033	0.127
1571	19,623	27.23	9.50	3.71	1.40	1.38	3.19	1.83	0.452	0.031	0.128
1581	19,700	26.84	9.63	3.82	1.42	1.67	2.96	1.87	0.458	0.032	0.116
1591	19,778	26.81	9.54	3.75	1.39	1.72	3.03	1.81	0.457	0.032	0.136
1701	20,628	26.50	9.47	3.78	1.37	1.91	3.00	1.78	0.454	0.033	0.129
1711	20,705	26.53	9.52	3.76	1.40	1.73	2.96	1.85	0.459	0.033	0.115
1721	20,782	26.85	9.53	3.78	1.37	1.42	3.06	1.88	0.459	0.032	0.128
1731	20,860	26.64	9.03	3.65	1.31	1.77	2.99	1.75	0.438	0.032	0.149
1741	20,937	17.62	6.27	2.60	1.58	14.04	2.49	1.13	0.299	0.033	0.238
1751	21,014	26.78	9.48	3.76	1.38	1.27	2.98	1.87	0.464	0.031	0.123
1761	21,092	25.57	9.26	4.07	1.32	2.40	2.88	1.74	0.445	0.033	0.123
1771	21,169	25.24	9.10	3.77	1.32	3.30	2.82	1.68	0.429	0.035	0.128
1781	21,246	24.49	8.97	3.68	1.26	4.00	2.77	1.56	0.416	0.036	0.122
1791	21,323	26.52	9.60	3.73	1.36	1.87	2.90	1.76	0.454	0.034	0.180
1801	21,401	27.17	9.79	3.93	1.36	1.54	2.98	1.82	0.457	0.035	0.132
1811	21,478	26.79	9.69	3.87	1.36	2.22	2.88	1.77	0.457	0.035	0.124
1821	21,568	26.69	9.55	3.75	1.33	2.47	3.05	1.66	0.444	0.034	0.150
1831	21,658	24.44	8.97	4.04	1.28	4.37	2.90	1.49	0.413	0.034	0.133
1841	21,748	24.49	9.11	3.74	1.30	4.48	2.73	1.53	0.418	0.036	0.149
1851	21,838	26.67	9.68	3.70	1.34	2.20	2.94	1.74	0.452	0.037	0.129
1891	22,198	25.37	9.54	3.75	1.28	2.15	2.99	1.65	0.436	0.032	0.123
1901	22,288	26.12	9.35	3.68	1.25	1.47	3.10	1.66	0.428	0.035	0.133
1911	22,378	24.94	8.96	3.73	1.21	3.28	2.85	1.55	0.408	0.032	0.133
1921	22,468	25.93	9.46	3.88	1.30	2.01	2.98	1.70	0.448	0.034	0.122
1931	22,558	25.89	9.73	3.98	1.31	1.97	2.88	1.73	0.460	0.034	0.121
1941	22,648	26.22	9.41	3.72	1.30	1.52	2.93	1.74	0.452	0.033	0.116
1951	22,738	26.11	9.21	3.91	1.29	2.09	2.89	1.74	0.445	0.034	0.146
1961	22,828	24.57	8.96	3.77	1.22	3.48	2.77	1.56	0.419	0.031	0.148
2231	24,880	25.13	8.80	3.67	1.30	4.10	2.90	1.58	0.420	0.031	0.131
2241	24,935	22.01	8.16	3.40	1.25	6.08	2.47	1.41	0.383	0.034	0.135
2251	24,990	23.60	8.71	3.74	1.25	4.09	2.44	1.59	0.421	0.034	0.119
2261	25,045	24.44	8.80	3.68	1.25	3.56	2.59	1.67	0.428	0.031	0.119
2271	25,100	24.29	8.84	3.59	1.27	3.60	2.47	1.75	0.421	0.032	0.103
2281	25,155	25.11	9.24	3.89	1.28	3.96	2.78	1.59	0.434	0.036	0.126
2291	25,209	21.70	8.10	3.53	1.48	9.05	2.63	1.38	0.386	0.043	0.220
2301	25,349	24.46	8.92	4.07	1.21	4.60	2.60	1.59	0.430	0.035	0.129
2311	25,489	23.83	8.83	3.82	1.24	5.64	2.57	1.54	0.414	0.032	0.133
2321	25,629	25.52	8.98	3.89	1.23	4.33	2.71	1.73	0.413	0.035	0.121
2331	25,769	24.62	9.03	3.77	1.25	4.97	2.65	1.59	0.428	0.033	0.133
2341	25,909	23.95	8.66	3.85	1.21	4.26	2.58	1.57	0.412	0.031	0.132
2351	26,049	23.87	8.70	3.62	1.17	4.18	2.57	1.60	0.403	0.033	0.119
2361	26,189	24.56	9.24	3.93	1.29	2.98	3.08	1.62	0.442	0.033	0.132
2371	26,329	23.99	8.93	3.64	1.21	2.85	2.57	1.53	0.428	0.031	0.122
2381	26,469	24.91	9.00	3.72	1.24	2.96	2.70	1.58	0.428	0.031	0.134
2391	26,609	25.74	9.57	3.91	1.31	1.74	2.78	1.66	0.452	0.032	0.109
2401	26,749	24.20	8.79	3.93	1.22	3.20	2.60	1.57	0.422	0.032	0.125
2411	26,889	26.33	9.96	3.97	1.32	1.67	2.83	1.77	0.465	0.033	0.133
2421	27,029	26.34	9.97	4.03	1.32	1.37	2.84	1.74	0.473	0.031	0.133
2431	27,169	26.02	9.85	4.05	1.34	2.02	2.74	1.75	0.472	0.034	0.126
2441	27,309	22.67	8.35	3.16	1.14	0.94	2.52	1.46	0.379	0.022	0.104

Appendix D
Core MD02-2520 (Gulf of Tehuantepec) - Major Elements

Depth (cm)	Age (yrs BP)	Si wt. %	Al wt. %	Fe wt. %	Mg wt. %	Ca wt. %	Na wt. %	K wt. %	Ti wt. %	Mn wt. %	P wt. %
2451	27,449	26.93	9.63	3.77	1.37	1.48	2.97	1.80	0.458	0.031	0.118
2461	27,589	27.11	9.73	3.65	1.37	1.26	3.01	1.84	0.467	0.030	0.120
2471	27,729	26.57	9.63	3.82	1.31	1.70	2.95	1.72	0.463	0.032	0.117
2481	27,869	27.31	9.44	3.68	1.34	1.38	2.96	1.76	0.460	0.029	0.112
2491	28,012	26.62	9.44	4.00	1.36	2.09	2.90	1.79	0.459	0.033	0.139
2501	28,126	25.52	9.35	4.00	1.29	2.42	2.91	1.65	0.442	0.033	0.131
2511	28,239	26.33	9.52	3.91	1.31	2.05	2.97	1.70	0.454	0.031	0.122
2521	28,353	26.93	9.70	3.77	1.31	1.22	2.92	1.75	0.460	0.029	0.119
2531	28,466	26.78	9.65	3.81	1.32	1.82	2.84	1.82	0.452	0.029	0.116
2541	28,580	26.21	9.76	3.97	1.33	1.51	2.86	1.79	0.470	0.032	0.126
2551	28,693	26.73	10.09	3.87	1.36	1.21	2.85	1.85	0.483	0.034	0.122
2561	28,807	26.77	9.70	3.91	1.40	1.42	2.96	1.84	0.468	0.032	0.118
2571	28,920	26.40	9.65	3.86	1.37	2.04	2.81	1.82	0.467	0.033	0.144
2581	29,034	27.23	9.61	3.84	1.37	1.16	3.00	1.80	0.463	0.031	0.119
2591	29,147	26.98	9.72	3.80	1.38	1.69	3.06	1.78	0.466	0.032	0.160
2601	29,261	25.36	9.31	3.87	1.33	2.22	2.76	1.74	0.449	0.033	0.139
2611	29,374	25.21	9.41	3.96	1.32	2.25	2.71	1.71	0.446	0.031	0.127
2621	29,488	25.45	9.75	3.86	1.28	2.13	2.82	1.68	0.446	0.031	0.122
2631	29,601	23.44	9.23	3.94	1.24	3.83	2.49	1.52	0.430	0.035	0.136
2641	29,715	24.67	9.48	3.98	1.27	2.96	2.65	1.63	0.448	0.033	0.155
2651	29,828	25.63	9.89	3.93	1.31	2.07	2.81	1.75	0.467	0.032	0.141
2661	29,942	22.46	8.71	3.54	1.36	5.63	2.54	1.48	0.406	0.039	0.163
2671	30,055	24.03	9.17	3.93	1.22	3.59	2.59	1.62	0.433	0.035	0.131
2681	30,169	23.23	8.96	3.72	1.20	4.38	2.50	1.53	0.418	0.033	0.152
2691	30,225	25.40	9.87	4.08	1.32	2.20	2.64	1.77	0.463	0.031	0.146
2701	30,282	24.74	9.51	3.96	1.36	2.53	2.70	1.77	0.455	0.035	0.126
2711	30,396	25.02	9.66	4.02	1.33	2.60	2.73	1.76	0.455	0.032	0.117
2721	30,509	24.73	9.55	3.94	1.32	2.87	2.74	1.70	0.451	0.032	0.124
2731	30,623	25.82	9.85	3.88	1.36	1.67	2.97	1.77	0.463	0.034	0.136
2741	30,736	25.66	9.68	4.00	1.32	1.47	3.08	1.72	0.455	0.032	0.136
2751	30,850	26.60	10.15	3.97	1.34	1.23	2.96	1.78	0.475	0.031	0.126
2761	30,963	26.90	9.85	3.81	1.40	1.08	2.92	1.89	0.481	0.028	0.111
2771	31,077	26.45	9.72	3.87	1.42	1.64	2.92	1.87	0.470	0.033	0.145
2781	31,190	26.38	9.77	4.14	1.36	1.38	2.85	1.76	0.466	0.032	0.136
2791	31,304	26.34	9.63	4.02	1.37	2.15	2.86	1.78	0.464	0.033	0.128
2811	31,531	24.99	9.37	4.05	1.29	3.40	2.78	1.63	0.445	0.032	0.147
2821	31,644	24.96	9.29	3.86	1.30	3.52	2.70	1.58	0.440	0.035	0.142
2831	31,758	27.15	9.62	3.77	1.32	1.28	3.04	1.80	0.455	0.030	0.139
2841	31,871	26.15	9.87	3.93	1.34	1.68	2.88	1.74	0.466	0.032	0.158
2851	31,985	26.36	9.74	4.00	1.31	1.59	2.88	1.77	0.467	0.032	0.154
2861	32,098	26.25	9.74	3.96	1.31	1.77	2.90	1.72	0.466	0.034	0.138
2871	32,212	25.08	9.30	3.89	1.34	3.35	2.80	1.62	0.441	0.035	0.143
2881	32,325	26.81	9.77	3.77	1.34	1.24	2.95	1.79	0.464	0.030	0.136
2891	32,439	27.14	9.55	3.89	1.38	1.50	3.05	1.78	0.452	0.030	0.272
2901	32,554	25.74	9.61	4.03	1.47	2.20	2.70	1.99	0.467	0.031	0.117
2911	32,671	25.75	9.45	3.98	1.35	2.09	2.83	1.77	0.452	0.030	0.154
2921	32,788	26.29	9.82	3.91	1.33	1.49	2.82	1.85	0.471	0.035	0.134
2931	32,905	25.84	9.54	3.91	1.33	1.33	2.81	1.79	0.466	0.034	0.137
2941	33,022	25.77	9.70	3.93	1.34	2.30	2.80	1.74	0.460	0.033	0.153
2951	33,139	26.23	9.63	3.91	1.34	1.93	2.79	1.78	0.465	0.034	0.149
2961	33,256	26.64	9.97	4.13	1.37	1.34	2.87	1.83	0.478	0.033	0.143
2981	33,490	26.88	9.89	4.16	1.39	1.38	2.98	1.84	0.475	0.032	0.136
2991	33,607	27.11	10.12	4.12	1.42	1.72	2.90	1.93	0.486	0.034	0.143
3001	33,724	26.00	9.66	3.91	1.36	2.43	2.73	1.81	0.455	0.036	0.144
3011	33,841	26.52	9.92	3.95	1.30	1.94	2.90	1.80	0.457	0.037	0.145
3021	33,958	27.57	10.13	3.89	1.34	1.71	3.02	1.80	0.460	0.037	0.151
3031	34,075	25.61	9.45	3.89	1.33	3.05	2.81	1.71	0.446	0.033	0.131
3041	34,192	25.67	9.73	4.24	1.31	2.29	2.73	1.75	0.460	0.035	0.137
3051	34,309	26.33	9.66	3.93	1.34	1.94	2.84	1.81	0.462	0.037	0.150
3061	34,426	26.25	9.62	4.12	1.34	2.17	2.87	1.81	0.454	0.036	0.127
3071	34,543	26.45	9.54	4.15	1.35	1.93	2.85	1.85	0.451	0.035	0.126
3081	34,660	26.44	9.62	3.78	1.39	2.32	2.76	1.92	0.457	0.035	0.116
3091	34,777	27.39	9.60	3.79	1.32	1.33	3.20	1.81	0.445	0.029	0.136
3101	34,894	26.92	9.93	4.05	1.39	1.42	2.94	1.93	0.467	0.032	0.147
3111	35,011	26.32	9.72	3.86	1.38	2.50	2.79	1.90	0.466	0.035	0.143
3121	35,128	26.05	9.84	4.02	1.39	2.40	2.84	1.83	0.468	0.035	0.150
3131	35,245	25.81	9.83	3.96	1.33	2.63	2.76	1.74	0.464	0.035	0.167
3141	35,362	25.60	9.70	4.03	1.37	3.05	2.87	1.70	0.456	0.039	0.147
3151	35,479	26.47	9.90	4.12	1.40	1.77	2.87	1.84	0.472	0.035	0.165
3161	35,596	25.99	9.72	4.02	1.36	2.56	2.79	1.79	0.469	0.036	0.137

Appendix D
Core MD02-2520 (Gulf of Tehuantepec) - Major Elements

Depth (cm)	Age (yrs BP)	Si wt. %	Al wt. %	Fe wt. %	Mg wt. %	Ca wt. %	Na wt. %	K wt. %	Ti wt. %	Mn wt. %	P wt. %
3171	35,713	26.91	9.99	4.11	1.39	1.52	2.93	1.86	0.478	0.037	0.157
3181	35,830	26.24	9.94	4.05	1.38	2.18	2.84	1.78	0.465	0.035	0.150
3186	35,889	26.28	9.97	4.16	1.39	1.37	2.87	1.89	0.473	0.035	0.126
3191	35,900	18.50	6.99	2.90	1.68	13.30	2.56	1.27	0.325	0.059	0.273
3192	35,912	11.98	4.58	2.02	1.80	21.53	1.75	0.87	0.227	0.081	0.334
3194	35,924	19.15	7.29	3.28	1.57	11.92	2.45	1.28	0.341	0.056	0.262
3196	35,935	26.59	10.09	4.22	1.37	1.55	2.83	1.85	0.475	0.033	0.140
3201	35,947	26.24	9.71	4.13	1.36	2.06	2.76	1.82	0.460	0.033	0.149
3211	36,064	26.83	9.89	3.90	1.38	1.42	2.96	1.84	0.454	0.032	0.157
3221	36,181	26.90	9.69	3.80	1.31	1.70	2.99	1.87	0.451	0.033	0.150
3231	36,298	26.19	9.73	4.01	1.34	2.37	2.89	1.72	0.451	0.034	0.151
3241	36,415	26.38	9.70	4.14	1.45	1.78	2.86	1.86	0.460	0.036	0.158
3251	36,532	26.68	9.50	3.83	1.44	1.46	2.93	1.86	0.450	0.036	0.159
3261	36,649	26.09	9.55	4.20	1.38	1.73	2.82	1.81	0.457	0.032	0.148
3271	36,766	26.87	9.66	3.91	1.41	1.19	2.96	1.89	0.464	0.035	0.159
3281	36,883	26.52	9.43	4.06	1.42	1.55	2.90	1.91	0.458	0.035	0.143
3291	37,000	25.99	9.29	4.00	1.44	2.08	2.87	1.91	0.454	0.035	0.144
3311	37,300	26.55	9.96	4.17	1.48	1.02	2.61	2.17	0.478	0.030	0.116
3321	37,552	27.12	9.81	3.78	1.37	1.11	2.82	1.99	0.483	0.030	0.126
3331	37,804	26.84	9.80	4.07	1.39	1.24	2.85	1.93	0.478	0.034	0.126
3341	38,056	26.97	9.74	3.79	1.38	1.41	2.90	2.00	0.472	0.034	0.133
3351	38,308	27.14	9.81	3.84	1.39	1.29	2.81	2.02	0.489	0.033	0.140
3361	38,560	26.69	9.46	3.76	1.31	2.11	2.68	2.02	0.464	0.031	0.129
3371	38,812	25.93	9.36	3.89	1.33	2.75	2.46	2.01	0.458	0.033	0.115
3381	39,064	26.65	9.61	4.05	1.36	1.23	2.85	1.93	0.468	0.036	0.145
3391	39,316	27.20	9.72	3.67	1.32	1.32	2.99	1.87	0.455	0.033	0.134
3401	39,568	27.65	9.55	3.59	1.36	1.17	3.05	1.90	0.458	0.031	0.117
3411	39,820	27.18	9.73	3.77	1.31	1.29	2.88	1.91	0.463	0.033	0.113
3421	40,072	27.17	9.66	3.75	1.34	1.42	2.90	1.91	0.466	0.035	0.109
3431	40,324	27.49	9.92	3.69	1.30	1.28	2.91	1.88	0.458	0.034	0.123
3441	40,576	27.38	9.72	3.79	1.27	1.26	2.91	1.90	0.446	0.034	0.111
3451	40,828	27.53	9.79	3.64	1.34	1.30	2.92	1.89	0.463	0.035	0.133
3461	41,080	27.62	9.64	3.84	1.25	1.50	2.96	1.94	0.448	0.035	0.133
3471	41,332	27.34	9.95	3.79	1.37	1.22	2.78	2.09	0.476	0.036	0.110
3481	41,584	27.79	9.63	3.69	1.21	1.22	2.83	1.95	0.439	0.039	0.105
3491	41,836	28.30	9.22	3.39	1.17	1.12	2.99	2.04	0.409	0.037	0.102
3501	42,088	29.74	8.86	2.89	1.02	1.09	3.05	2.38	0.352	0.042	0.095
3511	42,340	30.32	8.54	2.59	0.87	1.15	3.16	2.44	0.310	0.050	0.121
3521	42,592	27.11	9.92	3.63	1.24	1.47	2.88	1.86	0.442	0.034	0.133
3531	42,844	27.10	9.97	3.91	1.29	1.37	2.91	1.80	0.458	0.034	0.135
3541	43,096	27.22	10.00	3.82	1.31	1.32	2.88	1.85	0.467	0.034	0.128
3551	43,348	26.93	9.98	3.96	1.31	1.32	2.88	1.81	0.466	0.032	0.133
3561	43,474	27.03	10.01	3.85	1.32	1.31	2.92	1.77	0.464	0.036	0.143
3571	43,600	26.70	9.83	3.98	1.37	1.19	2.85	1.83	0.464	0.033	0.143
3581	43,852	26.87	9.54	3.85	1.36	1.55	3.02	1.75	0.453	0.035	0.185
3591	44,104	27.12	9.66	3.98	1.31	1.29	2.76	1.87	0.460	0.036	0.125
3601	44,356	27.59	9.14	3.55	1.37	1.31	3.06	1.75	0.446	0.030	0.211
3611	44,608	27.54	9.32	3.76	1.33	1.13	2.99	1.80	0.457	0.031	0.132
3621	44,860	27.67	9.11	3.77	1.38	0.99	2.96	1.93	0.454	0.029	0.116
3631	45,112	27.30	9.49	3.83	1.37	0.98	2.72	1.92	0.474	0.029	0.110
3641	45,238	27.40	9.54	3.86	1.24	1.17	2.90	1.72	0.451	0.033	0.126
3651	45,364	27.23	9.67	3.78	1.27	1.19	2.83	1.75	0.471	0.029	0.126
3661	45,490	27.18	9.59	3.77	1.31	1.12	2.90	1.82	0.469	0.028	0.127
3671	45,616	26.71	9.66	4.05	1.35	1.17	2.77	1.82	0.470	0.035	0.116
3672	45,742	24.85	11.13	5.12	1.86	0.79	2.13	2.39	0.606	0.047	0.067
3681	45,868	26.53	9.83	3.88	1.30	1.18	2.76	1.87	0.473	0.035	0.124
3691	45,994	26.75	9.52	3.91	1.32	1.15	2.76	1.93	0.472	0.032	0.132
3701	46,120	26.87	9.35	3.83	1.28	1.35	2.88	1.80	0.446	0.032	0.120

Appendix E
Core MD02-2518 (Mazatlan) – Colour Reflectivity

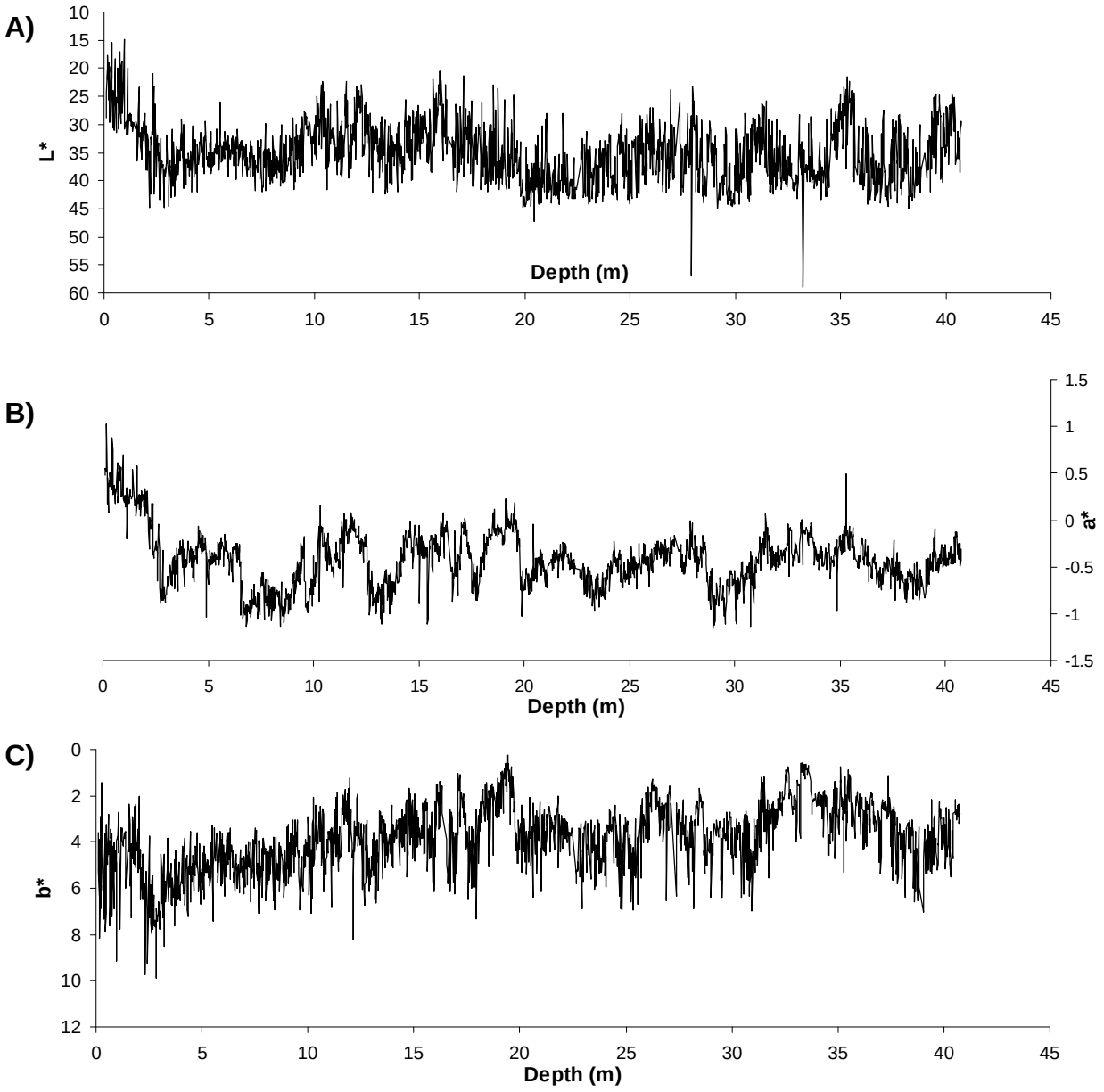

Comparison of colour reflectance in sediments from core MD02-2518 collected in Mazatlan Basin. A) Lightness (L*) of sediments measured as a percentage of light reflected. B) Plot of chromaticity values (a*) ranging from green (negative) to red (positive). C) Plot of chromaticity variable (b*) with values ranging from blue (lower values) to yellow (higher values).

The entire dataset of physical properties of core MD02-2518 can be found at:
http://doi.pangaea.de/10.1594/PANGAEA.95610

Appendix F
Core MD02-2520 (Gulf of Tehuantepec) – Colour Reflectivity

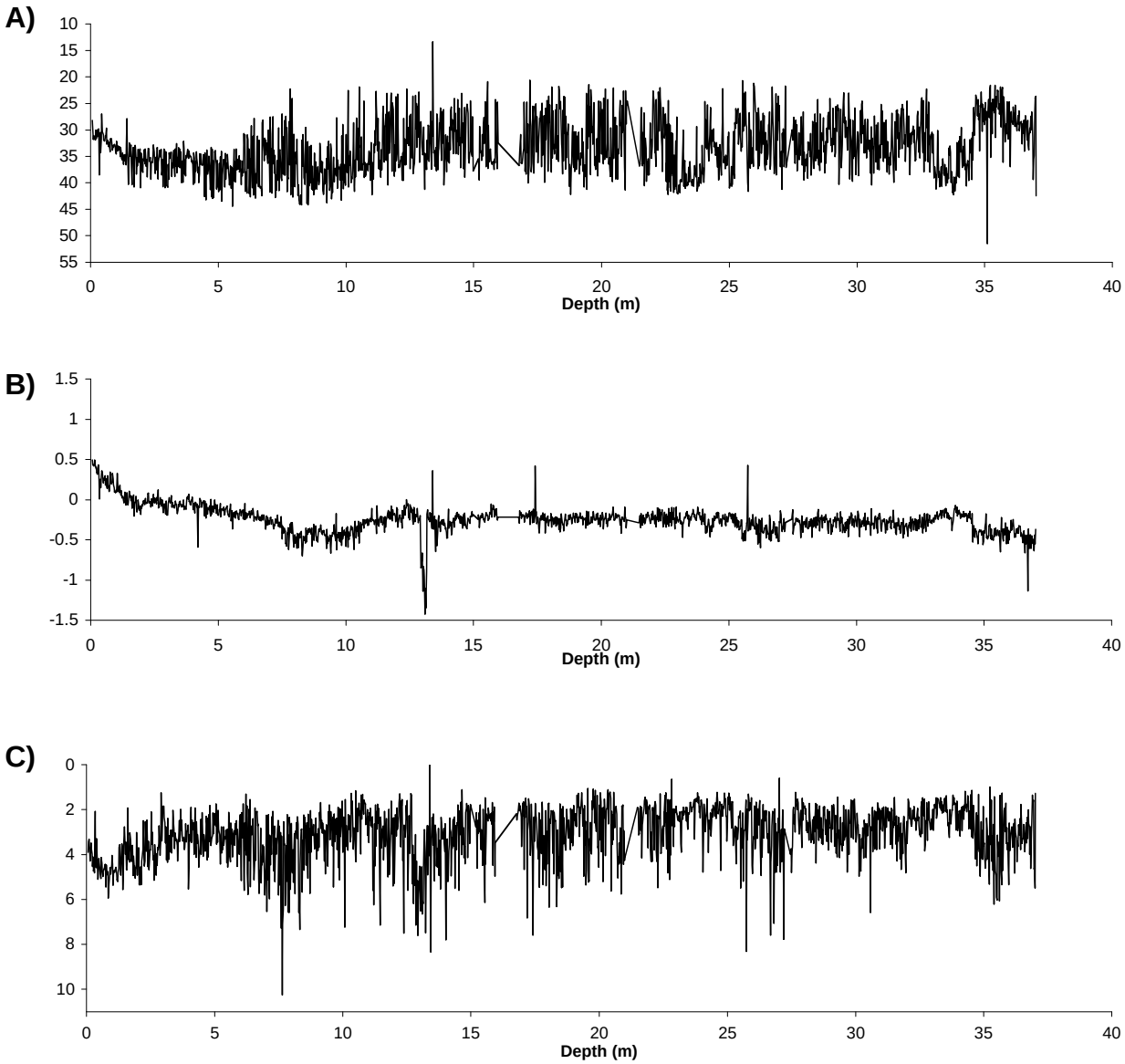

Comparison of colour reflectance in sediments from core MD02-2520 collected in the Gulf of Tehuantepec. A) Lightness (L*) of sediments measured as a percentage of light reflected. B) Plot of chromaticity value (a*) ranging from green (negative) to red (positive). C) plot of variable (b*) with values ranging from blue (lower values) to yellow (higher values).

The entire dataset of physical properties of core MD02-2520 can be found at:
http://doi.pangaea.de/10.1594/PANGAEA.95612